"Na^+-coupled betaine symporters involved in osmotic stress response in prokaryotes and eukaryotes"

Dissertation

Zur Erlangung des Grades

Doktor der Naturwissenschaften

Am Fachbereich Biologie

der Johannes Gutenberg-Universität Mainz

Eva Sabine Schweikhard

geb. am 09.02.1982 in Mainz

Mainz, 24.10.2013

(D 77)

Die vorliegende Arbeit wurde in der Abteilung Strukturbiologie am Max Planck Institut für Biophysik in Frankfurt am Main durchgeführt und an der Johannes Gutenberg-Universität, Fachbereich Biologie, als Dissertation angenommen.

This work was performed in the department of Structural Biology at the Max Planck Institute of Biophysics in Frankfurt/Main and accepted as a dissertation in the department of Biology from the Johannes Gutenberg University of Mainz.

Dekan:

1. Berichterstatter:
2. Berichterstatter:

Tag der mündlichen Prüfung: 02.04.2014

Parts of this thesis have been published, are in revision or in preparation for publication:

Schweikhard, ES; Kuhlmann, SI; Kunte, HJ; Grammann, K and Ziegler CM
Structure and Function of the Universal Stress Protein TeaD and Its Role in Regulating the Ectoine Transporter TeaABC of *Halomonas elongata* DSM 2581T,
Biochemistry, 2010, Vol.49, Issue10, Pages 2194-204

Schweikhard, ES and Ziegler, CM
Amino acid secondary transporters: toward a common transport mechanism,
Curr Top Membr, 2012, Vol.70, Pages 1-28

Schweikhard, ES; Burckhardt, BC; Joos, F; Koshy, C; Fenollar-Ferrer, C; Forrest, LR; Kempson, SA and Ziegler, CM
Role of *N*-glycosylation in osmotic stress-regulated renal betaine transport,
Biochem J, *in revision*

Schweikhard, ES; Burckhardt, BC; Burckhardt, G; Bonner,JS; Ziegler CM and Kempson SA
Mutation of a single threonine in the cytoplasmic N-terminus disrupts trafficking of the renal betaine/GABA transporter during hypertonic stress,
in preparation

Koshy, C; **Schweikhard, ES**; Perez, C; Gärtner, RM; Yildiz, Ö and Ziegler, CM
Structural evidence for functional lipid interactions in the betaine transporter BetP,
Embo J, *in press*

Table of contents

Abbreviations

% [v/v]	percentage volume per volume
% [w/v]	percentage weight per volume
% [w/w]	percentage weight per weight
˚C	degree Celsius
2D	two-dimensional
3D	three-dimensional
Å	Angström(s)
AdiC	Arginine/agmatine antiporter
amp	ampicilin
AP	alkaline phosphatase
APS	ammonium persulfate
Aa	Amino acid
BCCT	Betaine/carnitine/choline transporter
BetP	Glycine-betaine permease
BL21 (DE3)	*E. coli* BL21(DE3)
BN	Blue Native
bp	base pairs
BSA	bovine serum albumine
cmc	critical micelle concentration
CRT	Creatine transporter
Cymal-5	5-Cyclohexyl-1-pentyl-*β*-*D*-maltoside
Da	Dalton
DAT	Dopamine transporter
DM	*n*-Decyl- *β*-*D*-maltoside
DDM	*n*-Dodecyl- *β*-*D*-maltoside

Abbreviations

DNA	desoxyribonucleic acid
dNTP	deoxyribonucleotide triphosphate
D. melanogaster	*Drosophila melanogaster*
E. coli	*Escherichia coli*
et al	*et alia*
eV	electron volt (1eV = 1(e/C) J = $1{,}602\times10^{-19}$J)
FTO	Flow through
GAT	GABA transporter
hr	hours
His_{10}	Deca-histidine tag
HEK	Human embryonic kidney
HPLC	High pressure liquid chromatography
IPTG	Isopropyl-*β*-*D*-thiogalactopyranosid
k	kilo
kDa	kilo Dalton
l	liter
LB	Luria Bertani
LeuT	sodium-dependent leucine transporter
LPR	lipid-to-protein ratio
M	moles per litre
M	Marker
m	milli
MDCK	Madin Darby canine kidney
mg	milligramm
Mhp1	Benzyl-hydantoin transporter
min	minute(s)
ml	milliliter
MW	molecular weight

NaCl	sodium chloride
NET	Norepinephrine transporter
nm	nano meter
NSS	neurotransmitter sodium symporters
OD_{600nm}	Optical density at 600 nm
ORF	open reading frame
PAA	polyacrylamide
PAGE	Polyacrylamide gel electrophoresis
PC	phosphatidylcholine
PCR	polymerase chain reaction
pdb	protein data base
PE	phosphatidylethanolamine
PEG	Polyethylenglykol
Pfu	*Pyrococcus furiosus*
PG	Phosphatidylglycerol
pI	isoelectric point
P. pastoris	*Pichia pastoris*
PVDF	Polyvinylidene fluoride
RNA	ribonulceid acid
rpm	revolutions per minute
RT	room temperature
SDS	Sodium Dodecyl Sulfate
SEC	Size exclusion chromatography
sec, s	second(s)
SerT	Serotonin transporter
SLC6	solute carrier 6 family
T	temperature
t	time

TauT	taurine transporter
TBS	Tris-buffered saline
TEMED	N, N, N', N'-Tetramethylendiamin
TLC	thin layer chromatography
TM	transmembrane
Tris	2-amino-2-hydroxymethyl-propan-1,3-diol
vSGLT	*Vibrio parahaemolyticus* sodium/galactose symporter
wt	wild type
YNB	yeast nitrogen base
µl	microliter

Amino acids in One- and Three-letter code:

A	Ala	alanine	M	Met	methionine
C	Cys	cysteine	N	Asn	asparagine
D	Asp	aspartate	P	Pro	proline
E	Glu	glutamate	Q	Gln	glutamine
F	Phe	phenylalanine	R	Arg	arginine
G	Gly	glycine	S	Ser	serine
H	His	histidine	T	Thr	threonine
I	Ile	isoleucine	V	Val	valine
K	Lys	lysine	W	Trp	tryptophane
L	Leu	leucine	Y	Tyr	tyrosine
			x		variable

1 Introduction

1.1 Organic osmolytes: a common defense strategy

Fluctuations in external osmolarity cause cellular osmotic stress. Although the degree of changes in osmolarity differs in prokaryotes and eukaryotes, the accumulation of organic osmolytes is a common defense strategy against osmotic stress in both organisms (Singh et al., 2009a). Osmolytes are classified into four chemical groups (Yancey et al., 1982; Venkatesu et al., 2007): Polyols, amino acids and their derivatives, and methylamines (Yancey et al., 1982). Under certain osmotic conditions cations like K^+, and anions like glutamate can act as osmolytes and under very specific conditions (see below) urea can act as an osmolyte, too (Braun, 1985; Kwon et al., 2009). Organic osmolytes in prokaryotes are mainly termed 'compatible' solutes (Yancey, 2005). In eukaryotes the osmolytes are further subdivided into 'compatible' and 'counteracting' osmolytes depending on their effects on the functional activity of proteins (Borowitzka and Brown, 1974; Bowlus and Somero, 1979; Yancey et al., 1982) (Figure 1). Compatible solutes are preferentially excluded from the first hydration shell of proteins promoting proper conformational folding. This occurs either as direct osmolyte-macromolecule interactions or through osmolyte-induced changes in the water structure, effecting macromolecular stability (Yancey et al., 1982). Due to their chemical properties compatible solutes can be accumulated to high concentrations without affecting the metabolism of the cell. Amino acids like proline, glycine, taurine and ectoine or polyols like glycerol, sorbitol, *myo*-inositol, trehalose and sucrose are known to act as compatible osmolytes (Borowitzka and Brown, 1974; Bowlus and Somero, 1979; Wang and Bolen, 1996; Yancey, 2005). They are mainly found in archaea, fungi, algae, and insects, amphibians, terrestrial plants and in the mammalian kidney protecting the cells against high-salt environments, extreme temperatures and dehydration (Yancey et al., 1982). The amino acid derivates taurine and ectoine occur mainly in marine animals, although taurine is also found in some mammalian organs (Uchida et al., 1991). 'Counteracting' osmolytes, like trimethylamine N-oxide (TMAO), glycerophosphorylcholine (GPC), Dimethylsulfonopropionate (DMSP) can also be accumulated to high amounts, but they

furthermore enhance protein stability in the presence of the perturbing solute urea (Figure 1) (Yancey and Somero, 1979; Yancey and Burg, 1990; Burg et al., 1996; Venkatesu et al., 2009).

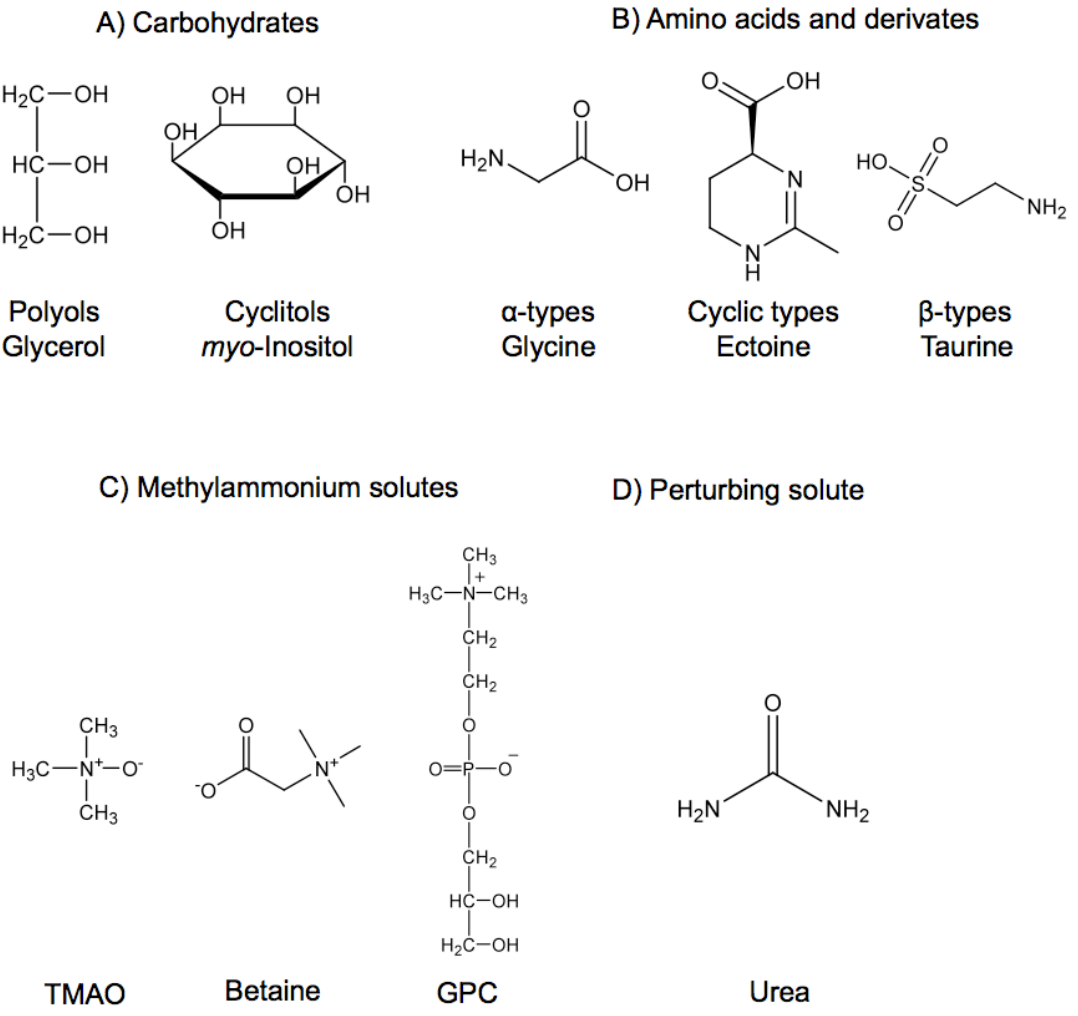

Figure 1: Examples of organic osmolytes, which are divided into 'compatible' and 'counteracting' osmolytes. The compatible osmolytes are classified into two subclasses: carbohydrates A) and amino acids with derivates B). The 'counteracting' osmolytes are splitted into methylammonium and methylsulfonium solutes C); here only the methylammonium group is shown. Urea is shown separately as perturbing solute D). TMAO, trimethyl N-oxide; GPC, glycerophosphorylcholine.

1.2 The osmolyte betaine counteracts urea

The trimethylammonium compound betaine (N,N,N-trimethylglycine) acts as an efficient osmolyte in all three kingdoms of life (Feng et al., 2001; Schliess and Haussinger, 2002; Lang, 2007). It can either be synthesized by the oxidation of choline or it is directly taken up through nutrition (Muñoz-Clares et al., 2010). The biosynthetic pathway for betaine synthesis is a two-step oxidation of choline with betaine aldehyde as an intermediate. It is found in both prokaryotes and eukaryotes (Rhodes and Hanson, 1993; Galinski and Trüper, 1994) and involves homologous enzymes. In *E. coli* the membrane-bound FAD-containing choline dehydrogenase (BetA) is needed in the first oxidation step of the betaine synthesis. BetA oxidizes choline to betaine aldehyde and in the second step the betaine aldehyde dehydrogenase (BetB) converts betaine aldehyde into the end product betaine (Lamark et al., 1991; Kempf and Bremer, 1998). These highly substrate-specific bacterial dehydrogenases share 26.7 % sequence identity with their mammalian relatives. Both mammalian dehydrogenases are stress-induced (Brocker et al., 2010) and expressed in kidney and liver and are particularly found in mitochondria, the cytosol and the nucleus, where they synthesize betaine for protecting all important cell compartments against osmotic stress (Chern and Pietruszko, 1999; Brocker et al., 2010). Besides its role in osmoregulation, betaine is a methyl donor for remethylation of homocysteine to methionine (Lever and Slow, 2010). During hypertonic stress bacterial cells accumulate up to 1 M betaine (Singh et al., 2009b), whereas the intracellular betaine concentration in renal medullary cells is around 100 mM and in the human blood plasma the betaine concentration is 20 μM – 144 μM (Laryea et al., 1998; Lever et al., 2004). Disruption of betaine-mediated volume regulation can cause apoptosis in renal medullary cells (Haussinger, 1996; Dmitrieva and Burg, 2005; Reinehr and Haussinger, 2006) and betaine is reported to counteract loss of enzyme activities caused by thermal stress in *E. coli* (Caldas et al., 1999). In bacteria urea is a product of nitrogen metabolism. In marine fishes the average urea concentration is about 400 mM, which can also cause perturbing effects on proteins (Yancey et al., 1982), but these organisms use urea and methylamines in a ratio of 2:1 to counteract osmotic stress (Yancey et al., 1982).

One major task of betaine in mammals is to counteract the destabilizing action of urea on protein structures (Yancey et al., 1982). Urea is a chaotropic agent that alters the water structure surrounding proteins and nucleic acids (Yancey et al., 1982). Urea disrupts hydrophobic interactions (Nozaki and Tanford, 1963; Yancey and Somero, 1979; Singh et al., 2009b) and forms hydrogen bonds (Bennion and Daggett, 2003; Smith, 2004; Cannon et al., 2007) with residues at the protein surface resulting in dehydration and unfolding (Creighton, 1991; Zou et al., 1998; Wu and Wang, 1999). Moreover, post-translational modification of proteins can also be caused through high urea concentrations resulting in carbamoylation or carbonylation near neutral pH (Kraus and Kraus, 2001; Nystrom, 2005). Urea penetrates the membrane but does not induce significant osmosis in contrast to salt, therefore, the counteraction of urea by betaine is not an osmotic stress response *per se* (Singh et al., 2009a). In the complex arrangements of tubuli in the kidneys, urea can even act as an osmolyte (Braun, 1985; Kwon et al., 2009) involved in regulated water re-absorption in the renal medulla (Wirthensohn et al., 1989; Kwon et al., 2009). Nevertheless, high urea concentrations exceeding 300 mM cause cell death (Michea et al., 2000) and counteracting urea is therefore the essential function of betaine in the renal medulla (Burg et al., 1996).

Besides betaine, glycerophosphorylcholine (GPC) is another methylamine organic osmolyte in renal medullas (Garcia-Perez and Burg, 1991) counteracting the perturbing effects of urea (Burg et al., 1996; Burg and Peters, 1998). GPC is synthesized from phosphatidylcholine (PC) by phospholipase A_2 and lysophospholipase (Bauernschmitt and Kinne, 1993) in inner renal medulla cells. GPC is preferred in renal cells, because its accumulation depends, besides on high concentrations of NaCl, on the extracellular urea concentration, whereas betaine accumulation is only regulated according to the increased external tonicities (Beck et al., 1998). As a consequence GPC tissue concentrations are related to that of urea (Peterson et al., 1992; Nakanishi et al., 1993; Sone et al., 1995) and are usually higher than betaine concentrations (Cowley et al., 1990; Beck et al., 1992a; Beck et al., 1992b; Peterson et al., 1992; Nakanishi et al., 1993; Sone et al., 1993; Nakanishi et al., 1994; Sone et al., 1995; Nakanishi et al., 1996). Both, betaine and GPC are excluded from the first hydration shell of proteins by repulsive interaction with the protein backbone. This occurs either as direct

osmolyte-macromolecule interactions or through osmolyte-induced changes in the water structure, effecting macromolecular stability (Yancey et al., 1982).

1.3 Osmolyte transporters in prokaryotes and eukaryotes

Exposure of bacterial cells to either hypo- or hyperosmotic stress triggers rapid water fluxes across the semipermeable cytoplasmic membrane resulting in changes in turgor, which is affecting many physiological processes (Ziegler et al., 2010). Under hyperosmotic conditions water efflux causes dehydration of the cytoplasm. The cell counteracts by changing the content of the remaining free cytoplasmic water through accumulation of ions and organic osmolytes, mostly betaine (Figure 2). Accumulation of betaine in prokaryotes and eukaryotes is facilitated by specific uptake systems (Figure 2), e.g. primary active ABC-transporters or secondary transporters (Wood, 2007; Berntsson et al., 2010; Ziegler et al., 2010).

In bacteria, both transporter types have been shown to exhibit osmosensing and osmoregulatory properties (Berntsson et al., 2010; Ziegler et al., 2010) both on the level of gene expression and transport activity, however, not always both at the same time. In some bacteria, i.e. in *Listeria monocytogenes,* betaine ABC-transporter and betaine secondary transporter work in conjunction; one is regulated on the expression level, the other on the activity level (Watson et al., 2009). Several reviews on the role of primary and secondary transporters in osmotic stress response provide a broad overview on bacterial osmoregulation (Poolman et al., 2002; Wood, 2007). The bacterial Na^+-coupled betaine symporter BetP is one of the best-investigated osmoregulated transporters to date, both structurally and functionally (Kramer, 2009; Kramer and Ziegler, 2009). BetP belongs to the BCCT-family (**b**etaine-**c**arnitine-**c**holine-**t**ransporter) (Ziegler et al., 2010) and is exclusively specific for betaine, which is co-transported along with two Na^+-ions (Figure 2), leading to extremely high accumulation concentrations of betaine inside the cell.

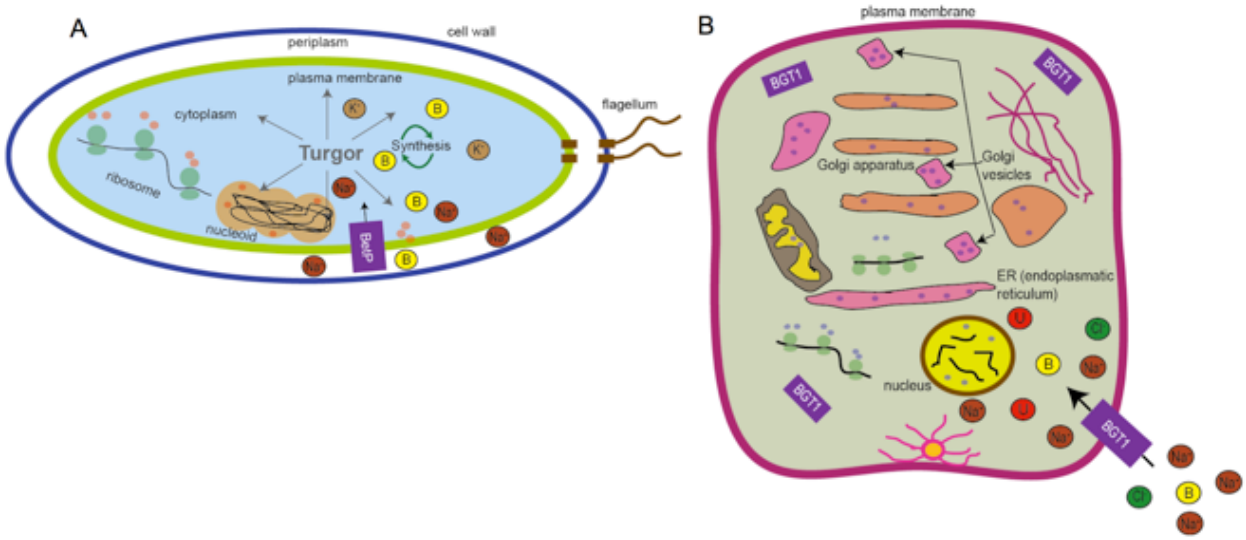

Figure 2: Osmotic stress response in prokaryotic and eukaryotic cells. Under hyperosmotic stress conditions cells accumulate compatible solutes, e.g. betaine (B, yellow) by specific transporters like BetP in prokaryotes (A) and BGT1 (both purple) in eukaryotes (B). Under isotonic conditions BGT1 is mainly found intracellular and it is inserted into the membrane under hyperosmotic conditions. Transport is coupled to Na^+ (brown circles) for both BetP and BGT1 but for BGT1 in an additional Cl^- -dependent manner (green circles). The intracellular K^+ concentration (light brown) is a measure for osmotic stress in prokaryotic cells. In eukaryotic cells betaine counteracts the unfolding actions of urea (light red circles).

BetP acts both as an osmosensor and an osmoregulator. It senses osmotic stress *via* its long, positively charged C-terminal domain and responds with instant regulation of its transport activity. BetP activation depends on certain stimuli related to osmotic stress like an increased cytoplasmic K^+ concentration (Schiller et al., 2004) and physical changes in the membrane. The N-terminal extension is also essential for activity regulation in BetP (Peter et al., 1998). Structural data were crucial to mechanistically describe the various regulatory interactions in BetP. The crystal structure of BetP recently solved to 3.35 Å resolution (Ressl et al., 2009b) reveals the trimeric architecture as well as the structure of the osmosensing C-terminal domain forming an extended α-helix protruding into the cytoplasm. The structure provides a basis to explain an osmoregulatory mechanism, which involves the formation of an homo-trimeric state of BetP (Kramer and Ziegler, 2009).

The BCCT-family comprises mainly bacterial betaine transporters. To date no functional BCCT-type betaine transporters were identified in eukaryotes (Ziegler et al., 2010), although several functional archaeal BCCT-type transporters are found (Ziegler et al., 2010), which share a moderate sequence identity of about 25-35 % with BetP. This raises the question why such extremely efficient BCCT betaine uptake systems like BetP are obsolete in mammalian osmoregulation. In fact, transport and regulation in mammalian osmolyte transporters is far less understood compared to the bacterial systems. This is mainly due to missing structural information. Generally, regulatory processes in mammalian cells are much more complex, often depending on several additional interaction partners (Muller et al., 2006; Armsen et al., 2007).

In mammals, the equilibrium of both hydration and compatible solute concentration is an important physiological factor (Bourque, 2008). Therefore, osmotically-induced regulation of gene expression, metabolic activity and osmolyte transport is found in diverse tissues and organs, e.g. kidney (Miyakawa et al., 1998), lung (Fedan et al., 1999), cardiovascular system (Zhou et al., 1997) and musculoskeletal system (Urban et al., 1993). Transporters of the **n**eurotransmitter-**s**odium-**s**ymporter (NSS) family facilitate osmolyte transport in mammals. The exact nomenclature for this family is solute carriers 6 (SLC6), according to the human genome organization (Broer, 2006), which is divided in different subfamilies depending on their substrate specificity (Figure 3). The first subfamily includes osmolyte transporters for the inhibitory neurotransmitter GABA (h/m/rGAT1, SLC6A1; mGAT4 = h/rGAT3, SLC6A11; mGAT2 = h/rBGT1, SLC6A12 and mGAT3 = h/rGAT2, SLC6A13) and for the osmolytes betaine (mGAT2/BGT1, SLC6A12), taurine (mTauT, SLC6A6) and creatine (rCRET, SLC6A8) (Figure 3, circled in green). The second subfamily comprises monoamine transporters for dopamine (DAT, SLC6A3), serotonine (SerT, SLC6A4) and norepinephrine (NET, SLC6A2) (Figure 3, circled in red). The third subfamily are the amino acid transporters splitted into Amino Acid transporters I and II (Figure 3, circled in black). Amino acid transporters I include the glycine transporters 1 and 2 (Glyt1, SLC6A9 and GlyT2, SLC6A5), the proline transporter (ProT, SLC6A7) and the neutral and basic amino acid transporter ($B(0^+)$, SLC6A14), Amino acid transporters II involves the orphan-transporters (NTT73,

NTT5, NTT4, XTRP2, B(0)AT1 and XTRP3, SLC6A15-20). The prokaryotic group (Figure 3, circled in blue) comprises archaeal and bacterial transporters like the leucine transporter $LeuT_{Aa.}$ from *Aquifex aeolicus* (Nelson, 1998; Livesay et al., 2007). In the following the SLC6 nomenclature will be kept to distinguish between the different osmolyte NSS transporters.

The osmolyte subfamily (Figure 3, circled in green) is the largest subfamily with certain members also transporting the neurotransmitter GABA even though that is not an osmolyte. GABA transporters GAT1, BGT1, GAT2 and GAT3 (refered to human and rat nomenclature, which is different from the mouse nomenclature (see above) and (Skovstrup et al., 2010)) differ with respect to their substrate spectra, as GAT1 and GAT3 exclusively transport GABA. BGT1 so far known as GAT2 in mouse (Chen et al., 2004), transports both GABA and betaine (Borden, 1996; Chen et al., 2004). All four GABA transporters have been cloned and described with respect to their pharmacologic properties (Guastella et al., 1990; Borden et al., 1992; Liu et al., 1992; Lopez-Corcuera et al., 1992; Yamauchi et al., 1992; Liu et al., 1993). The transporters share around 50 % amino acid sequence identity with each other. TauT can also accept GABA as a substrate but transport activity is low (Tomi et al., 2008). CRET only alters its substrate specifity after mutations based on the GABA transporters (Dodd and Christie, 2007).

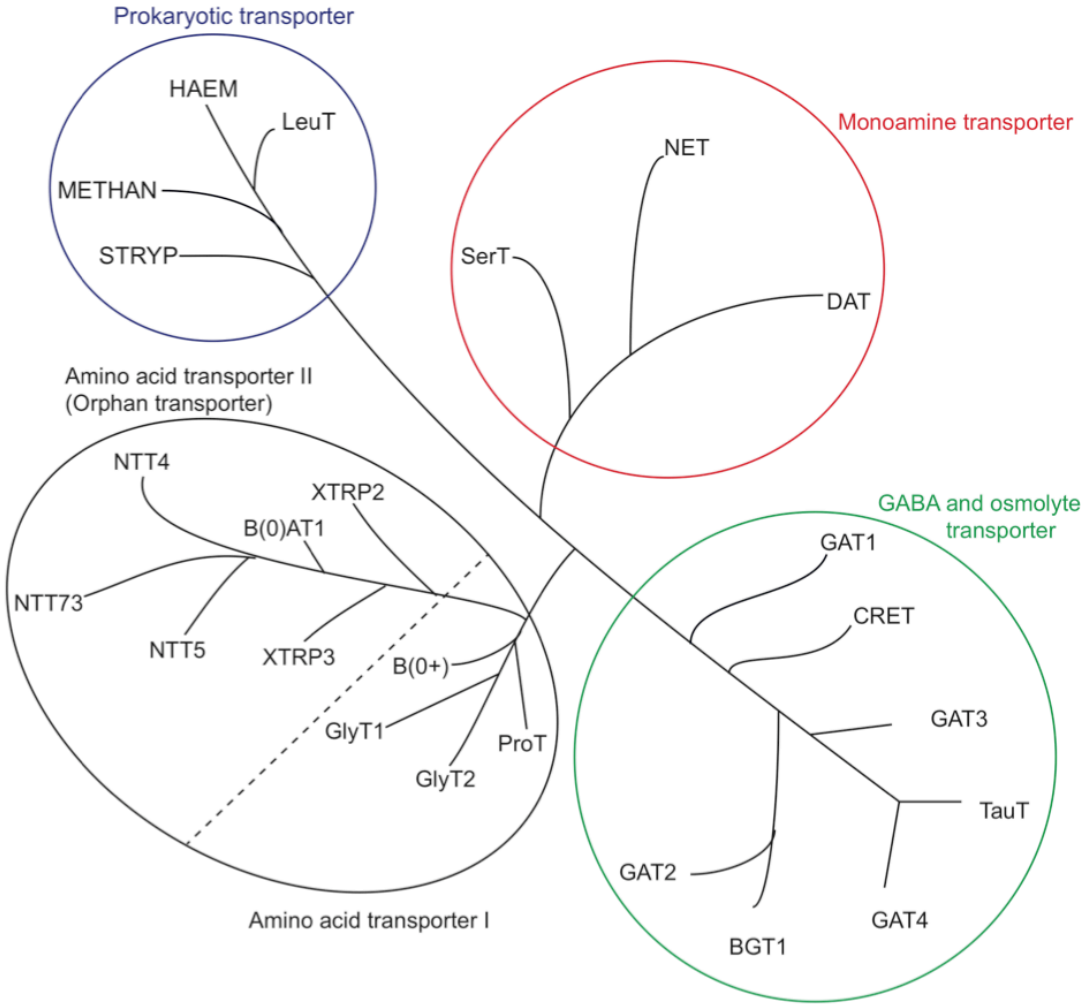

Figure 3: Phylogenetic tree of the SLC6-family. The tree is composed of the five major subfamilies. The families are divided into their chemical class of substrates (monoamines (red circle), GABA and osmolytes (green circle), the two amino acid transporter groups I and II (black circle, separated by a dashed line)) and the prokaryotic members (blue circle) of this family. HAEM is a gene of *Haemophilus influenzae*; METHAN is a gene from *Methanococcus jannashii* and STRYP is a gene from *Symbiobacterium thermophilum*. LeuT, leucine transporter; SerT, serotonine transporter; NET, noradrenaline transporter; DAT, dopamine transporter; GAT1, 2, 3, 4, GABA transporter 1, 2, 3, 4; CRET, creatine transporter; TauT, taurine transporter; BGT1, betaine/GABA transporter; GlyT1/2,glycine transporter 1/2; B(0+), neutral and basic amino acid transporter; XTRP2, neutral amino acid transporter; XTRP3, sodium/imino-acid transporter 1; B(0)AT1, neutral amino acid transporter; NTT/4/5/73, orphan transporter.

1.4 Structural information on SLC6 transporters

SLC6 transporters are predicted to contain 12 transmembrane (TM) spanning α-helices with both NH2- and COOH-termini facing the cytoplasm (Broer and Gether, 2012) (Figure 4). The large extracellular loop 2 (EL2) between TM segments 3 and 4 contains potential N-glycosylation sites (Broer and Gether, 2012) and for the serotonin transporter, SERT disulphide bond formation is crucial for obtaining a functional conformation of EL2 (Chen et al., 1997) (Figure 4). Additionally, several phosphorylation sites are loacted in the intracellular loops (ILs).

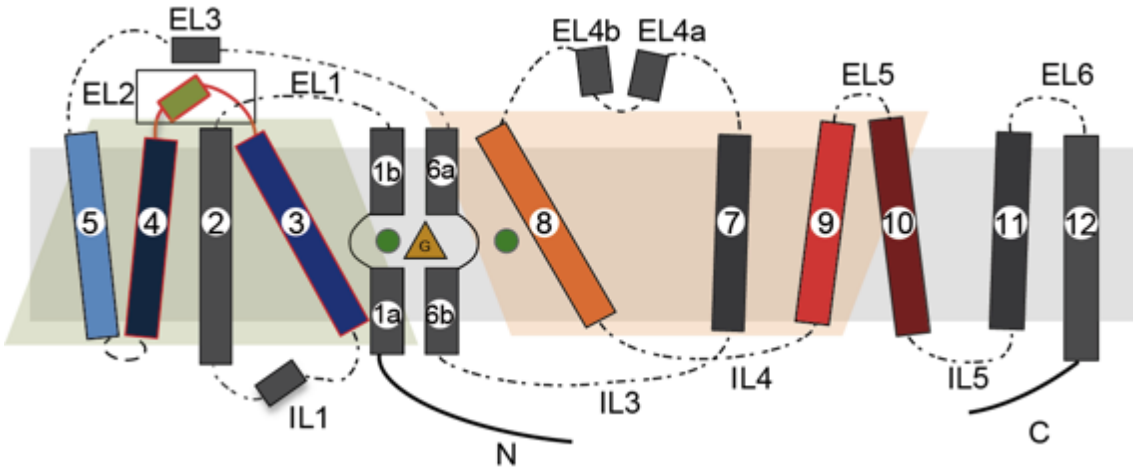

Figure 4: Topology of SLC6 transporters. Transporters of the SLC6 family have 12 transmembrane helices with both N- and C-termini facing the cytoplasmic side of the membrane. The transporter core is formed by two inverted repeats of five TM helices with repeat 1, TM1 - TM5 (light green background) and repeat 2, TM6 - TM10 (light orange background). TM11 and TM12 do not belong to the inverted repeats. The most prominent loop harboring several *N*-glycosylation sites and probable disulphide bonds in the eukaryotic members is EL2 between TM3 and TM4 (black rectangle and highlighted in red). The position of the substrate GABA (G) and the two sodium ions are represented as orange triangle and green circles, respectively.

Very recently a structure of an eukaryotic dopamine transporter from *Drosophila melanogaster* was published (Penmatsa et al., 2013) but until then no structural information was available on any of the eukaryotic SLC6 transporters. However, the crystal structure of the bacterial homologue $LeuT_{Aa}$ (Yamashita et al., 2005) has contributed tremendously to the understanding of eukaryotic neurotransmitter transporters, such as SERT (Ravna et al., 2006),

DAT (Ravna et al., 2003; Gedeon et al., 2010), GAT1 (Pallo et al., 2007; Zomot et al., 2007) and CRET (Christie, 2007), even though the sequence identity between the prokaryotic and the eukaryotic members of the SLC6-family is only 20-25 % (Yamashita et al., 2005). The fact that LeuT shares the same overall fold with other sequence-unrelated transporter families has contributed fundamentally to the understanding of the molecular transport mechanism of transporters owing this type of fold (Lolkema and Slotboom, 2003; Brett et al., 2005; Lolkema and Slotboom, 2008; Abramson and Wright, 2009; Gouaux, 2009; Krishnamurthy et al., 2009). In this context, it is important to note that also transporters of the BCCT family share this important fold (Figure 5), like the Na^+-coupled betaine transporter, BetP and the Na^+-independent carnitine transporter, CaiT, an antiporter, which is not involved in accumulating molecules inside the cell under osmotic stress conditions (Ressl et al., 2009a; Schulze et al., 2010).

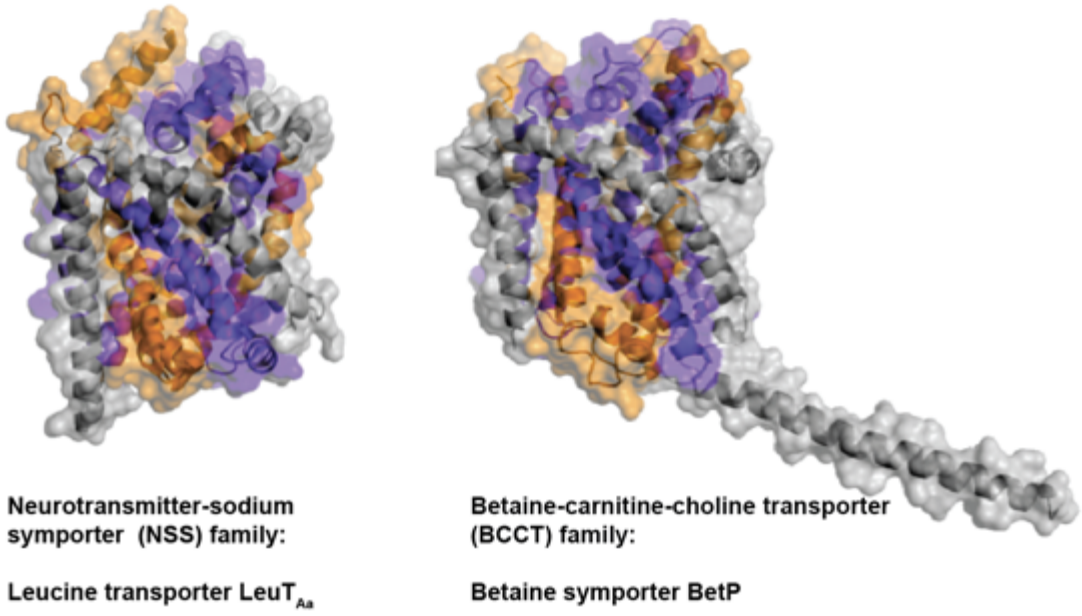

Figure 5: Overall fold of members of the NSS and BCCT family. Transporters of the NSS family (leucine transporter, LeuT, left; pdb code: 2A65) share the same overall fold with transporters of the BCCT family (betaine transporter, BetP, right; pdb code: 2WIT).

The mechanism of substrate binding and translocation in SLC6 transporters was discussed based on theoretical and computational deduction for SERT (Forrest et al., 2008) and DAT

(Indarte et al., 2008) using the LeuT X-ray crystal structure to calculate models of these transporters. Most recently a homology model was provided for a member of the osmolyte subfamily, GAT1, based on this homology model and functional validations, several residues involved in GABA binding could be identified (Skovstrup et al., 2010).

1.5 The betaine/GABA transporter BGT1

1.5.1 Function of BGT1 in osmotic stress response in renal medulla

Medullar cells have to cope with extreme changes in extracellular osmolality from diuresis (low medullary solute concentrations) to antidiuresis (high medullary solute concentrations) (Beck et al., 1998). The interstitial solution of the renal medulla is always fluctuant and cells are constantly facing variable hypertonicity. The highly variable osmolality in urine depending on the hydration state results in osmotic stress. Osmolality of the renal medulla reaches over 1,000 mosmol/kg in humans (Kwon et al., 2009). Both, diluted (< 100 mosmol/kg) and concentrated urine (> 4,000 mosmol/kg) must be adjusted without changing the amount of total solute excretion (Kwon et al., 2009).

Transcriptional osmoregulation in mammalian cells is one important osmotic stress response and was investigated in detail. The transcription factor TonEBP is an important transcriptional regulator for the accumulation of organic osmolytes in mammalian cells (Woo et al., 1999). The activity of TonEBP increases with extracellular hypertonicity. TonEBP promotes transcriptional stimulation of the two SLC6-transporters BGT1 and TauT, but also of one of the sodium/myo-inositol symporters (SMIT), a member of the Na^+-dependent solute symporter (SSS-) family comprising transporters that are specific for e.g. sugars, nucleosides, amino acids and vitamins (Reizer et al., 1994). Furthermore, TonEBP activates also the rate-limiting biosynthetic enzymes aldose reductase (AR) for sorbitol synthesis and the neuropathy target esterase (NTE, a phospholipase B) for GPC synthesis (Miyakawa et al., 1998; Trama et al., 2002; Na et al., 2003; Ito et al., 2004; Gallazzini et al., 2006).

Besides the transcriptional activation of the *bgt1* gene under hypertonicity (Uchida et al., 1993b), plasma membrane insertion of BGT1 is regulated by membrane tonicity (Kempson

and Montrose, 2004). Under isotonic conditions only a small amount of BGT1 is present in the plasma membrane, during hypertonicity, BGT1 is observed mainly in basolateral plasma membranes and betaine/GABA transport is up-regulated (Kempson et al., 2003).

Up- and down-regulation of BGT1 initiated by changes of the extracellular osmolarity occurs slowly in cultured cells within 24 hr. However, a comparative rapid downregulation (within 30 min) of BGT1 mediated substrate transport in response to extracellular ATP, adenosine, and calcium was previously demonstrated in MDCK cells (Kempson et al., 2006; Kempson et al., 2008). Inhibition of BGT1 transport by protein kinase A (PKA) and protein kinase C (PKC) was shown as a post-translational regulation of the uptake of osmolytes (Preston et al., 1995). This finding, suggesting a regulatory role of PKC on BGT1, was accompanied by an increased internalization of BGT1 from the plasma membrane (Massari et al., 2005; Kempson et al., 2006). BGT1 phosphorylation on serines and threonines was previously reported in response to PKC activation in MDCK cells (Massari et al., 2005). AMP-activated protein kinase activity was also shown to be a powerful down-regulator of BGT1 (Munoz et al., 2012), whereas the Janus-activated kinase-2 (JAK2) and the serine/threonine Tau-tubulin-kinase 2 (TTBK2), which are both activated upon hyperosmotic shock, were reported to be powerful stimulators of BGT1 (Hosseinzadeh et al., 2012; Almilaji et al., 2013).

However, the molecular mechanism of osmo-sensing and subsequent regulatory membrane insertion of BGT1 is still unknown. Controlled folding by *N*-glycosylation might be one regulatory mechanism, as *N*-glycans are reported to affect targeting and functional insertion into the plasma membrane of different proteins (Lis and Sharon, 1993; Kukuruzinska and Lennon, 1998). The role of *N*-glycosylation sites in the extracellular loop 2 (EL2) of SLC6 transporters has been widely discussed (Tate and Blakely, 1994; Melikian et al., 1996; Nguyen and Amara, 1996; Li et al., 2004; Cai et al., 2005; Straumann et al., 2006), although the results are inconsistent between different transporters. EL2 connects transmembrane (TM) helices 3 and 4, two helices that are involved in conformational changes during transport in the NSS family (Forrest et al., 2011). The number of *N*-glycosylation sites in EL2 varies among members of the NSS family from two in BGT1 to four in the dopamine transporter DAT. As a consequence individual NSS transporters seem to be differently affected by *N*-

glycosylation (Tate and Blakely, 1994; Nguyen and Amara, 1996; Li et al., 2004; Cai et al., 2005; Straumann et al., 2006). For instance, mutations of two of the three *N*-glycosylation sites in the GABA transporter GAT1 expressed in *Xenopus* oocytes yielded a reduction of substrate turnover rates and significantly changed the affinity to sodium (Cai et al., 2005), while the dopamine transporter, DAT, showed reduced inhibitor affinity when *N*-glycosylation was altered (Li et al., 2004).

Besides the kidneys, BGT1 is found in the brain and in the liver (Kempson and Montrose, 2004; Zhou et al., 2012). Most likely, BGT1 mediates the transport of the neurotransmitter GABA in the brain, however with lower affinity ($K_{M\ (GABA)}$= 20 – 100 μM (Chen et al., 2004)) compared to other GABA transporters, e.g. GAT1 ($K_{M\ (GABA)}$= 7 μM (Borden, 1996)). Both, betaine and GABA transport are chloride-dependent and coupled to the transport of three sodium ions (Rasola et al., 1995; Matskevitch et al., 1999), which might be required to provide a sufficient driving force in order to achieve an intracellular renal medullary cell betaine concentration of around 100 mM (Laryea et al., 1998; Lever et al., 2004). It is unknown to date, if betaine transport itself is similary regulated in BGT1 as it is observed for BetP. The LeuT X-ray crystal structure as well as the several homology models based on the LeuT structure show limitations (Ravna et al., 2003; Ravna et al., 2006; Christie, 2007; Zomot et al., 2007) to fully explain osmolyte transport and osmoregulation. Therefore, in this work BGT1 will be compared to BetP, a structural homologue of the SLC6 family, to analyze if structural and functional investigations on BetP can be extended to understand transport and regulation in BGT1.

1.6 BGT1 and BetP: Bacterial and eukaryotic betaine transporters share the same overall fold

For GAT1, the LeuT structure contributes to some extend to the understanding of GABA transport (Pallo et al., 2007), but so far nothing is known about key residues involved in betaine and GABA transport of BGT1. The BetP structure as well as two structures of the BetP-homologue CaiT (Schulze et al., 2010) reveal a very characteristic coordination of

trimethylammonium compounds like betaine by the indole groups of several tryptophans forming an aromatic substrate-binding box (Ressl et al., 2009a). These tryptophans contribute to the μM affinity of BetP for betaine. Similar aromatic substrate coordination would not be present in BGT1 when GABA and betaine share the same substrate-binding site as was proposed by the LeuT structure and by the GAT1 homology model.

It is suggested for BetP that the formation of a homo-trimer is related to regulatory properties. The trimeric architecture is a consequence of the unique structural elements characterizing the fold of the BCCT-family (Ziegler et al., 2010), which is not shared with other LeuT-fold transporters. Monomer interactions also involve the osmosensing C-terminal helix interacting with the cytoplasmic loop 2 and the C-termini of the other two BetP monomers. This interaction network is the basis of BetPs osmoregulatory abilities (Kramer and Ziegler, 2009). However, the oligomeric state of the eukaryotic osmoregulatory transporter BGT1 is yet unknown. Nevertheless, the structural information on C- terminal interactions with loop2 in BetP might be extended to understand regulatory properties in BGT1 due to an intriguing structural similarities in LeuT-fold transporters (Abramson and Wright, 2009). An important structural feature to keep in mind is the topological shift between LeuT and BetP. In LeuT, the transporter core comprises TM1-TM10 (Figure 4) whereas in BetP TM3-TM12 form the transporter core (Figure 6). Additional structural elements, like additional TM helices, for other LeuT-fold transporters are located either at the N- or C-terminal ends (Figure 6). This is of importance for the comparison between BetP and BGT1, because due to the topology shift loop2 (L2) in BetP, which interacts with the C-terminal domain, corresponds to the N-terminal domain of BGT1 (red rectangle, Figure 6). Interestingly, the N-terminal domains in the osmolyte SLC6-transporters are also involved in activity regulation by syntaxin 1A, and phosphorylation through protein kinase C (PKC), as shown for GAT1 (Beckman et al., 1998; Wang et al., 2003), CRET (Strutz-Seebohm et al., 2007), GAT2 (Chen et al., 2004) and GAT3 (Chen et al., 2004). Syntaxin 1A belongs to the vesicle associated membrane protein family and acts as a down-regulator for transport activity through interactions with the aspartic residues in the N-terminal domain of GAT1 (Beckman et al., 1998). PKC activation

leads to transporter phosphorylation of GAT1 and CRET and thereby down-regulating the transport capacity by activating endocytosis. Also, the N-terminus of the monoamine transporters are required for mediating amphetamines, e.g. a highly conserved threonine residue at position 81 is also phosphorylated by PKC, mutations to alanine in SERT, DAT and NET failed to support amphetamine-induced efflux (Sucic et al., 2010). This is a striking similarity to BetP, where the interaction of L2 with the C-terminal domain of BetP is similary based on ionic interaction with an aspartic acid residue, and it is speculated that this interaction down-regulates BetP by restraining the flexibility of the bundle helices (Ressl et al., 2009b).

Further on, the N-terminal domain in BetP would correspond to the C-terminal domain in BGT1 (Figure 6, green rectangle).

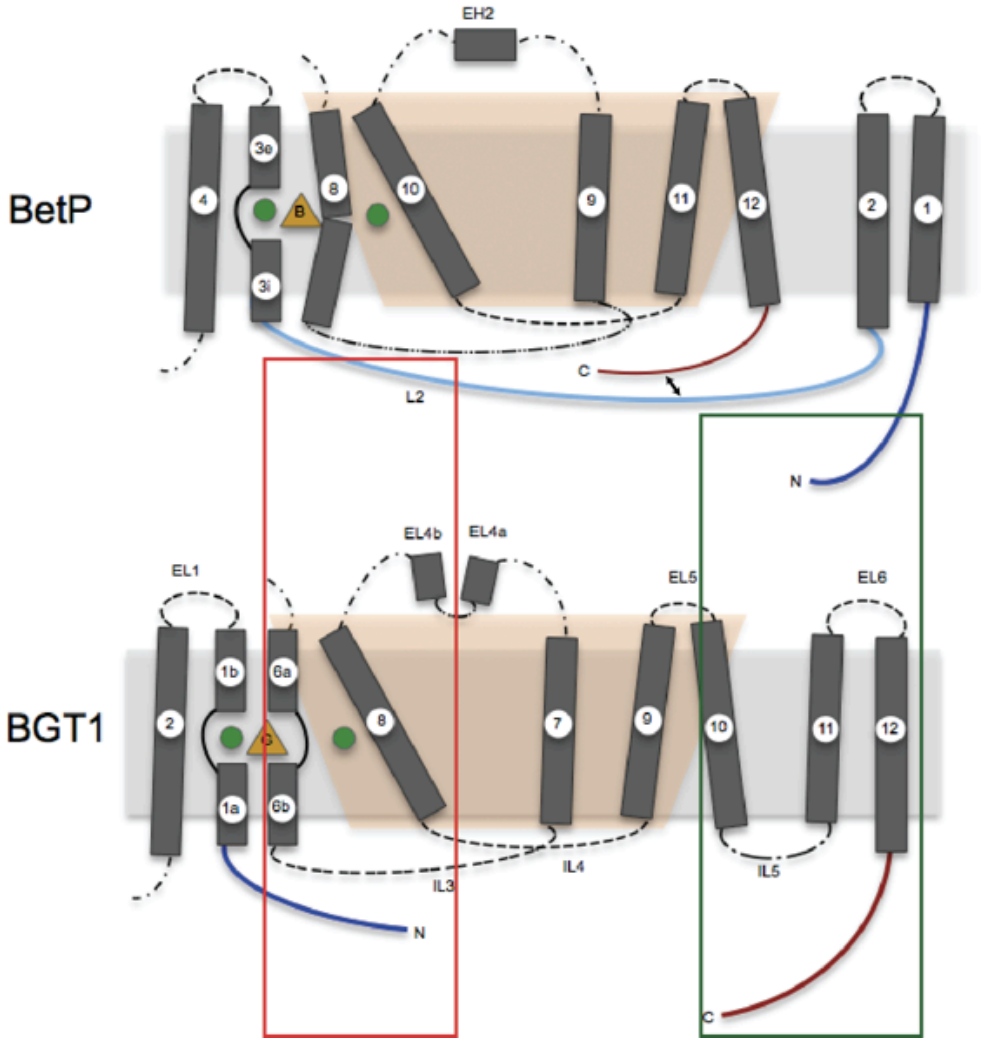

Figure 6: Topology of BetP (missing TM5, 6 and h7) and BGT1 (missing TM3, 4 and 5). The positions of GABA and betaine are shown as yellow triangles labeled with 'B' for betaine and 'G' for GABA. The two sodium ions are shown as green circles. Due to a shift in topology by 2 TM helices, loop2 (L2) in BetP corresponds to the N-terminal domain of BGT1 (red rectangle) and the N-terminal domain of BetP corresponds to the C-terminal domain of BGT1 (green rectangle).

The N-terminal domain of BetP functions as a regulation modulator during hyperosmotic stress and there is strong evidence that this occurs by a mutual interaction with the C-terminal domain. The C-terminal domain in BGT1 contains regulatory features, too, e.g. a PDZ association motif which prevents the protein from internalization when interacting with the PDZ protein mLin-7 (Kempson and Montrose, 2004). A conserved motif in the C-terminal

domain of GAT1 (^{566}RL^{567}) is a binding site for the COPII coat component Sec24D and the residues (^{733}DD^{734}) in Sec24D are also required to interact with GAT1 and two additional family members. These binding partners of the serotonin and dopamine transporters are necessary to export the proteins from the endoplasmatic reticulum to the plasma membrane (Farhan et al., 2007). Additionally, Farhan *et al*. identified a motif of three hydrophobic residues (^{569}VMI^{571}) in the C-terminus of GAT1 that is required to export GAT1 from the ER-Golgi intermediate compartment to the plasma membrane (Farhan et al., 2008).

A homo-trimeric state for BGT1 would not necessarily be required for regulation, because this transporter has several interaction partners, which in BetP might be mimicked by the interaction of L2 with the C-terminal domain. In this context osmosensing and/or osmoregulation might be out-sourced in BGT1. However, the the catalytic transport cycle in BGT1 is likely to be influenced by similar interactions within the N-terminal and C-terminal domains as are observed in BetP and therefore it can be assumed that substrate binding and release might be regulated in a similar way by locking or loosening the flexible bundle helices. Without structural information of the terminal domains of BGT1 in hand, the regulatory interactions observed in BetP could help to design experiments to identify crucial regulatory residues in BGT1.

1.7 Aims of this work

BGT1, a member of the neurotransmitter sodium symporter (NSS) family, facilitates betaine and GABA uptake. Transport is upregulated under hypertonic conditions when increasing amounts of intracellular BGT1 are inserted into the plasma membrane by a yet unknown mechanism. Re-establishing isotonicity results in subsequent depletion of BGT1 from the plasma membrane. The overall goal of this thesis is to contribute to a better understanding of the fascinating transport and regulation properties of BGT1, also in a molecular level by a thorough functional analysis and by structural studies using the prokaryotic BetP as a template. The following questions are addressed on detail:

Protein kinase C (PKC) is known as a down-regulator of many NSS transporters leading to the activation of endocytosis and consequently results in a decreased number of transporters in the plasma membrane.
BGT1 phosphorylation on serines and threonines was reported previously in response to PKC activation in MDCK cells (Massari et al., 2005). To understand the influence of PKC phosphorylation on BGT1, several potential phosphorylation sites will be mutated. Furthermore, the responses to PKC mediated activators, the cellular distribution and the consequences on substrate transport of these BGT1 mutants will be determined and compared to BGT1 wildtype. The PKC-interaction will be further investigated by immunoblotting against a PKC specific antibody.

N-glycosylation of the large extracellular loop (EL2) between TM3 and TM4, a topological feature, which is common in all members of this family, might as well play an important role for BGT1. Although the number and positions of these *N*-glycosylation sites are not conserved throughout the family, they are all located at homologous positions within EL2. So far, no investigations have been carried out concerning the two predicted *N*-glycosylation sites (N171 and N183) in BGT1 and to what extend *N*-bound glycans affect BGT1 function, stability and/or folding. Therefore, the functional importance of these two *N*-glycosylation sites will be investigated in this study.

No structural information of BGT1 is available to date, but the structure of $LeuT_{Aa}$ (Yamashita *et al.*, 2005) has contributed tremendously to the understanding of eukaryotic neurotransmitter transporters as SERT (Ravna *et al.*, 2006), DAT (Ravna *et al.*, 2003), GAT1 (Zomot *et al.*, 2007) and CRET (Christie, 2007). However, the sequence identity of the prokaryotic and the eukaryotic members of the NSS-family is only 20-25 % (Yamashita *et al.*, 2005) and the LeuT structure as well as several homology models showed limitations in explaining osmolyte transport and transport regulation.
Therefore, multiple different expression systems will be tested in order to find a suitable heterologous expression system for BGT1, in which expression and subsequent purification yield sufficient amounts of stable protein to perform qualitative analysis that will eventually lead to further structural studies using 2D and 3D crystallization.

Even though there is no significant sequence similarity between the BCCT- and the NSS family the overall fold suggestes that the different gene families have not only a common ancestor but also conserved structure-function relationship regarding the mechanism of how substrate and sodium transport is coupled. Moreover, the highly specific bacterial betaine transporter BetP might serve as a bacterial homologue for BGT1 and could also explain some characteristics of osmolyte transport of transporters within the NSS-family. Hence, detailed analysis of BetP regarding mutagenesis studies and transport measurements will be performed in order to transform BetP into a '*surrogate*' to reduce its naturally high affinity for betaine and to transform it into a BGT1-like betaine/GABA transporter. Additionally, 3D crystallization and structure determination of these specifically altert BetP mutants will be attempted. In this way it might be possible to deduced substrate coordination and ion coupling in BGT1.

2 Materials and Methods

2.1 Materials

2.1.1 Instruments

Table 1: Overview of instruments used in this work.

Instrument	name	company
Analytical balance	Excellence	Sartorius, Göttingen
BeadBeater	BeadBeater	Biospec Products (Bartlesville, OK, USA)
Cell disruptor	Art. Nr. B0-012	Constant Systems, Northants
Centrifuge	Avanti J-30 I	Beckman, Fullerton
Centrifuge	J6-MI	Beckman, Fullerton
Centrifuge *table top*	5415 C	Beckman, Fullerton
Demineralization machine		Millipore, Schwallbach
Cary 50 UV-Vis Spectrometer	Varian	Hoefer, San Francisco
Crystallization roboter	*Mosquito*™	TTP Labtech LTD
Incubator	Hereaus TypB6	Heraeus, Hanau
Magnetic stirrer	RCT basic	IKA Labortechnik, Staufen
Microplate reader		MWG Biotech, Ebersberg
Photometer	Biophotometer	Eppendorf, Hamburg
Powersupply	Power Pac 300	Biorad, München
Scintillation counter	TRI-CARB 1500 scintillation	Canberra-Packard

	counter	
SDS-PAGE	Mighty Small SE250/SE260	Hoefer, San Francisco
Shaker	Multitron AS120	Infors AG, Bottingen
Superose 6/Superdex 200	Ettan LC systems	GE Healthcare
T3 Thermocycler		Biometra, Göttingen
Ultracentrifuge	Optima L-70K	Beckman, Fullerton
Waterbath	Julabo U3	Julabo, Seelbach

2.1.2 Synchrotron

Table 2: Synchrotron beamlines for testing crystals.

Synchrotron	Beamline ID	Wave length (ג)	Properties
SLS Swiss Light Source (Villigen, Switzerland)	PX II	0.97973 nm	Third Generation Synchrotron; Detector: maar225 CCD
ESRF European Synchrotron Radiation Facility (Grenoble, France)	ID 29	0. 34 nm	Second Generation Synchrotron, fixed Wave length; Detector: Quatum ADSC-

2.1.3 Chemicals

Chemicals were used from Anatrace, AppliChem, Avanti, Biomol, Bio-Rad, Fermentas, GE Healthcare, Glycon, Fluka, Gibco, and Hampton research, Invitrogen, Merck, New England Biolabs, Qiagen, Roche, Roth, Serva and Sigma-Aldrich.

2.1.4 Reagent kits

flashBAC 5 reaction kit	Oxford Expression Technologies
QIAprep Spin Miniprep Kit	Qiagen (Hilden)
QIAquick PCR Purification Kit	Qiagen (Hilden)
QIAquick Gel Extraction Kit	Qiagen (Hilden)
QuikChange® Site-Directed Mutagenesis Kit	Stratagene, Agilent Technologies (Waldbronn)
1 kb Ladder DNA Standard	Roth (Karlsruhe)
Prestained Protein Marker	Fermentas (St. Leon-Roth)
Broad Range Prestained Protein Marker	New England Biolabs (Schwalbach)
Multi-Copy Pichia Expression Kit	Invitrogen (Karlsruhe)
EasySelect Pichia Expression Kit	Invitrogen (Karlsruhe)

2.1.5 Enzymes

Pfu DNA-Polymerase	Fermentas (St. Leon-Roth)
Restriction endonucleases	New England Biolabs (Schwalbach)
T4 DNA-Ligase	New England Biolabs (Schwalbach)
PreScission™ -Protease	GE Healthcare (München)
Alkaline Phosphatase	Roche (Mannheim)

2.2 Media and antibiotics

2.2.1 Medium for *E. coli* expression

Luria Bertani (LB) Medium

Bacto-tryptone	10 g/L
Bacto-yeast extract	5 g/L
NaCl	10 g/L

2.2.2 Media for *P. pastoris* expression

MD(H)

YNB	1.34 % (w/v)
Dextrose	20 % (w/v)
Biotin	$4x10^{-5}$ % (w/v)

MGY(H)

YNB	1.34 % (w/v)
Glycerol	1 % (w/v)
Biotin	$4x10^{-5}$ % (w/v)
(Histidine (H)	0.004 %, in case of *His*-deficiency)

MM(H)

YNB	1.34 % (w/v)
Methanol	0.5-1 % (w/v)
Biotin	$4x10^{-5}$ % (w/v)
(Histidine (H)	0.004 %, in case of *His*-deficiency)

YPD

Yeast extract	10 g/L
Peptone	20 g/L
Dextrose (glucose)	20 % (w/v)

All media were autoclaved, except YNB, biotin and dextrose, which were filtered sterile. For preparing plates, 1.5 % (w/v) bacto-agar was added. If necessary the solutions were cooled to approximately 60 °C and the antibiotics needed were added.

2.2.3 Media for Tissue culture

2.2.3.1 MDCK and HEK cells

DMEM/HAMS F12	500 ml
Fetal bovine serum	10 % (v/v)
Pen/strep	50 U/ml
Trypsin/EDTA	0.25 %

2.2.3.2 Insect cells

TNM-FH	500 ml
Fetal calf serum	5 %
L-glutamine	2 %
Gentamycin	50 µg/ml
Vitamin B12	5.38 µg
Pluronic®68	0.1 %

(Medium is light sensitive)

2.2.4 Antibiotics

Ampicillin	100 mg/ml
Carbenicillin	50 mg/ml
Kanamycin	50 mg/ml
Penicillin/Streptomycin	10,000 µg/ml
Gentamycin	50,000 µg/ml

2.3 Buffer and solutions

Colony-blot lysis-buffer	50 mM Tris-HCl, pH 7.5 100 mM NaCl 10 mM $MgCl_2$ 50 mM β-mercaptoethanol 6 M Urea 2 % (w/v) SDS
TBS-buffer	50 mM Tris-HCl, pH 7.6 150 mM NaCl
PBS-buffer (phosphate buffer saline)	140 mM NaCl 2.5 mM KCl 6.5 mM Na_2PO_4 1.5 mM K_2HPO_4 adjusted to pH 7.4
Basal salts	68.1 mM $(NH_4)_2SO_4$ 40 % (w/v) glycerol 5.4 mM $CaSO_4$ * 2 H_20 104.4 mM K_2SO_4 60.5 mM $MgSO_4$ * 7 H_20 adjusted to 3.2 L with A. dest.
Trace elements	233.8 mM $FeSO_4$ * 7 H_20 0.82 mM biotin 24.03 mM $CuSO_4$ * 5 H_20 0.53 mM NaI 17.8 mM $MnSO_4$ * H_20 8.3 mM Na_2MoO_4 * 2 H_20 0.32 mM H_3BO_3 2.1 mM $CoCl_2$ 146.7 mM $ZnCl_2$ 0.5 % H_2SO_4

The trace elements were filtered sterile (0.45 μm) and stored in the dark at room temperature

2.4 Organisms

2.4.1 Bacterial strains (*E. coli*)

Strain	Genotype	Reference
DH5α^{TM}-T1^{R}	F$^-$ Φ80*lac*ZΔM15 Δ(*lac*ZYA-*arg*F)U169 *rec*A1 *end*A1 *hsd*R17(r_k^-, m_k^+) *pho*A *sup*E44 *thi*-1 *gyr*A96 *rel*A1 *ton*A (Confers resistent to phage T1)	Killmann *et al.*, 1996
MKH13	*araD39 (argF-lac) U169 relA51 rps150 flbB5301 deoC ptsF25 Δ(putPA)101 Δ(proP)2 Δ(proU)*	Haardt *et al.*, 1995
XL1 Blue	*B F$^-$ hsdSB (rB$^-$, mB$^-$) gal dcm ompT (DE3)*	Novagen (Schwalbach)

2.4.2 Eukaryotic cells

Strain	Genotype	Reference
HEK-293	*human embryonic kidney*	ATC (Rockville, MD)
MDCK II	*Madin Darby canine kidney*	ATC CCL-34 (Rockville, MD)
Pichia pastoris SMD1163	*his4, pep4, prb1*	Invitrogen (Karlsruhe)
Sf9	Pupal ovarian cells of *Spodoptera frugiperda*	ATC CRL-1711 (Rockville, MD)

2.4.3 Plasmids

Plasmid	Resistance	Properties	Reference
pASK-IBA5 betP	Amp^R	pASK-IBA5 with *betP* cloned using the BsaI and HindIII restriction sites	(Rubenhagen et al., 2000)
pASK-IBA7 ΔN29EEE44/45/46AAA	Amp^R	pASK-IBA7 with *betP* cloned between the BsaI and HindIII restriction sites; 29 N-teminal amino acids deleted and codon exchange at E44A, E45A and E46A	(Ressl et al., 2009a)
pSPORT1_BGT1	Amp^R,	pSPORT with *bgt1* cloned between the XhoI and BamHI restriction sites	(Yamauchi et al., 1992)
pEGFPC3_BGT1	Amp^R,	pEGFPC3 with *bgt1* cloned using the XhoI and BamHI restriction sites	(Kempson et al., 2003)
pPIC3.5k_BGT1syn	Amp^R, G418	pPIC3.5k with synthetic *bgt1* cloned using the EcoRI and NotI restriction sites	This work
pVL1393_BGT1syn	Amp^R	pVL1393 with synthetic *bgt1* cloned using the EcoRI and NotI restriction sites	This work
pTLN_BGT1	Amp^R	pTLN with *bgt1* cloned between the XbaI and XhoI restriction sites	This work
pSKB2LNB_BGT1	Kan^R	pSKB2LNB with *bgt1* cloned using the NotI and XhoI restriction sites	This work
pET28a_BGT1	Amp^R	pET28a with *bgt1* cloned using the XhoI restriction site	This work

2.4.4 Oligonucleotide primers

2.4.4.1 BGT1 project

Label	Sequence	Description
BGT1_syn_EcoRI_for	ggcggcgaattcatggactacaaggacgatga	Sense primer with *Eco*RI restriction site for the *P. pastoris* optimized BGT1-gene
BGT1_syn_NotI_rev	attccagcggccgctccgcccaagtgagtctc	Anti-sense primer with *Not*I restriction site for the *P. pastoris* optimized BGT1-gene
BGT1_nat_NotI_for	accattgcggccgcatggacagaaaagtggcagtcccc	Sense primer with *Not*I restriction site
BGT1_nat_XhoI_ST_rev	ggcggcctcgagCTAcaagtgggtctccttctcccc	Anti-sense primer with *Xho*I restriction site and stop codon
BGT1_nat_XbaI_s	attacctctagaatggacagaaaagtggcagtcccc	Sense primer with *Xba*I restriction site
BGT1_nat_XhoI_as	attccgctcgagctacaagtgggtctccttctcccc	Anti-sense primer with *Xho*I restriction site
BGT1_nat_XhoI_s	ggcggcctcgagcacaagatggacagaaaagtggcagtcccc	Sense primer with *Xho*I restriction site
BGT1_nat_XhoI_ST_His_8_as	ggcctcgagCTAgtgatggtggtgatggtggtgatgcaagtgggtctccttctcccc	Anti-sense primer with *Xho*I restriction site, stop codon and His_8 tag
BGT1_nat_N171D_s	cattgcatggactttcttgaccactcgggagcccgc	Sense primer to mutate the asparagine at position 171 to aspartate
BGT1_nat_N171D_as	gcgggctcccgagtggtcaagaaagtccatgcaatg	Anti-sense primer to mutate the

		asparagine at position 171 to aspartate
BGT1_nat_N183D_s	gcgacctcctctgaggacttcacctcacctgtc	Sense primer to mutate the asparagine at position 183 to aspartate
BGT1_nat_N183D_as	gacaggtgaggtgaagtcctcagaggaggtcgc	Anti-sense primer to mutate the asparagine at position 183 to aspartate
BGT1_nat_F293A_s	ggcacccagatcttcgcctccttcgccatctgc	Sense primer to mutate the phenylalanine at position 293 to alanine
BGT1_nat_F293A_as	gcagatggcgaaggaggcgaagatctgggtgcc	Anti-sense primer to mutate the phenylalanine at position 293 to alanine
BGT1_nat_F293W_s	ggcacccagatcttctggtccttcgccatctgc	Sense primer to mutate the phenylalanine at position 293 to tryptophane
BGT1_nat_F293W_as	gcagatggcgaaggaccagaagatctgggtgcc	Anti-sense primer to mutate the phenylalanine at position 293 to tryptophane
BGT1_nat_Q299A_s	tccttcgccatctgcgcgggtgcctgactgcc	Sense primer to mutate the glutamine at position 299 to alanine
BGT1_nat_Q299A_as	ggcagtcaggcaccccgcgcagatggcgaagga	Anti-sense primer to mutate the glutamine at position 299 to alanine
BGT1_nat_Q299F_s	tccttcgccatctgcttcgggtgcctgactgcc	Sense primer to mutate the glutamine

		at position 299 to phenylalanine
BGT1_nat_Q299F_as	ggcagtcaggcacccgaagcagatggcgaagga	Anti-sense primer to mutate the glutamine at position 299 to phenylalanine
BGT1_nat_Q299W_s	tccttcgccatctgctgggggtgcctgactgcc	Sense primer to mutate the glutamine at position 299 to tryptophan
BGT1_nat_Q299W_as	ggcagtcaggcacccccagcagatggcgaagga	Anti-sense primer to mutate the glutamine at position 299 to tryptophan
BGT1_nat_E52A_s	ctgtcagtggccgggggcgatcattgggctgggc	Sense primer to mutate the glutamate at position 52 to alanine
BGT1_nat_E52A_as	gcccagcccaatgatcgcccggccactgacag	Anti-sense primer to mutate the glutamate at position 52 to alanine
BGT1_nat_E52F_s	ctgtcagtggccgggttcatcattgggctgggc	Sense primer to mutate the glutamate at position 52 to phenylalanine
BGT1_nat_E52F_as	gcccagcccaatgatgaacccggccactgacag	Anti-sense primer to mutate the glutamate at position 52 to phenylalanine
BGT1_nat_E52Q_s	ctgtcagtggccgggcagatcattgggctgggc	Sense primer to mutate the glutamate at position 52 to glutamine
BGT1_nat_E52Q_as	gcccagcccaatgatctgcccggccactgacag	Anti-sense primer to mutate the glutamate at position 52 to glutamine
BGT1_nat_N326D_s	gccctctgcttcctggacagtgccaccagcttc	Sense primer to mutate the asparagine at position 326 to aspartate

BGT1_nat_N326D_as	gaagctggtggcactgtccaggaagcagagggc	Anti-sense primer to mutate the asparagine at position 326 to aspartate

2.4.4.2 BetP project

BetP/BetA_A148E_s	tccatgatgtttgctgaaggtatgggtattggt	Sense primer to mutate the alanine at position 148 to glutamate
BetP/BetA_A148E_as	accaatacccatacttcagcaaacatcatgga	Anti-sense primer to mutate the alanine at position 148 to glutamate
BetP/BetA_G149I_s	atgatgtttgctgcaataatgggtattggtttg	Sense primer to mutate the glutamine at position 149 to isoleucine
BetP/BetA_G149I_as	caaaccaatacccattattgcagcaaacatcat	Anti-sense primer to mutate the glycine at position 149 to isoleucine
BetP/BetA_M150I_s	atgtttgctgcaggtataggtattggtttg	Sense primer to mutate the methionine at position 150 to isoleucine
BetP/BetA_M150I_as	caaaccaatacctatacctgcagcaaacat	Anti-sense primer to mutate the methionine at position 150 to isoleucine
BetP/BetA_M150E_s	atgtttgctgcaggtgaggtattggtttg	Sense primer to mutate the methionine at position 150 to glutamate
BetP/BetA_M150E_as	caaaccaataccctcacctgcagcaaacat	Anti-sense primer to mutate the

		methionine at position 150 to glutamate
BetP/BetA_M150E_W374A_s	ttctactgggcatgggcgatctcttggtcacca	Sense primer to mutate the tryptophan at position 374 to alanine
BetP/BetA_M150E_ W374A_as	tggtgaccaagaagagatcgccatgcccagtag aa	Anti-sense primer to mutate the tryptophan at position 374 to alanine
BetP/BetA_M150E_W373F _s	atcttctactgggcattctggatctcttggtca	Sense primer to mutate the tryptophan at position 373 to phenylalanine
BetP/BetA_M150E_ W373F_as	tgaccaagagatccaagtgcccagtagaagat	Anti-sense primer to mutate the tryptophan at position 373 to phenylalanine

2.5 Molecular biological and – gene transfer methods

2.5.1 Polymerase chain reaction (PCR)

The polymerase chain reaction (PCR) is used to amplify a certain DNA-segment in a series of cyclic repeated steps of DNA denaturation, annealing and elongation. During the first denaturation step (95 °C) the DNA double-strand is separated into two single-stranded DNA molecules allowing annealing of the primers in the second part to bind to the complementary DNA single strands (50 – 60 °C). In the last step a DNA-polymerase is activated at 68 °C to elongate the primers at the 3'-OH end synthesizing a new DNA strand complementary to the template.

For preparative PCR amplification the *Pfu*-Polymerase (Fermentas, St. Leon-Roth) was used because of its 3' – 5' exonuclease activity, which corrects evoked mutations during amplification.

Component	***Volume (µl)***
DNA template (150 ng/µl)	3
sense primer (10 mM)	5
anti-sense primer (10 mM)	5
dNTP mix (each 2 mM) (Clonetech, Heidelberg)	3
Pfu-Polymerase (Fermentas, St. Leon-Roth)	1
Pfu-Polymerase buffer (10x) (Fermentas, St. Leon-Roth)	5
H_20 (autoclaved)	28

Step	***Temperature (°C)***	***Time (min)***	***Cycle***
Denaturation	95	3	1
Denaturation	95	1	30
Hybridization	T_{hybr}	0.5	30
Elongation	72	x	30
Final elongation	72	5	1
	4	∞	1

The hybridization temperature T_{hybr} for the oligonucleotide primers can be calculated using the following equation:

$$T_{hybr} = N_{AT} \text{ x } 2\ °C + N_{GC} \text{ x } 4°C - 5\ °C$$

N_{AT} and N_{GC} are each the sum of adenine/thymine and guanine/cytosine pairs of the oligonucleotide primers respectively. Usually the hybridization temperature was set at 45 – 55 °C depending on the length of the primers.

The elongation time x depends on the length of the DNA fragment to be amplified and on the polymerase activity. For the *Pfu*-polymerase an elongation activity of 500 base pairs per minute is exhibited.

2.5.2 DNA cleavage using restriction endonucleases

Double-stranded DNA was hydrolytic cleaved using restriction endonucleases from New England Biolabs (Schwalbach) according to the manufacturer's instructions. The amount of inserted unit of enzymes can be calculated:

$$\frac{\text{Units of enzyme}}{\text{amount of DNA}\,(\mu g)} = \frac{\text{length of } \lambda \text{ DNA} \cdot \text{restriction sites in y DNA}}{\text{length of y DNA} \cdot \text{restriction sites in } \lambda \text{ DNA}}$$

length of λ DNA (reference) = 48502 bp
length of y DNA = variable
restriction sites in y DNA = variable
restriction sites in λ DNA = tables in NEB catalog
amount of DNA (µg) = variable

For preparative DNA-restrictions the amount of DNA was 2 – 4 µg in a volume of 50 µl. Analytical reactions were carried out in a reaction volume of 20 µl with 2 µl reaction buffer (10 x) and the calculated amount of enzyme added. The incubation time and temperature were chosen according to the enzymes optimum. The reaction was stopped by adding 4 µl of DNA-sample buffer.

Purification of cleaved DNA fragments was done by either PCR Purification Kit (Qiagen) or by agarose gel electrophoresis and subsequently extraction with QIAquick Gel Extraction Kit (Qiagen) according to the manufacturer's instructions.

2.5.3 Agarose gel electrophoresis

Separation of DNA fragments was achieved by agarose gel electrophoresis. It was used both to analyze restriction probes and to isolate DNA fragments after restriction or after PCR reaction. DNA samples were transferred with 6 x DNA sample buffer (40 % (w/v) sucrose, 0.25 % (w/v) bromphenol blue) before loading on a 0.8 – 1.2 % (w/v) agarose gel in 1 x TAE buffer (40 mM Tris-acetate (pH 8.3), 1 mM EDTA) at 6 V/cm distance of electrodes). Ethidium bromide, which is an organic fluorescent dye and intercalates with the DNA nucleotides was added to the agarose gel. For visualization of the DNA the intercalated fluorescent dye was illuminated in an UV-Illuminator (MWG Biotech) at the excitation wavelength $\lambda = 312$ nm.

2.5.4 DNA concentration and purity

The DNA concentration and purity was determined photometrically (BioPhotometer, Eppendorf). The concentration of double-stranded DNA can be calculated based on the optical density (OD) at the absorption maximum of nucleic acids at the wavelength (λ) of 260 nm (OD_{260}). The reference value for a pure 50 µg/ml DNA solution is $OD_{260} = 1$. The purity of a DNA solution can be estimated from the OD_{260} to OD_{280} ratio (Glasel, 1995), since aromatic amino acids in proteins absorb light at $\lambda = 280$ nm and therefore indicate the presence of protein contaminants. An OD_{260} to OD_{280} ratio of 1.8 - 2.0 points to a pure DNA solution.

2.5.5 Ligation of DNA fragments

In the ligation reaction an endonuclease-restricted insert DNA and a complementary restricted vector DNA are covalently linked by the T4 DNA-ligase (200 U, New England Biolabs, Schwalbach). For a ligation reaction in a total volume of 20 µl, 10 ng of linearized vector

DNA was mixed with a 3 – 5 fold molar excess of insert DNA together with 5 U T4 DNA-ligase and 2 µl of T4 DNA-ligase buffer (10x). The reaction was incubated overnight at 4 °C.

2.5.6 Site-directed mutagenesis

The QuikChange Site Directed Mutagenesis Kit (Agilent Technologies, Waldbronn) was used to insert point mutations. The mutagenesis primers with the changed bases were synthesized and used according to the manufacturer's instructions.

2.5.7 *In vitro* RNA synthesis

For RNA synthesis it is important to ensure RNAse-free conditions (gloves, DEPC-treated water, autoclaved tips and tubes).

To linearize the template DNA 3 µg plasmid DNA (BGT1_pTLN) were digested (1h, 37 °C, 10 U of enzyme) in a total volume of 50 µl with the specific enzyme in appropriate buffer condition. The linearized template DNA was further purified using ROCHE High-Pure-PCR-Product-Purification-Kit (Roche):

350 µl of binding buffer was added (guanidiniumisothiocyanate content makes the probe "RNA-grade") and shortly vortexed. Spin columns were put into collection tubes, loaded with samples and centrifuged (14,000 rpm, RT, 20 seconds; Eppendorf-centrifuge). The flow through was discarded. 500 µl of wash buffer was added to the columns, centrifuged (14,000 rpm, RT, 20 seconds; Eppendorf-centrifuge) and the flow through was again discarded. Subsequently, 200 µl of wash buffer was added and centrifuged (14,000 rpm, RT, 30 seconds; Eppendorf-centrifuge). The spin columns were then placed into fresh and autoclaved Eppendorf tubes and the column material was incubated for one minute with 50 µl DEPC-treated water (Ambion). The DNA was eluted by a subsequent centrifugation step (14,000 rpm, RT, 30 seconds, Eppendorf-centrifuge). The eluted DNA solution was concentrated (speedvac) to 15 µl to ensure a final concentration of 0.5 µg DNA in 3 µl solution.

In vitro RNA-synthesis was carried out using the mMessage mMachine Kit (Ambion) (appropriate kit according to promoter (SP6, T7, T3)) in a 10 µl reaction volume as follows:

5 µl NTP-cap mix
3 µl linearized template DNA solution
1 µl transcription buffer (e.g. SP6-Kit "10x Rxn Buffer")
1 µl (appropriate) RNA-Polymerase (e.g. SP6-Kit "Enzyme Mix")

The reaction was incubated for 1.5 – 2 h at 37 °C.

Subsequently, the RNA was precipitated by adding 12.5 µl LiCl solution (provided by the mMessage mMachine Kit; stored at -20 °C) and 15 µl DEPC-treated water (Ambion). The solution was mixed, briefly centrifuged and placed for at least 30 minutes at -20 °C (incubation overnight is also possible). After precipitation at -20˚C, the RNA was pelleted by centrifugation (14,000 rpm, 4°C, 15 minutes; Eppendorf-centrifuge). The supernatant was completely removed from the brownish RNA pellet (which was sometimes hard to see). A second short centrifugation step and using a smaller pipette tip was sometimes necessary to remove the supernatant completely.
To purify the RNA, 150 µl 70 % RNA grade ethanol (stored at -20 °C) was added to the RNA pellet. The solution was gently mixed before centrifugation (14,000 rpm, RT, 5 minutes; Eppendorf-centrifuge). The pellet usually appeared white and the supernatant was again completely removed. The RNA pellet was briefly dried in a speedvac (about 2 minutes at RT) and re-dissolved in 12 µl DEPC-treated water (Ambion). The solution usually yielded an RNA concentration of about 1 µg/µl.
To ensure integrity of the RNA, 0.3 - 0.5 µl RNA was mixed with 5 µl loading buffer (mMessage mMachine Kit, Ambion) and loaded onto a 1 % agarose gel (cast the gel freshly about 1 h before use) supplemented with ethidium bromide (0.5 µg/ml).
The gel was run with fresh TAE-buffer at 80 to 90 V for 1 hour. The RNA should show a clear band structure (several bands are possible due to secondary structure). Degradation would show up as a broad smear. The concentration of the RNA solution was determined photometrical (BioPhotometer, Eppendorf).

2.5.8 Preparation and transformation of chemically competent *E. coli* cells

The Chung TSS-method (Chung et al., 1989) was used to produce chemically competent *E. coli* cells. An overnight culture (37 °C, 125 rpm) of a particular *E. coli* strain was grown in 100 ml LB medium. The culture was re-adjusted to an OD_{600} of 0.1 and further grown to early exponential phase (OD_{600} = 0.4). The cells were slowly cooled down (30 min at 4 °C) and centrifuged (2500 g, 4 °C, 10 min). The supernatant was decanted and the pellet was resuspended in 1/10 of the original culture volume with TSS medium (10 % (w/v) PEG8000, 5 % (v/v) DMSO, 50 mM $MgCl_2$, 15 % (v/v) glycerol in LB medium, sterile filtered). Aliquots (100 – 200 µl) of the cell suspension were flash frozen in liquid nitrogen and stored at -80 °C.

The transformation of QuikChange PCR- or ligation products was set up with either 10 µl of the reaction solution or 25 – 50 ng of circular vector DNA from Mini- or Maxi-Prep-Isolation. Competent *E. coli* cells were thawed on ice and DNA was added. After incubation on ice for 30 minutes, a heat shock at 42 °C for 1 minute was administered and 1 ml LB medium was added. The cells were incubated at 37 °C for 1 hour. During this time the plasmid-coding antibiotic resistance genes located on the inserted vector are expressed. After incubation the cells were centrifuged for 5 minutes at 5000 g. The supernatant was removed, the cell pellet resuspended in the reflux medium and plated on LB-agar plates with the corresponding antibiotics for selection. Plates were incubated overnight at 37 °C.

2.5.9 Isolation of vector DNA and DNA sequencing

Colonies of transformed cells were grown in 5 ml LB medium overnight at 37 °C with the corresponding selection marker. Cells were pelleted for 10 minutes at 5000 g and 20 °C. The vector DNA was isolated using QIAprep Spin Mini- or Maxiprep Kit (Qiagen) according to the manufacturer's instructions. DNA sequencing was done either by SRD (Bad Homburg) or Seqlab (Göttingen).

2.5.10 Glycerol stock of bacteria

A single isolated *E. coli* colony was grown overnight (37 °C, 125 rpm) in 2 ml LB medium containing the selection marker. After addition of 30 % (v/v) glycerol the culture was flash frozen in liquid nitrogen. These glycerol stocks were stored at -80 °C.

2.6 Biochemical methods

2.6.1 Protein production in *E. coli*

Heterologous expression of recombinant proteins in *E. coli* is influenced by many factors, e.g. the bacterial strain, media, temperature or the concentration of the inductor. Also, the choice of the vector can have an influence on the production rate, on the number of copies of the recombinant plasmid, the promoter for the production of the recombinant proteins or the choice of the localization (N- or C-terminus) of the affinity tag which can influence the amount and quality of the produced recombinant protein as well. In this work, pASK-IBA5 and pASK-IBA7 were used for the expression of BetP and BetA, respectively. For the BGT1 construct vectors of the pET-system (pET28a, Novagen) and pSKB2LNB (a derivative of the pET28a, in which the Thrombin-restriction site was exchanged against a Prescission site) were used. BGT1 **analytical heterologous protein production** was first tested in 50 ml scale. An overnight culture (150 rpm, 37 °C) of 5 ml was used to inoculate 50 ml LB medium supplemented with the appropriate antibiotic. This culture was grown at 37 °C and 180 rpm to an OD_{600} of 1. IPTG (final concentration 1 mM) was added to start over-production of recombinant BGT1 for 4 h at 30 °C with shaking (150 rpm).

For BetP **preparative heterologous protein production** *E. coli*- One Shot®Invitrogen DH5α^{TM}-T1 cells were used. Transformed DH5α - T1 cells were grown over night at 37 °C with shaking (180 rpm) in 100 ml of LB medium supplemented with carbenicillin (50 µg/ml). 10 ml of this culture were used to inoculate 2 l LB medium (start OD_{600} = 0.15) supplemented with the same antibiotic. The cells were grown at 37 °C and shaking (120 rpm) until they reached an OD_{600} of 1 – 1.5 (~ 3 hours). Induction of the over-expression of *betP* was initiated

with anhydrotetracycline (final concentration 200 µg/l) until cells reached the stationary phase.

For **substrate transport measurements in cells**, transformed *E. coli* MKH13 cells with a particular strep-*betP* mutant were used. A 5 ml LB medium over night culture, grown at 37°C and supplemented with 50 µg/ml carbenicillin was used to inoculate 10 ml of the same type of media and appropriate antibiotic to an OD_{600} of 0.15. After incubation of 1 hour at 37˚C with shaking the cells reached an OD_{600} of 0.5 and *bet*P mutant gene over-expression was induced by adding anhydrotetracycline to a final concentration of 200 µg/l. Cells were harvested after 2 hours of expression, washed twice and resuspended in buffer containing 25 mM KPi buffer (pH 7.5) and 100 mM NaCl. In the last resuspension step 20 mM glucose was added.

2.6.1.1 *E. coli* cell lysis and membrane preparation

After reaching the stationary phase (~ 2 hours after induction of gene over-expression), cells were harvested by centrifugation (4200 rpm, 4˚C, 20 minutes; Low-Speed Beckman J6-MI Centrifuge, rotor type JS4.2). The supernatant was discarded and the cell pellet was resuspended and homogenized using a homogenizer in buffer containing 100 mM Tris-HCl (pH 7.5) and 0.1 mM PefaBloc (Biomol). After this step the cell suspension was either directly used to prepare membranes or frozen and stored at -20 °C or -80 °C.

Resuspended cells were lysed using a cell disruptor (Constant Systems) at 1.8 kbar and 4 °C. The cell disruptor presses cells through a narrow nozzle (diameter: 0.5 mm) with high pressure. After passing the nozzle cells are rapidly expanded and break due to the sudden release of high pressure.

Cell debris was removed by centrifugation at 12,500 rpm (Avanti J-30 I, rotor type JLA-16.250) for 30 minutes at 4 °C. Membranes were harvested by ultra-centrifuging the supernatant at 45,000 rpm (Beckman Optima L-70K, rotor type Ti45) for one hour at 4 °C. The membrane pellet was resuspended in buffer containing 50 mM Tris-HCl (pH 7.5) and 17.4 % glycerol and adjusted to a concentration of 10 mg/ml. The membrane solution was either directly solubilized or frozen in liquid nitrogen and stored at -20 °C.

2.6.1.2 Solubilization of BetP

Membranes containing BetP WT or mutants were diluted 1:4 in buffer containing 50 mM Tris-HCl (pH 7.5), 8.6 % glycerol and 200 mM NaCl and solubilized with 2 % n-Dodecyl β-D-maltoside (DDM) when purified for crystallization. After a 15 minutes incubation step on ice under stirring, NaCl was added to a final concentration of 200 mM and incubation was continued for additional 40 minutes. The soluble fraction was separated from the insoluble material by ultracentrifugation (45,000 rpm, 4 °C, 45 minutes; Beckman Optima L-70K, rotor type Ti45). The soluble fraction was diluted 1:4 in buffer containing 50 mM Tris-HCl (pH 7.5), 8.6 % glycerol and 200 mM NaCl.

2.6.2 Protein production in *Pichia pastoris*

The cultivation of *Pichia pastoris* cells was carried out at 30 °C in a shaker (HT Multitron, Infors, Bottmingen, Switzerland) at 250 rpm. The doubling time of *Pichia pastoris* in the logarithmic growth phase is about 2 hours. The following equation was used to get a certain optical density after a define time,

with: $$N = N_0 e^{\sigma t}$$

N = Final OD_{600}, (OD_{600}, which should be reached after t hours)
N_0 = Starting OD_{600}, (OD_{600}, which is calculated, so that the culture has an OD_{600} with N after t hours)
σ = 0.346 for YPD medium and 0.231 for MGY(H)-medium
t = time of growth (in hours)
This equation was solved for N_0 and resulted in the OD_{600} that a starting culture should have for the final culture to reach a certain OD_{600} after t hours. The volume needed is due to the actual OD_{600} of the starting culture and the culture volume of

$$V = \frac{N_0 Vol}{X}$$

For the protein production the pPIC3.5k vector (Invitrogen) was used.

2.6.2.1 Production of electro competent *P. pastoris* cells and transformation

The transformation of *P. pastoris* cells was carried out by electroporation (Becker and Guarente, 1991). A single fresh colony of the protease-deficient *P. pastoris* strain SMD1163 grown on an agar plate was transferred into YPD-medium. This starting culture was shaken over night at 30 °C. After reaching an OD_{600} of 2-8, 50 ml MGYH media were inoculated with a sufficient volume of starting culture so that an OD_{600} of 1.3-1.5 could be reached after a define time (minimum 8 hours). The cells were then pelleted at 2000 rpm (Sigma 3-16K centrifuge) for 5 minutes at 4 °C, resuspended in 50 ml cold, sterile *A. dest*. and again centrifuged (2000 rpm, 4 °C, 5 minutes, Sigma 3-16K centrifuge). A second washing step in 25 ml cold, sterile *A. dest*. was applied, followed by centrifugation (2000 rpm, 4 °C, 5 minutes, Sigma 3-16K centrifuge). The cell pellet was resuspended in 2 ml cold and sterile sorbitol (1 M), centrifuged (2000 rpm, 4 °C, 5 minutes, Sigma 3-16K centrifuge) and finally resuspended in 100 µl sterile, cold sorbitol (1 M). For transformation by electroporation, 80 µl competent cells were shortly mixed with 10 µl of linearized, recombinant plasmid (5-30 µg in sterile *A. dest.*) in a pre-cooled MicroPulser cuvette (diameter 2 mm gap, Biorad) and subsequently electroporated in a GenePulser system (Biorad) with a voltage of 1.5 kV and a capacity of 25 µF and 200 Ω. The restriction enzyme for linearization of the plasmid was chosen from the particular kit (EasySelect Pichia Expression Kit or Multi-Copy Pichia Expression Kit, Invitrogen, Karlsruhe). For the transformation of BGT1 30 µg plasmid DNA was linearized with 100 units of SacI enzyme at 37 °C for 4 hours. The linearized DNA was concentrated to 10 µl by evaporation in a speedvac vacuum centrifuge. Directly after electroporation 1 ml of sterile sorbitol (1 M) was added to the cuvette. The suspension was applied to a 15 ml Falcon tube and incubated at 30 °C for 1 hour. Subsequently the cells (100-400 µl) were plated on four MD plates (Selection for His^+ mutants) and incubated at 30 °C for 2-3 days.

MD plates: 1.34 % (w/v YNB, 0.005 % (w/v) biotin, 2 % (w/v) dextrose, 1.5 % (w/v) agar. 800 ml of water was autoclaved with agar and dextrose, then cooled to 60 °C, then the other solutions were added.

YPD plates: 1 % (w/v) yeast extract, 2 % (w/v) peptone, 2 % (w/v) dextrose, 2 % (w/v) agar

2.6.2.2 Selection of *P. pastoris* transformants

The heterologous protein expression in *P. pastoris* is strongly dependent on gene dosage. The number of genes integrated into the *Pichia* genome depends on the level of Geneticin resistance (for pPIC3.5K). The resistance to the antibiotic can be used to detect transformants (clones), which harbor multiple copies of the gene of interest (Andre et al., 2006).

In order to screen a high number of clones, colonies from the first selection (His^+ selection) were inoculated in sterile 96-well microtiter plates containing 150 µl YPD medium in each well and incubated over night at 30 °C. The clones grown in the microtiter plate were replica-copied onto multiple YPD-agar plates with increasing concentration of Geneticin (0.025, 0.05, 0.075, 0.1 and 0.2 mg/ml). These selection plates were incubated for 3 days at 30 °C. Colonies grown at the highest antibiotic concentration were inoculated in fresh sterile 96-well microtiter plates containing YPD medium and incubated overnight at 30 °C. These clones were then replica-plated onto a sterile nitrocellulose membrane placed on a MGY-agar (pPIC3.5k) rectangular dish and incubated for 2 to 3 days at 30 °C. Colonies grew on the nitrocellulose-membrane as nutrients were taken up through the nitrocellulose membrane. The nitrocellulose membrane was then transferred to a MM-agar plate to induce expression of the gene of interest and production of the heterologous protein. The MM-agar plate was incubated for 24 hours at 30 °C. Afterwards, the nitrocellulose-membrane was placed on Whatman filter paper presoaked in Lysis-buffer (50 mM Tris-HCl (pH 7.5), 100 mM NaCl, 10 mM $MgCl_2$, 50 mM β-mercaptoethanol, 6 M urea, 2 % SDS) and incubated at 65 °C for 3 hours in a closed vessel (to prevent evaporation) to lyse the cells after expression. Cell debris on the nitrocellulose-membrane was removed with de-ionized water. To test and compare the expression of each clone the membrane was further blocked with 5 % skim milk powder in TBS and subsequently immuno stained comparable to Western blot analysis (chapter 2.6.8.3). Colonies with the highest expression levels showed the strongest signal (distinguishable as a ring) on the nitrocellulose-membrane. These colonies were used for further expression tests in liquid media. Nine clones were chosen from the colony blot and tested for differences in the amount of produced target protein. In order to test the protein production, MGY liquid

cultures were adjusted to an OD_{600} of 4 and an appropriate culture volume was centrifuged (2000 rpm, RT, 5 minutes; Heraeus Labofuge 400R, rotor type 75008172). The cell pellet was resuspended in 50 ml MM medium to start induction. 24 hours after induction the cells were harvested (2000 rpm, 4 °C, 10 minutes; Heraeus Labofuge 400R, rotor type 75008172) and resuspended in 3 ml TBS buffer. Cell breakage was achieved by adding ice-cold glass beads (0.5 mm diameter) and vortex mixing for ten 30 second bursts at 4 °C. Unbroken cells, cell debris and glass beads were removed by centrifugation (4500 rpm, 4 °C, 20 minutes; Heraeus Labofuge 400R, rotor type 75008172). The pellet was washed once more with the equal volume of buffer and centrifuged again. The supernatants of the two centrifugation runs were combined and further centrifuged (45000 rpm, 4 °C, 2 hours; Beckmann, model L8M, rotor type Ti50) to pellet the membranes. The membrane pellet was resuspended in TBS buffer and protein content was further investigated by Western blot analysis.

2.6.2.3 Storage of the highest expressing *P. pastoris* clone

In the *P. pastoris* system the transformed gene is stably integrated into the *P. pastoris* genome. Therefore, it is important to store the highest expressing clone properly after selection. To prepare glycerol stocks of highly expressing transformants, *P. pastoris* cells were grown in YPD-medium to an OD_{600} of 1 to 2 at 30 °C with shaking. Glycerol was added to a final concentration of 30 % (v/v) in 1 ml aliquots. Glycerol stocks were stored at – 80 °C.

2.6.3 Preparative protein production in *P. pastoris*

Large-scale protein production was either performed in shaking flasks or in a fermenter (INFORS AG). An advantage of the fermentation is that cells grow to a much higher cell density than they do in shaking flasks but the protein production rate can be diminished. In general, shaking flasks were used at first to test if the recombinant target protein was at all over-expressed. Finally, fermentation for production of the recombinant protein was established in order to overcome the more time-consuming shaking cultures.

2.6.3.1 Protein production in shaking flasks

A pre-culture of 50 ml *bgt*1-transformed *P. pastoris* in MGY (BMG or BMGY) was grown to an OD_{600} of 4 and then centrifuged (3000 rpm, RT, 30 minutes; Beckman J6-MI Centrifuge, rotor type JS4.2). For expression induction, cells were resuspended to an OD_{600} of 1 in MM (BMM or BMMY) medium and grown for 20-24 hours at 30 °C with shaking at 260 rpm. After 20-24 hours of expression the culture was centrifuged (4200 rpm, 4 °C, 20 minutes; Beckman J6-MI centrifuge, rotor type JS4.2) and the cell pellet was resuspended in lysis buffer (50 mM Tris-HCl, pH 7.5, 200 mM NaCl, 10 % (w/v) glycerol. The cell suspension was stored at -80 °C until further use.

For **transport measurements in cells**, 3 ml of a *bgt*1-transformed *P. pastoris* culture were divided into 2 Falcon tubes. The OD_{600} of the culture ranged between 40 and 60. Cultured cells were centrifuged (4000 rpm, RT, 10 minutes; Sigma 3-16K centrifuge) and washed twice in 10 ml transport buffer (150 mM NaCl, 10 mM Tris-HEPES, pH 7.4, 1 mM $MgCl_2$ and 1 mM $CaCl_2$) in order to remove the rich medium. A third centrifugation step was done and the final cell pellet was resuspended to a final volume of 400-600 µL (1 OD_{600}/10 µl) with transport buffer (Doring et al., 1998).

2.6.3.2 Yeast fermentation

Large-scale cultures were grown in a 5 l fermenter (INFORS AG, Bottmingen, Switzerland) using a protocol with a glycerol fed-batch strategy (Parcej and Eckhardt-Strelau, 2003), which allows accumulation of biomass prior to induction with methanol (Stratton et al., 1998) and sodium hexametaphosphate as the phosphate source (Curless et al., 1996).

The fermenter was autoclaved with 3.2 l of basal salts. Before fermentation trace salts (4.4 mg/l) and 400 ml of Na^+-hexametaphosphate (10 x, 250 g/l, sterile filtered and kept at RT) were added. A 400 ml starting culture grown in MGY to an OD_{600} of 6 to 8 was used to inoculate the medium in the fermenter. The fermentation temperature was kept at 30 °C and the pH of 5 maintained constant with an ammonium hydroxide solution (16 % ammonium). The dissolved oxygen level was set to 20 to 30 %. The glycerol fed-batch process was initiated after around 20 hours of batch culture and cells were fed for 20 hours (approximately 500 ml glycerol solution (50 % (w/v), supplemented with 12 ml/l trace elements), followed by

a four hours of carbon-source starvation. Subsequently the methanol-feeding phase (10 % (v/v), supplemented with 12 ml/l trace elements) was continued for 24 hours (500 ml methanol).

After fermentation the cells were harvested by centrifugation (4200 rpm, 4 °C, 20 minutes; Beckman J6-MI centrifuge, rotor type JS4.2) and the pellets were stored at -80 °C until further use.

P. pastoris cell lysis and membrane preparation

For membrane preparation from cells grown in the fermenter or in shaking flasks cells were first resuspended in 200 ml lysis buffer (50 mM Tris-HCl (pH 7.5), 200 mM NaCl, 10 % (w/v) glycerol and protease inhibitors) and filled in the pre-cooled BeadBeater (Hamilton Beach, model IG918) chamber with the same volume of ice-cold glass beads (0.5 mm diameter, Carl Roth GmbH, Karlsruhe). The chamber was screwed on the ice-water jacket before it was closed with the rotor assembly. The jacket was then filled up completely with ice and cold water and placed on the BeadBeater motor. Cells were broken in three passages each one minute with a five minutes break in between. The supernatent was removed by pipetting and the glass beads were washed twice with each 25 ml of lysis buffer. The supernatants were combined and centrifuged (4500 rpm, 4 °C, 20 minutes; Heraeus Labofuge 400R, rotor type 75008172) to pellet cell debris. The supernatant was further centrifuged (40,000 rpm, 4 °C, 1 hour; Ultracentrifuge Beckman Model, L8M, rotor type Ti45) and the membrane pellet was resuspended and homogenized in lysis buffer and stored at – 80 °C until further use.

2.6.4 Protein production in baculovirus-infected insect cells

The *Sf*9 cell line (pupa ovarian cells, a sub strain of *Spodoptera frugiperda Sf*21 cells) was used for recombinant protein production. The doubling time of *Sf*9 cells lies between 4 and 24 hours at 27 °C. Cells can grow both in adherent and suspension culture.

2.6.4.1 Sub culturing from adherent monolayer

To maintain the cell line (*background cultures*) two cultures were weekly inoculated from a 25 cm^2 flask (NuncClone™) with adherent confluent monolayer culture (about 1-1.5 x 10^6 cells/ml). These background cultures were inoculated into 25 cm^2 flasks with two different volumes from an earlier cell passage (e.g. one flask was inoculated with 0.4 ml and the other one with 0.8 ml, *i.e.* one particular volume and its double volume). This is usually enough to guarantee the confluence of the culture for up to 5-7 days after sub-culturing (usually on the 6^{th} day). If necessary, volumes and incubation time can be increased/decreased to reach a complete confluent monolayer. To get a 175 cm^2 complete monolayer in 6 days the entire volume (2 ml) of cells grown is a 25 cm^2 monolayer culture were used. For each new passage fresh complete medium was added to a new flask (2 or 10 ml for 25 or 175 cm^2 flasks, respectively). The flask with cells grown in a monolayer was mildly beaten 4-5 times to detach the cells. The detached cells were carefully shaken and the desired volume was transferred into fresh flasks with the aforementioned volumes of medium.

To uniformly distribute the cell suspension the flask was carefully shaken again and let stand for at least 15-30 minutes on an even plane to allow the cells to attach. After attachment of the cells to the flask bottom the medium consequently cleared and was replaced by fresh medium. The medium of the two previous background cultures was as well replaced by fresh complete medium (5 or 30 ml for 25 or 175 cm^2 flasks respectively). The flasks were incubated at 27 °C with the lid slightly unscrewed to allow gas circulation.

2.6.4.2 Freezing and storing of *Sf*9 cells

From a 175 cm^2 flask with a grown monolayer culture, cells were detached and counted. Cells should be in the exponential growth and more than 98 % healthy (≈ 1 x 10^6 cells/ml). The cells were collected by centrifugation (1000 g, RT, 5 min). The old medium was removed and fresh complete medium was added to resuspend the cell pellet in a final concentration of 2 x 10^7 cells/ml. Aliquots of one volume of freezing medium (see below) with one volume of cellular suspension were prepared and kept on ice for half an hour. The aliquots were first stored at -20 °C for 1 hour before transferring them to -80 °C for 1-2 hours. Finally, the aliquots were transferred and stored in the atmosphere of liquid nitrogen.

Freezing Medium: 85 % complete medium
15 % DMSO (sterile)

2.6.4.3 Transfection of *Sf*9 cells – obtaining a virus stock

Transfection was done in a 6-well plate (NunclonDelta, 6). 1 ml of fresh complete medium without FCS was added into each well and 1.28 x 10^6 cell/well were seeded to have a starting monolayer with 60-70 % confluence. Cells were allowed to attach for at least 30 minutes. The medium was completely removed and replaced with 1 ml fresh complete medium without FCS. This washing step was repeated 3 times, with a ten-minute incubation period between steps. The cells were therefor in total washed 4 times. To prepare the transfection mixture the following components were mixed in the indicated order in a sterile 2 ml Eppendorf tube:

5 µl synthBGT1_pVL1393 (500 ng)
5 µl flashBAC DNA (100 ng)
10 µl sterile water
30 µl Lipofectamine (Invitrogen)
(Negative control: only DMMH-medium)

After adding Lipofectamine all components were mixed well by pipetting up and down. After 15 minutes incubation at RT the transfection mixture was directly added into the well. The 6-well plate was placed in a box with wet paper on the bottom and let stand for 4-24 hours at 27 °C. After incubation 1 ml of fresh complete medium supplemented with 10 % FCS was added and the incubation was continued for another 6-7 days. The appearance of infected cells is very different from non-infected control cells. Infected cells look wizened compared to non-infected cells.

To collect the virus stock only the supernatant of a well was used and transferred into a sterile 2 ml Eppendorf tube. The virus containing solution was centrifuged (6000 rpm, RT, 10 minutes; Eppendorf-centrifuge) to remove dead cells and cell debris whereas the virus containing supernatant was transferred into a sterile 2 ml Eppendorf tube. This virus stock was stored at 4 °C in the dark.

Virus collection from a non-adherent shaking culture was done in the same way by removing cells by centrifugation, collecting the virus containing supernatant and storing the virus solution at 4 °C in the dark.

To amplify the virus stock a 25 cm^2 adherent culture was infected by adding 100 µl of the aforementioned virus stock; in parallel a 50 ml shaking culture was infected with 1 ml virus stock. After 6-7 days of incubation at 27 °C, cells were checked for infection and the virus of infected cells was collected as described before. One aliquot (usually 1 ml) of this virus stock was frozen at -80 °C and stored as "master virus stock". From the 50 ml cultures the virus titer was determined and at the same time a second round of virus amplification was started in a 500 ml shaking culture assuming a virus titer from the first stock of 1 x 10^7 pfu/ml. After 6-7 days of incubation at 27 °C, the virus was collected and the titer was determined for this virus stock.

2.6.4.4 Determining the virus titer by using the End-point dilution method

A sterile 96 well plate was used to determine the virus titer. Wells were seeded with 10^4 healthy cells/well in 100 µl of medium from a monolayer culture (175 cm^2 flask).

The virus solution was diluted from 10^{-1} to 10^{-9}. For a 10^{-1} dilution 50 µl virus stock were mixed with 450 µl fresh medium. From this virus dilution 10 µl were added in each well according to the following scheme:

A1-A2 only cells (100 µl healthy cells)
A3-A5 dilution 10^{-2} (100 µl healthy cells plus 10 µl of the 10^{-1} virus stock dilution)
A6-A8 dilution 10^{-3} (100 µl healthy cells plus 10 µl of the 10^{-2} virus stock dilution)
A9-A12 dilution 10^{-4} (100 µl healthy cells plus 10 µl of the 10^{-3} virus stock dilution)

Then a complete row for each dilution starting from 10^{-5} (B) up to 10^{-9} (F) was seeded. The plate was incubated for 6 days at 27 °C in a box with wet paper.

Virus titer calculation by End-point dilution assay:
After 6 days of incubation the plate was checked under the microscope and notes were taken if the cells looked infected (+) or not. The cell infection had to be evaluated over a period of three days starting from the sixth day post infection.

	1	2	3	4	5	6	7	8	9	10	11	12
A			+	+	+	+	+	+	+	+	+	+
B	+	+	+	+	+	+	+	+	+	+	+	+
C		+	+			+	+		+	+	+	
D			+			+						+
E					+				+			
F							+		+			+

1. Cell infection evaluation table:

Dilution	Number of positive well	Number of negative well	Δ positive *	Δ negative **	% Δ positive
-5	12	0	27	0	100
-6	7	5	15	5	75
-7	3	9	8	14	36
-8	2	10	5	24	17
-9	3	9	3	33	8,3

* Sum of positively infected cells in the wells from the highest to the lowest virus stock dilution assuming that positive infection at higher dilution will also result in viral infection at lower dilution.

** Sum of negatively infected cells in the wells from the lowest to the highest virus stock dilution assuming that a lower virus stock dilution resulting in no cell infections will also show no infection at higher dilution.

1. Determine the first % Δ positive (column 6 in the evaluation table) value that exceeds 50 %. This value, for example 75 %, is the parameter a in the equation to calculate the point dilution (PD) parameter. Then determine the first % Δ positive value that is smaller than 50 %. This value, 36 % in my example, is the parameter b in the following equation.
2. Calculate the PD parameter by calculating (a-50)/(a-b). The result in this example is 0.64.
3. Calculate the log of the Tissue Culture Infection Dilution (TCID) at which 50 % of the cells are infected. The $\log_{TCID50}$ is calculated by subtracting the PD parameter (0.64) from the corresponding logarithmic dilution factor of a (in this case - 6). The result for my example is $\log_{TCID50}$ = -6 – 0.64 = -6.64.
4. The titer of the virus stock is $1/10\log_{TCID50}$ ($4.37x10^6$ in this case). The actual number of viruses in 1 ml is $1/10\log_{TCID50}$ x 100 (4.37×10^8 in my example).

The Plaque Forming Unit (pfu)/ml is calculated by multiplying the virus number per ml by 0.69. The result for my example is $4.37 \times 10^8 \times 0.69 = 3.02 \times 10^8$ pfu/ml.

2.6.4.5 Shaking Culture

The minimum cell amount to start a shaking culture should be $3 \times 10^5 – 5 \times 10^5$ cells/ml. Starting from a monolayer culture cells usually require 4 - 5 days to reach a concentration above 1×10^6 cells/ml. When starting from a shaking culture (5×10^5 cells/ml) this density is usually reached after 3 days of incubation. Cells growing in shaking flasks should be sub-cultured when reaching a concentration above 1×10^6 cells/ml.

2.6.4.6 Infecting a shaking culture

The multiplicity of infection (m.o.i.) depends on the aim of infection. This could be either infection to amplify the virus or to produce proteins. The starting cell density of the culture also depends on the aim.

	m.o.i.	*Starting: cells/ml*
Culture for virus amplification	0.01	5×10^5
Culture for protein production	10	2.5×10^6

For virus amplification the cell density grown as shaking culture was diluted with the appropriate volume. For protein production cells were grown in suspension culture and collected by centrifugation in a sterile bottle (1000 g, RT, 10 min). The supernatant was carefully removed to avoid loosing cells. The very soft cell pellet was resuspended in the appropriate volume of fresh medium to reach the required cell density.
For infection the required volume of fresh medium was applied before the appropriate cell density was added. At last the virus was pipetted to the culture before it was incubated for several days.

2.6.4.7 Cell harvesting after infection and expression

After 6 days of protein expression flasks were checked for contamination. A non-contaminated culture showed a yellow deposit ring at the medium shaking level. A sample of each flask was also checked under the microscope to verify cell infection and general health of the culture (e.g. culture contamination by bacteria). A contaminated culture was discarded.
Cells were counted both because cell lysis requires a specific cell density and the calculated cells counts were compared with the number of cells from the original starting culture to estimate cell viability during infection and protein expression. Cells were collected by centrifugation (6000 rpm, 4 °C, 10 minutes; Beckman centrifuge, JL 4.2) and the supernatant was carefully removed completely by pipetting while the bottles were kept on ice. The cell pellet was resuspended in buffer (50 mM Tris pH 7.5, 200 mM NaCl, 10 % glycerol, Roche Protease Inhibitor) by pipetting up and down several times in a final volume of medium that resulted in a cell density of 5×10^6 cells/ml. Cells were either directly lysed or stored at -80 °C until further use.

After centrifugation, the centrifugation bottles were washed with 200 ml of 1 M NaOH to inactivate the virus and then 3 times rinsed with water. All washing solutions were collected and autoclaved. The culture flasks were also washed with 1 M NaOH, and then filled with water (or any other liquid produces during cell culturing) to a level higher than the deposit ring that results from shaking the cell culture (usually the flasks were filled to ¾ of the maximum flask volume). The flasks and solutions were autoclaved before the liquid was discarded. The flasks were cleaned by washing with detergent, rinsed with water and autoclaved again for further use.

2.6.4.8 Expression test in 6 well plates and Benzonase assay for cell lysis

An expression test in 6-well plates was carried out for seven days post infection (d.p.i) and cells were checked every 24 hours. At least one well with non-infected cells was kept until the record of the last daily time point was taken and the status of the cell culture was verified. Fresh medium (1 ml) was added to each well before 1.28 x 10^6 cells/well were seeded from a monolayer culture and left for at least 30 min to allow cells to attach. The medium was removed and 2 ml fresh medium was added. The cells were infected with an m.o.i. of 10 and incubated for one hour (infection period) at 27 °C. The virus-containing medium was replaced by fresh medium and the plate incubated in a box with wet paper at 27 °C for 24 hours. The cells were then collected from each well by resuspending them in the 2 ml medium containing in each well and transferred into sterile 2 ml Eppendorf tubes. The cells were counted and diluted to a density of 6 x 10^5 cells/ml. The cell solution was centrifuged (6000 rpm, RT, 10 minutes; Heraeus Labofuge 400R, rotor type 75008172), the supernatant removed and the cell pellet stored at -20 °C.

Benzonase assay for cell lysis:

Benzonase buffer: 50 mM Tris-HCl
1.5 mM $MgCl_2$
1 % SDS

Benzonase (stock): 3U/µL in the above buffer without SDS

PI buffer (100x): 500 µg/ml leupeptin
100 mM EDTA
100 µM E64
200 µg/ml pepstatin A
1 mg/ml aprotinin

Instead of PI buffer: *Complete EDTA free protease inhibitor cocktail (Roche)*:
1 tablet dissolved in final 2 ml of water supplemented with 100 mM EDTA)

PMSF (100x): 100 mM PMSF (dissolved in water: isopropanol)

The above mentioned cell pellet was resuspended on ice in:

85.6 µl of Benzonase buffer
1.2 µl 100x PI
1.2 µl 100x PMSF
2 µl Benzonase (3U/µL)

The reaction was incubated on ice for 15-60 minutes. Another 1.2 µL of 100x PMSF plus 30 µl 4x SDS-PAGE sample buffer was added. 10-20 µl of this solution were loaded onto an SDS-gel (≈ 5-10 x 10^4 cells/lane) to run an SDS-PAGE.

2.6.4.9 Cell breakage and membrane preparation

In buffer containing 50 mM Tris-HCl (pH 7.5), 200 mM NaCl, 8.6 % glycerol and Roche protease inhibitor resuspended cells (5 x 10^6 cells/ml) were lysed using a Parr bomb (Parr

Instrument Company) at 34 bar and 4 °C. The cell solution was three times applied to the Parr bomb with a break of 30 minutes in between.
Cell debris was removed by centrifugation (12,500 rpm, 4 °C, 10 minutes; Avanti J-30 I, rotor type JLA-16.250), the supernatant was collected and centrifuged for one hour at 45,000 rpm and 4°C (Beckman Optima L-70K, rotor type Ti45) to collect membranes. The membrane pellet was resuspended into buffer containing 50 mM Tris-HCl (pH 7.5) and 17.4 % glycerol before the membrane solution was either directly solubilized or frozen in liquid nitrogen and stored at -20°C for further use.

2.6.4.10 BGT1 solubilization

The solutions of membranes either from *P. pastoris or D. melanogaster* (*Sf*9 cells) containing BGT1 were adjusted to a total protein concentration of 5 mg/ml. For 2D crystallization and reconstitution buffer containing 50 mM Tris-HCl (pH 7.5), 10 % glycerol and 200 mM NaCl was used and the protein was solubilized in 2 % n-Dodecyl β-maltoside (DDM) for 1 hour on ice while stirring. When BGT1 was purified to attempt 3D crystallization, the protein was solubilized in the same buffer (see above) but in 2 % DM for at least 40 minutes on ice while stirring. After solubilization the soluble fraction was separated from the insoluble material by ultracentrifugation (45,000 rpm, 4 °C, 45 minutes; Beckman Optima L-70K, rotor type Ti45). The supernatant was further used for purification.

2.6.5 Protein production in *Xenopus laevis* oocytes

A standard oocyte Ringer solution (ORi) was used for oocyte preparation, storage, and for electrophysiological measurements. ORi contained 110 mM NaCl, 3 mM KCl, 2 mM $CaCl_2$, 5 mM HEPES/Tris pH 7.5. GABA and betaine were added to ORi in the following concentrations: 0.01; 0.025; 0.05; 0.1, 0.25; 0.5, and 1 mM. All chemicals were purchased from Sigma-Aldrich (Taufkirchen, Germany). Stage V and VI oocytes from *Xenopus laevis* (Nasco, Fort Atkinson, WI, USA) were separated by an overnight treatment with collagenase (Typ CLS II, Biochrom, Berlin, Germany), subsequently washed in calcium-free ORi and maintained at 16 – 18 °C in ORi containing again a calcium concentration of 2 mM. One day

after removing the oocytes from the frog, each oocyte was injected with 50 nl ORi containing 12.5 ng cRNA coding either for wildtype BGT1 or mutants. 23 nl 0.5 mg/ml tunicamycin dissolved in ORi, 10 units/ml PNGase F in ORi or 23 nl ORi alone were injected separately approximately 1 hour after the injection of either the cRNA or an equivalent amount of ORi (negative controls). Oocytes were maintained at 16 – 18$^{\circ C}$ in ORi supplemented with 50 µM gentamycin and 2.5 mM sodium pyruvate. After 3 to 4 days of incubation with daily medium changes, oocytes were used for electrophysiological measurements. Oocyte injection and cultivation were performed by Prof. Dr. Burckhardt (University Göttingen).

2.6.5.1 *Xenopus laevis* oocytes lysis and membrane preparation

Preparation of membranes was carried out as described previously (Broer, 2010). The lysates were separated on 12.5 % SDS-PAGE and then electro-transferred onto PVDF-membranes which were previously activated by methanol. The membrane was blocked with 5 % (w/v) skim milk powder for 1h at room temperature and then incubated over night at 4 °C with affinity-purified rabbit polyclonal antibody to dog BGT1 (Proteintech Group), diluted 1:1000 in 0.5 % (w/v) skim milk powder, followed by a 2 hours incubation with affinity-purified polyclonal antibody to rabbit coupled to alkaline phosphatase, diluted 1:1000 in 0.5 % skim milk powder.

Fractionation of oocytes membranes was carried out according to the protocol from Broer (Broer, 2010) with minor changes. Briefly, 80 WT-RNA injected untreated oocytes (WT), 100 WT-RNA injected oocytes treated with tunicamycin ($WT^{+Tun)}$ or PNGase F (WT^{+P}), respectively or 150 NN171/183DD-RNA injected oocytes were homogenized in 1 ml, 1.5 ml and 2 ml "homogenization buffer 2": 320 mM sucrose, 50 mM Tris pH 7.5, 1 mM EDTA, 1 mM Pefabloc, respectively by pipetting up and down. The suspension was centrifuged twice at 1000 g for 10 minutes at 4 °C. The supernatants were transferred on a sucrose gradient: 2 ml [2M], 3.2 ml [1.3 M], 3.2 ml [1 M], 2 ml [0.6 M] and centrifuged in a swing-out rotor at 40,000 rpm (Beckman Optima L-70K, rotor type SW40) for 4 hours at 4 °C. Sucrose solutions were prepared in "TE-buffer" (50 mM Tris-HCl pH 7.5, 1 mM EDTA, 5 mM $MgCl_2$). 1 ml fractions were collected from the bottom, diluted 4-fold with 150 mM sucrose in "TE-buffer" and centrifuged at 50,000

rpm in a Ti70 (Beckman) rotor for 2 hours at 4 °C. Membrane pellets were resuspended in 15 µl SDS-PAGE sample buffer for electrophoresis and Western blotting as described above.
According to Broer (Broer, 2010), the rough ER (rER) is detected in fractions 2-3, the plasma membrane (PM) in fraction 5 and the trans-Golgi network (TGN) in fractions 9-10.

2.6.6 Protein production in MDCK cells

MDCK cells (CCL-34, from American Type Culture Collection (Rockville, MD)) were used as described previously (Kempson et al., 2003). Enzymatic deglycosylation with PNGase F was carried out by adding 10 units/ml PNGase F to the hypertonic medium and an incubation of 6 hours at 37 °C prior measuring. For transient expression MDCK cells were transfected using GeneJammer (Stratagene) according to the manufacturer's instructions.

2.6.6.1 MDCK cell lysis and membrane preparation

Cell monolayers in six-well plates were placed on ice and washed twice with isotonic or hypertonic TBS (50 mM Tris-HCl (pH 7.6), 150 mM NaCl). The cells were lysed by the addition of lysis buffer (1 % Triton X-100, 150 mM NaCl, 5 mM EDTA, 10 % glycerol, 50 mM Tris-HCl (pH 7.5), and protease inhibitors (cOmplete EDTA-free Protease Inhibitor Cocktail Tablets, Roche)). Cells were collected by scraping, sonicated for 5 seconds, incubated for 15 minutes at 4 °C, and centrifuged at 13,000 *g* for 15 minutes at 4 °C. The supernatant was collected and stored at -80 °C before further use. Aliquots of the supernatant were assayed for protein content by the BCA method (Pierce). Before being loaded (5–10 µg/lane) on a 12 % SDS gel, the supernatant samples were incubated in SDS sample buffer, containing 100 mM dithiothreitol, for 10 minutes at 65 °C.

2.6.6.2 Purification with StrepTactin®-affinity chromatography

For BetP, WT and mutants were purified via their N-terminal StrepII-tag (NH2-WSHPOFEK-COOH) (IBA, Göttingen). 2 – 3 ml of StrepTactin® material was equilibrated with five column volumes (CV) of buffer A (50 mM Tris-HCl (pH 7.5), 8.7 % glycerol, 200 mM NaCl, 0.05 % DDM) before the diluted solubilized fraction was loaded over night at 4 °C. After loading three washing steps were applied:

For crystallization: (1) 6 to 8 CV buffer A supplemented with 0.05 % DDM, slowly

(2) 6 to 8 CV buffer A supplemented with 0.05 % DDM and 300 mM NaCl, fast

(3) 6 to 8 CV buffer A supplemented with 0.6 – 1.2 % Cymal-5, slowly

The protein was eluted with 5 mM of desthiobiotin added to buffer A supplemented with either 0.05 % DDM or 0.6 – 1.2 % Cymal-5. Elution fractions of 500 µl were collected. The protein concentration of each fraction was checked using the Bradford assay (Bradford, 1976).

2.6.6.3 Purification with Immobilized Metal Ion Affinity Chromatography (IMAC)

Recombinantely expressed BGT1 fused either to an N-terminal hexa-histidine (His_6-tag, *E. coli* cell-free expression), a C-terminal octa-histidine (His_8-tag, *D. melanogaster* expression) or a C-terminal deka-histidine tag (His_{10}-tag, *P. pastoris* expression) was purified via Ni-NTA Agarose (Sigma- Aldrich, Munich). This method is based on the binding of the histidine residues to the divalente cations (e.g. Ni^{2+}), which are immobilized to nitrilotriacetic (NTA) to the column material. 1 ml of Ni-NTA resin was equilibrated with ten column volumes (CV) of equilibration buffer (50 mM Tris-HCl (pH 7.5), 10 % glycerol, 200 mM NaCl, 10 mM Imidazole, supplemented with either 0.05 % DDM or 0.1 % DM) before the solubilized fraction was incubated together with the Ni-NTA material for 2 hours at 4 °C. The binding of his-tagged protein to Ni-NTA results in a chelate complex between one Ni^{2+}-ion, and two histidine residues of the his-tag. After incubation the mixture was applied to a 10 ml chromatography column (Biorad, Munich). Unspecifically bound proteins were removed by several washing steps (see below) with equilibration buffer supplemented with low but raising concentrations of imidazole (10 - 30 mM). The protein was eluted with equilibration buffer supplemented with 240 mM imidazole and either 0.05 % DDM, 0.1 % DM or 0.6 – 1.2 % Cymal-5. Aliquots of 500 µl were collected and analyzed using the Bradford assay (Bradford, 1976). Fractions containing the highest protein concentrations were pooled.
Equilibration and washing steps were performed as follows.

For reconstitution: (1) 2 CV equilibration buffer supplemented with 0.05 % DDM

(2) 2 CV equilibration buffer supplemented with 0.05 % DDM and 10-30 mM imidazole

For crystallization: (1) 2 CV equilibration buffer supplemented with 0.05 % DDM or 0.1 % DM

(2) 2 CV equilibration buffer supplemented with 0.05 % DDM or 0.1 % DM and 10 mM imidazole

(3) 2 CV equilibration buffer supplemented with 0.6 – 1.2 % Cymal-5 and 20 mM imidazole

2.6.6.4 Purification with Immunoaffinity-FLAG-tag

The second purification step of heterologously expressed BGT1 in *P. pastoris* involved immunoaffinity by immobilized antibodies (Anti-FLAG M2 Agarose, Sigma-Aldrich). A FLAG-tag, which is an octa-peptide consisting of the amino acids "DYKDDDDK", is fused to the N-terminus of BGT1 followed by a *PreScission* cleavage site. The pooled fractions after IMAC purification were incubated with the pre-equilibrated Anti-FLAG M2 Agarose for 2 hours at 4 °C and constant stirring. Subsequently the mixture was applied to a 10 ml chromatography column (Biorad, Munich). The agarose was washed with 5 column volumes of washing buffer (25 – 50 mM Tris-HCl (pH 7.5), 200 mM NaCl, 10 % glycerol and 0.05 % DDM or 0.1 % DM or 0.6 – 1.2 % Cymal-5) to remove unbound and unspecifically bound proteins. The target protein was eluted with washing buffer supplemented with FLAG peptide (100 µg/ml, Sigma-Aldrich).

2.6.6.5 Size exclusion chromatography (SEC)

Size exclusion chromatography (SEC) was used for both **preparative** and **analytical** purposes. A Superose™ 6 10/300 column (GE Healthcare) connected to an ÄKTA system (GE Healthcare) was used for **preparative SEC**, equilibrated with buffer containing 25 mM Tris-HCl (pH 7.5), 200 mM NaCl and either 0.6 – 1.2 % Cymal-5 or 0.1 % DM before the concentrated protein solution was injected. The flow rate was set to 0.2 ml/min and fractions

of 0.2 ml were collected. The fractions containing the target protein were pooled after SDS-gel electrophoresis.

For **analytical SEC** a Superose™ 6 (3.2/30) column (GE Healthcare) connected to an ETTAN LC system (GE Healthcare) was used. The column was equilibrated with buffer containing 25 - 50 mM Tris-HCl (pH 7.5), 200 mM NaCl and either 0.6 – 1.2 % Cymal-5 or 0.1 % DM. The flow rate was kept at 50 µl/min.

All buffers used for SEC were filtered (exclusion size 0.2 µm) and degassed.

2.6.6.6 Ultra Filtration

Saltorius concentrators with a molecular weight cut-off of 50,000 or 100,000 kDa were used to concentrate a protein solution by centrifugation at 4 °C according to manufactures instructions.

2.6.7 Protein concentration

2.6.7.1 Bradford Assay

The Bradford assay (Bradford, 1976) was used to determine the protein concentration either pure or in membrane solution. The Coomassie Brilliant Blue G250 dye in the Bradford Reagent (Sigma-Aldrich) forms a complex with the basic (arginine, lysine and histidine) and the hydrophobic (phenylalanine, tryptophan and tyrosine) amino acids. This complex stabilizes the anionic form of the dye and causes a bathochromic shift in the absorption maximum from 465 nm to 595 nm, when protein is bound. The protein concentration could be measured with a calibration curve calculated from a BSA standard (Photometer BioPhotometer, Eppendorf).

2.6.7.2 Protein denaturing method

By measuring the absorbance at 280 nm, the protein concentration of purified protein was calculated. The ExPASy ProtParam tool (www.expasy.ch/tools/protparam.html) was used to get the extinction coefficient ε and the molar mass M_r of the BGT1 amino acid sequence. The

protein was first denatured in 6 M guanidinium hydrochloride; the latter was also used as a reference. The protein concentration was calculated using the following equation:

$$c(BGT1) = \frac{Abs.(\lambda_{280}) * 100}{\varepsilon(BGT1)} * M_r(BGT1)$$

ε (BGT1) = 144,950 M_r = 69,292 Da

2.6.7.3 Amido Black assay

The Amido Black method (Schaffner and Weissmann, 1973) was used to determine the protein concentration reconstituted into liposomes. The Amido Black method is a very sensitive method by which the total protein concentration in the sample can be measured up to 0.75 µg/ml. Trichloroacetic acid (TCA) precipitates the protein collected on a membrane filter and visualized by the dye Amido black.

A 2 – 10 µl sample was diluted with water to a final volume of 225 µl. Then 30 µl buffer (1 M Tris-HCl, (pH 7.4), 2 % (w/v) SDS) and 50 µl 90 % (v/v) TCA was added, vortexed and incubated at room temperature for 5 minutes. A Millipore filter (type HAWP02500, 0.45 µm) was marked with pencil dots and soaked in water before placing on a suction unit. The samples were carefully and slowly dropped onto the marked spots, sucked through the filter with a vacuum pump and directly washed with 200 µl 6 % (v/v) TCA. At the end, after applying all samples, the whole filter was washed with 1 – 2 ml 6 % (v/v) TCA, transferred into a petri dish with Amido Black solution (0.25 % (w/v) Amido Black, 45 % (v/v) methanol, 10 % (v/v) acetic acid) and incubated for 2 - 10 minutes. The filter was then rinsed with water to remove excess solution before it was incubated for 3 minutes in destaining solution (90 % (v/v) methanol and 2 % (v/v) acetic acid). The filter was again washed with water and the blue colored protein spots were cut out and transferred into Eppendorf reaction tubes. 1 ml of elution solution (25 mM NaOH, 50 µM EDTA and 50 % (v/v) ethanol) was added to the tubes to destain the filter spots under shaking for 10 – 30 minutes at room temperature. The absorption of the solution was measured at 630 nm. A concentration range from 0 – 10 µg BSA was used to determine the standard curve.

2.6.8 Polyacrylamid gel electrophoresis (PAGE)

2.6.8.1 Blue-Native (BN)-PAGE

Blue Native PAGE was carried out as described by Schägger and von Jagow (Schagger and von Jagow, 1991), to detect undenatured proteins after purification. Negative charges of Coomassie Blue G250 are tightly bound to the native solubilized proteins after purification and determine their electrophoretic mobility.

4 – 16 % Tris-Glycine gels (Invitrogen) were used, protein samples (5 – 10 µg) were mixed with NativeMark™ Unstained Native Protein marker (Invitrogen) and loaded onto the gel. The gel was started at 80 V for 30 minutes to concentrate the protein samples in the stacking gel and then run at 150 V for 4 hours at 4 °C. The gels were distained with 10 % (v/v) Ethanol and 10 % (v/v) Glacial acetic acid.

Anode buffer	50 mM BisTris (pH 7)
Cathode buffer	50 mM Tricine 15 mM BisTris (pH 7) 0.02 % Coomassie-Brilliant-Blue G-250

2.6.8.2 Sodium dodecyl sulfate polyacrylamide gel electrophoresis (SDS-PAGE)

SDS-PAGE is a method to determine the purity of a protein sample under denaturing conditions (Laemmli, 1970). The proteins are separated according to their electrophoretic behavior. 10 % separating gels with 4 % stacking gels (Table 4) were prepared in a multiple gel-casting (Hoefer) and stored at 4 °C. Prior electrophoresis the protein samples were denatured and linearized in 4x sample buffer containing the anionic detergent SDS and loaded onto the gel. The gel electrophoresis was performed at 80 V until all the samples were concentrated within the stacking gel and then run at constant voltage of 120 V. Gels were stained with Coomassie Brilliant Blue R 250 by the protocol of Studier (Studier, 2005) and distained over night.

Table 1: SDS-PAGE gel mixture for five Tris Glycine polyacrylamid gels.

Buffer	*10 % Separating gel*	*4 % Stacking gel*
1.5 M Tris-HCl, pH 8.8	7.5 ml	-
0.5 M Tris-HCl, pH 6.8	-	5 ml
40 % (v/v) Acrylamide	7.5 ml	2 ml
10 % (w/v) SDS	300 µl	200 µl
H_2O	14.6 ml	12 ml
TEMED	100 µl	100 µl
10 % (w/v) APS (fresh)	25 µl	20 µl
Bromphenol blue	-	800 µl

Sample buffer (4x)	25 mM Tris-HCl pH 8
	2.5 % (w/v) SDS
	2.5 % (w/v) β-Mercaptoethanol
	12.5 % (w/v) Glycerol
	0.4 % (w/v) Bromphenol blue
SDS-PAGE buffer	25 mM Tris-HCl pH 7
	200 mM Glycine
	0.1 % (w/v) SDS

Coomassie staining solutions:

Solution I	50 % (v/v) Ethanol
	10 % (v/v) Acetic acid
Solution II	50% (v/v) Ethanol
	7.5 % (v/v) Acetic acid
Coomassie Stock Solution	95 % (v/v) Ethanol
	0.25 % (v/v) Coomassie Brilliant Blue G250

Silver staining:

SDS-PAGE gels were stained with silver stain using the protocol of Nestrenko et al. (Nesterenko et al., 1994).

Table 2: Solutions for silver stain

Step	*Component*	*Concentration*	*Wash/Incubation*
Fixation	Acetone	50 % (v/v)	5 min
	TCA	1.8 % (v/v)	
	CH_2O	0.015 %	
Rinse	Water		3 x 5 sec
Incubation	Acetone	50 % (v/v)	5 min
Pretreat	$Na_2S_2O_3$ * $5H_20$	0.017 % (v/v)	1 min
Rinse	Water		2 x 5 sec
Impregnate	$AgNO_3$	0.27 % (v/v)	8 min
Rinse	Water		2 x 5 sec
Develop	Na_2CO_3	0.02 g/ml	10-20 sec
	CH_2O	0.0154 % (v/v)	
	$Na_2S_2O_3$ * $5H_20$	0.004 % (v/v)	
Stop	Acetic acid	1 % (v/v)	30 sec
Rinse	Water		

2.6.8.3 Western blot analysis

For Western-blotting proteins after SDS-PAGE the SDS-gel was transferred to a methanol-activated polyvinylidene difluoride (PVDF) membrane (Immobilon™ -P Transfer Membrane, pore size 0.45 µm, MILLIPORE) and the proteins were blotted onto the PVDF membrane via a "semi-dry" blot system (Trans-Blot® SD, Biorad). The target protein can be detected using specific antibodies.

A PVDF membrane was shortly activated in 100 % (v/v) methanol and placed on four layers of blot paper (Whatman 3MM filter paper (Schleicher & Schüll)) previously soaked in transfer buffer (100 mM Tris-HCl pH 8.3, 192 mM Glycine, 0.2 % (w/v) SDS, 10 % (v/v) methanol), on the anode of a blot apparatus (Trans-Blot® SD, Biorad). The SDS gel was applied on top of the PVDF membrane and covered with four Whatman papers soaked in transfer. Western blotting was carried out at 15 V for 35 minutes.

After blotting the membrane was incubated in 5 % (w/v) skim milk powder or in 3 % (w/v) BSA in TBS (blocking buffer) for 1 hour at room temperature to block unspecific binding sites. The membrane was subsequently washed 3 times in TBS-buffer and for immuno-detection incubated in primary antibody (1 : 1000 dilution in 0.5 % (w/v) skim milk powder in 1 x TBS) for 2 hours at room temperature or over night at 4 °C. The membrane was washed 3 times in TBS-buffer before incubating with the secondary antibody coupled to Alkaline Phosphatase (1 : 1000 dilution in 0.5 % (w/v) skim milk powder in TBS) for 2 hours at room temperature. The PVDF membrane was washed again 3 times with TBS-buffer before developing specific antibody binding in 10 ml solution of water dissolved with a tablet of SigmaFAST™ BCIP/NBT (Sigma-Aldrich) until bands appeared. The membrane was washed with deionized water to stop the reaction.

Table 3: Primary and secondary antibodies used for Western blotting

Antibody	*Dilution*	*Source*
Monoclonal Anti-polyHISTIDINE clone HIS-1	1 : 1000 in 0.5 % (w/v) skim milk powder in TBS	Sigma-Aldrich
Monoclonal Anti-FLAG® clone M2	1 : 1000 in 0.5 % (w/v) skim milk powder in TBS	Sigma-Aldrich
Monoclonal Anti-BGT1 (dog, 595-613)	1 : 1000 in 0.5 % (w/v) skim milk powder in TBS	Proteintech Group
Monoclonal Anti-StrepTagII IgG1	1 : 4000 in TBS	IBA
Anti-Mouse IgG (whole molecule)-Alkaline Phosphatase, antibody produced in rabbit	1 : 1000, 1 : 4000 in 0.5 % (w/v) skim milk powder in TBS or when Anti-StrepTagII was used in TBS	Sigma-Aldrich
Anti-Rabbit IgG (whole molecule)-Alkaline Phosphatase, antibody produced in goat	1 : 1000 in 0.5 % (w/v) skim milk powder in TBS	Sigma-Aldrich

2.6.8.4 Thin-layer chromatography (TLC)

Thin layer chromatography was performed to analyze lipids bound to solubilized BetA and BGT1 after purification and compared to lipid standards.

35 µg of purified protein in detergent solution, 0.5 µg detergent solution (DDM) and 100 µg of each standard sample were loaded onto a pre-coated HPTLC-silica gel plate (10x10 cm^2, pre-coated, Silicia 60, Merck) about 2 cm from the base. Lipids were separated either in acetone : chloroform : methanol : water : acetic acid = 2 : 1 : 1 : 0.5 : 5 or in chloroform : methanol : water = 69 % : 27 % : 4 % (v/v/v) and for two-dimensional TLC a solvent of chloroform : methanol : ammonia = 13 : 7 : 1 was used for the second dimension. After drying, lipids were first visualized by iodine vapour (unspecific lipid dye) (Gasser et al., 1977) to detect all lipids non-specifically. Secondly, phospholipids were detected using molybdenum blue spray reagent (1.3 % (w/v) molybdenum oxide (MoO_3) (Sigma-Aldrich) in 4.2 M sulfuric acid, 1 : 1 dilution) (Müthing and Radloff, 1998). The phospholipids appeared as blue spots.

2.6.8.5 Protein reconstitution into liposomes

Reconstitution of BGT1 into liposomes was carried out based on a reconstitution method by sodium-cholate dialysis and subsequently SEC-mediated removal of detergent (Radian and Kanner, 1985) and best results could be obtained by a Bio-Beads (SM-2 Macroporous Beads, Bio-Rad) detergent removal method. For reconstitution either liver polar lipids (Liver Polar Lipid Extract, Avanti), brain polar lipids (Brain Polar Lipid Extract, Avanti), PC (Soy PC, Avanti), DOPE (18:1 (Δ9-Cis) PE, Avanti) or mixtures of PC and brain polar lipids (ratio 3.5 : 1) as well as PC : PE (ratio 1 : 1) both partially supplemented with cholesterol 5 % (v/v) were used.

A lipid aliquot in chloroform was dried under a nitrogen gas stream and subsequently resuspended in Reconstitution buffer (120 mM KP_i, pH 6.8, 1 % glycerol, 10 mM Tris-SO_4, pH 7.4, 0.5 mM EDTA, 1 mM $MgSO_4$) to a final concentration of 20 mg/ml. Aliquots of 400 µl were frozen in liquid nitrogen and stored at -80 °C.

A lipid aliquot, when frozen, was slowly thawed at RT or directly extruded 20 times through a 400 nm membrane filter (Polycarbonate Membrane, pore size = 400 nm, Avestin) and diluted 1 : 4 in Reconstitution buffer. The liposomes were titrated with Triton X100 (10 % stock solution (w/v)) to the onset of solubilization, detected by measuring light absorbance at 540 nm. Subsequently, purified protein was added at a lipid-to-protein ratio of 40 : 1 (w/w). After 30 minutes of incubation at RT under gentle agitation Bio-Beads (SM-2 Macroporous Beads, Bio-Rad) were added step-wise to remove detergent. Proteoliposomes were collected by ultra-centrifugation at 100,000 g for 35 minutes at 20 °C, washed twice and resuspended in Reconstitution or KP_i buffer to a final lipid concentration of 60 mg/ml from which aliquots of 50 µl were prepared, frozen in liquid nitrogen and stored at -80 °C. Each reconstitution was checked by freeze-fracture electron microscopy.

Table 4: Lipids used for reconstitution of BGT1

Abbreviation of the lipid	*Lipid (wt/wt%)*	*Source*
POPC	1-palmitoyl-2-oleoyl-*sn*-glycero-3-phosphocholine	Avanti polar lipids
DOPC	1,2-dioleoyl-*sn*-glycero-3-phosphocholine	Avanti polar lipids
DMPC	1,2-dimyristoyl(Δ54)-*sn*-glycero-3-phosphocholine	Avanti polar lipids
PCegg	L-α-lysophosphatidylcholine (Egg, Chicken)	Avanti polar lipids
PCsoy	L-α-lysophosphatidylcholine (Soy)	Avanti polar lipids
PCsoy +	L-α-lysophosphatidylcholine (Soy) + 1-palmitoyl-2-oleoyl-*sn*-glycero-3-	Avanti polar lipids

POPE	phosphoethanolamine	
PCsoy +	L-α-lysophosphatidylcholine (Soy) + 1-palmitoyl-2-oleoyl-*sn*-glycero-3-phospho-(1'-*rac*-glycerol)	Avanti polar lipids
POPG		Avanti polar lipids
Asolectin +	45.7 % PC, 22.1 % PE, 18.4 % PI, 6.9 % PA, 6.9 % unknown +	Sigma-Aldrich +
Brain polar lipids	12.6 % PC, 33.1 % PE, 4.1 % PI, 18.5 % PS, 0.8 % PA, 30.9 % unknown	Avanti polar lipids
Liver polar lipids	42 % PC, 26 % PE, 9 % PI, 1 % lyso PI, 5 % cholesterol, 17 % others, incs. Neutral lipids	Avanti polar lipids

2.6.8.6 Transport measurements in *E. coli* MKH13 cells

Uptake of [^{14}C]-betaine (Moravek Biochemicals and Radiochemicals, U.S.A) in *E. coli* cells was performed as described previously (Ott et al., 2008). *E. coli* MKH13 expressing a particular strep-*bet*P derivative was expressed at 37°C in LB medium containing carbenicillin (50 µg/ml), cells were induced with anhydrotetracycline [200 µg/l] at an OD_{600} of 0.5. After 2 hours the cells were harvested, washed in

buffer containing 25 mM KP_i buffer (pH 7.5) and 100 mM NaCl and then resuspended in the same buffer containing 20 mM glucose. For all uptake measurements the external osmolality was adjusted using different concentrations of KCl (200 – 1200 mOsmol/kg). For measurement of betaine or GABA uptake cells were incubated for 3 minutes at 37°C in the appropriate osmolality buffer before adding 250 µM [^{14}C]-betaine (specific radioactivity of 90 µCi/mmol). For K_m- and v_{max} -determination at variable betaine or GABA concentrations, cells were incubated for 3 minutes at 37°C in buffer with an external osmolality of 800 mOsmol/kg. Samples were filtered through glass fiber filters (APFF02500, Millipore,

Schwalbach, Germany) at different time intervals, and washed twice with 2.5 ml of 0.6 M KP_i buffer (pH 7.5). The radioactivity on the filters was determined by liquid scintillation counting. Kinetic constants were derived by curve fitting of the uptakes rates versus the substrate concentration with GraphPad Prism version 5.0c for Mac OS X, GraphPad Software (Motulsky, 1999).

2.6.8.7 Transport measurements in *P. pastoris* cells

Uptake of [^{3}H]GABA (Moravek Biochemicals and Radiochemicals, USA) in *P. pastoris* cells was performed as described (Doring et al., 1998). *P. pastoris* cells expressing BGT1 were harvested (3,000 g, 4 °C, 10 minutes) and washed twice in 25 mM KP_i buffer (pH 7.5), then resuspended in the same buffer to 1 OD * 10 μl^{-1}. For uptake measurements 10 µl cells were incubated with 40 µl of Uptake buffer (120 mM KP_i buffer (pH 6.8), 10 mM Tris-SO_4 (pH 7.4), 0.5 mM EDTA, 1 mM $MgSO_4$, 150 mM NaCl) supplemented with 0.2 µCi [^{3}H] GABA and for inhibition studies supplemented with NNC 05-2090 to a final concentration of 2 µM prior incubation. The empty vector (pPIC3.5k) was measured as a control and subtracted. GABA uptake was measured at various intervals after cell samples were passed through glass fiber filters (ME 25 type, 0.45 µm pore size, Millipore). The reaction was stopped by washing twice with 2 ml of ice-cold 25 mM Tris-buffer pH 7.5. The radioactivity retained on the filters was quantified by liquid scintillation counting. For uptake measurements incubation of the substrate was measured at different periods of time and for K_M and V_{max} determination the concentration of [^{3}H]GABA was varied. The kinetic constants were derived by Michaelis-Menten curve fitting of the uptake rates versus the substrate concentration with GraphPad Prism version 5.0c for Mac OS X, GraphPad Software (Motulsky, 1999).

2.6.8.8 Transport measurements in MDCK and HEK-293 cells

Na^+- dependent [^{3}H]GABA (Moravek Biochemicals and Radiochemicals, USA) uptake was determined in 6-well plates (Kempson et al., 2003). Inhibition studies were performed by adding NNC-05-2090 to a final concentration of 2 µM just prior incubation. Enzymatic deglycosylation with PNGase F was carried out by adding 10 units/ml PNGase F to both the

isotonic and hypertonic sucrose medium. The reactions were incubated for 6 hours at 37°C prior measuring. MDCK cells were transiently transfected using GeneJammer (Stratagene) according to the manufacturer's instructions.

GraphPad Prism version 5.0c for Mac OS X, GraphPad Software (Motulsky, 1999) was used for kinetic constants calculations, which were derived by Michaelis-Menten curve fitting of the uptake rates versus the substrate concentration. All transport measurements were repeated five times.

HEK-293 cells were transiently transfected using Fugene 6 (Roche, Germany) according to the manufacturer's instructions. Na^+- dependent [^{3}H]GABA uptake in HEK-293 cells was carried out by Prof. Dr. Kempson (Indiana University, USA).

2.6.8.9 Transport measurements in Liver polar lipid proteoliposomes

Uptake measurements of [^{3}H]GABA (Moravek Biochemicals and Radiochemicals, USA) into proteoliposomes containing BGT1 was performed by preloading proteoliposomes with a saturating concentration of non-radioactive substrate, usually 5 mM of GABA (Sigma-Aldrich) was used. Substrate was added to the proteoliposomes and subsequently loaded by three rounds of freeze thawing. Proteoliposomes were extruded through a 400 nm polycarbonate membrane filter (Polycarbonate Membrane, pore diameter 400 nm, Avestin) and washed with KP_i buffer to remove extra liposomal substrate. Collection of proteoliposomes was carried out by ultracentrifugation (100,000 g, 20 °C, 35 minutes) and resuspended to a final concentration of 60 mg of lipid/ml. To measure sodium/chloride-driven uptake, proteoliposomes were diluted 200-fold in Reconstitution buffer supplemented with 150 mM NaCl. At time points of 5 to 30 seconds, [^{3}H]GABA incorporated into the proteoliposomes was determined with scintillation counter TRI-CARB 1500 (Canberra-Packard). Transport measurements were repeated three times.

2.7 Biophysical methods

2.7.1 Two-Electrode Voltage Clamp

Two-electrode voltage clamp analyses on *Xenopus laevis* oocytes were carried out 3 - 4 days after cRNA and tunicamycin injection at room temperature. Oocytes were placed into a 0.5 ml chamber on the stage of a microscope and impaled under direct view with borosilicate glass microelectrodes filled with 3 M KCl (BioMedical Instruments, Zöllnitz, Germany). Current recordings at -60 mV were performed using a two-electrode voltage clamp device (OC725A, Warner, Hambden, CT, USA) in the voltage clamp mode.

Data were provided as means ± SEM. Paired Student's t-test was used to show statistically significant difference of the GABA- or betaine-associated currents in the absence and presence of PNGase F. Statistical significance was set at $p<0.05$ (*). Michaelis-Menten constants (K_m) for GABA in the absence and presence of tunicamycin were determined by SigmaPlot software (Systat Software, Point Richmond, CA, USA) using the Michaelis-Menten equation $I = I_{max} \cdot [S]/(K_m + [S])$, where I is the current, I_{max} is the maximum current observed at saturating substrate concentrations, K_M is the substrate concentration at half-maximal current, and S is the substrate concentration. All two-electrode voltage clamp measurements were performed by Prof. Dr. Birgitta Burckhardt (University Göttingen).

2.7.2 Mass spectrometry

Mass spectrometry is a method for determination the masses of molecules by ionization to generate molecule fragments and measure their mass-to-charge ratios.

In this work, samples were analyzed at the "Zentrum für Molekulare Medizin (ZMMK, Cologne) with ESI-MS/MS (electrospray ionization-mass spectrometry) to identify the protein and a specific phosphorylation site in the N-terminal domain of BGT1.

2.7.3 Freeze-fracture electron microscopy

A small sample of proteoliposome suspension (2 µl, final lipid concentration 60 mg/ml) was pipetted between two copper plates (sample holder). Subsequently, the sample was frozen in

liquid ethane at -180 °C. Freeze-fracture of proteoliposomes was carried out with a BAF 060 machine (Bal-Tec) at a temperature of -130 °C and a pressure of $2x10^{-7}$ mbar. To reinforce the replica the resulting fracture planes were shadowed with platinum/carbon followed by pure carbon shadowing. For removal of organic material the replica was floated with sulfuric acid (40 - 50 % (v/v)) for 10 hours, washed several times with water and analyzed in an EM208S electron microscope (FEI Company). Images were collected on a 1K x 1K slow-scan CCD camera (TVIPS). All freeze-fracturing and imaging steps were performed by Friederike Joos and Susann Kaltwasser (MPI of Biophysics).

2.7.4 Immunogold-labeling

Immunogold-labeling was carried out for localization studies of a protein within a cell by using a primary antibody raised against an antigenic epitope of the target protein and a secondary antibody labeled with gold particles, which binds to the primary antibody. Immunogold labeling and electron microscopy were performed by Friederike Joos (MPI of Biophysics).

2.7.5 Two-dimensional crystallization

For membrane proteins two-dimensional crystallization is one of the established methods for structure determination. Purified protein and lipids are mixed with detergent and the latter is removed by dialysis, dilution or absorption leading to densely packed proteoliposomes or crystallization of the protein. The critical factors, which influence the 2D crystallization, are lipids, lipid-to-protein ratio (LPR), protein- and detergent-concentration, pH, salt concentration and ionic and nonionic additives as well as temperature, which influences lipid fluidity, rate of detergent removal and critical micelle concentration (cmc) of the detergent.

The protein yield for 2D crystallization can be relatively low but determines the choice of the dialysis device, starting from dialysis cassettes (≥ 100 µl volume) over glass capillaries ("hockey sticks", (Kuhlbrandt, 1992) and dialysis bags (50 µl volume) to Mini-Slyde-A-Lyzers and dialysis buttons (5 – 10 µl volume).

The dialysis time is not only influenced by temperature but also by the characteristics of the detergent (e.g. high cmc detergents dialyze within days whereas low cmc detergents take weeks) and the dialysis volume.

2D samples are screened using an electron microscope after detergent removal. To do so the samples are negatively stained with uranyl acetate on a glow discharged carbon coated copper grid.

The quality of crystalline areas was investigated by applying Fourier transform analysis to detect possible crystal reflections.

2.7.5.1 Preparation of lipids

Lipids (Avanti polar lipids) dissolved in chloroform were dried under a stream of nitrogen gas and resuspended in 1 % β-DM to a final concentration of 4 mg/ml. Aliquots were frozen in liquid nitrogen and stored at -80 °C.

2.7.5.2 Two dimensional crystallization of BGT1

2D crystallization trials were set up by incubating lipid with purified protein over night at 4 °C. If necessary the reaction was supplemented with buffer (50 mM Tris-HCl (pH 7.5), 200 mM NaCl, 10 % glycerol) to give a desired volume. LPR was varied from 0.1 to 3 and protein concentrations from 0.5 to 3 mg/ml.

Table 5: Lipids used for 2D crystallization of BGT1

Abbreviation of the lipid	*Lipid (wt/wt%)*	*Source*
POPC	1-palmitoyl-2-oleoyl-*sn*-glycero-3-phosphocholine	Avanti polar lipids
DOPC	1,2-dioleoyl-*sn*-glycero-3-phosphocholine	Avanti polar lipids
DMPC	1,2-dimyristoyl(Δ54)-*sn*-glycero-3-phosphocholine	Avanti polar lipids

PCegg	L-α-lysophosphatidylcholine (Egg, Chicken)	Avanti polar lipids
PCsoy + POPE	L-α-lysophosphatidylcholine (Soy) + 1-palmitoyl-2-oleoyl-*sn*-glycero-3-phosphoethanolamine	Avanti polar lipids
Asolectin + Brain polar lipids	45.7 % PC, 22.1 % PE, 18.4 % PI, 6.9 % PA, 6.9 % unknown + 12.6 % PC, 33.1 % PE, 4.1 % PI, 18.5 % PS, 0.8 % PA, 30.9 % unknown	Sigma-Aldrich + Avanti polar lipids
Liver polar lipids	42 % PC, 26 % PE, 9 % PI, 1 % lyso PI, 5 % cholesterol, 17 % others, incs. Neutral lipids	Avanti polar lipids

2.7.5.3 Detergent removal

Mini Slyde-A-Lyzers (Pierce) and dialysis cassettes with molecular weight cut-offs of 10 kDa were used for detergent removal with sample volumes ranging from 50 – 200 µl. The samples were dialysed against buffer containing 50 mM Tris-HCl (pH 7.5), 150 mM NaCl, 5 % MPD, 5 % glycerol, 2.5 mM $CaCl_2$, 3 mM NaN_3 at temperatures between RT and 37 °C for 4 – 6 weeks.

2.7.6 Electron microscopy

2.7.6.1 Negative staining and data collection

A 2 µl sample was applied on a glow discharged carbon-coated copper grid (400 mesh) for 1 minute. The excess solution was removed with a filter paper (Whatman paper No. 4). The grid was washed once with 2 µl 1 % uranyl acetate and incubated with 2 µl 1 % uranyl acetate for 1 – 2 minutes. The excess uranyl acetate solution was removed with filter paper. The grid was inserted into an electron microscope (EM208) equipped with a LaB_6 filament and operated in low-dose mode with 10 – 20 electrons/Å at an acceleration voltage of 120 kV. Images were

taken on a CCD camera with 2k x 2k or 1k x 1k pixel size and evaluated by Fourier transform calculation.

2.7.7 X-ray crystallography

X-ray crystallography is the most used method to obtain a three dimensional molecular structure from a crystal at atomic resolution. Crystals are exposed to an X-ray beam and the resulting diffraction pattern contains information about the crystal packing symmetry and the size of the repeating unit forming the crystal. The degree of internal crystal order is directly correlated to the amount of atomic information incorporated in the diffraction pattern. The intensities of the spots can be used to calculate a map of the electron density. To permit the building of the molecular structure various methods can be used to improve the quality of this map using the protein sequence until it is of sufficient clarity. The resulting structure is further refined to adopt a thermodynamically favored conformation by fitting the map more accurately (Smyth and Martin, 2000).

2.7.7.1 Three-dimensional crystallization

The major bottleneck in 3D crystallization is the expression of functional membrane proteins in sufficient amounts (Barnard et al., 2007). When pure and homogeneous protein could be obtained, the growth of well-ordered, single three-dimensional crystals diffracting to high resolution and therefore suitable for X-ray analysis is another rate-limiting step in the overall process of structure determination (Caffrey, 2003).

Protein crystals grow in a supersaturated solution after formation of a stable nucleus.

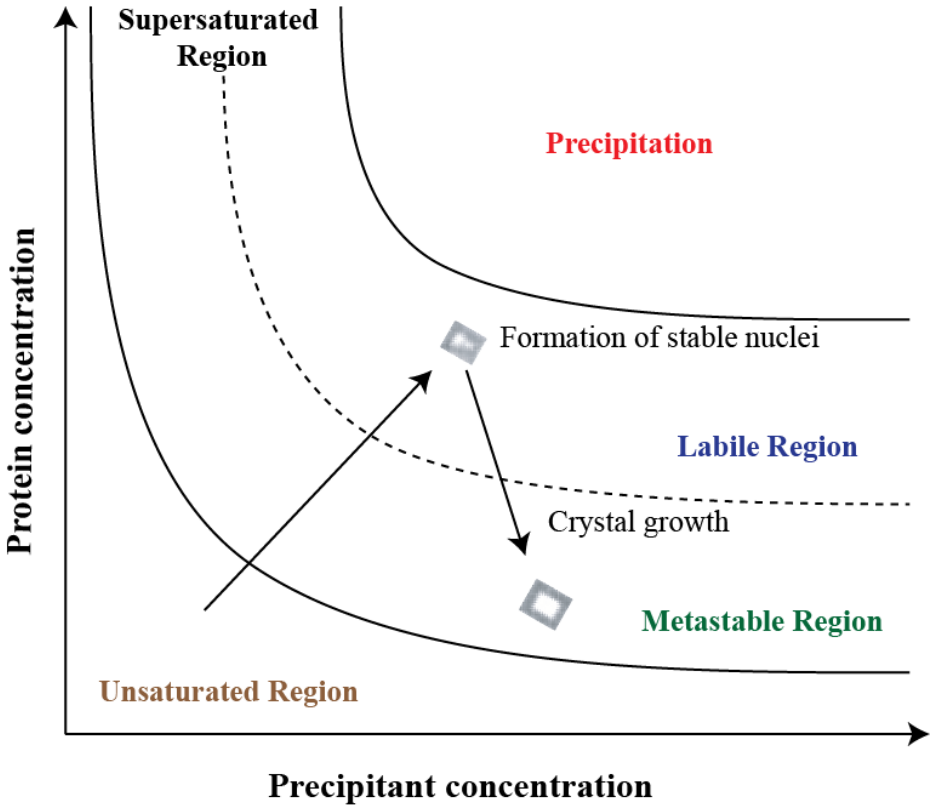

Figure 7: Phase diagram for protein crystal growth. The phase diagram shows three regions. In the unsaturated region (brown) protein crystals cannot form due to low protein concentration. The supersaturated region (black) is divided into two sub-regions, in the metastable region (green) crystal growth is possible but nucleation occurs in the labile region (blue) at higher saturation levels. In the precipitation region (red) protein and precipitant concentrations are high enough leading to protein precipitation.

The phase diagram (Figure 7) represents the relation between protein and precipitant concentration. Supersaturated solutions are necessary to form protein crystals. Low protein and/or precipitant concentrations will cause unsaturation where no protein crystals can grow. The line separating the unsaturated region from the supersaturated region is characterized as the solubility curve. An unsaturated or metastable crystallization setup will appear clear, however, the possibility of crystal growth in the metastable region is given through seeding. Protein precipitation occurs when the protein concentration and precipitant concentration increase beyond the labile phase leading to aggregates and therefore is not useful for crystallographic studies. In the labile region crystal nucleation and initial growth occur. The protein concentration depletes during crystal formation causing a shift from the labile to the

metastable zone. Besides the precipitant (e.g. salts, PEG, jeffamine, MPD), the temperature, pH and the crystallization method itself are important factors that influence protein crystal nucleation and growth.

Hanging and sitting drop are the two most commonly used vapor diffusion methods for protein crystallization. BetP and BGT1 were crystallized using the hanging drop vapor diffusion method (Figure 8). The reservoir- and protein-solution are mixed and placed on top of the reservoir in a closed chamber. Initially, the concentration of precipitant in the reservoir is higher than in the drop, water molecules vaporize from the drop until the osmolarity of the drop and the reservoir are in equilibrium. Due to the loss of water in the drop the protein and precipitant concentration increase continuously.

Initial crystallization trials for BGT1 and BetP-ΔN_M150E (BetP-ΔN will be further named BetA) were done using commercial protein crystallization screens IndexTM, Crystal Screen™ and Crystal Screen II™ screens from Hampton, the MbClass™ and MbClass II™ screens from Qiagen, the MemStart™ and MemSyst™ screens from Molecular Dimension and the JBScreen Basic™ and JBScreen Membrane™ screens from Jena Bioscience. All screening crystallization trials were performed in 96-well sitting drop plates using the *Mosquito*TM (TTPLabtech, UK) pipetting robot. The reservoirs of the 96-well sitting drop plate were manually filled with 100 µl of crystallization solution. Typically, the crystallization drops were prepared using 400 nl of protein solution (5 mg/ml) plus 400 nl of reservoir solution. The crystallization plates were incubated at different temperatures (4 °C, 12 °C and 18 °C). Optimization of crystallization conditions for BetA_M150E were performed in pre-greased 24-well plates (Hampton Research) by hanging drop vapor diffusion at 18 °C.

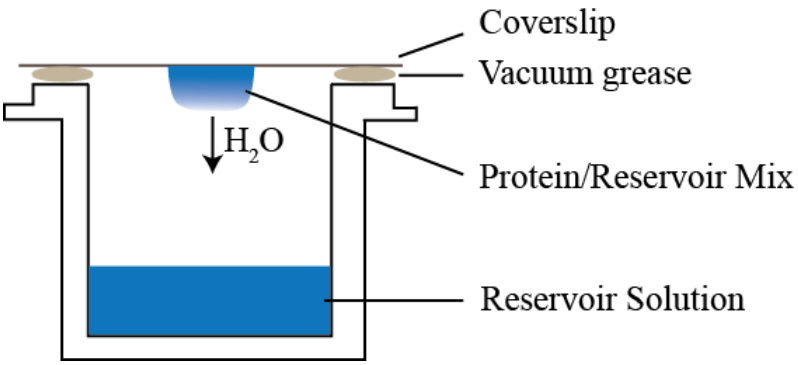

Figure 8: Schematic representation of the hanging-drop protein crystallization method.

2.7.7.2 Cryocrystallography

The main advantage of Cryocrystallography is the significant reduction in X-ray-induced radiation damage suffered by a crystal held in the high-intensity X-ray beam during data collection. Cryocrystallography is performed by holding the crystal in a constant liquid nitrogen stream at a temperature of 100 K. The diffusion of primary radicals produced by energy loss of the X-rays due to absorption in the crystal, which in turn give rise to secondary radicals, is substantially reduced at low temperatures (Garman and Doublie, 2003).

To protect the protein crystal during freezing it is transferred into a solution of cryoprotectant agents to prevent the crystal from damage caused by ordered crystalline ice formation during flash freezing. Cryoprotectant agents are water-soluble organic materials reducing the overall freezing point of the solution, preventing the formation of crystalline ice but promoting the formation of vitreous ice. Latter does not expand on formation and therefore does not damage the protein crystals (McPherson, 1999). Cryoprotectants, like PEG 400 or glycerol, penetrate into the solvent-filled channels of protein crystals (Garman and Schneider, 1997; Garman and Doublie, 2003) and interact with water molecules.

BetP and BGT1 crystals were picked with a nylon loop (LithoLoop™; Hampton Research, Molecular Dimensions) and cryoprotected with 30 – 35 % (w/v) PEG 400 buffered with Reservoir solution.

2.7.8 Data collection

Diffraction of BGT1 crystals and high-resolution data sets of BetP crystals were collected at the European Synchrotron Radiation Facility (ESRF, Grenoble, France) ID29 or at the Max-Planck beamline of the Swiss Light Source (SLS, Villigen, Switzerland) PXII. Data collection was performed under a permanent cryo-stream. Three test images were collected each 60° or 90° apart before collecting a complete data set. These three images were indexed and data collection was optimized with the program STRATEGY of the MOSFLM package (Leslie, 1992).

2.7.9 Data processing

Diffraction data were processed with MOSFLM (Leslie, 1992) or XDS (Kabsch, 1993). Data analysis was carried out in three stages: First, **Autoindexing** to get the lattice type, the crystal unit cell and crystal orientation parameters. Second, **Indexing** of all images to compare the diffraction measurements to the spots predicted on the basis of the autoindexing parameters, assign the Miller indices hkl and calculate the diffraction intensities for each spot in all the collected images. Third, **Scaling** to merge together the data of all collected images and calculate the structure factor amplitudes for each reflection (identified by the indices hkl). Beside the completeness of the data set, the signal-to-noise ratio (I/,I) as well as the Rmerge factor were used to judge data quality with the following equation:

$$R_{merge} = \frac{\Sigma_{hkl}\Sigma_i \left| |F_{hkl}| - F_{hkl}(i) \right|}{\Sigma_{hkl}\Sigma_i |F_{hkl}(i)|}$$

$|F_{hkl}(i)|$ = the value of structure factor amplitude of the i-th reflection with Miller indices hkl

$|F_{hkl}|$ = the final value of the structure factor amplitude

2.7.9.1 Correction for diffraction data anisotropy

Diffraction anisotropy is a directional dependence in diffraction quality. Diffraction anisotropy is commonly observed in protein crystallography and it is attributed to whole-body anisotropic vibration of unit cells, for example crystal packing interactions being more ellipsoidal than spherical. The directional dependence coincides with reciprocal cell directions a*, b* and c*, frequently. Anisotropy can affect the R-factors due to numerous poorly measured reflections. To overcome this problem, an ellipsoidal truncation (Strong et al., 2006) is used, by which an ellipsoidal resolution boundary on the data is imposed, in contrast to a conventional spherical boundary, so that the weak reflections falling outside the ellipsoidal boundary are removed from the data set and the refinement process. By degrading the appearance of electron density maps, anisotropy can also influence the R-factors and therefore impeding model-building attempts. Anisotropy from the data set can be eliminated by applying resolution dependent scale factors (equivalent to B-factors) through anisotropy correction algorithms to three principle directions of the data set, decreasing the magnitude of the structure factors with resolution at equal rates in all three dimensions. The magnitude of the reflections in the weakly diffracting direction is then scaled up while the magnitude of the reflections in the strongly diffracting direction is scaled down. Unfortunately, then the high-resolution reflections in the strongly diffracting direction of the crystal are diminished to the point that they contribute only little to the electron density map; hence, the lack of details in the map. To correct this problem a negative isotropic B-factor is applied to the data set to restore the magnitude of the high-resolution reflections to their original values. In the end, the electron density maps improve immensely in detail. The anisotropic data can be corrected by using the server http://services.mbi.ucla.edu/anisoscale/ (Strong et al., 2006).

2.7.10 Phasing

2.7.10.1 The phase problem

The generation of an electron density map is a critical component in crystallography. The electron density map is important since it guides the creation of the protein model. Each

diffraction spot is defined by three parameters, which need to be refined to calculate the electron density map of a protein. These parameters are the diffraction spot's index (hkl), intensity (I_{hkl}) and its phase angles (α_{hkl}) of the reflections. From a diffraction pattern only two of these parameters are measured.

The diffraction pattern is collected with the spot positions and intensities. The intensity of the spots allow for the calculation of the amplitude. From the spacing of the reflections the volume of the crystal (V_c) can be determined. The phase angles (α_{hkl}) are not recorded during crystallographic data collection. Since the phase is not determined it creates a problem, "the phase problem" in crystallography. The challenge is to reconstruct the electron density map by approximating phases.

2.7.10.2 A method to solve the phase problem

Molecular Replacement (MR):

Molecular replacement is used to solve the phase problem for an unknown structure by placing the atomic model for a related, known structure in the unit cell of the unknown structure in such a way as to best reproduce the observed structure factors. The known model, once placed, may be used to calculate phases, which in combination with the observed structure factors for the unknown structure allow the model to be rebuilt and refined. The calculation involves a 6 dimensional search over all possible orientations and translations of the known model in the unit cell of the unknown structure. This calculation is generally too time consuming to perform in full, so it is usually split into two parts:

- A 3 dimensional search over all possible orientations to determine the orientation of the model.

- A 3 dimensional search over all possible translations to determine the position of the orientated model.

Rotation:

A rotation function is used to find the correct orientation of the model in the crystal lattice. This may be achieved by testing the agreement between the Patterson functions calculated from the model and from the data at various relative orientations. The rotation function can be thought of as a convolution in a rotational space. At the relative orientation that superposes the model onto the crystal, the product of the two Patterson functions - which are maps of interatomic vectors - should have a large value. The usual way to compute the rotation function is by a fast Fourier method (Crowther, 1972).

Translation:

A translation function places the oriented molecule in the asymmetric unit in such a way as to give the best fit to the observed data. It is typically performed by Fourier methods. The signal from the translation function is generally stronger than from the rotation function. Therefore it may be necessary to take multiple rotation function solutions and attempt to perform a translation function for each, using the results of the translation function to identify the correct rotation function result. This process is automated in modern molecular replacement software. The dimensionality of the translation search may depend upon the space-group. In the case of several molecules in the asymmetric unit, locating the first copy fixes the origin and subsequent translation searches must be over the entire unit cell. The structure solved in this work was determined by applying MR using as search model the BetP structure with pdb code 4c7r and the program PHASER (McCoy et al., 2007) was used.

2.7.10.3 Structure refinement

Model building and model refinement is a repetitive interactive process of building an atomic model based on an electron-density map. After every cycle refining the structure using the refined phase angles as a basis for calculating a new electron density map and building a new model. The $2F_{obs}$ - F_{calc} Fourier coefficient amplitudes map displays the atomic model with normal weights and indicates errors in the model by its contribution of the difference Fourier map (Messerschmidt, 2007). The electron density map is improved in such a way that amino acid side chains can be correctly assigned through repetitive cycles of model building and/or

model refinement. To minimize the difference between the calculated and observed structure factors the parameters of the initial model (x, y, z coordinates, overall and/or individual atomic displacement parameter (B-factor), scaling factor) are adjusted. The quality of the crystallographic model can be estimated from the crystallographic R-factor (Drenth, 2007). Geometric and stereochemical restrains (bond length, bond angles and dihedral angles) are applied to the structural model during refinement. The Ramachandran plot (Ramachandran et al., 1963) is used to verify the conformation of the main chain folding in which the dihedral angles Φ and Ψ are plotted against each other for each residue. The angles are correct when they lie in the energetically favored regions of secondary structures such as α-helices, β-sheets and defined turn structures (Messerschmidt, 2007). The BetP mutant structure was refined with iterative cycles of manual rebuilding of each polypeptide chain using the program COOT (Emsley and Cowtan, 2004), coordinates and isotropic B-factor were refined using the program PHENIX (Terwilliger et al., 2008). Validation of the final models was performed using the server MolProbity (Chen et al., 2010).

2.7.10.4 Figures of structures

Figures of protein structures were generated using the program PyMol (DeLano, 2002). Superpositions were carried out with the SSM or LSQ (Krissinel and Henrick, 2004) superposition routine of COOT (Emsley and Cowtan, 2004).

3 Results

3.1 Expression of BGT1 for functional studies

3.1.1 Expression of BGT1 in MDCK cells

Renal BGT1 was originally cloned from Madin-Darby canine kidney (MDCK) cells (Uchida et al., 1993a). MDCK cells and stably transfected MDCK cells with BGT1 cloned into pEGFPC3 vector resulting in an NH_2-terminal EGFP tag (EGFP_BGT1) were kindly provided by Prof. Dr. Kempson (Indiana University, Indianapolis, USA).

For localization studies MDCK cells were either maintained in isotonic or exposed to hypertonic medium (500 mosmol/kg) for 24 hours to induce BGT1 insertion into the plasma membrane (Uchida et al., 1993b; Kempson et al., 2003).

Immuno-blotting against GFP allowed comparing the expression of EGFP_BGT1 protein exposed to isotonic (Iso) and hypertonic (Hyp) growth medium for 24 h and demonstrated an increase in abundance after 24 h of hypertonic stress (Figure 9 A). Under isotonic conditions EGFP_BGT1 fusion protein was restricted to compartments in the cytoplasm (Figure 9 B). In contrast, under hypertonic conditions it can be assumed that BGT1 is primarily inserted into the plasma membrane (Figure 9 C) to provide up-regulated betaine transport (Kempson et al., 2003).

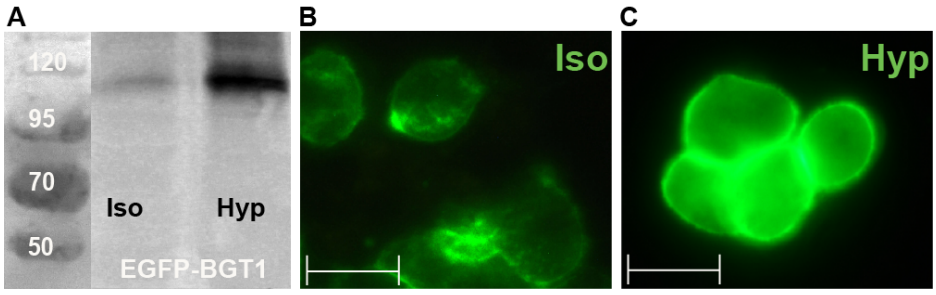

Figure 9: Western blot and Fluorescence microscopy of EGFP-BGT1 expression in MDCK cells. (**A**) Western blot of MDCK cell lysates expressing EGFP-BGT1 exposed to iso- (Iso) and hypertonic (Hyp) growth medium reveals a single band of the WT protein at 120 kDa accounting for the 27 kDa EGFP-tag (WT_{EGFP}) and resulting in an increase in protein expression during hypertonicity. Fluorescence microscopy of MDCK cells under iso- (**B**, Iso) and hypertonic (**C**, Hyp) conditions (24 hours) expressing WT_{EGFP} demonstrates a clear subcellular distribution to the plasma membrane under hypertonicity. (Scale bar: 20 µm).

3.1.2 Expression of BGT1 in *Xenopus laevis* oocytes

Wild type (WT) BGT1 cDNA was cloned into pTLN Vector (gift from Prof. Bamberg group, department of Biophysical Chemistry, Max Planck Institute of Biophysics) with XbaI and XhoI restriction sites (see Table 2.4.3).

PCR was carried out as described in material and methods (chapter 2.5.1). Positive clones were verified by restriction with the corresponding enzymes used for cloning. The correct insertion and sequence of each construct was confirmed by DNA sequencing. *pTLN-BGT1* was further linearized using *MluI*. Linearized DNA was then purified with High Pure PCR Product Purification Kit (Roche) and concentrated up to 25 µg for in vitro RNA-synthesis (chapter 2.5.7) using the mMESSAGE mMACHINE SP6 Kit (Ambion, USA).

WT BGT1 is detected below 70 kDa on the Western blot (Figure 10 A, WT). Cell surface expression was also assayed by immunogold-labelling of thin-sectioned *Xenopus* oocytes against a BGT1 specific antibody (Figure 10 B, WT).

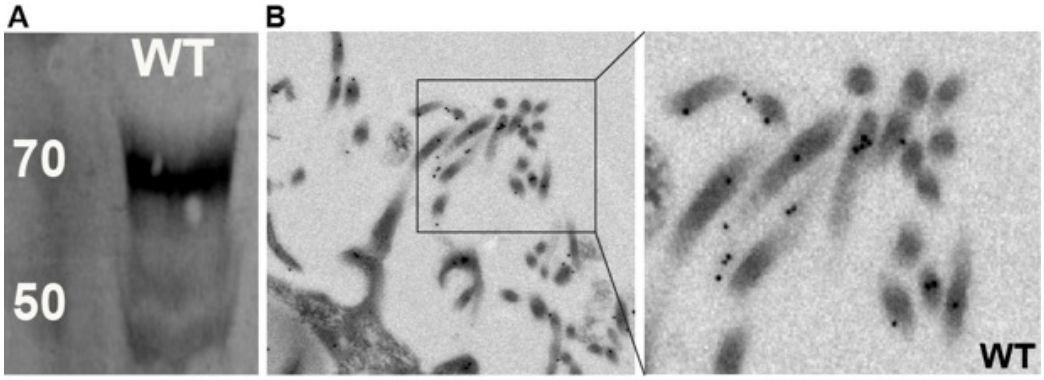

Figure 10: Western blot and Immunogold-labelling of BGT1 expression in *Xenopus* oocytes. (**A**) Western blot analysis against a α-BGT1 antibody resulted in a protein band that runs at around 70 kDa. (**B**) Immunogold labelling of thin-sectioned oocytes containing BGT1-WT reveals the abundance of the WT in the plasma membrane.

3.1.3 Regulation of BGT1

Superfusion of WT-BGT1 expressing oocytes with either 1 mM GABA or 1 mM betaine in ORi produced inward currents within the potential range between -90 and 0 mV. At −60 mV, K_M values of 0.020 ± 0.003 mM for GABA (5 oocytes from 4 donors) and 0.18 ± 0.05 mM for betaine (3 oocytes from 3 donors) were calculated by SigmaPlot using least square fit analysis (Figure 11). These data confirm previous reports (Yamauchi et al., 1992; Matskevitch et al., 1999) that WT-BGT1 has an apparent affinity for GABA that is 10-fold higher than the affinity for betaine.

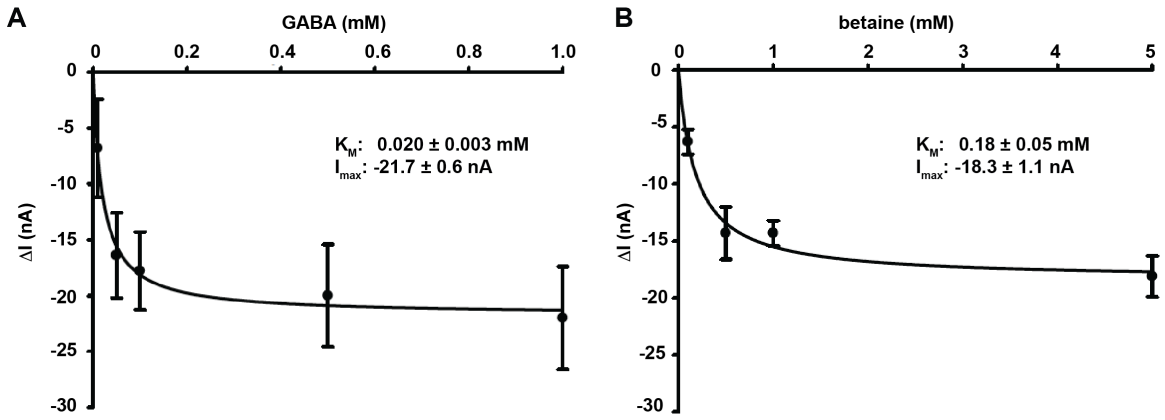

Figure 11: GABA- and Betaine-dependent currents in oocytes expressing WT-BGT1. (**A**) GABA-associated currents, measured at -60 mV were plotted as a function of the applied GABA concentration. (**B**) Betaine-associated currents, measured at -60 mV were plotted as a function of the applied betaine concentration. Data represent mean values of 5 oocytes from 4 donors and 3 oocytes from 3 donors, respectively.

3.1.3.1 PKC-dependent transporter down-regulation

Cellular kinases and phosphatases are suggested to regulate SLC6 transporter expression, activity, trafficking and degradation. Specific phosphorylation sites within this family have not been identified although SLC6 transporters are known as phosphoproteins. Both, the N- and C-terminal domains comprise a number of kinase consensus sequences as the N-terminus integrates input signals provided by regulatory modifications such as phosphorylation (Figure

13 A) and the C-terminus contains, besides phosphorylation sites (Figure 13 A), sequence elements that allow for docking of components of the ER-export machinery.

The N- and C-terminal domains of BGT1 were modeled in collaboration with Dr. Lucy Forrest and Dr. Cristina Fenollar-Ferrer (Computational Structural Biology Group, MPI of Biophysics) using the Rosetta software (Kaufmann et al., 2010) to get folded conformations.

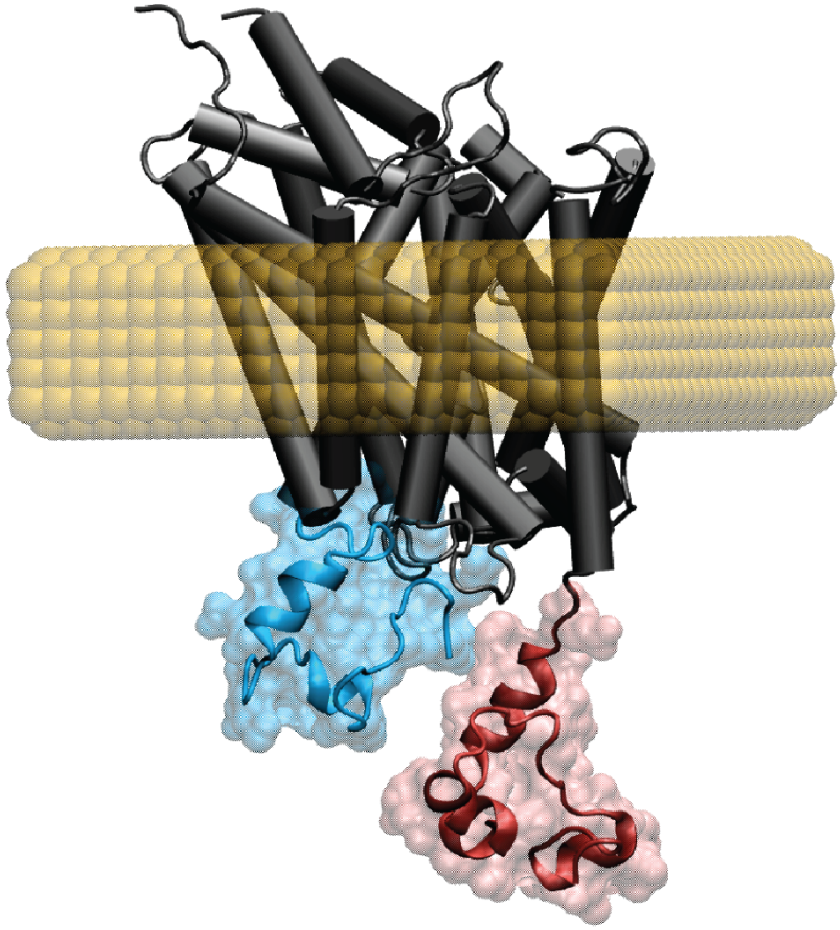

Figure 12: Homology model of BGT1 embedded in a membrane with N- and C-terminal domains facing the cytoplasm. The model was made with the structure of LeuT (pdb code: 2A65) used as a template. The N- and C-terminal domains (colored in blue and red, respectively) were modeled with Rosetta. This program uses the abinitio-folding approach, so that the structure can directly be obtained from the sequence without using any template. (Kindly provided by Dr. Cristina Fenollar-Ferrer, Computational Structural Biology Group, MPI of Biophysics).

The amino acid sequence of BGT1 includes amongst others consensus sequences for phosphorylation by protein kinase C (PKC) in its N- and C-terminal domain raising the possibility that although transcription is the major site of regulation that results in modification of BGT1 activity in response to changes in tonicity, more rapid post-translational regulation may be mediated by changes in the activity of PKC.

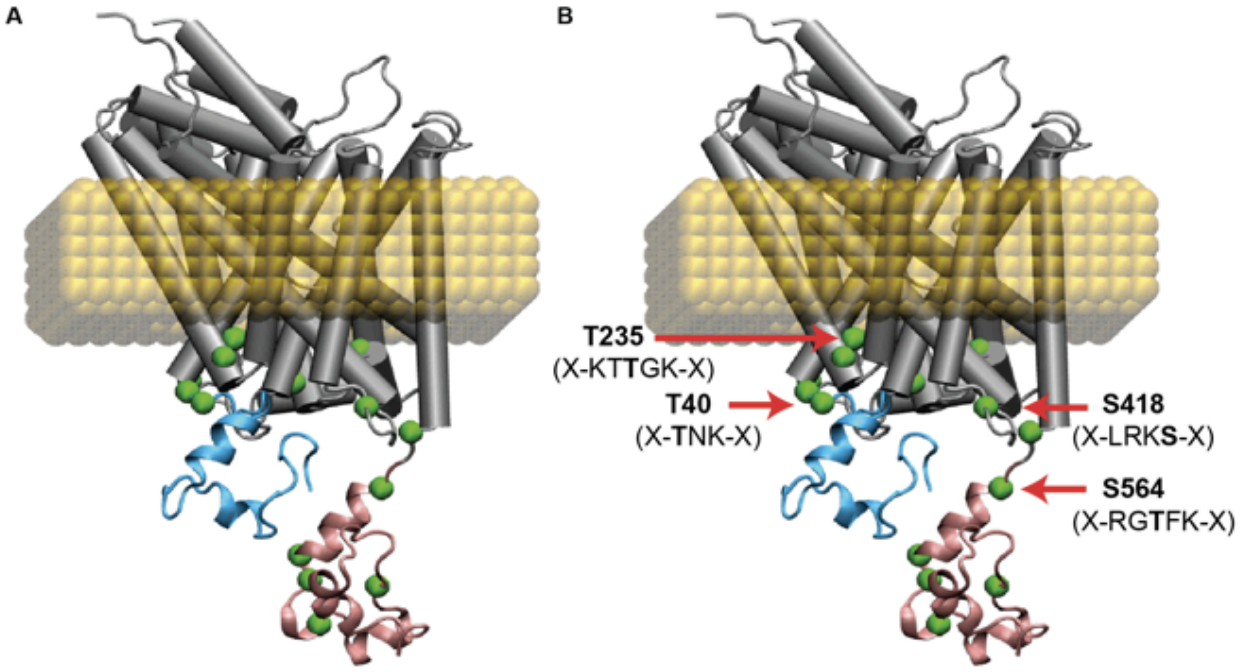

Figure 13: Potential phosphorylation sites in the terminal domains of BGT1. (**A**) Overview of potential phosphorylation sites marked as green dots in the homology model of BGT1 based on the LeuT structure (pdb code: 2A65). (**B**) Four potential phosphorylation sites, T40, T235, S418 and S564, are highly conserved across species and were mutated to alanine. Images were kindly provided by Dr. Cristina Fenollar-Ferrer, Computational Structural Biology Group, MPI of Biophysics).

BGT1 phosphorylation on serines and threonines accompanied by internalization of BGT1 from the plasma membrane was reported previously in response to PKC activation in MDCK cells (Massari et al., 2005).

In *Xenopus* oocytes GABA-associated currents were sensitive to the PKC activators PMA (phorbol 12-myristate 13 acetate) and a diacylglycerol analog DOG (dioctanoyl-*sn*-glycerol). Significant inhibition of GABA-associated currents occurred after a 30 minutes preincubation of the oocytes in ORi containing 5 µM DOG (Figure 14 A). Extending the incubation time to

60 minutes did not enlarge the effect. DOG had no effect on the currents in mocks (Figure 14 A). At −60 mV, the GABA-mediated currents decreased by 93.6 ± 5.1 % ($p<0.01$; 7 oocytes from 3 donors). When WT-BGT1 expressing oocytes were treated for 60 minutes with 10 μM staurosporin, there was only a small, insignificant reduction in GABA associated currents compared to controls (Figure 14 B, grey column compared to black column). Application of 5 μM DOG in the continuous presence of staurosporin (Figure 14 B, white column) prevented the DOG-mediated inhibition of the current. These experiments were performed in paired experiments on 5 oocytes from 4 donors. PMA, another activator of the PKC, affected also GABA-mediated currents (Figure 14 C). At –60 mV, GABA-mediated currents decreased by 53.0 ± 19.9 % (4 oocytes from 3 donors) upon a 30 minutes incubation in 100 nM PMA. The inactive analog 4αPMA inhibited the GABA current only by 13.9 ± 4.9 % (3 oocytes from 3 donors). These observations suggest a role for PKC in mediating the down regulation of BGT1 transport by DOG and PMA.

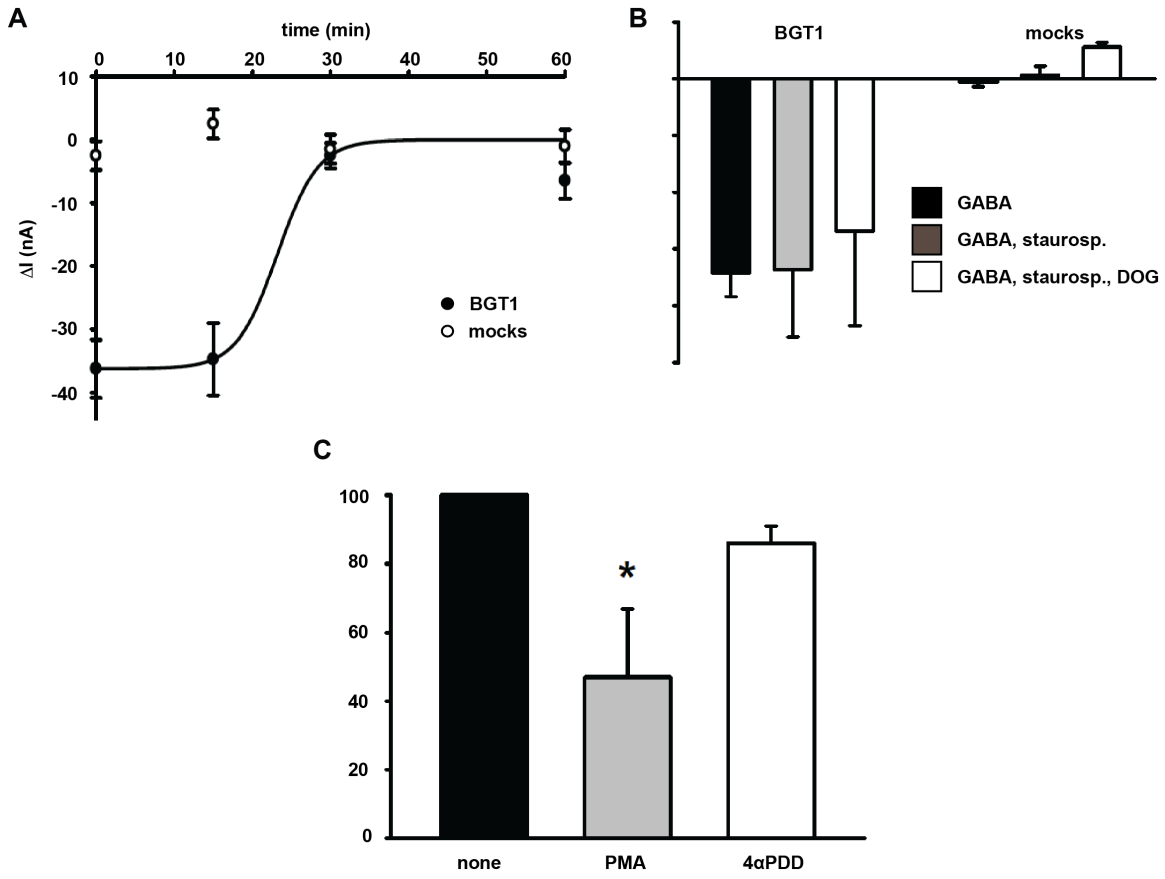

Figure 14: Effect of PKC activators and inhibitors on WT-BGT1-expressing oocytes compared to mocks. (**A**) At a holding potential of –60 mV, 5 µM DOG inhibited the GABA (1mM)-associated currents in a time-dependent manner. Data were taken from both BGT1-expressing oocytes (filled circles) and mocks (open circles) and show mean ± SD from 7 oocytes from 3 donors. (**B**) Pretreatment with 10 µM staurosporine markedly reduced the inhibitory action of DOG. GABA (1 mM)-associated currents are shown for BGT1-expressing oocytes and mocks either without treatment (black columns), after 60 min incubation in 10 µM staurosporine (grey columns), or with an additional treatment of 5 µM DOG (white columns). Data are mean ± SD from 5 oocytes from 4 donors at a holding potential of –60 mV. (**C**) A 30 min treatment with PMA but not inactive 4αPDD inhibited GABA-associated currents. GABA-associated currents in the presence of PMA (100 nM) or 4αPDD (100 nM) were expressed as a percentage of the steady state current evoked by GABA (1 mM) in the same BGT1-expressing oocyte. Whereas PMA, as observed in 4 oocytes from 3 donors, induced a significant inhibition (grey column, * $p<0.01$) of the currents, 4αPDD did not (white column) (3 oocytes, 3 donors). Currents induced in mocks were less than 5 % of those induced in BGT1-expressing oocytes and were therefore not shown.

Four potential phosphorylation sites on BGT1 (Figure 13 B) were mutated to alanine by site-directed mutagenesis. These sites are highly conserved in rat, mouse, human and dog BGT1,

based on multiple sequence alignments (http://genome.cs.mtu.edu/map.html). Single mutations were created at each site by substituting with the neutral amino acid alanine (A) in WT-BGT1.

All mutants, except mutant T40A, evoked GABA-sensitive currents comparable or even larger than the WT-BGT1 (Figure 15 A). GABA-associated currents obtained by T40A were –7.8 ± 2.2 nA (5 oocytes, 3 donors) as compared to –23.3 ± 11.8 nA (6 oocytes, 3 donors) in the wild type (Figure 15 B, black columns). These currents were inhibited by PMA (100 nM, Figure 15 B, grey columns) and the inhibition was significant for WT-BGT1 but not for T40A.

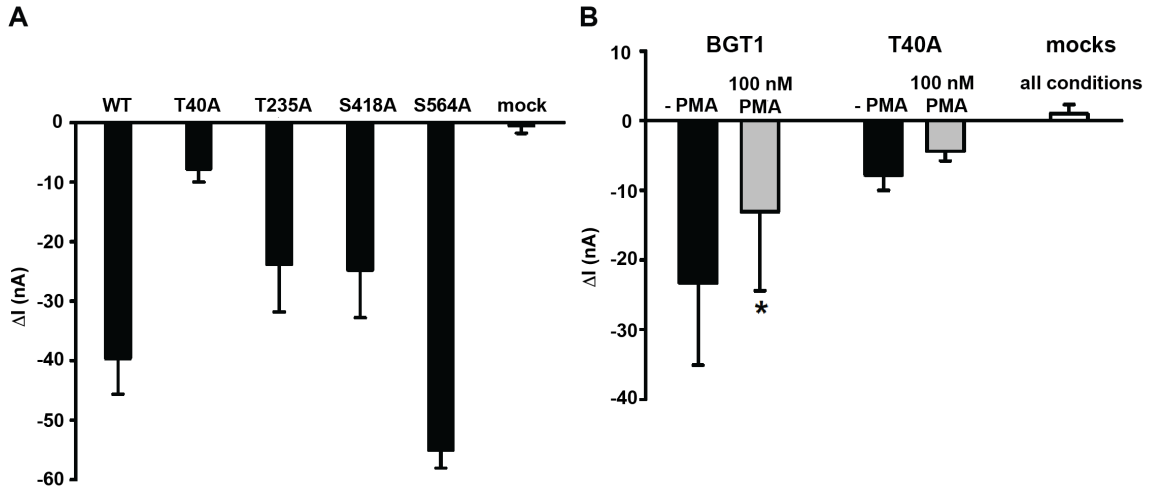

Figure 15: Effect of PMA on GABA-mediated currents in WT-BGT1 and the mutant T40A-expressing oocytes. (**A**) GABA-associated currents evoked by the wild type and mutants at –60 mV. The data represent 3 experiments. WT-BGT1 and two mutants were always expressed in the same batch of oocytes for a more precise comparison of the current amplitudes. (**B**) Currents evoked by 1 mM GABA were much larger in BGT1-expressing than in T40A-expressing oocytes. Application of 100 nM PMA for 30 min inhibited significantly the GABA-induced currents in BGT1-expressing oocytes (*$p<0.01$), but not in T40A-expressing oocytes ($p>0.10$). Data represent experiments on 6 oocytes from 3 donors for WT-BGT1 as well as for T40A.

Potential PKC phosphorylation sites were mutatetd in EGFP-tagged BGT1 as well. The mutants were characterized after expression in mammalian kidney cells to allow correlation of intracellular distribution and transport activity following adaptation to hypertonic growth medium. When expressed in MDCK cells in monolayer culture. All mutants except T40A

were localized primarily in the plasma membrane after 24 h of hypertonic stress (500 mOsm), similar to native BGT1. In contrast, the T40A mutant showed a scattered distribution in the cytoplasm, possibly in the region of the Golgi, and none was detected in the plasma membrane (Figure 16 A). Anti-GFP antibody was used for western blotting of whole cell lysates from HEK-293 cells expressing native EGFP-BGT1 or one of the mutants (Figure 16 B). These cells were used because of a much higher transfection efficiency compared to MDCK. The primary protein band was detected just below the 100 kDa marker in all mutants (Figure 16 B), identical to native EGFP-BGT1 (Kempson et al., 2003; Kempson et al., 2005). No free EGFP (26 kDa) was detected (Figure 16 B). This suggests indirectly that all mutants, including T40A, were expressed as full-length proteins.

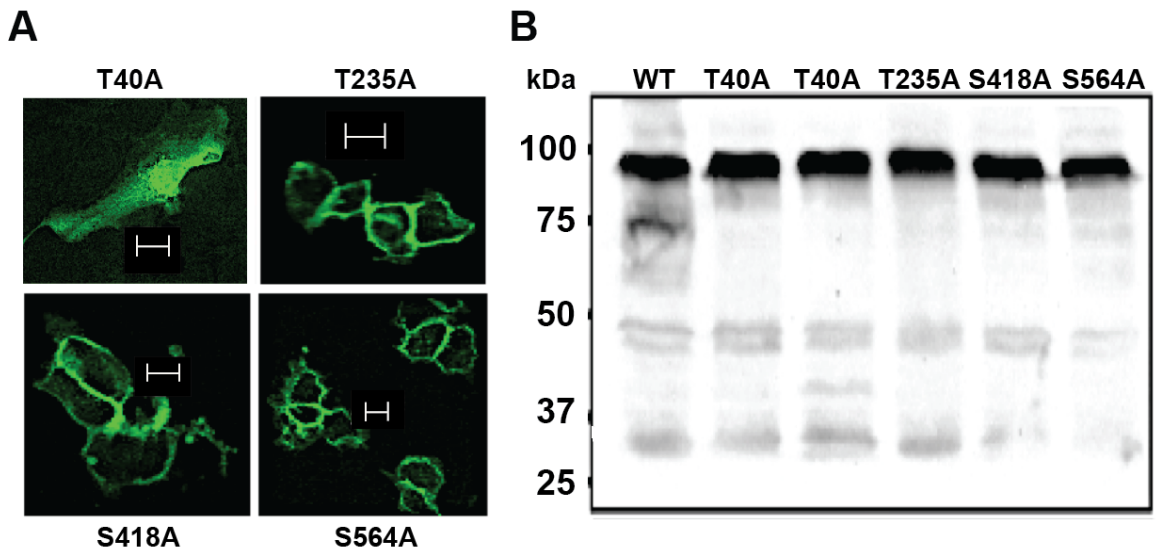

Figure 16: Expression of mutants of EGFP-BGT in MDCK cells in monolayer culture. (**A**) Following adaptation to 500 mOsm medium for 24 h confocal micrographs of live cells revealed normal plasma membrane localization of all mutants except T40A. (**B**) Western blots of whole cell lysates using anti-GFP antibody showed that all mutants had a molecular size similar to native EGFP-BGT1. (Scale bar: 20 µm). Confocal microscopy was performed by Prof. Dr. Kempson (Indiana University, USA).

The intracellular localization of T40A was confirmed after expression in polarized MDCK cells grown on permeable supports (Figure 17 A). The T235A, S418A and S564A mutants were located exclusively in the plasma membrane following 24 h incubation in hypertonic

growth medium. In contrast, T40A remained intracellular and close to the nucleus. This suggests that the cytoplasmic location observed in monolayer cultures (Figure 16 A) was not due to the lack or disorganization of basolateral protein trafficking. The response of the other mutants to PMA was tested after expression in MDCK cell monolayers followed by a 24 h adaptation period to hypertonic growth medium, as previously described (Kempson et al., 2006). Both wildtype EGFP-BGT and the mutants showed normal internalization after 45 minutes exposure to PMA. The PMA-treated cells showed clear intracellular evenly distributed fluorescence signals consistent with endocytic removal of the proteins from the plasma membrane, in contrast to untreated controls (Figure 17 B).

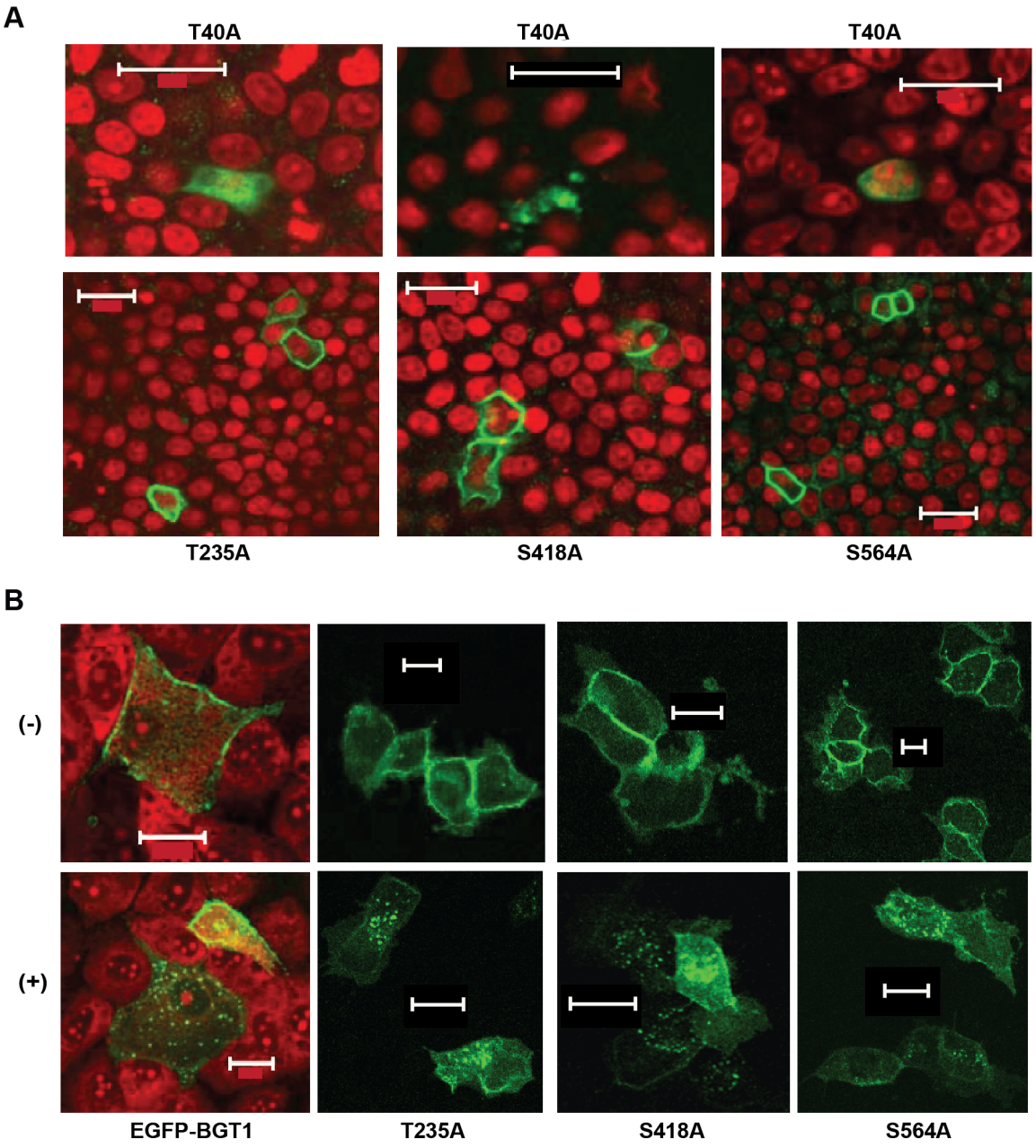

Figure 17: Distribution of WT and mutants in polarized MDCK cells following hypertonic stress and response to PMA. (**A**) In contrast to the other mutants, T40A remained intracellular (top row) in filter-grown MDCK cells during hypertonic stress (24 h), similar to the findings in monolayer culture (Figure 16 A). (**B**) Following a 24 h adaptation to hypertonic stress, treatment of monolayers with 75 nM PMA for 30 min (+, bottom row) led to an internalization of both mutants and wildtype EGFP-BGT1. Note the clear intracellular fluorescence signals compared to untreated controls (-, top row). Cells were fixed, permeabilized, and nucleic acids were stained with propidium iodide (red). (Scale bar: 20 µm). Confocal microscopy was performed by Prof. Dr. Kempson (Indiana University, USA).

EGFP-BGT and mutants were expressed in HEK-293 cells to assess functional responses to hypertonic stress and PMA. Hypertonic medium for HEK cells was routinely 400 mOsm and the treatment time was over night (16 h). These conditions did not lead to the excessive cell detachment observed at 500 mOsm during repeated washing steps performed for transport studies. Endogenous Na^+/GABA transport activity was very low in non-transfected HEK cells and in controls treated with Fugene6™ reagent only, both under isotonic and hypertonic conditions (Figure 18). Expression of wildtype EGFP-BGT and all mutants (except T40A) produced increases in GABA transport under isotonic conditions, possibly because over-expression leads to some unspecific plasma membrane localization. Adaptation to hypertonic medium increased GABA transport significantly by 3-7 fold except for T40A (black bars). The latter showed levels of transport equivalent to those in non-transfected and control cells, consistent with T40A remaining intracellular under all conditions. In short, the mutants (except T40A) showed wildtype-like upregulation of transport in response to hypertonic challenge, consistent with a predominant location in the plasma membrane (Figure 16). It was previously shown that hypertonic upregulation of transport is due primarily to redistribution of EGFP-BGT1 protein to the plasma membrane, rather than increased synthesis of EGFP-BGT1 protein (Kempson et al., 2003; Kempson et al., 2005). The response to PMA was determined in HEK cells previously adapted (16 h) to hypertonic medium, and transport activity is expressed relative to that of wildtype EGFP-BGT1 in untreated controls. This illustrates that in the absence of PMA (black bars, Figure 18 B) GABA uptake in mutant expressing cells was not significantly different from uptakes in cells expressing wildtype EGFP-BGT1. The exception was T40A, which showed only 6 % (hyperosmotic stress, no PMA) or 4 % (hyperosmotic stress, PMA treatment) of the uptake in untreated controls, compared to relative uptakes in Figure 18 A, black bars. After a 30 minutes treatment with 75 nM PMA there was significant inhibition of uptake in all mutant-groups except T40A. The degree of inhibition was similar to or exceeded 30 % inhibition observed in cells expressing wildtype EGFP-BGT1 (Figure 18 B). This proves that the mutations at T235, S418 and S564 did not interfere with the response to PMA, and strongly suggests that these may not be

important sites for phosphorylation by PKC. However, unexpectly T40 appears to play an important role in normal trafficking during hypertonic stress.

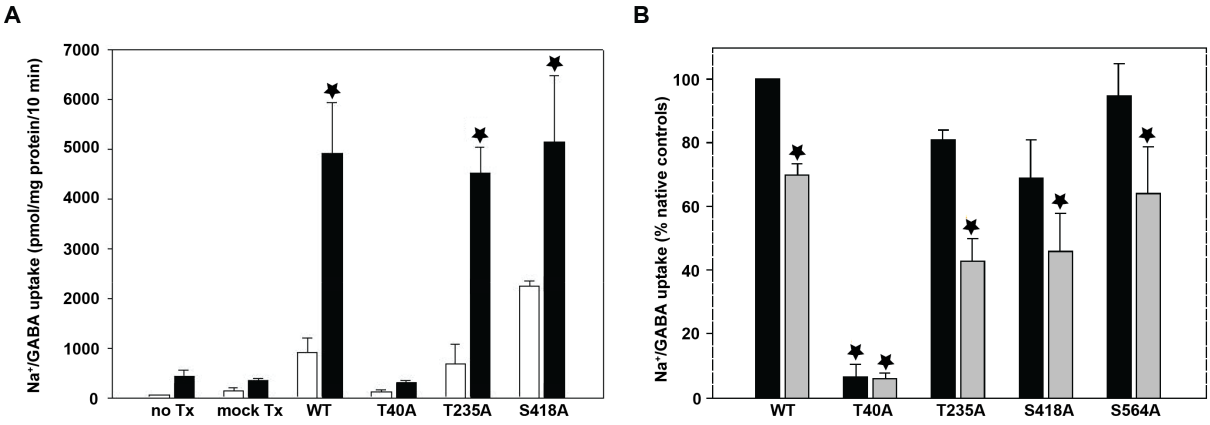

Figure 18: Na^+/GABA cotransport activity in HEK-293 cells expressing wildtype EGFP-BGT1 and mutants. (**A**) All mutants except T40A showed normal upregulation by hypertonic stress (16 h, black bars) compared to isotonic controls (open bars). Transport activity in non-transfected cells was very low. Data are mean ± SD of 3 separate experiments, ✱ $p<0.01$ compared to isotonic group. (**B**) Transport activity of wildtype EGFP-BGT and all mutants except T40A was inhibited by 30 min incubation with PMA (75 nM, grey bars). Data are mean ± SD of 3 separate experiments, ✱ $p<0.05$ compared to activity in untreated cells expressing wildtype EGFP-BGT1 (black bar). Transport studies in HEK-293 cells were carried out by Prof. Dr. Kempson (Indiana University, USA).

A phospho-specific antibody against T40 was used for defining the PKC specific interaction. This antibody detects the PKC phosphorylated T40 residue of BGT1 from a complex mixture of proteins in cells. Western blotting of whole cell lysates from HEK-293 cells expressing native EGFP-BGT1 and T40A, adapted to hypertonic medium (16 h) and treated for 1 hour with either PMA (75 nM) or DOG (5 µM) revealed that EGFP-BGT1 is phosphorylated by PKC (Figure 19 A, WT) while T40A is not (Figure 19 A, T40A).

Site-directed mutagenesis of T40 to glutamate mimics phosphorylation and restores normal function (Figure 19 B). Transport of T40E mutant is not different from wildtype BGT1 (Figure 19 B).

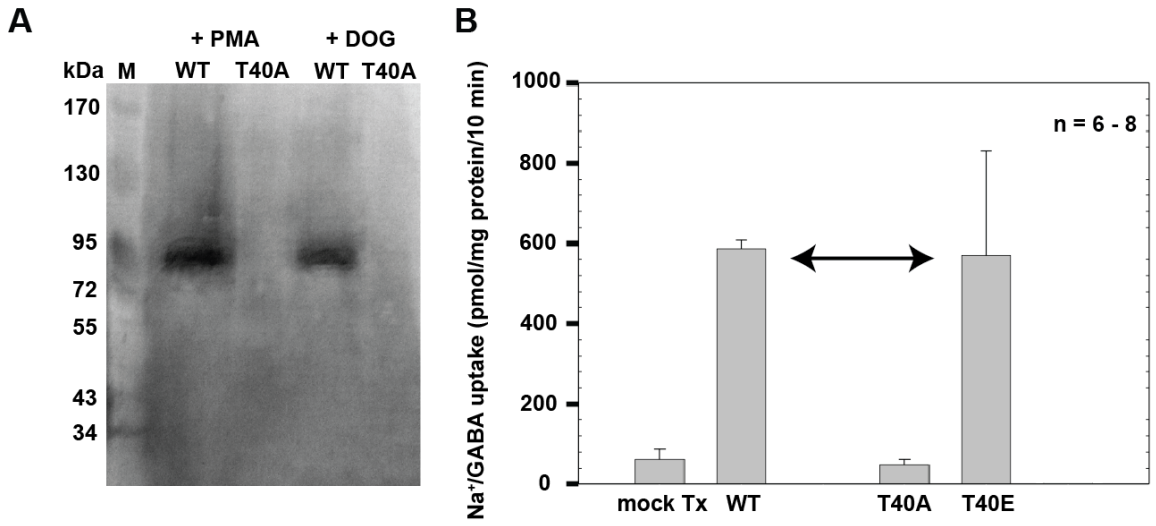

Figure 19: Phospho-specific Western blot and Na^+/GABA cotransport by HEK cells after transfection with BGT1 or mutants followed by hypertonic stress for 6 hours (450 mOsm). (**A**) Western blots of whole cell lysates using a phospho-specific antibody showed that after a 16 h adaptation to hypertonic medium and treatment with either 75 nM PMA or 5 µM DOG for 1 hour EGFP-BGT1 is phosphorylated by PKC but T40A is not. (**B**) Phosphorylation can be mimicked by substitution of T40 to glutamate and transport is similar to WT. Transport activity from T40A is not different to control mock-transfected (mock Tx) cells.

3.1.3.2 Role of *N*-glycosylation

N-glycosylation is one of the major co- and post-translational modifications of eukaryotic proteins. The majority of synthesized proteins undergo glycosylation in the rough ER (rER). The attached *N*-glycans are crucial for the functionality and structural fold of secreted membrane proteins, as some of those do not fold correctly or transport is affected when *N*-glysosylation is prevented (Stanley et al., 2009).

A multiple-sequence alignment of representative NSS transporters (Figure 20 A) reveals five distinct *N*-glycosylation sites in EL2, which are not simultaneously conserved in all members of this family. These sites are labelled according to their positions in EL2 from 1 (N-terminal) to 5 (C-terminal). There is no obvious pattern in distribution or number of sites for different branches of the NSS family. DAT contains four *N*-glycosylation sites (1, 2, 3, and 5). BGT1 is predicted to contain only two sites (Rasola et al., 1995), 3 and 5, while EL2 in other GAT

transporters accommodates site 4 in addition. In the creatine transporter CRT site 5 is missing but sites 3 and 4 are present. The taurine transporter TauT, which belongs to the SLC6 osmolyte branch like BGT1, contains sites 3 and 5, too, and in addition shares site 1 with the dopamine transporter DAT. Evidently, in all aforementioned transporters site 3, which is N171 in BGT1, is highly conserved.

According to the BGT1 homology model determined from LeuT (pdb code: 2A65) as a template, residues forming the *N*-glycosylation site 5 (Asn183-Phe184-Thr185) are located at the N-terminal end of the extracellular helical segment (Phe181-Val196) with Asn183 pointing towards Thr156 (Figure 20 C). Site 3 in BGT1 (Asn171-His172-Ser173) could not be modelled, as no equivalent region of EL2 (Ser150-Pro180) is present in the template.

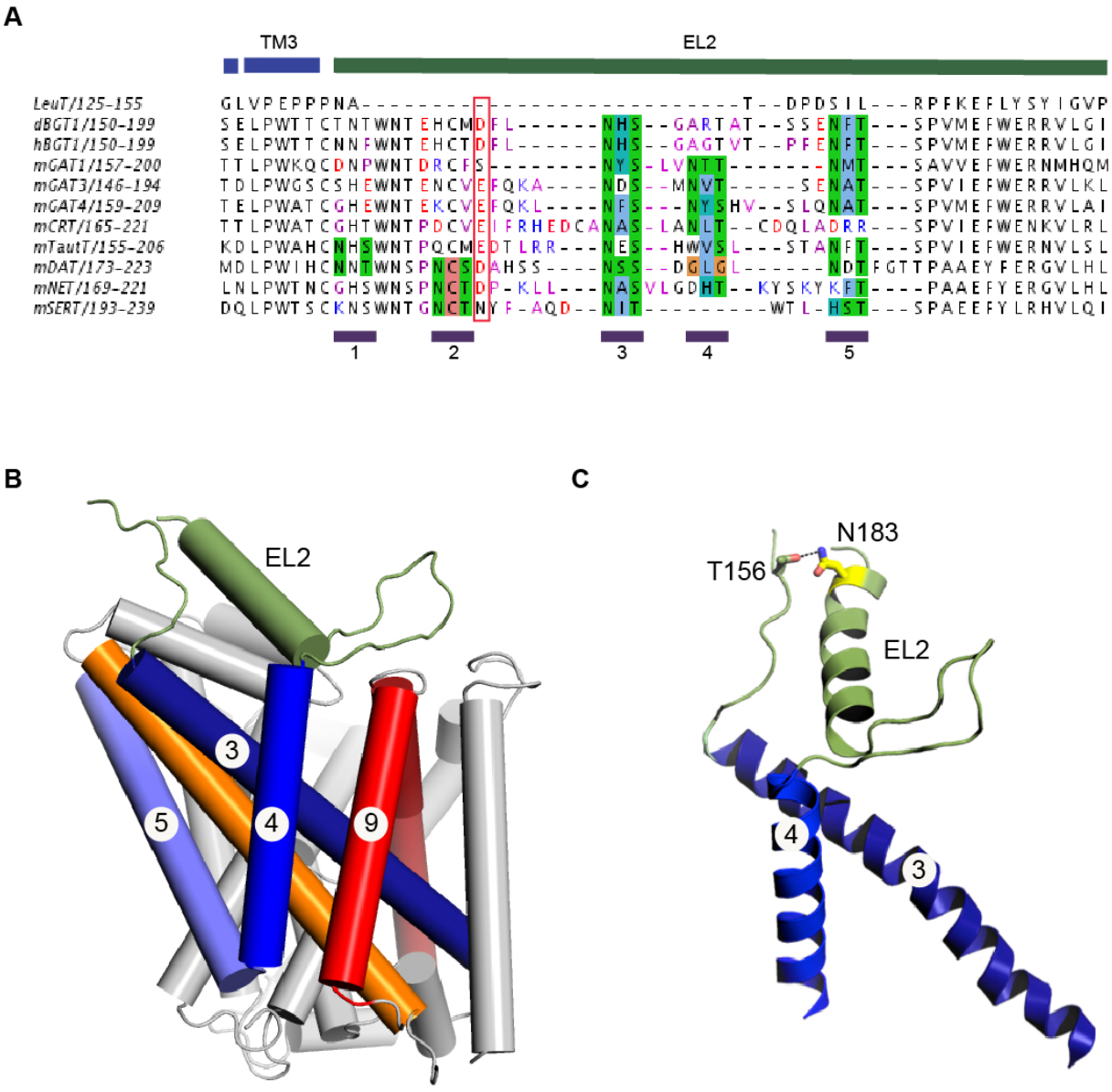

Figure 20: Homology model of the NSS family transporter BGT1 using the LeuT structure (pdb code 2A65) as template. (**A**) Sequence alignment of representative NSS family members with varying numbers of *N*-glycosylation sites in EL2. Five *N*-glycosylation sites are found in total, and are labelled as sites 1-5 (purple bars). Charged residues are colored blue and red. In purple basic, acidic and neutral amino acids are highlighted. Conserved charged residues within the family are labeled with a red box. (**B**) Homology model of BGT1 based on LeuT, shown as cartoons and viewed from the plane of the membrane, with loop EL2 in green. Specific transmembrane helices are highlighted. (**C**) Close-up view of extracellular loop EL2 and transmembrane helices 3 and 4, and glycosylation site 5, showing residues N183 (yellow) and T156 as sticks. A putative hydrogen bond is shown as a dotted line. The region between residues 159 and 179 was not modeled due to the lack of a template.

Localization and transport measurements of deglycosylated BGT1, achieved chemically, enzymatically and/or by mutagenesis, in *Xenopus laevis* oocytes were performed to compare to those of other NSS transporters (Tate and Blakely, 1994; Melikian et al., 1996; Nguyen and Amara, 1996; Li et al., 2004; Cai et al., 2005; Straumann et al., 2006). As BGT1 insertion into the plasma membrane is regulated by osmotic stress, which subsequently leads to an up-regulated substrate transport (Kempson et al., 2003), the effect of hypertonic conditions on BGT1-WT plasma membrane insertion and transport of substrate into *Xenopus laevis* oocytes were evaluated and compared to MDCK cells under the same conditions. The aim was to evaluate if BGT1 expressed in *Xenopus laevis* oocytes is processed and regulated in a similar way as BGT1 expressed in MDCK cells under the same hypertonic conditions. Oocytes were superfused with 10 mM GABA (Figure 21, black bar, 10 mM GABA), which led to inward currents of BGT1 expressing oocytes but not in water-injected control oocytes. After restoration from GABA, hypertonic conditions (455 mOsM, Figure 21, black bar, + 220 mM Sucrose)) led to inward currents in both, water-injected control oocytes (Figure 21 A) as well as in BGT1-expressing oocytes without any superfusion of substrate (Figure 21 B). Under these hypertonic conditions the effect of GABA was tested again (Figure 21, black bar, 10 mM GABA) but substrate-mediated currents in BGT1-expressing oocytes were abolished (Figure 21 B, black bars, + 220 mM Sucrose and 10 mM GABA). Applying again isotonic conditions (235 mOsM) restored the currents to values before creating osmostic stress.

However, the majority of oocytes did not survive long-term exposition (24 hours) of hypertonic conditions and therefore a putative osmotic-stress induced transport regulation was not detectable. In the following the role of *N*-glycosylation of BGT1 expressed in oocytes was investigated entirely under isotonic (ORi, 235 mOsM) conditions and these data were discussed only in the context of trafficking and transport, not in the context of regulation. The regulatory role of *N*-glycosylation was considered only when measurements were performed in MDCK cells.

The impact of *N*-glycosylation on the subcellular distribution of BGT1 in oocytes under normotonic conditions (235 mOsM) were investigated, focusing on the rough ER (rER), the trans-Golgi network (TGN) and the plasma membrane (PM). After 3 days expression, *N*-

glycosylated BGT1 is detected at ~ 60 kDa on the Western blot (Figure 21 C, WT) and is similarly distributed in all three compartments but nevertheless the main proportion is found in the plasma membrane (Figure 21 C, WT, PM). The stability and abundance of membrane-inserted BGT1 was determined after *N*-glycans were removed enzymatically by PNGase F. The loss of *N*-glycans after membrane insertion did not affect the amount of BGT1 found in the rER (Figure 21 D, WT^{+P}, rER) but led to a slightly increase in the TGN (Figure 21 D, WT^{+P}, TGN). The de-glycosylated BGT1 isoform (~ 50 kDa) is still observed in the plasma membrane without any apparent degradation (Figure 21 D, WT^{+P}, PM), implying that the remaining BGT1 fraction in the plasma membrane is stable even after removal of associated *N*-glycans though the loss of *N*-glycans leads to a partial depletion and causes internalization.

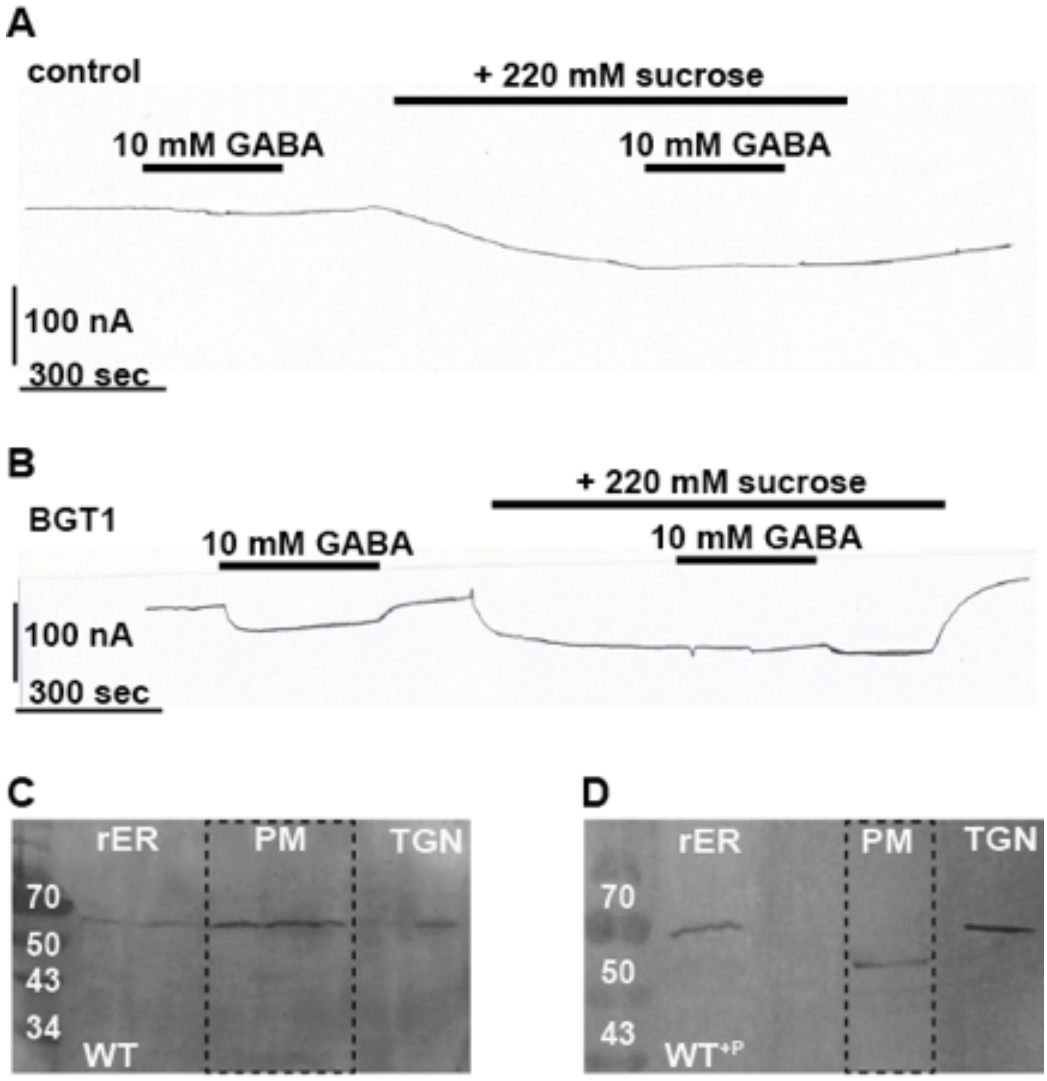

Figure 21: Response of BGT1 to GABA in the presence of hypertonic conditions and membrane distribution of *N*-glycosylated and de-glycosylated BGT1 in *Xenopus* oocytes. (**A**, **B**) Traces represent typical records as obtained on 3 oocytes from 3 different frogs. Oocytes were clamped at a potential of -60 mV and superfused with 10 mM GABA solved in ORi (black bar, 10 mM GABA). Hypertonic conditions were achieved by adding 220 mM sucrose to ORi (black bar, + 220 mM sucrose) and the effect of GABA (black bar, 10 mM GABA) was tested again. Hypertonic conditions led to inward currents in both water-injected- (**A**) as well as in BGT1-RNA-injected oocytes (**B**), but GABA-mediated currents were abolished under hypertonic conditions. (**C**) Distribution of WT and (**D**) WT^{+P} in the plasma membrane (PM), in the rough Endoplasmic Reticulum (rER) and in the trans-Golgi network (TGN) of oocytes.

Treatment of oocytes with tunicamycin during protein synthesis reveals the de-glycosylated BGT1-WT form at ~ 50 kDa on the Western blot (Figure 22 A, WT, +). The total amount of

un-glycosylated BGT1 in tunicamycin-treated oocytes appears very similar to that found in untreated cells (Figure 22 A, WT, - , +).

Both *N*-glycosylation sites in BGT1 were modified by replacing asparagine against aspartate either individually (N171D, N183D) or simultanously (NN171/183DD) to investigate them in greater detail. The expression levels for both single mutants and the double mutant is significantly reduced in absence or presence of tunicamycin (Figure 22 A, N171D, -, +; N183D, -, +; NN171/183DD, -, +).

The *N*-glycosylation site 3-mutant N171D shows a similar band shift to BGT1-WT after tunicamycin treatment (Figure 22 A; N171D, +) suggesting that *N*-glycans are attached to the remaining N183 site. Neither N183D nor NN171/183DD change electrophoretic mobility upon tunicamycin treatment (Figure 22 A, N183D, +; NN171/183DD, +) meaning that only one of the two sites, N183, contributes to the gain in molecular weight by *N*-glycosylation and that N171 is not post-translationally modified by *N*-glycans. Surprisingly, in Western blot analysis independent on tunicamycin treatment N183 mutants were always detected at the same position as *N*-glycosylated WT without tunicamycin treatment (Figure 22 A, N183D, - , +). This leads to the conclusion that also in the WT protein no *N*-glycans are associated with N171, which, although being highly conserved in the NSS family, appears to be non-glycosylated in BGT1.

NN171/183DD is enriched in the rER and undergoes some degradation in the TGN (Figure 22 B), perhaps due to a retarded targeting to the plasma membrane. Cell surface expression was also assayed by immunogold-labelling of thin-sectioned *Xenopus* oocytes against a BGT1 specific antibody (Figure 22 C, WT). Judged from the electron micrographs of thin sections the amount of N171D, N183D and NN171/183DD inserted into the plasma membrane is slightly and for the double mutant even significantly reduced (Figure 22 C, NN171/183DD). However, the fraction of NN171/183DD, which is abundant in the plasma membrane, does not show protein degradation in the Western blot analysis (Figure 22 B, PM) reflecting a stably inserted protein. The reduced membrane localization might reflect both, a decrease in the initial expression level and a specific effect on plasma membrane targeting of this mutant.

In summary, removal of the *N*-glycosylation site N183 by mutagenesis (N183D as well as NN171/183DD) results in a mutant, which is severely altered in overall expression and hence membrane abundance, but still retains its capability for membrane insertion.

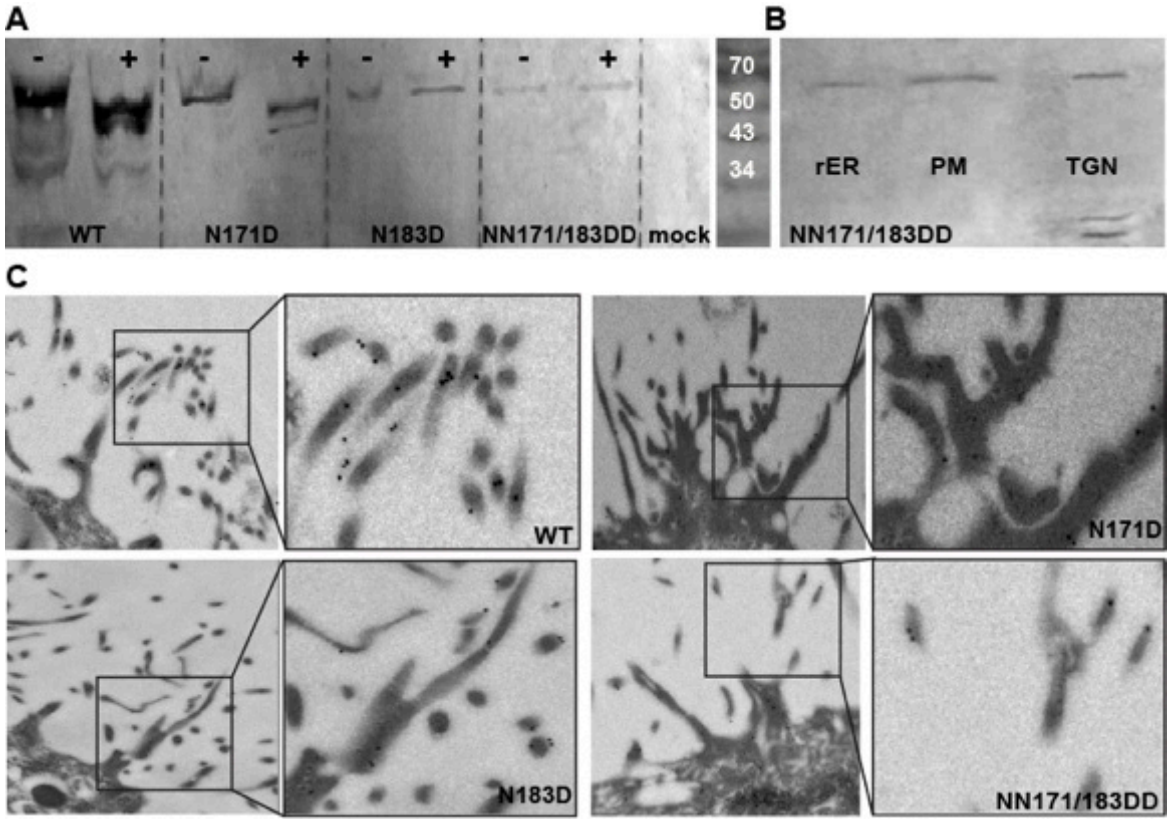

Figure 22: Expression and distribution of BGT1 and *N*-glycosylation site mutants in oocytes. (**A**) Western blot analysis using a BGT1 specific antibody on oocyte membranes containing mutants treated with (+) and without (-) tunicamycin. Treatment of oocytes with tunicamycin resulted in a 60 kDa glycosylated form (WT, -) and two un-glycosylated isoforms (WT, +) of 55 and 50 kDa. N171D treated with tunicamcyin (N171D, +) shows a shift similar to that observed for WT BGT1, with two isoforms at 55 and 50 kDa. N183D and NN171/183DD are detected at 60 kDa both with and without tunicamycin (N183D, +, -; NN171/183DD, +, -). The expression level of all, the single mutants to the point of the double mutant, is significantly reduced. (**B**) Fractionation of oocyte membranes showing the distribution of NN171/183DD in the plasma membrane (PM), in the rough Endoplasmatic Reticulum (rER) and in the trans-Golgi network (TGN), latter with minor degradation. (**C**) Immunogold labeling of thin-sectioned oocytes containing WT, N171D, N183D and NN171/183DD reveal the abundance of WT to higher amounts in the plasma membrane whereas N171D and N183D show a reduced abundance in the plasma membrane and NN171/183DD is detected only in very small amounts in the plasma membrane and stays mainly intracellular in the rER.

Functional analysis of *N*-glycosylated and de-glycosylated forms of BGT1 was carried out to shed light onto the consequences of *N*-glycan-linked EL2 on transport. GABA transport by BGT1-WT and mutants was investigated by two-electrode voltage clamp. Apparent K_M-values were determined at a holding potential of -60 mV (Table 6). The K_M of BGT1-WT for its substrate GABA is 11.7 ± 0.4 µM, which is in good agreement with a previous report (Matskevitch et al., 1999). N183D exhibits an apparent K_M value of 9.5 ± 1.2 µM for GABA, which is very close to that of BGT1-WT. The maximal inducible current of N183D is reduced by a factor of 2 accounting for the lower protein concentration in the plasma membrane. NN171/183DD substrate-associated currents were below detection limits (Table 6, NN171/183DD). Interestingly, the *N*-glycosylated N171D mutant has a significantly higher GABA affinity, which is five times higher than for BGT1-WT (Table 6, N171D).

GABA-induced currents of BGT1-WT were reduced by 80 % at -60 mV after *N*-glycosylation was prevented by tunicamycin (Table 6, BGT1-WT^{+Tun}). The apparent K_M-value also increased nearly 20-fold (Table 6, BGT1-WT^{+Tun}). Due to the apoptotic side effects of tunicamycin on all cellular components, these measurements have to be considered with caution, moreover as the amount of totally expressed BGT1 in tunicamycin-treated occytes is comparable to glycosylated BGT1-WT (Figure 22 A). Indeed, compared to *N*-glycosylated BGT1-WT only a threefold reduction in the apparent K_M was observed when *N*-glycans were removed by PNGase F after the protein was inserted into the plasma membrane (Table 6, BGT1-WT^{+P}). Therefore, chemical *N*-glycan removal in BGT1-WT by tunicamycin decreases the affinity of BGT1 for GABA and reduced GABA transport, while substitution of the *N*-glycosylation sites by charges does not alter significantly transport kinetics. Having investigated in detail the effect of *N*-glycosylation on trafficking, membrane insertion and transport its role on osmotic stress regulated membrane insertion was further examined, which is a phenomenon observed in MDCK cells. Thus, the major experiments performed in oocytes were repeated in MDCK cells for better comparison.

Table 6: Functional analysis of glycosylated, de-glycosylated and mutants of BGT1 in *Xenopus* oocytes. K_M-values and ΔI_{max} of BGT1 wildtype (BGT1-WT) expressed in *Xenopus* oocytes with and without treatment of tunicamycin ($^{+Tun}$) and PNGase F ($^{+P}$) as well as K_M-values for the single mutants (N171D, N183D) without treatment of tunicamycin and PNGase F for GABA are listed. For the double mutant (NN171/183DD) because of the low currents no K_M could be determined. Values were determined in at least three independent observations.

	$K_{M,\ -60\ mV}$ (μM)	$\Delta I_{max,\ -60\ mV}$ (nA)
BGT1-WT	11.7 ± 0.4	−47.0 ± 9.5
BGT1-WT^{+Tun}	209.0 ± 80	−10.0 ± 1.9
BGT1-WT^{+P}	29.4 ± 7.5	−16.6 ± 2.2
N171D	2.1 ± 0.5	−13.6 ± 1.1
N183D	9.5 ± 1.2	−21.1 ± 0.7
NN171/183DD	BD[a]	BD[a]

[a] Below detection (BD)

MDCK cells contain endogenous BGT1 (Kempson et al., 2003). *N*-glycosylation of N171 (site 3, Figure 20 A) and N183 (site 5, Figure 20 A) were investigated both for the endogenous form (Figure 23 A, WT_{end}) as well as for MDCK cells stably expressing BGT1 fused with an N-terminal 27 kDa EGFP-tag (Figure 23 B, EGFP-BGT1). Different to oocytes, MDCK cells were able to survive hypertonic conditions and therefore BGT1 plasma membrane insertion was induced in hypertonic medium (500 mOsM) (Figure 23 C, D, Hyp). As reported already in great detail in previous studies BGT1 is primarily inserted into the plasma membrane under hypertonic conditions (Uchida et al., 1993b; Kempson et al., 2003; Kempson et al., 2005) to provide up-regulated betaine transport (Kempson et al., 2003) and depleted and internalized under isotonic conditions (Kempson and Montrose, 2004). Endogenous BGT1 shows an electrophoretic mobility of about 90 kDa on the Western blot (Figure 23 A, WT_{end}, -), while PNGase F treated cells reveal de-glycosylated endogenous protein running at ~ 55 kDa (Figure 23 A, WT_{end}, +). *N*-glycosylation in MDCK cells seems to be more complex compared to *N*-glycosylation in oocytes. The de-glycosylated EGFP-

tagged BGT1 (EGFP-BGT1, +) was detected at a molecular weight of ~ 90 kDa accounting for the molecular weight of the 27 kDa EGFP tag, while the glycosylated form runs at ~ 120 kDa (Figure 23 B, EGFP-BGT1, -), which corresponds to a comparable shift to that of glycosylated and de-glycosylated endogenous BGT1 in MDCK cells (Figure 23 A, WT_{end}, -; WT_{end}, +).

In contrast to oocytes, which seem to withstand the apoptotic action of tunicamycin, MDCK cells were detrimentally affected by tunicamycin especially under hyperosmotic conditions. Therefore the effect of *N*-glycosylation on total expression of BGT1 in MDCK cells could not be examined in a similar way as for the oocyte expression. Consequently, the effect of *N*-glycan association on osmo-regulated insertion and depletion of BGT1 into or from the plasma membrane of MDCK cells was solely studied with PNGase F treatment (Figure 23 A, B,+ and Figure 23 D, Hyp^{+P}). After enzymatically removal of *N*-glycans, de-glycosylated BGT1 remains mainly in the plasma membrane (Figure 23 D, Hyp^{+P}) suggesting that removal of *N*-glycans does not trigger depletion of plasma membrane-inserted BGT1. Similary, as observed in oocytes, also in MDCK cells the removal of *N*-glycans from BGT1 after insertion into the plasma membrane does not seem to affect the location of the protein in the membrane as well as its stability. However, when PNGase F treated MDCK cells were exposed to isotonic medium after a hyperosmotic shock, de-glycosylated EGFP-BGT1 remains mainly in the plasma membrane (Figure 23 E, $Hyp^{+P}_{recovery}$). In contrast, EGFP-BGT1 is depleted from the membrane after hyperosmotic conditions return to normal isotonic conditions (Figure 23 E, $Hyp_{recovery}$). This happens as consequence for a down-regulation mechanism of osmoregulatory substrate transport (Kempson and Montrose, 2004). This result is the first indication that *N*-glycosylation of BGT1 in MDCK cells is involved at least in regulated membrane depletion.

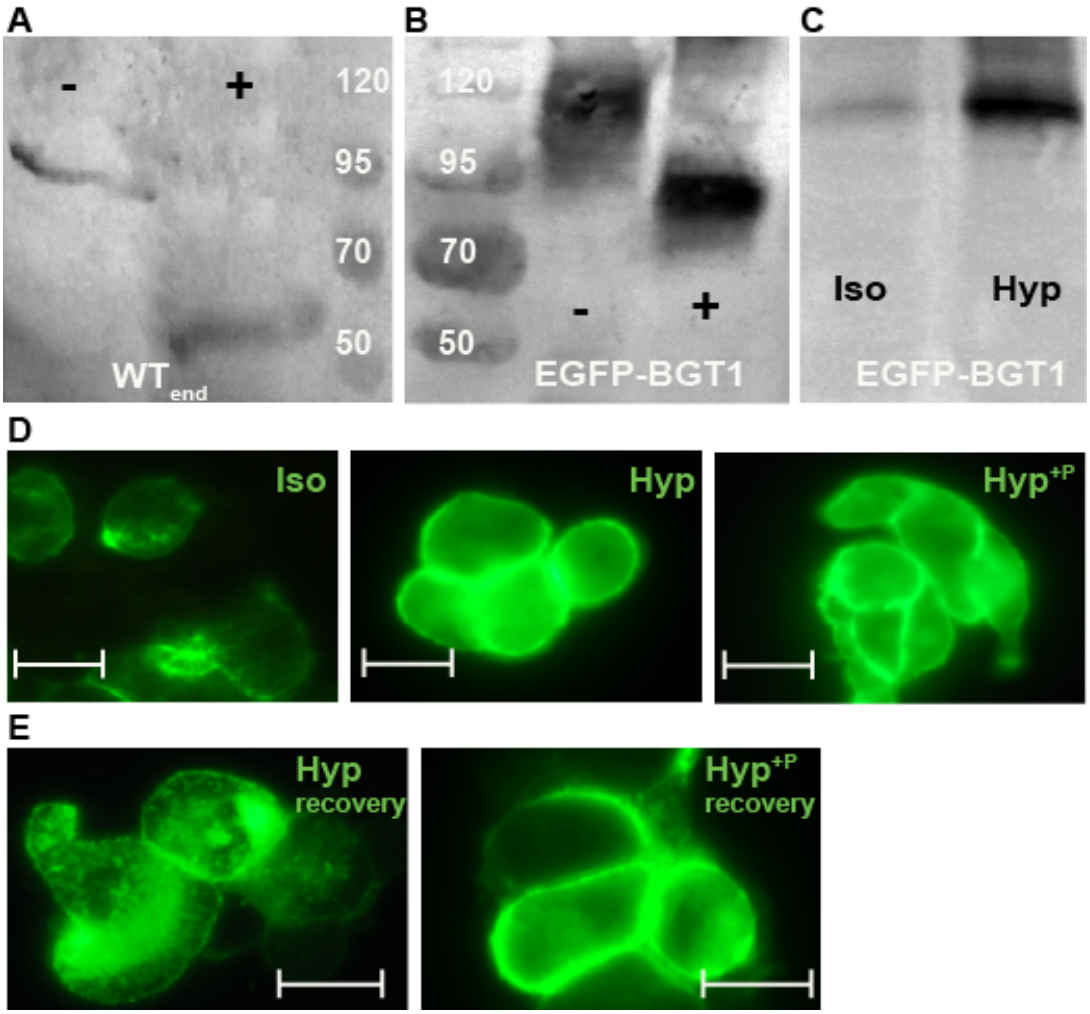

Figure 23: Plasma membrane distribution of de-glycosylated BGT1 in MDCK cells. (**A**) Western blot analysis of endogenous BGT1 (WT_{end}) before and after treatment with PNGase F (WT_{end}, +) using a BGT1 specific antibody reveal a band shift from 95 kDa (WT_{end}, -) to 55 kDa (WT_{end}, +). (**B**) Western blot of MDCK membranes stably expressing EGFP-BGT1 using a GFP-tag reveals a fully glycosylated form of BGT1 at 120 kDa accounting for the 27 kDa EGFP-tag (EGFP-BGT1, -) and a 95 kDa band of EGFP-BGT1 after PNGase F treatment (EGFP-BGT1, +). (**C**) EGFP-BGT1 exposed to iso- (Iso) and hypertonic (Hyp) growth medium resulting in an increase in protein expression during hypertonicity. (**D**) Fluorescence microscopy of MDCK cells under iso- (Iso) and hypertonic (Hyp) conditions (24 hours) expressing EGFP-BGT1 demonstrates a clear subcellular distribution to the plasma membrane under hypertonicity. The same hypertonic conditions and treatment with PNGase F for 6 hours (Hyp^{+P}) result in a partial redistribution of EGFP-BGT1. (**E**) Distribution of EGFP-BGT1 and EGFP-BGT1 treated with PNGase F for 6 hours in MDCK cells after 24 hours in hypertonic medium and then switched to fresh isotonic growth medium for further 24 hours ($Hyp_{recovery}$, $Hyp^{+P}{}_{recovery}$). (Scale bar (**D**, **E**): 20 µm)

[^{3}H]GABA uptake by endogenous BGT1 (WT_{end}) was measured in MDCK cells and K_M-values could be determined (Figure 24 A, B). The affinity of BGT1 for GABA expressed in MDCK cells was 3.4 times higher (Table 7) compared to what was detected by two-electrode voltage clamp measurements in oocytes (Table 6). After the MDCK cells were treated with PNGase F (Figure 24 A, open symbols), the apparent K_M-value was still increased by a factor of 1.3 (Table 7, WT_{end}^{+P}) compared to measurements in oocytes, indicating a smaller effect of *N*-glycosylation on BGT1 substrate affinity. However, the transport rates were reduced by a factor of 2 after PNGase F treatment (Table 7, WT_{end}^{+P}). These values were similar to the reduced maximal inducible currents measured in oocytes (Table 6).

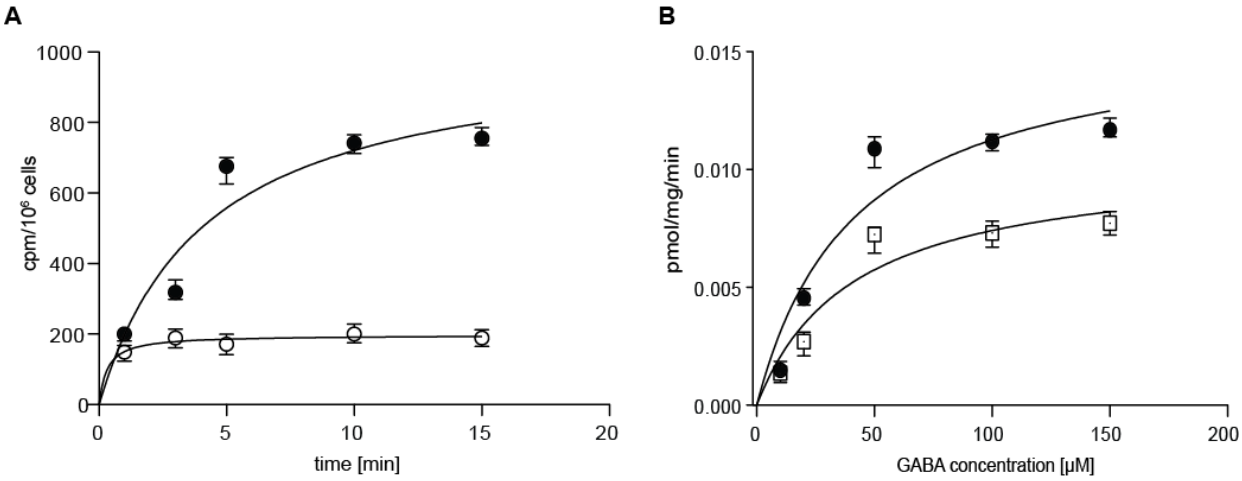

Figure 24: Activity of glycosylated and de-glycosylated endogenous BGT1 in MDCK cells. (**A**) Accumulation of [^{3}H]GABA in MDCK cells dependent on the time was measured after inducing hypertonic stress for 24h in cpm/10^6 cells (filled circles). Inhibition by NNC-5 2090 (2 µM) abolished the GABA uptake (open circles). Each point shows the average of at least five independent experiments. The error bars represent a mean ±SD of fivefold repeated measurements. (**B**) K_M-values of endogenous BGT1, WT_{end}, (filled circles) and de-glycosylated BGT1 after PNGase F, WT_{end}^{+P}, treatment (open triangles) were obtained from the uptake rates of [^{3}H]GABA in pmol per mg per min in MDCK cells. Each point shows the average of at least five independent experiments. The error bars represent a mean ±SD of five independent measurements.

Table 7: Functional characterization of glycosylated and de-glycosylated endogenous BGT1 in MDCK cells. K_M-values and v_{max} of endogenous BGT1 (WT_{end}) with and without treatment of PNGase F (WT_{end}^{+P}) of MDCK cells exposed to hypertonic conditions for 24 h. Values were determined in five independent observations.

	K_M (μM)	v_{max} (pmol/mg/min)
WT_{end}	40.3 ± 1.6	159.4 ± 3.3
WT_{end}^{+P}	55.4 ± 1.8	104.4 ± 2.1

GABA transport is slightly affected by *N*-glycosylation in both, oocytes and MDCK cells, although in both systems *N*-glycosylation is not essential for transport. In oocytes transport data revealed that the mutation N183D does affect trafficking and expression, but not essentially transport. Therefore N183D with respect to regulatory expression and plasma membrane insertion was investigated under both isotonic and hypertonic conditions in MDCK cells (Figure 25). Surprisingly, the amount of expressed and hence plasma membrane inserted N183D is not up-regulated, but strongly down-regulated under hypertonic conditions (Figure 25 A, B, Hyp). In contrast *N*-glycosylated EGFP-BGT1 behaves exactly *vice-versa* (Figure 25 C, D, Hyp). The difference in expression level of N183D might be associated with *N*-glycans at EL2, which might to be a regulatory parameter during translation, trafficking and insertion. The fact that the amount of plasma membrane inserted N183D is rigorously reduced under hypertonic compared to isotonic conditions (Figure 25) indicates that this site is majorly involved in a regulation mechanism of BGT1 in MDCK cells. The dramatic change in transcription level of N183D indicates furthermore an association with *N*-glycans at EL2 as a potential regulatory parameter during translation, trafficking and insertion.

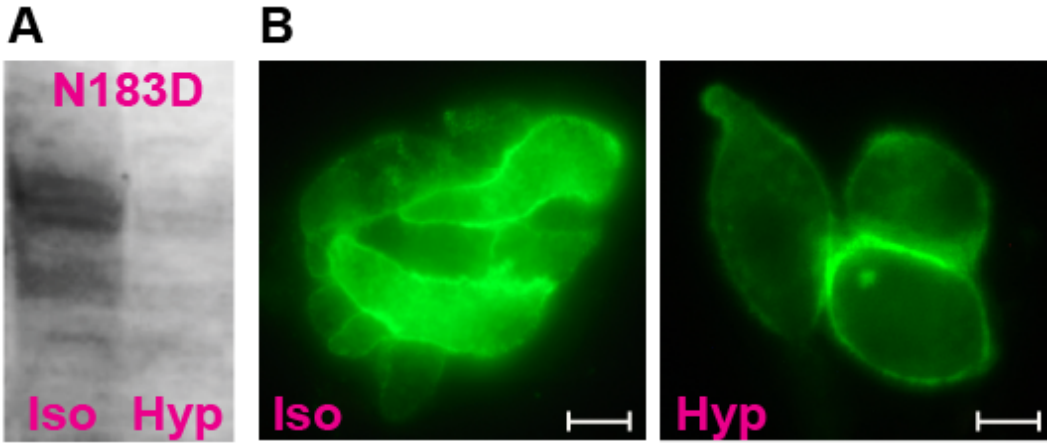

Figure 25: Expression and distribution of N183D under iso- and hypertonic conditions in MDCK cells. (**A**) Western blot analysis of N183D under iso- (Iso) and hypertonic (Hyp) conditions show a decrease in expression level during hypertonic growth conditions. (**B**) Fluorescence microscopy reveals that under isotonic conditions (Iso) N183D is located both in the plasma membrane as well as intracellular whereas under hypertonic conditions (Hyp) the overall amount of protein is strongly reduced. (Scale bar: 20 µm)

3.2 Expression of BGT1 for structural studies

With classical cell culture expression systems it is often difficult to obtain eukaryotic membrane proteins in sufficient amounts for structural studies. An initial consideration for heterologous expression is which system should be used for the production of the target mammalian membrane protein to have a good cell-surface expression and of course high levels of functional protein. To approach the best heterologous expression system for BGT1 as one individual eukaryotic membrane protein, the expression was tested in four different heterologous expression systems.

3.2.1 *In vitro* Expression of BGT1 in *E. coli*

The gene of full length native BGT1 from *Canis lupus* was cloned into the pSKB2LNB vector with an N-terminal His_6-tag (chapter 2.4.3) for *E. coli in vitro* expression.

Cell-free expression was carried out in collaboration with Stefan Haberstock (Prof. Dötsch, University of Frankfurt). Two different expression modes were tested, the **P-CF** (**P**recipitation-**C**ell **F**ree) mode, in which the protein is produced as precipitate and can be solubilized with different detergents afterwards and as a second system in the **L-CF** (**L**ipid-**C**ell **F**ree) mode where the protein is expressed in a hydrophobic environment through the addition of lipids. The extract source was from *E. coli* cells (S30 Extract).

An initial expression screen for P-CF under varying concentrations of Mg^{2+} ions within a range of 15 – 23 mM was set up to evaluate the best starting reaction conditions that were optimized in a second step (Figure 26). Western blot analysis indicates that BGT1 could be expressed in the P-CF mode with no strong dependency on Mg^{2+} ions. An intermediate concentration of 17 mM Mg^{2+} was selected for further reactions.

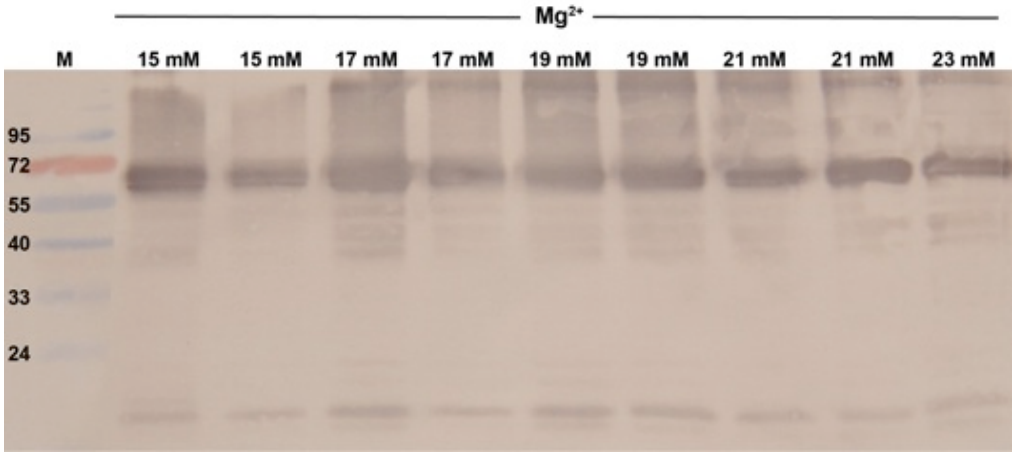

Figure 26: Western blot of BGT1 expressed in P-CF mode. Western blot analysis of BGT1 expressed in the P-CF mode with an Mg^{2+} ion concentration ranging from 15- 23 mM. BGT1 was detected as a dominant band at ~70 kDa with a BGT1-specific antibody. M: PageRuler™ Prestained Protein Ladder (Fermentas).

3.2.1.1 Solubilization and purification of BGT1

After expression in the P-CF mode, BGT1 was solubilized with 2 % LMPG, which is one of the most efficient detergents for solubilization of P-CF based expressed membrane proteins (Klammt et al., 2005). Solubilized membrane fraction was applied to the previous equilibrated Ni^{2+} column. The washing buffer (W1) contained 10 mM imidazole pH 8.0, 200 mM NaCl, 50 mM Tris pH 8, 10 % (w/v) glycerol and 0.1 % DDM (Figure 27). The protein was eluted with 250 mM imidazole pH 8.0 in the aforementioned buffer (Figure 27). Binding efficiency was not sufficient as most of the protein was found in the flow through (FTO, Figure 27) and the protein concentration of purified BGT1 was too low (45 µg) for structural analysis.

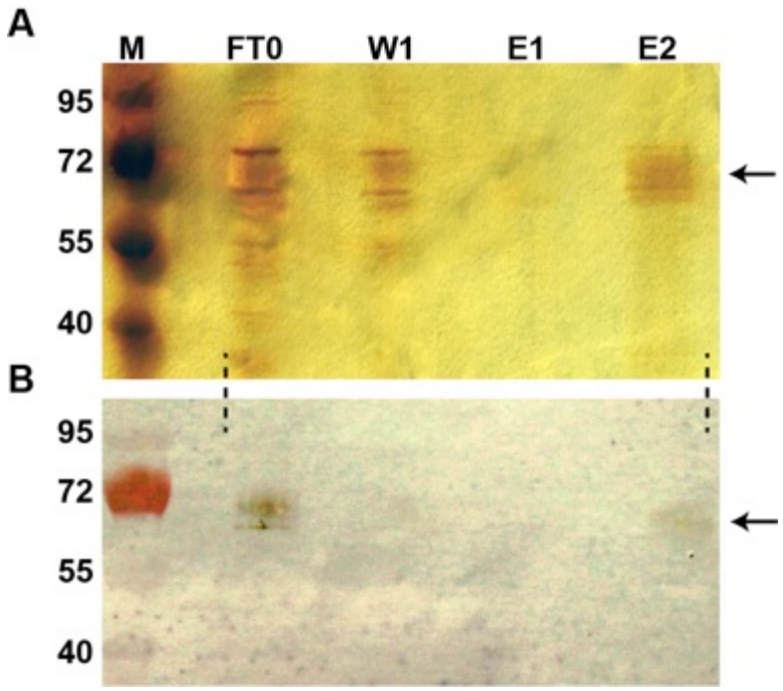

Figure 27: SDS-PAGE and corresponding Western blot of a BGT1 purification from P-CF mode. (**A**) Silver-stained SDS-PAGE and (**B**) Western blot against a BGT1- specific antibody. Native_BGT1 runs at 70 kDa (indicated by the arrow). Per lane M: Marker in kDa, FTO=: Flow through, W1: Wash1, E1 and E2: Elution fractions. M: PageRuler™ Prestained Protein Ladder (Fermentas).

An alternative option is the L-CF (lipid-based) mode, in which synthesized BGT1 has the possibility to integrate into supplemented liposomes. Different liposome mixtures were used that contained Asolectin with brain polar lipids (BPL) and DOPC with DOPE both supplemented with cholesterol (chol), DOPC alone and liver polar lipids (LPL) (chapter 2.6.8.5, Table 4) were tested in order analyze the potential incorporation by cotranslational translocation into artificial lipid bilayer (Table 8). The addition of an additional detergent (CHAPS) further simplified the solubilization of expressed BGT1 and therefore the incorporation of BGT1 into liposomes (Table 8, Figure 28).

Table 8: BGT1 expression in different liposomes mixtures in L-CF mode. 11 samples were tested with different liposomes, detergent concentrations and supplemented BGT1 DNA concentration. Positive incorporation is indicated by a checkmark.

Sample	Liposomes [mg/ml]	CHAPS [cmc]	DNA [ng/µl]	Incorporation
(Asolectin+BPL (3.5:1)), 5 % chol				
1	3	1.5	20	
2	3		20	
3	3	1.5	15	✓ (+ aggregates) Figure 28 A
4	3		15	
5	3	1.5	5	
6	3	1.5	10	✓ Figure 28 B
LPL				
7	3	1.5	15	✓ Figure 28 C
DOPC				

8	3	1.5	15	✓ (+ aggregates) Figure 28 D
DOPC+DOPE (1:1), 5 % chol				
9	3	1	15	✓ (+ aggregates) Figure 28 E
10	3	2	15	✓ Figure 28 F
11	3	3	15	✓ (+ aggregates) Figure 28 G

The L-CF-proteoliposomes were harvested by centrifugation after expression and analyzed by freeze-fracture EM. In general, samples with all tested lipids showed incorporated particles (Figure 28), while incorporation with Asolectin + BPL, 5 % cholesterol, 1.5 x cmc CHAPS and 15 ng/µl DNA (Figure 28 A), DOPC with 1.5 x cmc CHAPS and 15 ng/µl DNA (Figure 28 D) and DOPC with DOPE (1:1), 5 % cholesterol, 1 x cmc (Figure 28 E) showed most aggregates, little or no aggregation was obtained with Asolectin + BPL, 5 % cholesterol, 1.5 x cmc CHAPS and 10 ng/µl DNA (Figure 28 B), with LPL, 1.5 x cmc CHAPS and 15 ng/µl DNA (Figure 28 C) and with DOPC with DOPE (1:1), 5 % cholesterol, 2 x cmc and 15 ng/µl DNA (Figure 28 F) suggesting a correlation of supplemented detergent and DNA concentration in respect to the lipid composition. L-CF set-ups with either LPL, 1.5 x cmc

CHAPS and 15 ng/µl DNA (Figure 28 C) or DOPC with DOPE (1:1), 5 % cholesterol, 3 x cmc and 15 ng/µl DNA (Figure 28 G) showed best incorporation.

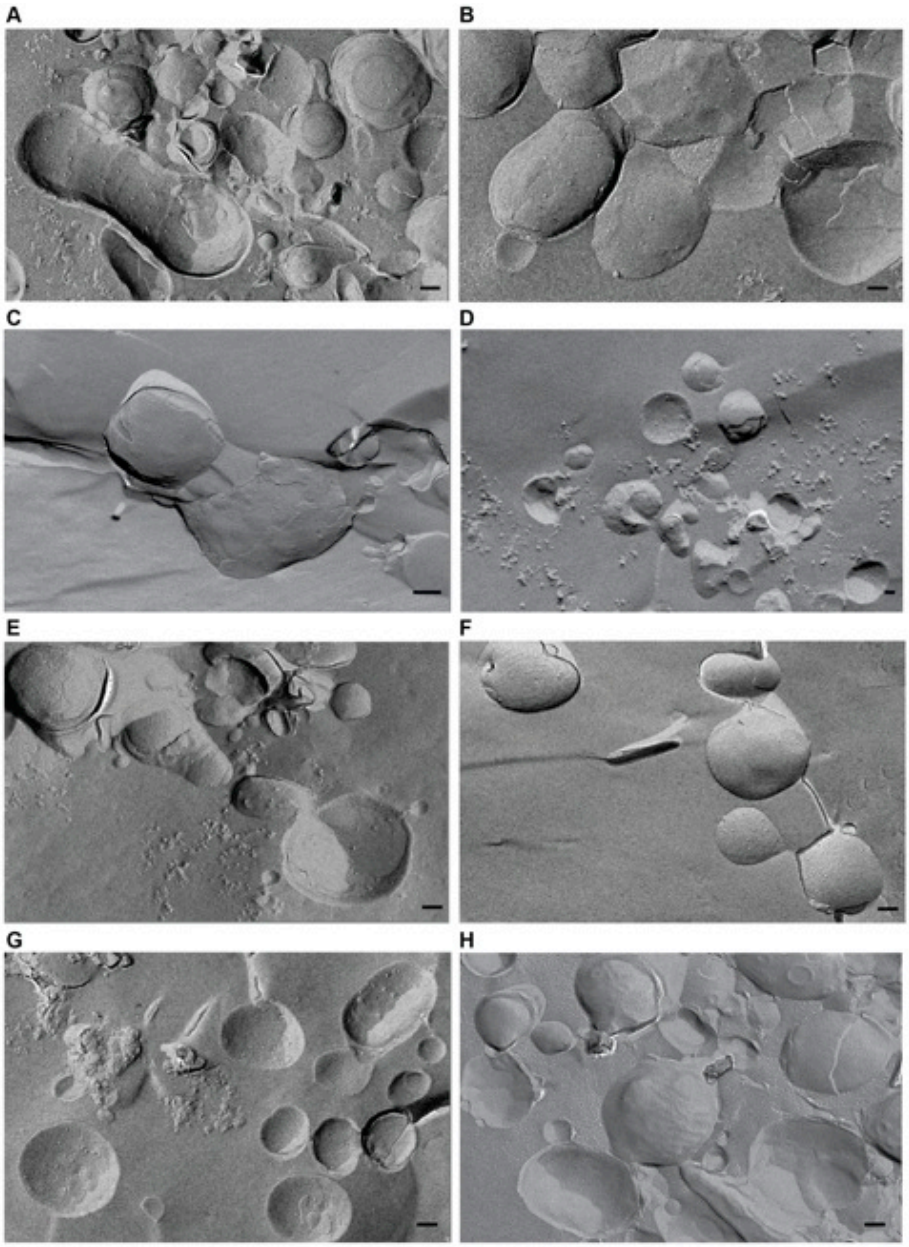

Figure 28: Freeze-fracture images of BGT1 incorporated into liposomes in L-CF mode. Incorporation was either achieved with liposomes of Asolectin and brain polar lipids (3.5:1) supplemented with 5 % cholesterol and addition of 15 or 10 ng/µl DNA (**A**, **B**), liposomes of liver polar lipids and 15 ng/µl DNA (**C**), liposomes of DOPC and 15 ng/µl DNA (**D**). In **A**-**D** the addition of CHAPS was 1.5 times the cmc. In **E**, **F** and **G** liposomes of DOPC and DOPE (1:1) supplemented with 5 % cholesterol, 15 ng/µl BGT1 DNA and 1, 2 and 3 times the cmc of CHAPS, respectively, are shown. As negative control the same experimental setup as shown in (**E**, **F** and **G**) without the addition of any DNA template was used (**H**). (Scale bar: 100 nm).

Sample 11 (Table 8 and Figure 28 G) was used for uptake measurements with [^{3}H]GABA. The protein concentration was around 0.03 mg/ml determined by the Amido Black method (chapter 2.6.7.3). BGT1 retains some degree of functionality (Figure 29, filled circles) in comparison to the control of empty liposomes produced in L-CF mode without added DNA template (Figure 29, filled squares) but the signal was too weak for more detailed analysis, like K_M measurements. This is probably due to improper post-translational modification, which does not take place in the *in vitro E.coli* expression system. Furthermore, there is even no machinery for post-translational modification of eukaryotic proteins in *E.coli* cells and it is no native environment present to regulate proper maturation of the osmoregulated protein.

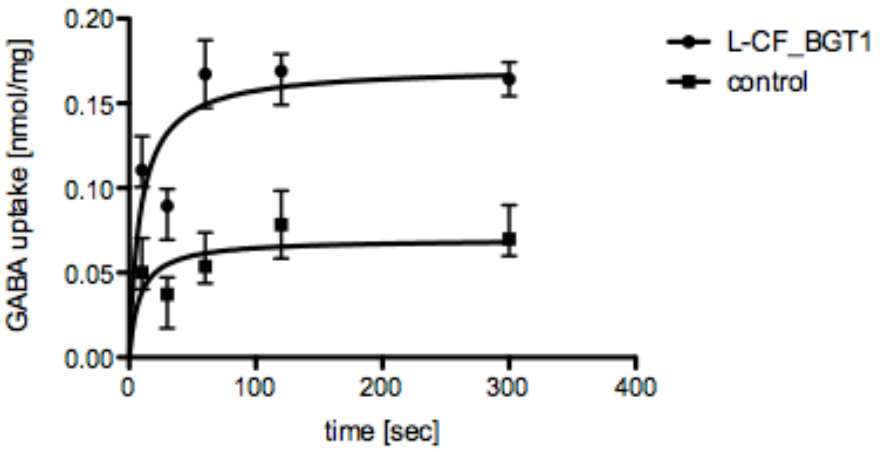

Figure 29: Activity of BGT1 expressed in *E. coli* L-CF mode. Accumulation of [^{3}H]GABA of BGT1 expressed in L-CF mode measured over time (filled circles). Empty liposomes were used as a control (filled squares). Each point shows an average of at least three independent experiments. The error bars represent a mean ±SD of threefold repeated measurement.

3.2.2 Expression of BGT1 in fly eyes of *Drosophila melanogaster*

Expression of BGT1 (BGT1_Dm) in the eyes of transgenic flies was carried out in collaboration with Dr. Valerie Panneels (Prof. Dr. Sinning, Biochemistry Center, Heidelberg University).

The gene of full length native BGT1 from *Canis lupus* was cloned into the pET28a vector used as a transfer vector (chapter 2.4.3) and was then sub-cloned into the pUAST vector (Prof. Dr. Sinning, Biochemistry center, Heidelberg university) for expression in the eyes of *D. melanogaster*. Expression and membrane preparation were performed by Dr. Valerie Panneels (Figure 30).

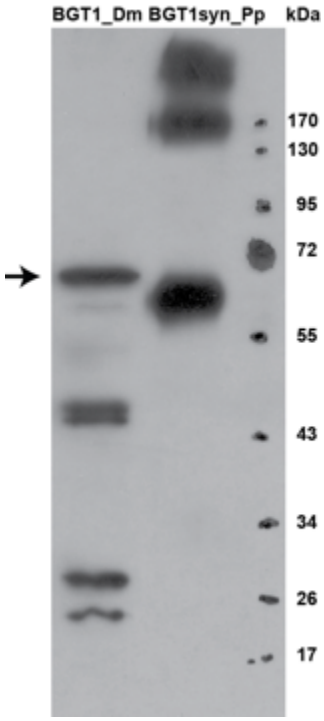

Figure 30: Western blot of BGT1 membranes expressed in fly eyes of *Drosophila melanogaster*. BGT1 (indicated by the arrow) runs at 70 kDa (BGT1_Dm). As a control BGT1syn expressed in *P. pastoris* (chapter 3.2.4, BGT1syn_Pp) was loaded, too. (Western blot analysis was carried out by Valerie Panneels, 1st antibody against BGT1, 2nd antibody conjugated with horseradish peroxidase). M: PageRuler™ Prestained Protein Ladder (Fermentas).

3.2.2.1 Solubilization and purification of BGT1_Dm

2.6 ml of *D. melanogaster* membranes with a concentration of 10.6 mg/ml were diluted to 4 mg/ml and solubilized with 2 % DDM for 1 hour on ice while stirring. After solubilization, the solubilized membrane fraction was applied on a pre-equlibrated Ni^{2+} column. The column was washed several times. The protein was finally eluted from the Ni^{2+} column with 250 mM imidazole pH 8.0 (Figure 31 A). BGT1 seems to form oligomers after expression; a monomeric and a dimeric form are detectable in Western blot analysis (Figure 31 A). Elution fractions E1 and the pooled fractions E2 to E4 were analyzed for *N*-glycosylation via PNGase digestion (Figure 31 B). For a portion of the protein detected at ~ 50 kDa in the flow through, the three washing steps and in E1 remained unclear if it was indeed BGT1 or unspecific binding of the BGT1-antibody to a different protein. Elution fraction E1 was treated with PNGase F as well. For the pooled elution fractions E2-E4 a clear band shift was detected for both the monomeric (Figure 31 B, Mon/Mon*) and the dimeric (Figure 31 B, Dim/Dim*) form and a second band below the monomer band appeared after PNGase F treatment, which could correspond to the un-glycosylated core-protein. This band is the pre-dominant band in the E1 fraction, in which this core-protein is mostly abundant. The part of the protein that does not bind to the Ni^{2+} column (Figure 31 A) seems to be the core-protein of BGT1.

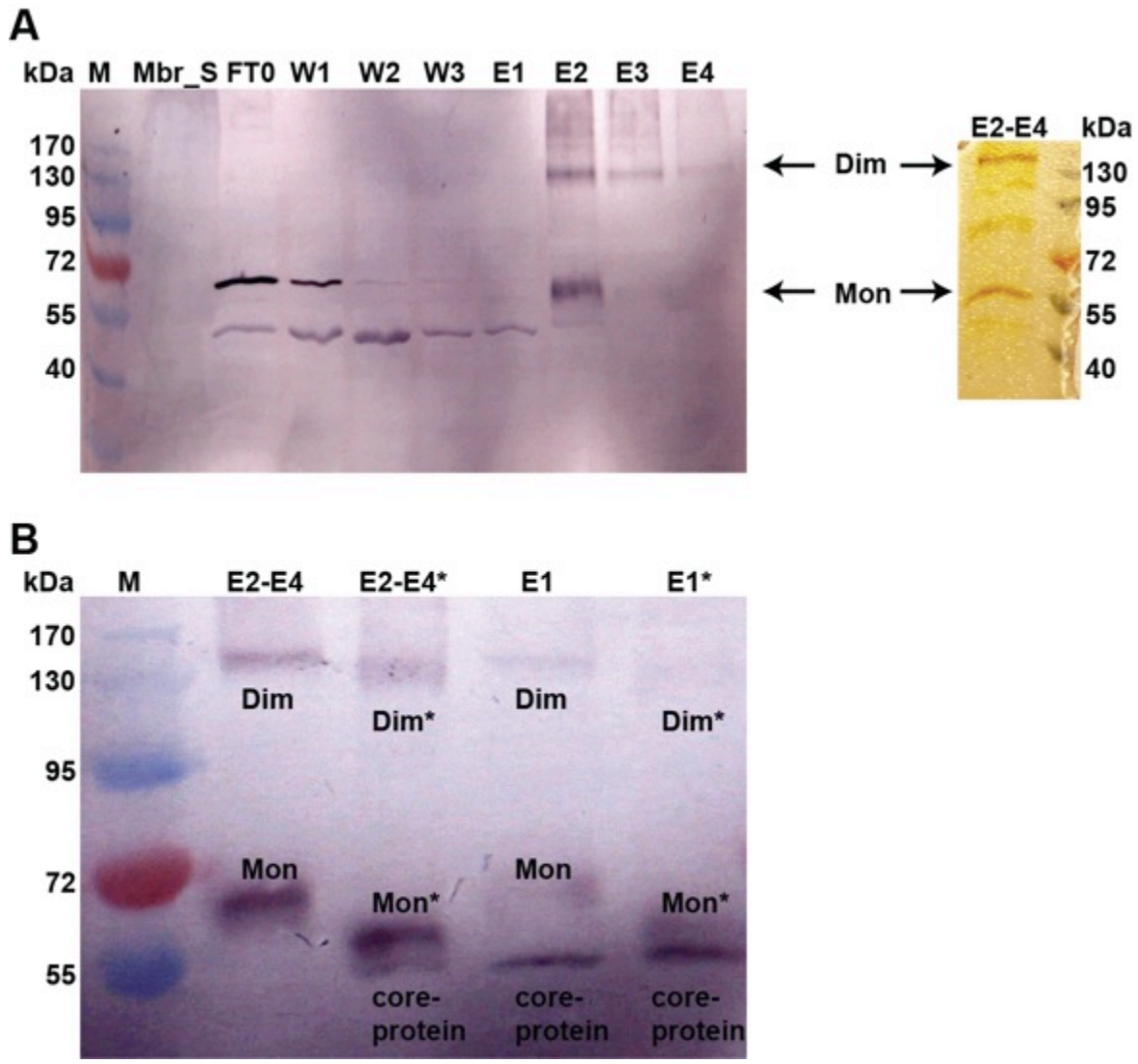

Figure 31: Western blot and SDS-PAGE of BGT1_Dm after Ni^{2+} column purification and PNGase F digestion. (**A**) The solubilized membrane fraction was loaded onto a Ni^{2+} column; the residual membranes after solubilization (Mbr_S) were loaded on the gel to check efficiency of DDM solubilization. The flow through (FTO) was discarded and the column was washed three times (W1, W2, W3) before the protein was eluted (E1, E2, E3, E4). In both the Western blot and the silver-stained SDS PAGE of pooled fractions E2-E4, the monomeric form (arrow, Mon) and the dimeric form (arrow, Dim) of BGT1 is detectable. (**B**) Elution fractions E2-E4 from (A) were pooled (E2-E4) and digested with PNGase F (E2-E4*), Elution fraction 1 (E1) was also digested with PNGase F (E1*). Both the dimer (Dim) and the monomer (Mon) showed a clear band shift after PNGase F treatment (Dim*, Mon*). The core-protein is unaffected (core-protein). M: PageRuler™ Prestained Protein Ladder (Fermentas).

After Ni^{2+} affinity chromatography, the protein concentration of BGT1_Dm was about 0.02 mg/ml determined by guanidinium hydrochloride method (chapter 2.6.7.2). Purified protein

was used for a reconstitution test with liver polar lipids in a lipid-to-protein ratio (LPR) of 3:1. The resulting proteoliposomes as assessed by freeze fracture showed partial incorporation of proteins into liposomes (Figure 32). For suitable transport studies, more purified protein would be necessary to achieve a more even distribution of protein into the liposomes.

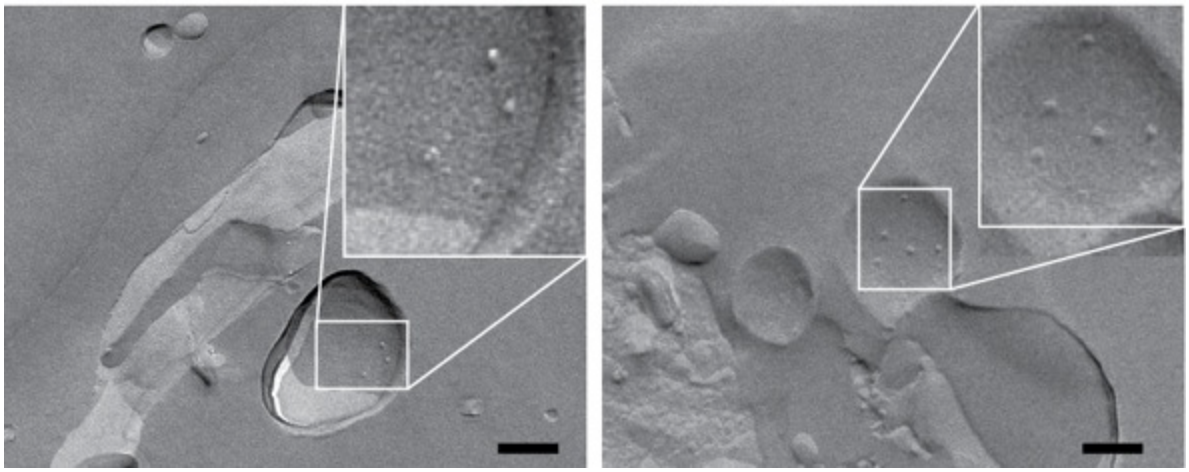

Figure 32: Freeze-fracture images of BGT1_Dm reconstituted into Liver polar lipids liposomes. Proteoliposomes were checked by freeze-fracture (performed by F. Joos, MPI of Biophysics). Reconstitution of BGT1_Dm was first tested with an LPR of 3:1. (Scale bar: 100 nm).

3.2.3 Expression of gene optimized BGT1 in *Sf9* cells

The codon optimized gene BGT1 (BGT1syn) (see chapter 3.2.4) from *Canis lupus* was cloned into the pVL1393 vector with an N-terminal FLAG-tag followed by a Prescission cleavage site and a C-terminal His_{10}-tag (BGT1syn_Sf9).

A small-scale expression test of *bgt1*syn_Sf9 was carried out in 6 well plates with adherent *Sf9* cells. The expression of *bgt1*syn_Sf9 was checked each 24 hours 7 days post infection (d.p.i.). After each day 6 x 10^5 cells were lysed using the Benzonase assay (chapter 2.6.4.8), from which 10 – 20 µl were loaded on a SDS gel [5 – 10 x 10^4 cells/lane] and analyzed by Western blotting. After 3 d.p.i. over-expression of *bgt1*syn_Sf9 was induced and remained constant until 7 d.p.i. (Figure 33). For large scale expression the optimum of 3 d.p.i was used to avoid aggregation of the protein.

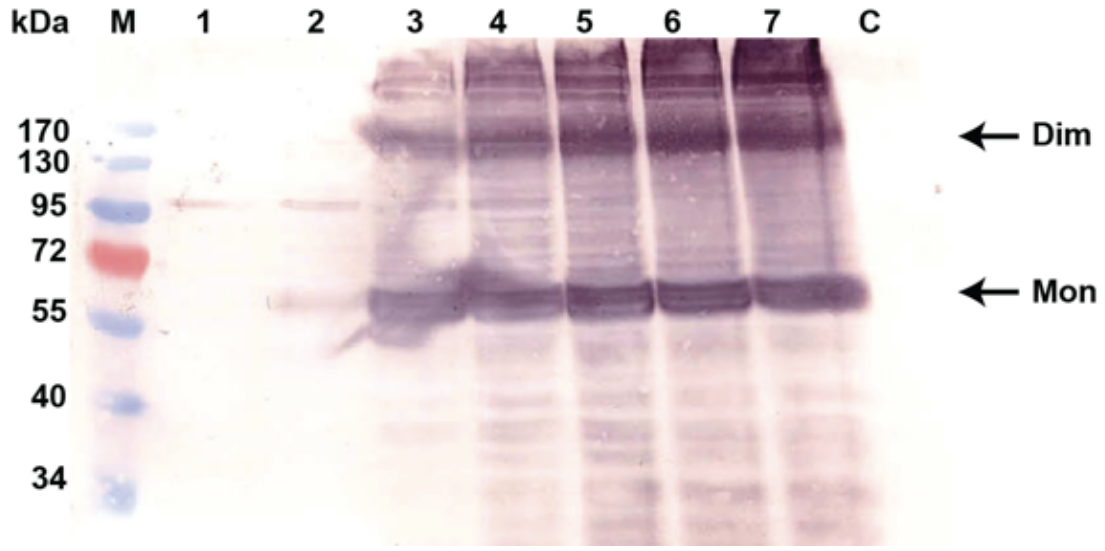

Figure 33: Western blot analysis of Sf9 cells containing overexpressed BGT1syn_Sf9 protein. 5 – 10 x 10^4 cells were loaded per lane after one until 7 d.p.i. (1-7). As a control (C) untransfected *Sf9* cells were loaded. *bgt1*syn_Sf9 was expressed after 3 d.p.i. and the protein was detectable as monomer (Mon) of around 70 kDa and as a dimer of around 140 kDa (Dim). M: PageRuler™ Prestained Protein Ladder (Fermentas).

3.2.3.1 Solubilization and purification of BGT1syn_Sf9

For a first solubilization and purification test a 50 ml suspension culture of transfected *Sf9* cells was harvested and 1.2 ml of membranes were obtained with a concentration of 10 mg/ml. Membranes were diluted (1:1) and split for a solubilization test with four different detergents (DDM, DM, Cymal-5 and OG). Solubilized membrane fractions and remaining membrane pellets after ultra-centrifugation were loaded on an SDS PAGE and further analyzed via Western blotting. All detergents could solubilize BGT1syn_Sf9 to some extend except for OG (Figure 34).

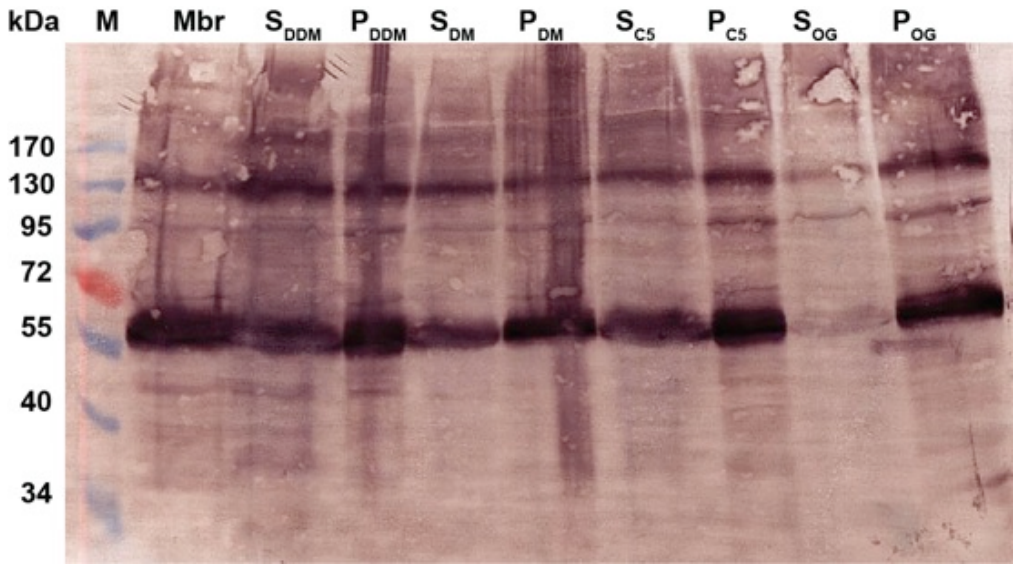

Figure 34: Western blot analysis of *Sf9* membranes after solubilization test. Membranes of *Sf9* cells expressing *bgt1*syn_Sf9 were loaded (Mbr) and alternating solubilized membrane fraction of each detergent ($S_{DDM,\ DM,\ C5,\ OG}$) and corresponding membrane pellet after solubilization ($P_{DDM,\ DM,\ C5,\ OG}$). All tested detergents solubilized BGT1syn_Sf9 except OG. M: PageRuler™ Prestained Protein Ladder (Fermentas).

Remaining membranes with a concentration of 10 mg/ml were diluted to 5 mg/ml and solubilized with 2 % DDM for 1 hour on ice while stirring. After solubilization, the solubilized membrane fraction was applied onto the Ni^{2+} column. The column was washed with 10 mM imidazole pH 8.0, 10 % glycerol, 50 mM Tris pH 7.5, 200 mM NaCl and 0.1 % DDM. The protein was eluted from the Ni^{2+} column with 250 mM imidazole pH 8.0 in the same buffer. The eluted fractions were further applied onto Anti-FLAG® agarose-beads, washed once with the same buffer used for Ni^{2+} column purification however without imidazole and eluted with 0.2 mg/ml FLAG peptide (Figure 35 A, B).

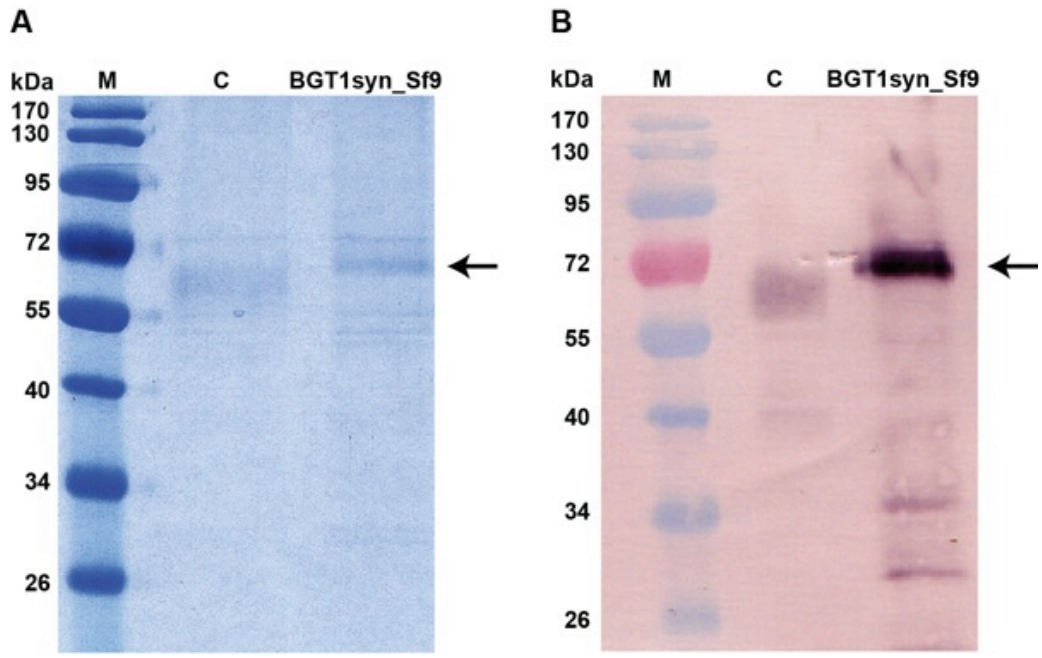

Figure 35: SDS-PAGE gel and Western blot of purified BGT1syn_Sf9. (**A**) The SDS-PAGE gel shows the final step after Anti-FLAG purification of BGT1syn_Sf9. (**B**) corresponding Western blot to the SDS-PAGE gel. Analysis was performed using a specific antibody against the FLAG-tag. As a control (**C**) another SLC6 transporter was loaded. M: PageRuler™ Prestained Protein Ladder (Fermentas).

The expression of *bgt1*syn_Sf9 in *Sf*9 cells appears very promising and will be continued in larger scale.

3.2.4 BGT1-gene optimization and expression in *Pichia pastoris*

When the codon usage of the target gene matches that of the host expression system, target gene expression can improve intensely. Codon-optimization of the *bgt1* gene was designed on the codon bias of AOX 1 (alternative Oxidase-) protein, which is highly expressed in *P. pastoris*. Furthermore, a N-terminal FLAG-tag followed by a Prescission protease sequence and a C-terminal His_{10}-tag were attached to the codon-optimized *bgt1*. As *N*-glycosylation can hinder crystallization of eukaryotic proteins and as it does not prevent its activity (chapter 3.1.3.2) both potential *N*-glycosylation sites (N171, N183) were mutated to Aspartates (NN171/183DD).

The optimized gene was synthesized and delivered in the pPUC57 vector by GenScript. This construct was used as template for PCR amplifications and for sub-cloning into *Sf9* (pVL1393_BGT1syn) and *P. pastoris* expression vectors (pPIC3.5k_BGT1syn) (chapter 2.4.3).

For integration into the *P. pastoris* genomic DNA, a plasmid containing gene optimized BGT1syn (BGT1syn_Pp) was transformed into the protease-deficient *P. pastoris* strain SMD1163 by electroporation resulting in clones containing multiple copies of the gene expression cassette. In microtiter plates (sterile 96 well plates) highly expressing clones according to their antibiotic resistance (G418) were identified by immuno-detection (Figure 36).

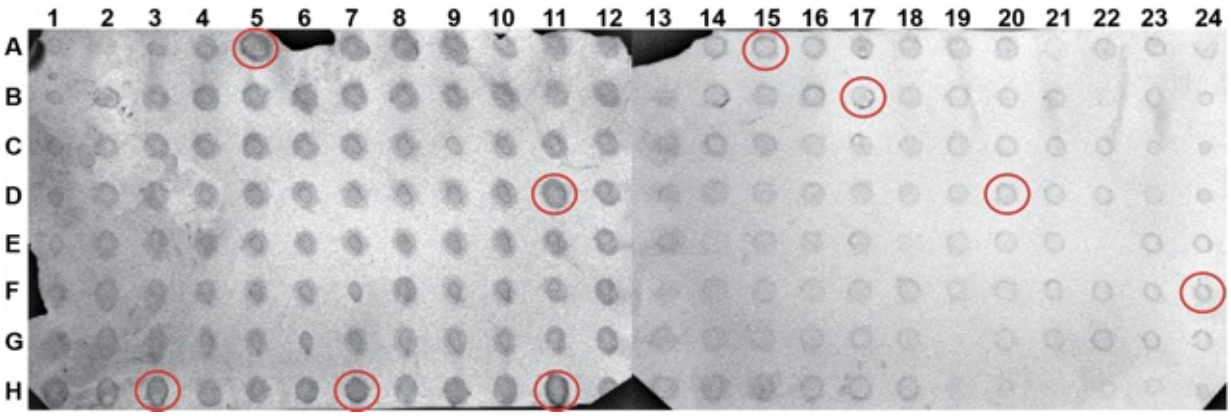

Figure 36: Analysis of bgt1-syn_Pp gene expression by dot blot. Analysis of *bgt1*syn_Pp expression in *P. pastoris* strain SMD1163. Cells were grown on nitrocellulose and subsequently lysed. The nitrocellulose membrane was then used for immuno-staining. Colonies with the darkest signal correspond to those having highest G418 resistance, and thus the highest expression level. Nine of these clones (red circles) were chosen for a second test in shaking culture.

Nine clones were grown in liquid media at 30 °C in MGY media to an OD_{600} of 2 to 6. Cells were diluted to OD_{600} of 1 in MM media to start induction. After 24 hours cells were harvested and verified by Western blotting of the corresponding membranes to identify the highest expressing clone (Figure 37). The following expressions, purifications and functional

analysis as well as 2D and 3D set-ups were carried out with the particular clone that gave the most prominent signal in this Western blot (H7, Figure 37).

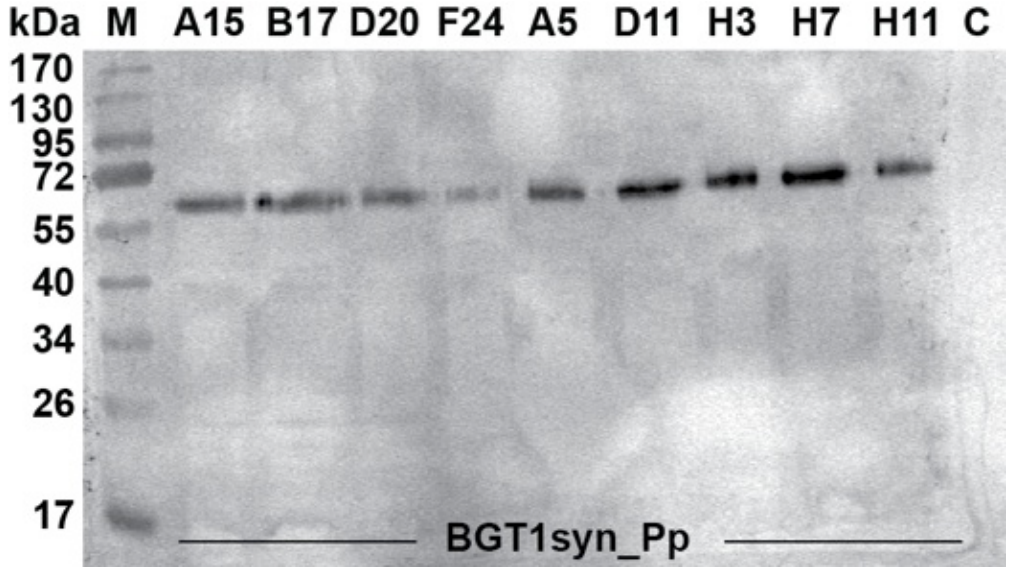

Figure 37: Expression analysis of BGT1syn_Pp in pPIC3.5k vector. Nine selected clones (Figure 36) were expressed in shaking cultures. After cell lysis, membranes of each construct were loaded on an SDS-gel and transferred onto a PVDF membrane for immuno-detection against the His_{10} tag of the recombinant protein (molecular weight approx. 65 kDa). Clone H7 had the most prominent signal of all tested clones. The labeling of the clones is the same as on the dot blot in Figure 36. As a control (C) only cells expressing empty vector was loaded.

To further optimize protein expression in *P. pastoris* the following growth media were tested: minimal (MGY, MM), semi-complex (BMG/BMM) or complex (BMGY/BMMY) medium at variying methanol concentration (0.5, 1 or 1.5 %), (Figure 38).

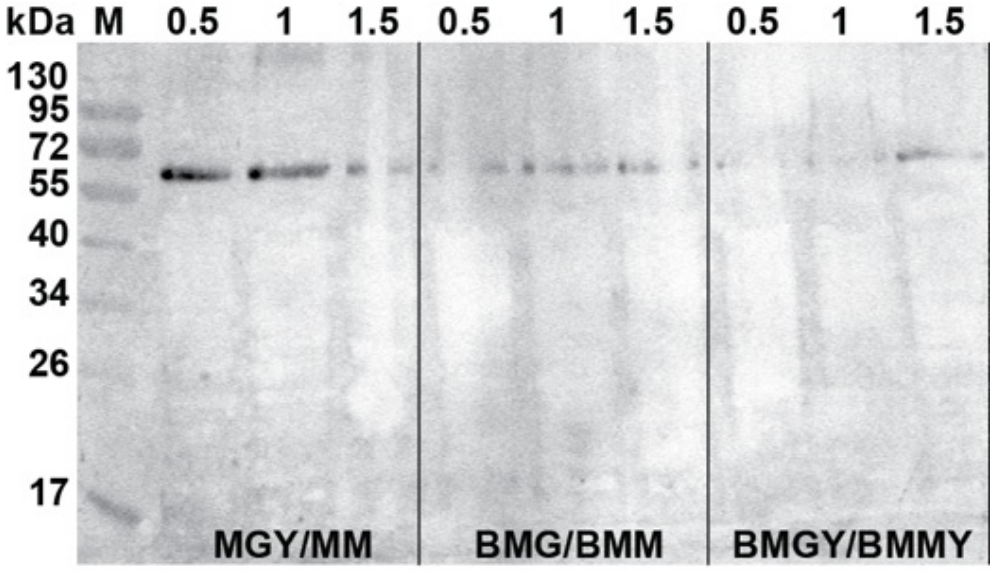

Figure 38: Western blot analysis of *P. pastoris* membranes containing BGT1syn_Pp expressed in different media and varied methanol concentrations. BGT1syn_Pp was either expressed in minimal medium (MGY/MM), semi-complex medium (BMG/BMM) or complex medium (BMGY/BMMY). Methanol concentration varied from 0.5, 1 or 1.5 % (indicated on top of the Western blot with 0.5, 1, 1.5).

Best expression was obtained with minimal media (MGY/MM) and 0.5-1 % of methanol for induction (Figure 38).

Localization studies of BGT1syn_Pp via immunogold labeling against a FLAG-tag specific antibody revealed BGT1syn_Pp in the plasma membrane and in the ER (Figure 39 A, black arrows). Accumulation of [^{3}H]GABA was measured in *P. pastoris* cells (Figure 39 B, filled circles), where the presence of the BGT1 specific inhibitor NNC-05-2090 (Thomsen et al., 1997) resulted in a significant reduction in transport (Figure 39 B, open circles), indicating that the transport is specific to BGT1. A K_M-value of 104.5 ± 28.8 µM could be determined (Figure 39 C). Western blot analysis using a specific antibody against BGT1 revealed stably expressed protein without any degradation (Figure 39 C, inset). These cell measurements imply already that BGT1syn_Pp is functional expressed.

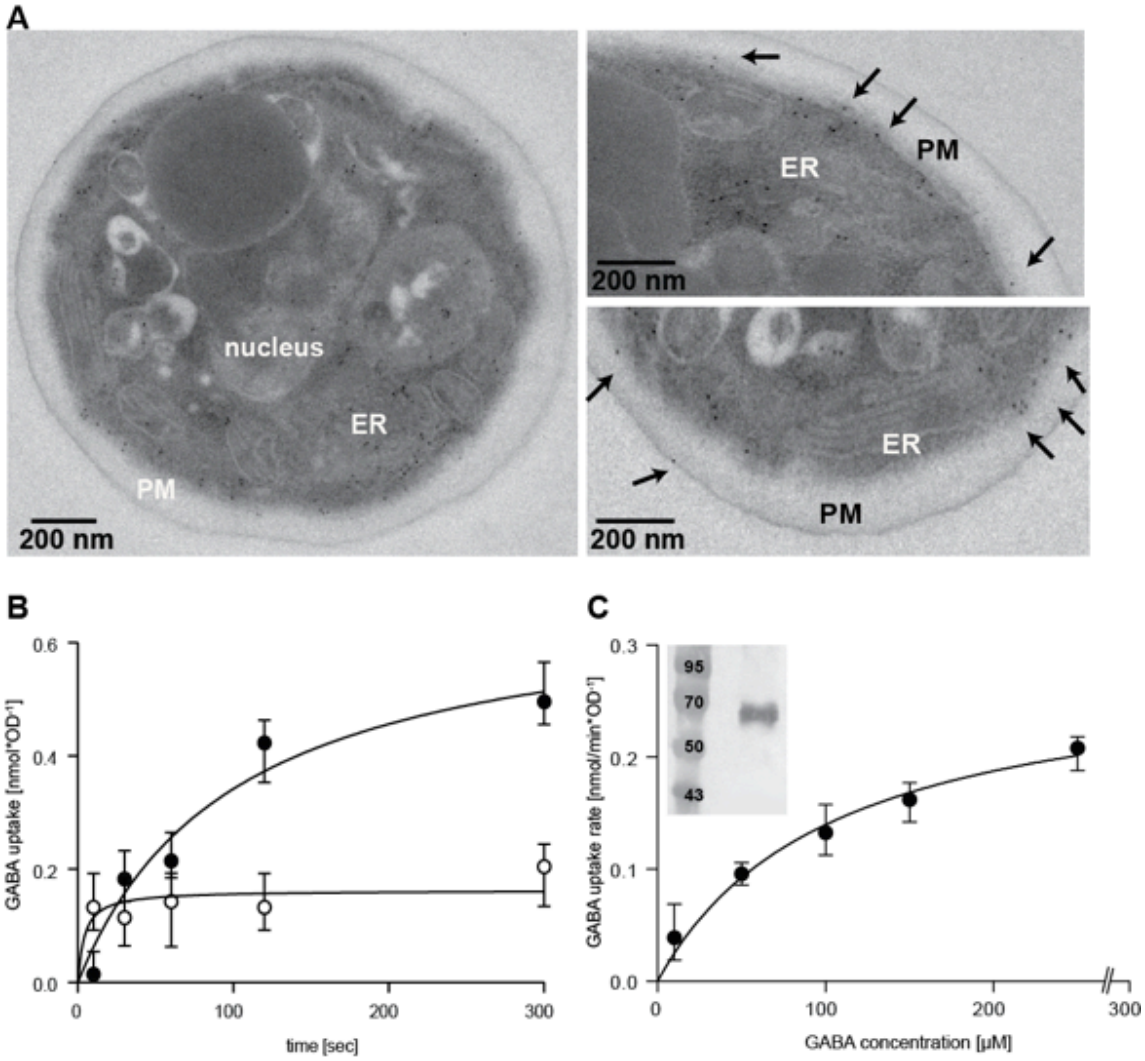

Figure 39: Postembedding immunogold labelling of recombinant BGT1syn_Pp in *Pichia pastoris*. (**A**). Localization of BGT1syn_Pp within the cell was monitored by immunogold labeling against the FLAG-tag. BGT1syn_Pp is found in the endoplasmatic reticulum (ER) and in the plasma membrane (PM), indicated by black arrows in the zooms on the distribution of the protein. (**B**) Accumulation of [^{3}H]GABA in nmol per min and OD_{600} was measured over time in *bgt1syn_Pp* transfected *Pichia pastoris* SMD1163 host cells (filled circles). Inhibition of GABA transport by NNC-05-2090 (2 µM) reduced the transport rate by half (open circles). The values measured on cells containing the empty vector pPIC3.5k are subtracted from the [^{3}H]GABA uptake values of cells containing *bgt1syn_Pp*. Each point shows the average of at least three independent experiments. The error bars represent a mean ±SD of triplicate experiments. (**C**) K_M-value of BGT1syn_Pp was measured by the uptake rates of [^{3}H]GABA in nmol per min and OD_{600} over the GABA concentration in µM. Each data point shows the average of at least three independent experiments. The error bars represent a mean ±SD of triplicated experiments. Western blot of NN171/183DD against a BGT1 specific antibody reveals that the protein is stably expressed without any degradation.

3.2.4.1 Solubilization of *P. pastoris* expressed BGT1syn

BGT1syn_Pp solubilizes in a number of different detergents; the most efficient ones were DM and DDM (Figure 40).

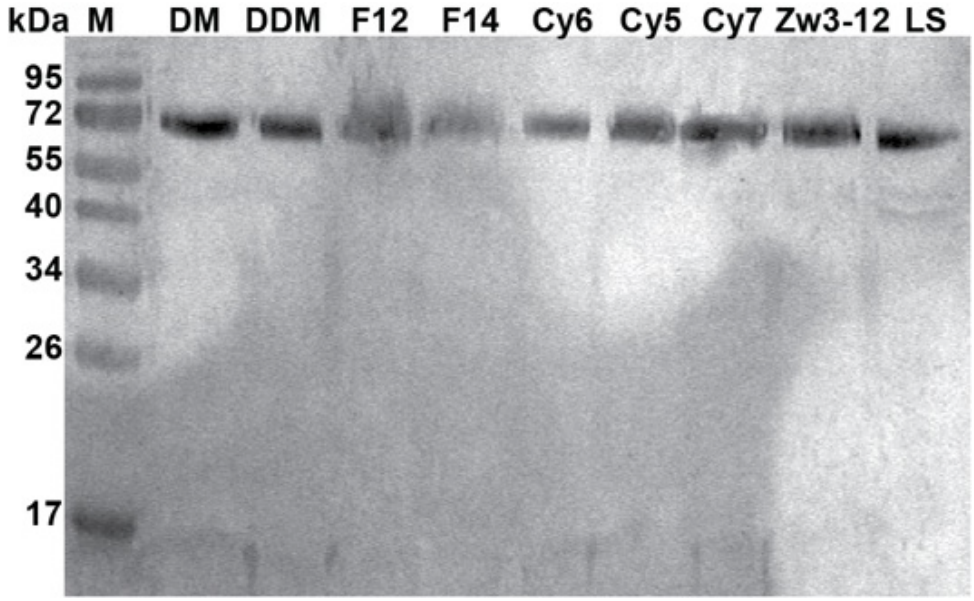

Figure 40: Solubilization tests of BGT1syn_Pp. Nine detergents were tested with a final concentration of 2 % each. DM = decylmaltoside, DDM = dodecylmaltoside, F12 and F14 = Foscholine 12 and 14, Cy6, 7 and 5 = Cymal-5, 6, 7; Zw3-12 = Zwittergent 3-12; LS = Laurorylsarcosine.

3.2.4.2 Purification and stability of BGT1syn_Pp

Since DM and DDM were the best detergents for solubilization of BGT1syn_Pp, both were used for initital purification tests. Additionally, an exchange to Cymal-5 during purification was tested. The BGT1 construct has an N-terminal FLAG- and a C-terminal His_{10}-Tag for protein purification by anti-FLAG agarose and/or by immobilized metal affinity chromatography (IMAC). Table 9 summarizes representative solubilization and purification tests of BGT1syn_Pp. After purification the protein was tested for stability and monodispersity by size exclusion chromatography (SEC) and BN-PAGE. SEC was pre-equlibrated to ensure that the protein does not aggregate during chromatography. Coomassie G250, which is the dye used in BN-PAGE, induces a charge shift on the protein and stays tightly bound during electrophoresis. Both methods are appropriate to test the stability of membrane proteins.

Table 9: Overview of BGT1_Pp Solubilization, Purification trials and further analysis.

Detergent (Solub)	IMAC (Nickel/Cobalt)		FLAG		SEC (Superose 6, 10/30)	Concentration (mg/ml)	Purity and Stability	2D / 3D, Reconstitution
	Wash	Elution	Wash	Elution				
1. **2 % DM**	10 mM Imidazole pH 8, 50 mM Tris-HCl pH 7.5, 200 mM NaCl, 10 % glycerol 0.1 % DM	250 mM Imidazole pH 8, 50 mM Tris-HCl pH 7.5, 200 mM NaCl, 10 % glycerol 0.1 % DM	50 mM Tris-HCl pH 7.5, 200 mM NaCl, 10 % glycerol 0.1 % DM	100 µg/ml FLAG-Peptide, 50 mM Tris-HCl pH 7.5, 200 mM NaCl, 10 % glycerol 0.1 % DM	50 mM Tris-HCl pH 7.5, 200 mM NaCl, 10 % glycerol 0.1 % DM	7.5	✓	**3D** (Hampton Index 1 &2, Hampton Crystal Screen, Qiagen Membrane Fract.)

2. **2 % DM**	10 mM Imidazole pH 8, 50 mM Tris-HCl pH 7.5, **150** mM NaCl, 10 % glycerol 0.1 % DM	**300** mM Imidazole pH 8, 50 mM Tris-HCl pH 7.5, **150** mM NaCl, 10 % glycerol 0.1 % DM	50 mM Tris-HCl pH 7.5, **150** mM NaCl, 10 % glycerol 0.1 % DM	100 µg/ml FLAG-Peptide, 50 mM Tris-HCl pH 7.5, **150** mM NaCl, 10 % glycerol 0.1 % DM			✓	
3. **2 % DDM**	10 mM Imidazole pH 8, **25** mM Tris-HCl pH 7.5, 150 mM NaCl, **5** % glycerol **0.04** % DDM	300 mM Imidazole pH 8, **25** mM Tris-HCl pH 7.5, 150 mM NaCl, **5** % glycerol **0.04** % DDM	**25** mM Tris-HCl pH 7.5, 150 mM NaCl, **5** % glycerol **0.04** % DDM	100 µg/ml FLAG-Peptide, **25** mM Tris-HCl pH 7.5, 150 mM NaCl, **5** % glycerol **0.04** % DDM		1.8	✓	**Reconstitution** Liver polar lipids; **2D** Lipids: Liver polar lipids, DMPC, PCegg (60 %) + 5 % cholesterol
4. **1.5 % DDM**	10 mM Imidazole pH 8, 50 mM Tris-HCl pH 7.5, 200 mM NaCl, 10 % glycerol 0.04 % DDM	250 mM Imidazole pH 8, 50 mM Tris-HCl pH 7.5, 200 mM NaCl, 10 % glycerol 0.04 % DDM	50 mM Tris-HCl pH 7.5, 200 mM NaCl, 10 % glycerol 0.04 % DDM	100 µg/ml FLAG-Peptide, **25** mM Tris-HCl pH 7.5, 200 mM NaCl, 10 % glycerol 0.04 % DDM	50 mM Tris-HCl pH 7.5, 200 mM NaCl, 10 % glycerol 0.04 % DDM		✓	

5. **2 % DDM**	**W1**: 5 mM Tris-HCl pH 7.5, 200 mM NaCl, **10** % glycerol **0.1** % DDM **W2**: 30 mM Tris-HCl pH 7.5, 300-500 mM NaCl, **10** % glycerol **0.1** % DDM **W3**: 50 mM Imidazole pH 8, 50 mM Tris-HCl pH 7.5, 200 mM NaCl, **10** % glycerol **0.1** % DDM	250 mM Imidazole pH 8, 50 mM Tris-HCl pH 7.5, 200 mM NaCl, 10 % glycerol **0.1** % DDM	50 mM Tris-HCl pH 7.5, 200 mM NaCl, 10 % glycerol 0.05 % DDM	100 µg/ml FLAG-Peptide, **25** mM Tris-HCl pH 7.5, 200 mM NaCl, 10 % glycerol 0.05 % DDM			✓	**Reconstitution** Liver polar lipids
6. **1.5 % DDM**	**30** mM Imidazole pH 8, 50 mM Tris-HCl pH 7.5, 200 mM NaCl, **10** % glycerol **0.05 % DDM**	250 mM Imidazole pH 8, 50 mM Tris-HCl pH 7.5, 200 mM NaCl, 10 % glycerol **0.05** % DDM → **Dialysis** over night against 50 mM Tris-HCl pH 7.5, 200				0.2	✓	**2D** Lipids: POPC, DOPC, DMPC LPR: 0.15, 0.3, 0.6

		mM NaCl, 10 % glycerol, 0.05 % DDM						
7. **2 % DM**	W1: 10 mM Imidazole pH 8, 50 mM Tris-HCl pH 7.5, 200 mM NaCl, 10 % glycerol, **0.6 % Cymal5** W2: 50 mM Imidazole pH 8, 50 mM Tris-HCl pH 7.5, 200 mM NaCl, 10 % glycerol **0.6 % Cymal5**	250 mM Imidazole pH 8, 50 mM Tris-HCl pH 7.5, 200 mM NaCl, 10 % glycerol, **1.2 % Cymal5**	50 mM Tris-HCl pH 7.5, 200 mM NaCl, **0.6 % Cymal5**	100 µg/ml FLAG-Peptide, 50 mM Tris-HCl pH 7.5, 200 mM NaCl, **1.2 % Cymal5**		4	✓	**3D** (Hampton Index 1 &2, Hampton Crystal Screen)

8. **2 % DM**	W1: 10 mM Imidazole pH 8, 50 mM Tris-HCl pH 7.5, 200 mM NaCl, 10 % glycerol, **0.6 % Cymal5** W2: 30 mM Imidazole pH 8, 50 mM Tris-HCl pH 7.5, 200 mM NaCl, 10 % glycerol **0.6 % Cymal5**	250 mM Imidazole pH 8, 50 mM Tris-HCl pH 7.5, 200 mM NaCl, 10 % glycerol, **0.6 % Cymal5**	50 mM Tris-HCl pH 7.5, 200 mM NaCl, **0.6 % Cymal5**	100 µg/ml FLAG-Peptide, 50 mM Tris-HCl pH 7.5, 200 mM NaCl, **1.2 % Cymal5**	**25** mM Tris-HCl pH 7.5, 200 mM NaCl, **1.2 % Cymal5**	5	✓	**3D** (MemGold)

9. **2 % DDM** **+ 30 mM Imidazole pH 8**	W1: 10 mM Imidazole pH 8, 50 mM **Tris-HCl pH 8**, 200 mM NaCl, 10 % glycerol, **2 mg/ml Asolectin**, **5 % cholesterol**, **5 mM GABA**, 0.1 % DDM W2: 30 mM Imidazole pH 8, 50 mM **Tris-HCl pH 8**, 200 mM NaCl, 10 % glycerol, **2 mg/ml Asolectin**, **5 % cholesterol**, **5 mM GABA**, 0.1 % DDM	250 mM Imidazole pH 8, 50 mM **Tris-HCl pH 8**, 200 mM NaCl, 10 % glycerol, **2 mg/ml Asolectin**, **5 % cholesterol**, **5 mM GABA**, 0.1 % DDM					✗ aggrega-tion	

10. **2 % DDM** **+ 30 mM Imidazole pH 8**	W1: 10 mM Imidazole pH 8, 50 mM Tris-HCl pH 8, 200 mM NaCl, 10 % glycerol, **5 mM GABA**, **10 mM β-mercaptoethanol**, 0.1 % DDM W2: **40** mM Imidazole pH 8, 50 mM Tris-HCl pH 8, 200 mM NaCl, 10 % glycerol, **5 mM GABA**, **10 mM β-mercaptoethanol**, 0.1 % DDM	250 mM Imidazole pH 8, 50 mM Tris-HCl pH 8, 200 mM NaCl, 10 % glycerol, **5 mM GABA**, **10 mM β-mercaptoethanol**, 0.1 % DDM	50 mM Tris-HCl pH 7.5, 200 mM NaCl, 10 % glycerol, 0.1 % DDM	100 µg/ml FLAG-Peptide, 50 mM Tris-HCl pH 7.5, 200 mM NaCl, 10 % glycerol, 0.1 % DDM		Protein splitted: After IMAC: 2, After FLAG: 1		Protein after IMAC: **Reconstitution**, Protein after FLAG: **2D** Lipid: DOPC LPR: 0.2, 0.5, 0.8

11. **2 % DM**	W1: 10 mM Imidazole pH 8, 50 mM Tris-HCl pH 8, 200 mM NaCl, 10 % glycerol, 0.1 % DM W2: **40** mM Imidazole pH 8, 50 mM Tris-HCl pH 8, 200 mM NaCl, 10 % glycerol, **0.6 % Cymal5**	250 mM Imidazole pH 8, **25** mM Tris-HCl pH 8, **100** mM NaCl, **5** % glycerol, **1 % Cymal5** **2. WGA: (**Binds to N-acetyl-β-D-glucosamine and Sialic acid) → FTO	**25** mM Tris-HCl pH 8, **100** mM NaCl, **5** % glycerol, **1 % Cymal5**	100 µg/ml FLAG-Peptide, **25** mM Tris-HCl pH 7.5, **100** mM NaCl, **2.5** % glycerol, **1 % Cymal5**		3	✓	**3D** **+ Inhibitor** (NNC-05-2090, 100 µM) PEG-suite nextal-Screen, Qiagen, JB Screens Mb 1-3 + Classic 5)
12. **2 % DDM**	W1: **15** mM Imidazole pH 8, **25** mM **Hepes pH 7**, 100 mM NaCl, 10 % glycerol, **1** mM **TCEP**, 0.05 % DDM W2: **40** mM Imidazole pH 8, **25** mM **Hepes pH 7**, 200 mM NaCl, **1** mM	250 mM Imidazole pH 8, **25** mM **Hepes pH 7**, 100 mM NaCl, **1** mM **TCEP**, 0.05 % DDM	**25** mM **Hepes pH 7**, 100 mM NaCl, **1** mM **TCEP**, **0.02** % DDM	100 µg/ml FLAG-Peptide, **25** mM **Hepes pH 7**, 100 mM NaCl, **1** mM **TCEP**, **0.02** % DDM		6	✓	**3D** (Molecular Dimensions : MemGold, MemSys)

	TCEP, 0.05 % DDM							
13. **2 % DDM**	10 mM Imidazole pH 8, 50 mM Tris-HCl pH 7.5, 200 mM NaCl, 10 % glycerol 0.05 % DDM	250 mM Imidazole pH 8, 50 mM Tris-HCl pH 7.5, 200 mM NaCl, 10 % glycerol 0.05 % DDM	50 mM Tris-HCl pH 7.5, 200 mM NaCl, 10 % glycerol 0.05 % DDM	100 µg/ml FLAG-Peptide, 50 mM Tris-HCl pH 7.5, 200 mM NaCl, 10 % glycerol 0.05 % DDM	50 mM Tris-HCl pH 7.5, 200 mM NaCl, 10 % glycerol 0.05 % DDM	2.5; 1.6	✓	**2D** Lipids: Liver polar lipids LPR: 0.1, 0.25, 0.5, 1, 1.5, 2, 3
Detergent for Solubilization	**Wash**	**Elution**	**Wash**	**Elution**	**SEC (Superose 6, 10/300, 10/30) Superdex 200 (10/300)**	**Concentration (mg/ml)**	**Purity and Stability**	**2D / 3D, Reconstitution**
	Nickel/Cobalt IMAC		**FLAG**					

The highest purity and best protein yield were achieved using Ni-NTA agarose (Sigma-Aldrich) followed by anti FLAG agarose (Sigma-Aldrich) during the purification (Figure 41). Size exclusion chromatography (SEC) was used to check protein stability after both purification steps with different buffers and detergents. The best buffer condition for solubilization and purification was Tris-HCl pH 7.5, 200 mM NaCl and 10 % glycerol. As binding of BGT1syn_Pp to the Ni^{2+}-column was strong under these conditions, the concentration of imidazole during washing steps could be increased to 50 mM during washing steps (Table 9, 5., 7.). During solubilization the addition of imidazole did not help to avoid unspecific binding (Table 9, 9., 10.) and was therefore only used during Ni^{2+} column washing steps. Elution of the protein was achieved with a concentration of 250-300 mM imidazole.

The FLAG-Tag at the N-terminal domain allowed a second purification step with which the protein purity could be significantly improved and yielded up to 95 % of pure protein and almost all impurities could be removed (Figure 41). The only disadvantage of two purification

steps is the loss of high amounts of protein but this was compensated by the level of purity achieved, which was not possible with only IMAC followed by SEC. A WGA-purification step could also increase the purity of the protein after IMAC purification as wheat germ agglutinin binds to *N*-acetylglucosamine and sialic acid of glycosylated proteins and deglycosylated BGT1syn_Pp could be collected in the flow through (Table 9, 11.). However, the specific anti-FLAG agarose step was essential for highly purified protein.

For biochemical measurements and 3D crystals, a stable and monodisperse protein sample is required; therefore after purification, the protein sample was tested for its stability and monodispersity by analytical size exclusion chromatography (SEC). For the analytical SEC, a Superose^{TM} 6 (3.2/30) column was pre-equlibrated with the appropriate buffer and the purified protein sample (50 µg) was loaded. The flow rate was set to 50 µl/min and fractions of 100 µl were collected using the Ettan LC system. Three of the aforementioned established purification protocols (Table 9, 1., 8., 13) resulted in qualitative best protein samples for 2D and 3D crystallization and reconstitution for uptake measurements and are shown in more detail in Figure 41.

The BGT1syn_Pp monomer showed a single peak at a retention volume of 1.97 ml (Figure 41 A) when solubilized and purified with DM as detergent (Table 9, 1., labeled in green). Interestingly, BGT1syn_Pp solubilized in DM and switched to Cymal-5 during purification (Table 9, 8., labeled in turquoise), resulted in a SEC profile with two peaks, with retention volumes of 1.59 ml and 1.97 ml, corresponding to the dimeric and the monomeric form of BGT1syn_Pp, respectively (Figure 41 B). When solubilized and purified in DDM (Table 9, 13, labeled in yellow), the protein eluted as a single peak with a retention volume of 1.99 ml, a smaller peak at 1.61 ml corresponds to the dimeric form of BGT1syn_Pp (Figure 41 C). Samples, which eluted in a single peak, were concentrated without loss of monodispersity and were used for 3 D and 2 D crystallization trials and for activity measurements.

In summary, the best size exclusion profile was obtained using 50 mM Tris-HCl pH 7.5, 200 mM NaCl and 10 % glycerol. As expected, the choice of the detergent has an influence on the oligomerization of the protein (Figure 41 B, C).

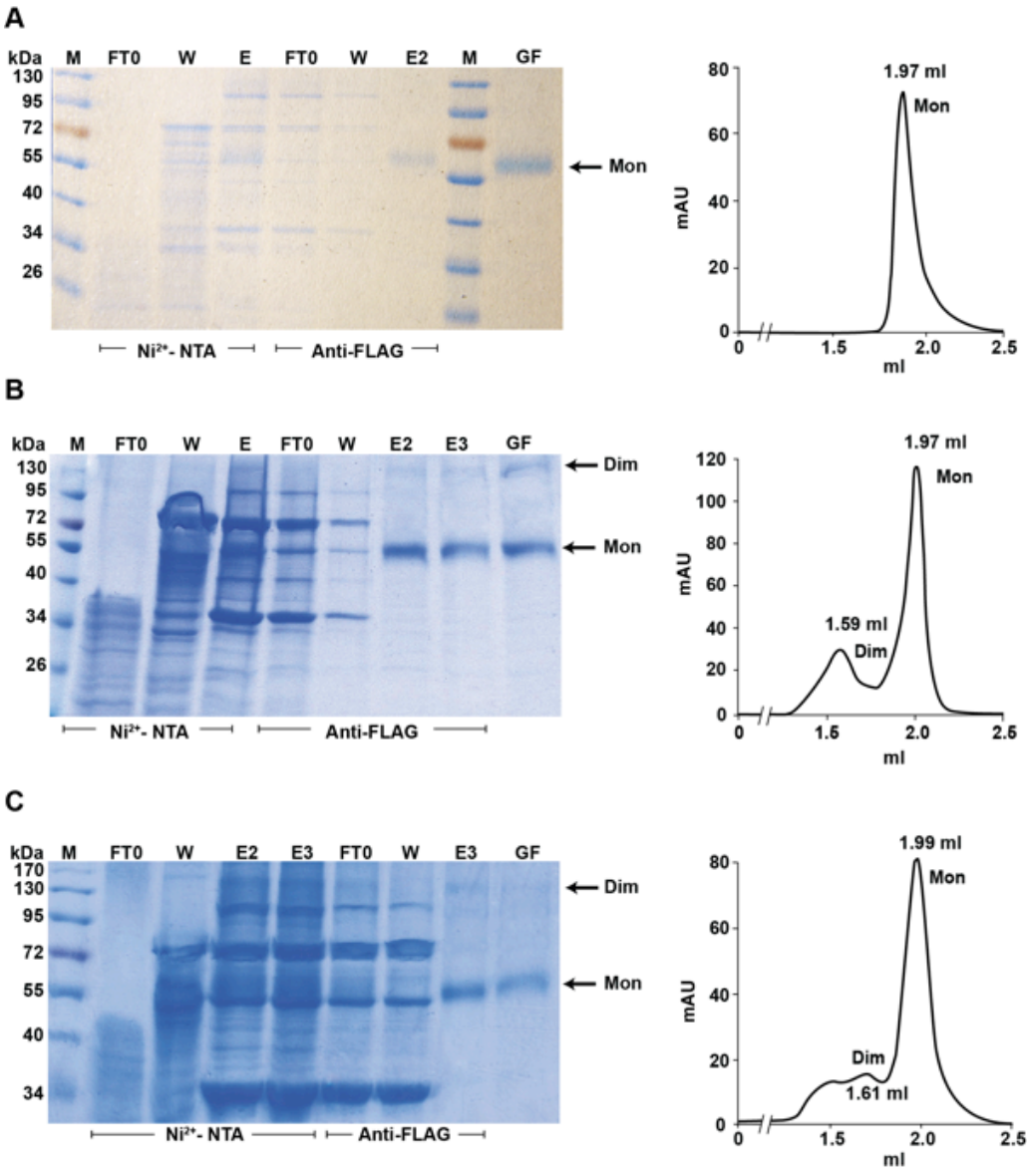

Figure 41: IMAC and Anti-FLAG purification followed by SEC of BGT1syn_Pp. The SDS-PAGE gels show three different purifications of BGT1syn_Pp using IMAC and an Anti-FLAG column (**A**-**C**). On the right side of each gel is the corresponding size exclusion chromatography profile shown. The detailed parameters of each of the three purifications are listed in Table 9 (1. marked in green, 8. marked in turquoise and 13. labeled in yellow). The solubilized membrane fraction of BGT1 was loaded onto a Ni^{2+}-column. After washing (W) the protein was eluted (E) with 250 mM imidazole pH 8.0 and directly loaded onto a pre-equlibrated Anti-FLAG column. After washing (W), the protein was eluted with 100 µg/ml FLAG-peptide and subsequently loaded onto a size exclusion column. The eluted protein after SEC was concentrated to either 5 mg/ml (GF) and used for 3D crystallization (**A**, **B**) or to 2.6 and 1.6 mg/ml and used for 2D crystallization (**A**, **C**). FTO = Flow through, M = PageRuler^{TM} Prestained Protein Ladder (Fermentas).

10 – 20 µg of purified protein was loaded onto 4 – 16 % gradient native gels. BGT1 purified in DM, DDM or Cymal-5 usually separated into three bands during electrophoresis (Figure 42). The first protein band ran to a size between 66 kDa and 146 kDa, the second protein band migrated to a size between 242 kDa and 480 kDa and the third protein band ran to a size between 480 kDa and 720 kDa according to the native protein marker (NativeMARK™ Unstained Protein Standard, life technologies). The first protein band indicates monomers of BGT1 (70 kDa) plus additional bound detergent molecules. The second band corresponds to BGT1 dimers (140 kDa) plus bound detergent molecules. The third band of BGT1 might contain BGT1 tetramers (560 kDa) surrounded by the detergent micelle. This band probably represents BGT1 dimer-dimer-interactions.

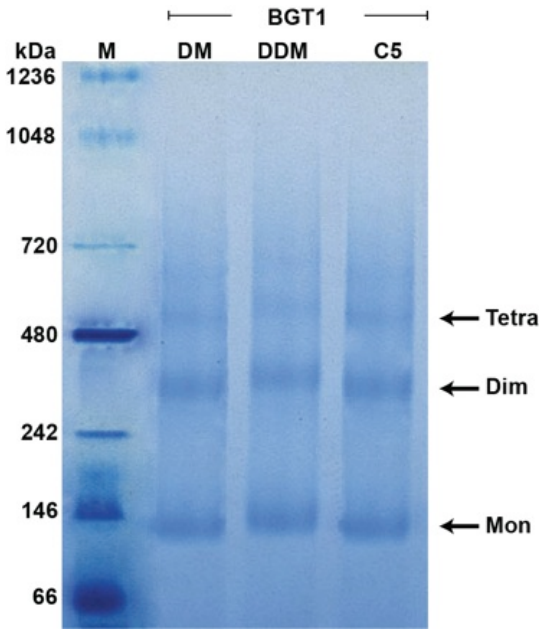

Figure 42: BN-PAGE gel of purified BGT1 in DM, DDM or Cymal-5. After purification of BGT1 the samples were checked for stability by BN-PAGE. The gel was loaded with 10 – 20 µg of purified protein. In the BN-PAGE gradient gel (4-16 %) three bands of BGT1 either purified in DM, DDM or Cymal-5 (C5) were detectable. The first band indicates a protein size between 66 kDa and 140 kDa and might correspond to a BGT1 monomer (Mon). The second protein band migrates between 242 kDa and 480 kDa and has the appropriate size of BGT1 dimers surrounded by a detergent micelle (Dim). The third band runs between 480 kDa and 720 kDa and might represent a tetramer of BGT1 plus detergent molecules (Tetra) according to the native protein marker (M, NativeMARK™ Unstained Protein Standard, life technologies).

Both methods, analytical SEC and BN-PAGE suggest that BGT1 is stable and monodisperse in detergent solutions containing DM, DDM or Cymal-5 after purification, which is a pre-requisite for further activity and structural studies.

3.2.4.3 Three- dimensional protein crystallization of BGT1syn_Pp

3D crystallization trials were set up when sufficient quantities of pure and homogenous BGT1syn_Pp were obtained. Protein samples in DM (Table 9, 1.) or Cymal-5 (Table 9, 8.) were concentrated to 7.5 mg/ml or 5 mg/ml, respectively. Commercially available screens from Qiagen, Hampton, Molecular Dimesions and Jena Bioscience were used for initial crystallization trials. Initial crystals of BGT1syn_Pp in DM were obtained with the condition 2.1 M DL-Malic acid pH 7.0 from Index^{TM} screen (Hampton) and had the form of small thin plates and needles (Figure 43 A). However, these crystals were too small and instable for fishing and further analysis. Initial crystals obtained from BGT1syn_Pp purified with Cymal-5 grew at 4 °C in 0.1 M MES pH 6.5 and 25 % (v/v) PEG550MME from the PEGSuite screen (Qiagen) and yielded in small and thin rectangels diffracting to a resolution of ~ 22 Å (Figure 43 B).

Each crystallization screen was set up with a protein batch from a new protein synthesis and purification due to the usually low total amount of expressed protein. Thus, the crystallization conditions varied depending on the particular protein batch aggravating reproducibility and systematic optimization of the crystals regarding quality and size.

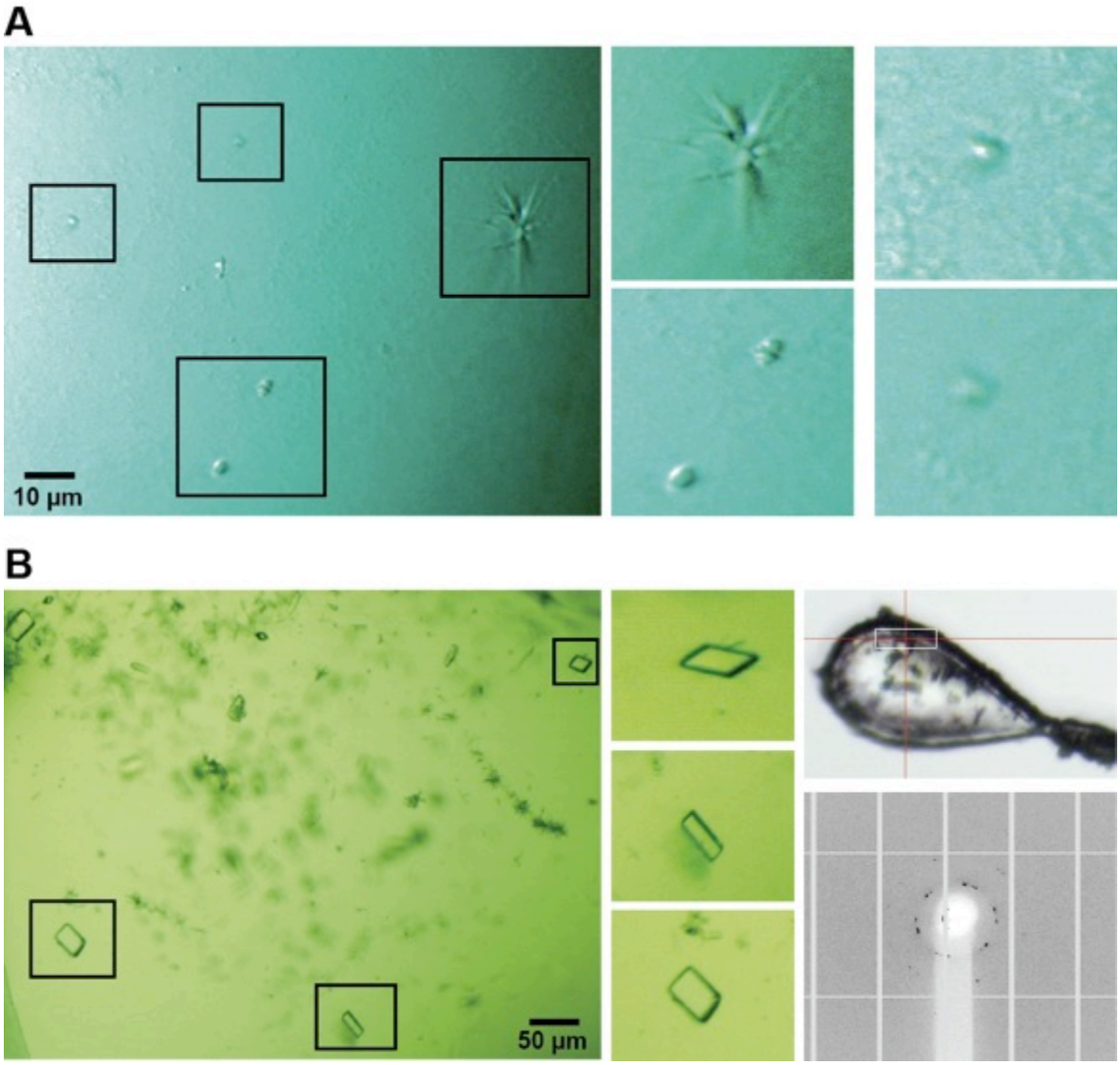

Figure 43: BGT1syn_Pp crystals and protein diffraction. Crystals of BGT1syn_Pp purified in DM (**A**) or Cymal-5 (**B**) were grown in 2.1 M DL-Malic acid pH 7.0 or 0.1 M MES pH 6.5 and 30 % (v/v) PEG300, respectively. From the latter, crystals of 30 µm size could be fished using a 0.1 mm loop. These crystals diffracted to ~ 22 Å resolution.

Notably, the fact that initial protein crystals of this canine betaine/GABA transporter could be obtained is a significant progress for further crystallization and structural studies. These first crystals indicate that the protein is able to form ordered, assembled packing and might eventually arrange even into proper crystal lattices.

3.2.4.4 Lipid analysis of BGT1syn_Pp

During detergent solubilization and subsequently purification membrane proteins are extracted from their lipid environment. Nevertheless, some lipids stay tightly bound to the purified protein, indicating that these lipids are important for functionality and stability of the protein. Analysing these particular lipids, which are bound to the protein after solubilization and purification might help to determine the conditions for protein reconstitution into liposomes for 2D crystallization or transport studies. The lipid composition was analyzed by thin-layer chromatography (TLC). Silicia gel TLC plates were loaded with heart, brain and liver lipids and detergent (DDM) as control to compare with the purified protein sample.

One lipid spot at the height of PC was observed in the protein sample (Figure 44), demonstrating that PC remained bound to BGT1syn_Pp after solubilization and purification.

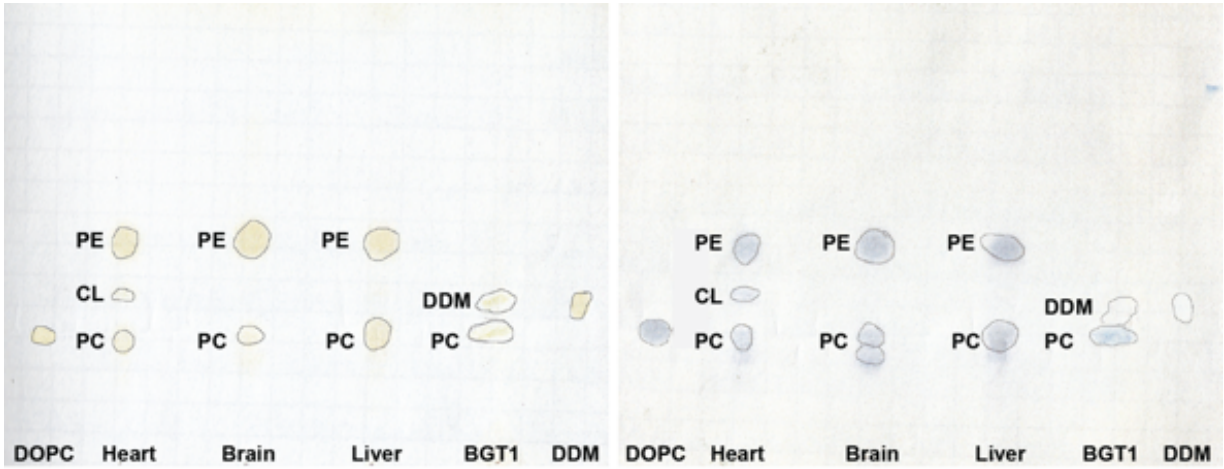

Figure 44: TLC plate of DOPC, heart, brain and liver polar lipids, DDM and BGT1syn_Pp. 50 µg of each sample were applied on a silicia gel TLC plate and separated in a mixture of chloroform : methanol : water (69 % : 27 % : 4 % (v/v)). The silicia gel plate was dried and stained with iodine vapour (left) to visualize carbon-carbon double bonds of unsaturated fatty acids and maltosides of detergent molecules (DDM or Cymals). Then the plate was further stained with molybdenum spray reagent (right) to detect phospholipids. As lipid standards DOPC, heart polar lipids (Heart), brain polar lipids (Brain) and liver polar lipids (Liver) were used and as detergent standard DDM (DDM) was used.

3.2.4.5 Two-dimensional crystallization of BGT1syn_Pp

To gain structural data of BGT1syn_Pp in lipid environment, the purified protein was reconstituted for two-dimensional crystallization. Due to the low amount of protein and thereby the small volume of crystallization conditions a systematic improvement of different crystallization conditions was not feasible.

Each crystallization screen was made with a new batch of protein because of the low yield of BGT1syn_Pp after each expression (0.1 – 2 mg/12 l of culture). Hence, crystallization results varied depending on each protein batch. Aside from other crucial parameters, three important factors influence 2D crystallization in general. First, the lipid to protein ratio (LPR) is important for the formation of vesicles or sheets, which crucially influences the crystallization of the protein. Second, the temperature at which the setups are incubated influences the lipid fluidity. Other crucial parameters are the dialysis time, protein stability and the cmc of the detergent. Low temperatures (e.g. 4 °C) are most favorable for protein stability but tend to have a negative effect on 2D crystallization due to the rigidity of the lipids at this temperature. Third, lipids also have an important influence on protein stability, functionality and crystallization. Lipid analysis with TLC (chapter 3.2.4.4) indicated that BGT1syn_Pp binds PC lipids. Consequently, for 2D crystallization of BGT1syn_Pp lipids from this class were used either alone (DOPC, POPC, DMPC, PCegg + 5 % cholesterol) or as a mixture (DOPC: DOPE, 1:1; Liver polar lipids).

In summary, different lipids and lipid combinations, an incubation temperatures of 27 °C or 37 °C were tested as well as the influence of the LPR varying from 0.1 – 3 (Table 10).

Table 10: Overview of crystallization conditions of BGT1syn_Pp.

Sample	Protein concentration [mg/ml]	LPR	Temperature °C	Lipid	Detergent (Protein)
A	2.5	0.1	27, 37	Liver polar lipids	DDM
B	1, 1.8	0.2	27, 37	DOPC, DOPC:DOPE (1:1), PCegg,60% + 5% chol.	DDM
C	2.5	0.25	37	Liver polar lipids	DDM
D	2.5	0.5	27, 37	DOPC, DOPC:DOPE (1:1), DMPC, PCegg,60% + 5% chol.	DDM
E	1, 1.8	0.8	27, 37	DOPC, DMPC, PCegg,60% + 5% chol.,	DDM
F	1.8, 2.5	1	27, 37	POPC, DOPC:DOPE (1:1), DMPC, PCegg,60% + 5% chol., Liver polar lipids	DDM
G	1.6	1.5	37	Liver polar lipids	DDM
H	1.6, 1.8	2	27, 37	POPC, DOPC:DOPE (1:1), DMPC, PCegg,60% + 5% chol., Liver polar lipids	DDM
I	1.6, 1.8	3	37	DOPC:DOPE (1:1), DMPC, PCegg,60% + 5% chol., Liver polar lipids	DDM

At an LPR of 0.5, 1, 2 and 3 and in the presence of liver polar lipids, protein-lipid patches formed at 37 °C (Figure 45). In some of these crystallization conditions loosely packed thin sheets and vesciles were detected, which made it difficult to detect crystals because of the weak contrast in negative stain. However, in general the formation of vesicles or sheets was

strictly dependent on the LPR, the temperature and the lipid combination but most of all on the protein batch itself.

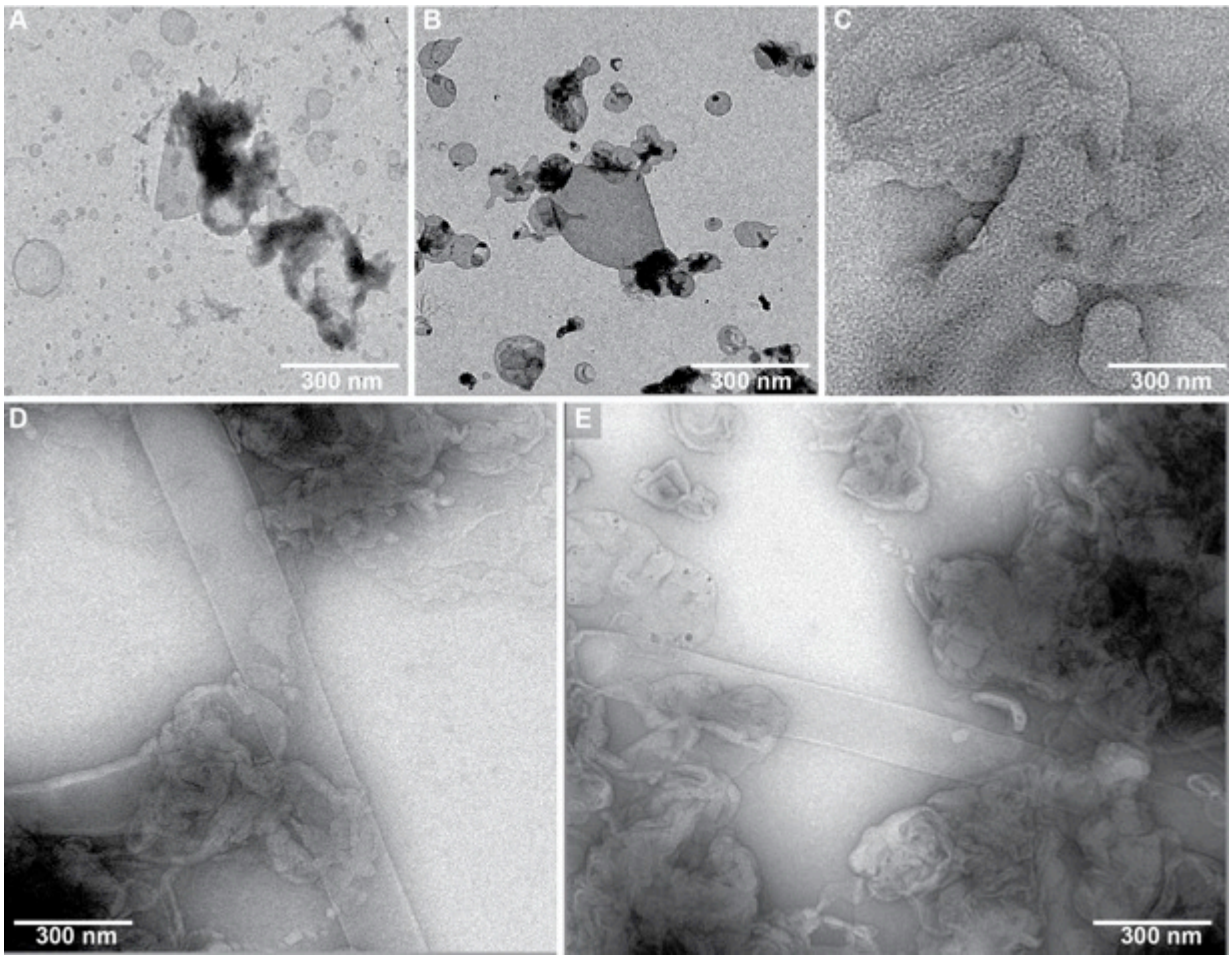

Figure 45: Electron micrographs of BGT1syn_Pp reconstituted at different LPRs. BGT1syn_Pp was purified in DDM, resulted in a concentration of 1.8 mg/ml and was reconstituted in Liver polar lipids for two-dimensional crystallization. The samples were dialyzed against 50 mM Tris pH 7.5, 150 mM NaCl, 5 % MPD, 5 % glycerol, 2.5 mM $CaCl_2$, 3 mM NaN_3 for four weeks at 37 °C. (**A**, **B**). Small protein-lipid patches and aggregates were observed at LPR 0.5 and 1, respectively. (**C**) Protein-lipid patches were obtained at LPR 2. (**D**, **E**) Larger patches and sheets were formed at LPR of 3.

Remarkably, the point that initial protein-lipid patches of this canine betaine/GABA transporter could be obtained is a significant step forward for further 2D crystallization and

hence structural studies. These first lipid-protein sheets indicate that the protein has already ordered, assembled packing.

3.2.4.6 Reconstitution of BGT1syn_Pp into liposomes

Reconstitution protocols as described by (Shouffani and Kanner, 1990) and (Ishmukhametov et al., 2005) were tested for reconstitution of BGT1syn_Pp into liposomes of DOPC, DOPC : DOPE (1 : 1) and Liver polar lipids. These reconstitutions were prepared with a LPR of 3 : 1. The resulting proteoliposomes were freeze-fractured and analyzed in the electron microscope. With the method of (Shouffani and Kanner, 1990) protein incorporation was observed whereas with the protocol of (Ishmukhametov et al., 2005) limited protein incorporated was achieved however not in sufficient amounts suitable for transport studies.

Furthermore, reconstitution of BGT1syn_Pp was performed by first forming liposomes of Liver polar lipids via extrusion (400 nm) and subsequent solubilization with Triton X-100. The detergent was removed with Biobeads and the lipid-to-protein ratio (LPR) was adjusted to 20 : 1. The resulting proteoliposomes were analyzed by freeze-fracture techniques (Figure 46) and showed moderately distributed protein in liposomes of 300-500 nm diameter. These proteoliposomes could be used for transport studies.

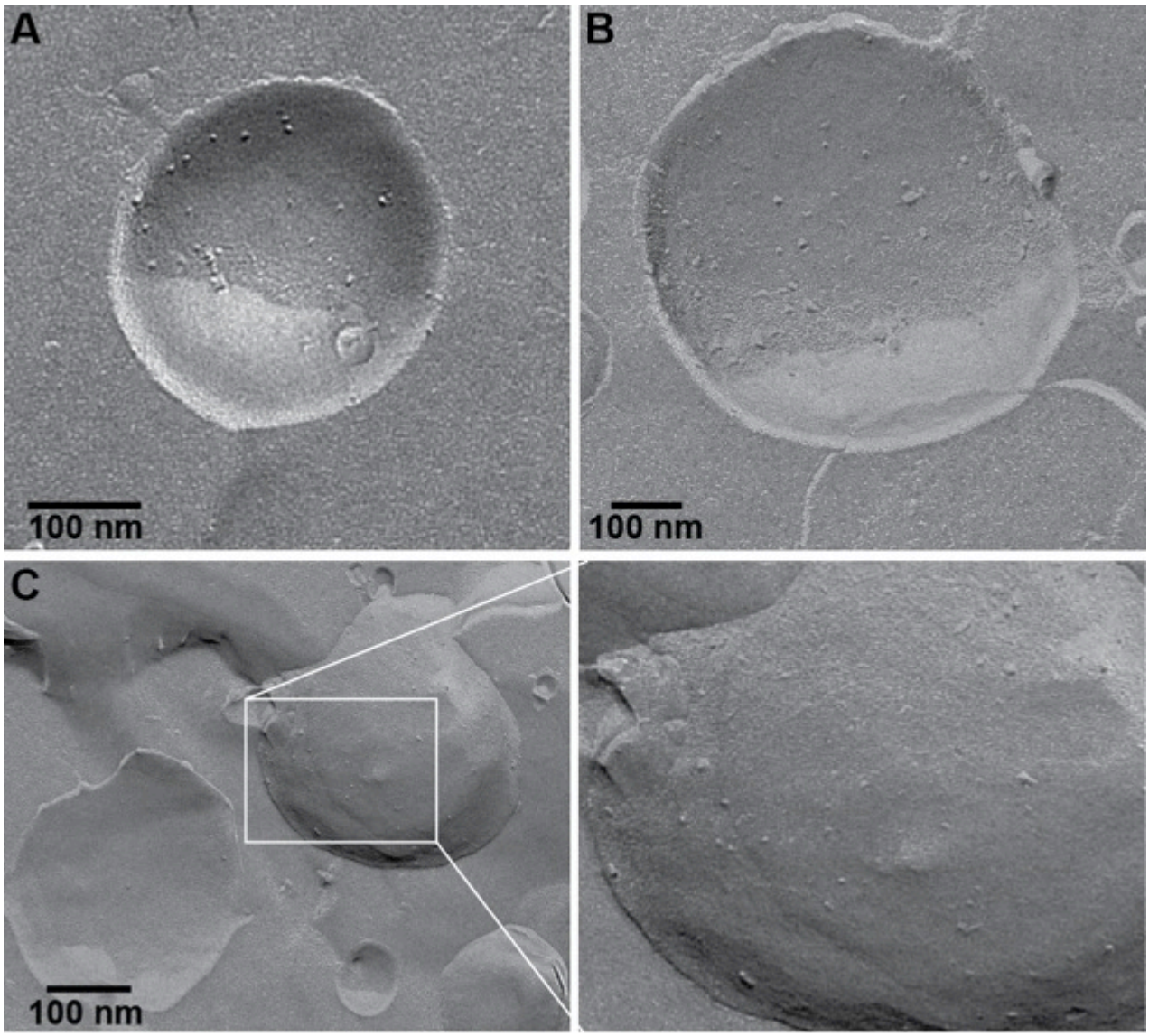

Figure 46: Freeze-fracture images of reconstituted BGT1syn_Pp into Liver polar lipids liposomes. BGT1syn_Pp was reconstituted into Liver polar lipids liposomes with an LPR of 20:1. The protein is moderately distributed into the liposomes, which were suitable for transport studies. Freeze-fracture images were performed by Friederike Joos (MPI of Biophysics).

3.2.4.7 Substrate transport studies

Functionality of purified BGT1syn_Pp was determined by [^{3}H]GABA substrate transport into proteoliposomes. The proteoliposomes (Figure 46) were first washed with Reconstitution buffer to remove residual detergent and to ensure non-permeability of the proteoliposomes. The proteoliposomes were preloaded with Reconstitution buffer supplemented with 250 mM NaCl to create a gradient over the membrane. In addition the proteoliposomes were, in a second step, preloaded with with a higher concentration of non-radioactive substrate (2 mM GABA) in order to reduce the probability of [^{3}H]GABA being transported out of the proteoliposomes from transporters that were reconstituted in the reverse direction. In this way saturation of [^{3}H]GABA in the proteoliposomes was achieved and could be measured after a certain time or with a certain concentration. Substrate transport was measured by recording the uptake of [^{3}H]GABA. [^{3}H]GABA uptake resulted in a saturation curve for proteoliposomes that were preloaeded with non-radioactive GABA (Figure 47, filled squares). BGT1syn_Pp was inhibited by the incubation with the specific BGT1 inhibitor, NNC-05-2090 (Figure 47, open squares). The protein concentration in the proeteoliposomes was measured using amido black assay (chapter 2.6.7.3).

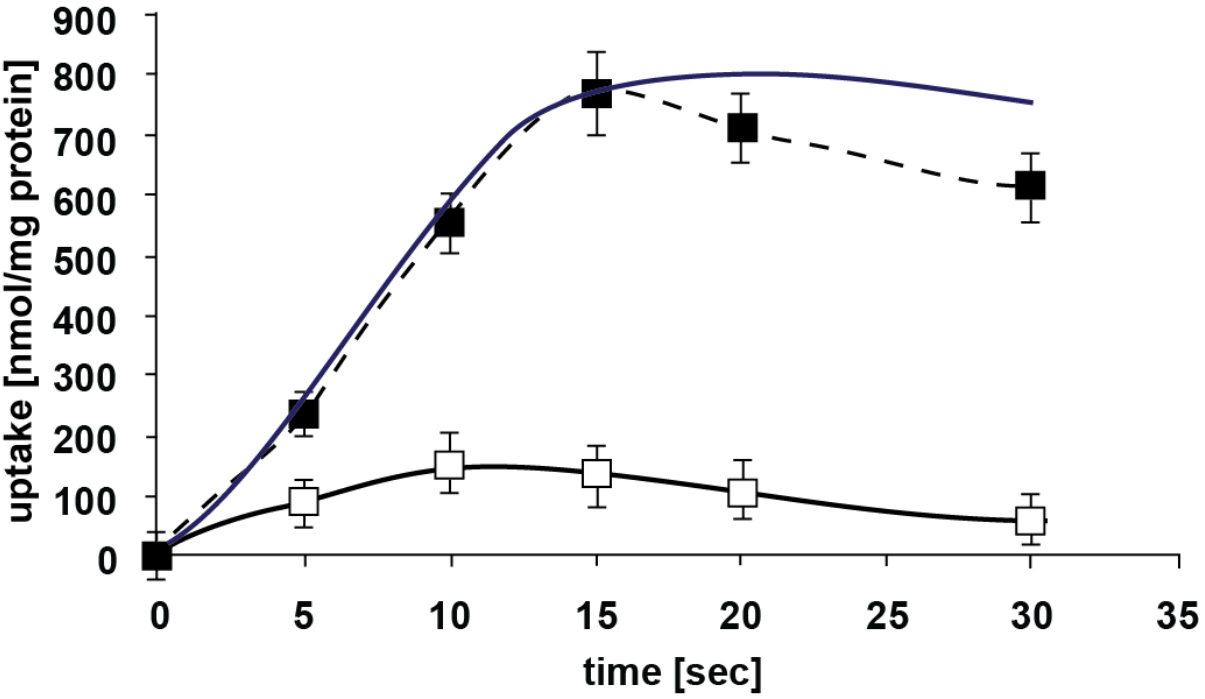

Figure 47: [^{3}H]GABA uptake into proteoliposomes with reconstituted BGT1syn_Pp. BGT1syn_Pp was reconstituted into liposomes with an LPR of 20. The proteoliposomes were preloaded with both 250 mM NaCl to create a gradient over the membrane and with non-radioactive GABA in order to reach saturation of [^{3}H]GABA while reducing the probability that [^{3}H]GABA is transported out of the proteoliposomes from transporters that are reconstituted in the reverse direction. Samples were taken at 5, 10, 15, 20 and 30 seconds (filled squares), an average of the uptake curve is shown in dark blue. As a control, BGT1 was inhibited with the specific inhibitor, NNC-05-2090 (open squares). An average of three independent measurements is shown.

3.3 BGT1 and BetP: Introduction of a potential substrate binding site in BetP

BetP shares the same overall fold with symporters of the NSS-family, i.e. it is a structural homologue of the NSS-symporter BGT1. BetP was used as a template to understand aspects of the transport mechanism in BGT1. A molecular mechanism as to how BGT1 is able to specifically transport two different substrates is still missing. BGT1 and BetP are not at all sequence related and in addition there is a topology shift by 2 transmembrane (TM) helices; TM1 in BGT1 corresponds to TM3 in BetP. Therefore the betaine- or GABA-binding site could not be identified from a sequence alignment without the BetP structure. To address these questions, a comparison of the BetP structure with a homology model of BGT1 (Figure 20 B) and subsequent mutagenesis studies in BetP were performed to mimic possible substrate interaction sites in BGT1. In a second step, corresponding mutations introduced in BGT1 might reveal coordination sites for possibly both substrates. A homology model of BGT1 was created based on the bacterial NSS-transporter $LeuT_{Aa}$ structure (pdb cod: 2A65) (Figure 20 B). The protein sequence of BGT1 was aligned with that of LeuT and adjusted using (Beuming et al., 2008) as reference for correct helix placements and optimal gap assignments. This final alignment was used to generate an energy-minimized and validated homology model.

Based on the BetP structure and the BGT1 model single key residues crucial for substrate specificity and ion coupling were identified. By introducing point mutations into the betatine transporter BetP, the betaine transport properties could be specifically altered. Recently, this strategy was very successfully applied to investigate H^+-coupled choline transport in a BetP mutant (Perez et al., 2011).

3.3.1 Betaine coordination in BGT1

The structure of BetP (Ressl et al., 2009a) reveals a very characteristic coordination of the substrate betaine. The trimethylammonium group of betaine is held in position by several tryptophans forming an aromatic substrate-binding box (Figure 48 A, inset). These aromatic

residues undergo major conformational changes when the transporter converts from an outward-facing to an inward-facing open state (Perez et al., 2012). The tryptophan-box coordinates betaine by cation-π interactions and thereby contributes to the µM affinity of BetP for betaine. BGT1 shows a 10 fold lower affinity for betaine and comprises seven phenylalanines in TM2 and TM6, the helices potentially important for substrate binding and transport. Some of these phenylalanines might also form an aromatic box, similar to that in BetP. The tryptophans in the binding pocket of BetP were substituted with phenylalanines obtaining single- (W189F), double- (W189/194F), triple- (W189/194/374F) and quadruple mutants (W189/194/374/377F) of BetP (diploma thesis Izabela Waclawska).

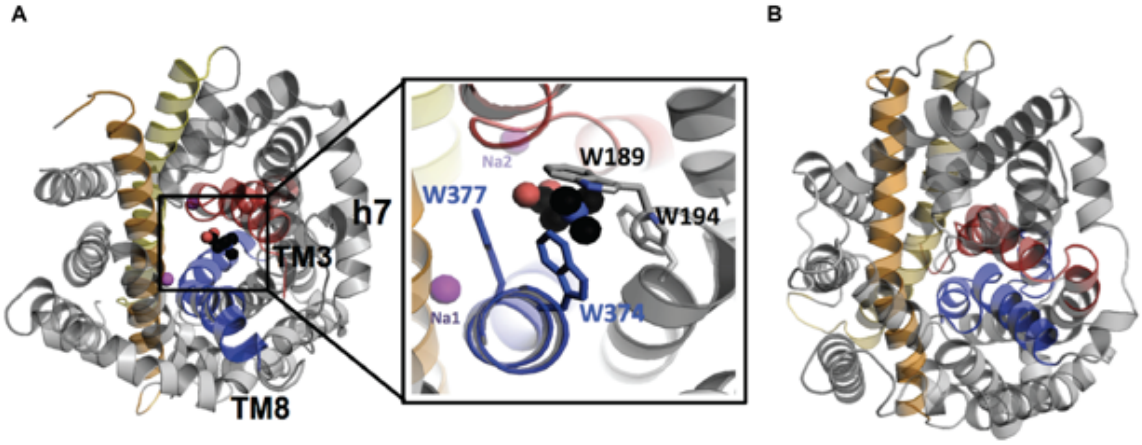

Figure 48: The structure of BetP reveals a 10 TM helix transporter core -TM3 to TM12- that corresponds to TM1 to TM10 in BGT1. (**A**) Top view from the periplasmic side on the structure of BetP and (**B**) top view on a homology model of BGT1 with $TM3_{BetP}$ and $TM1_{BGT1}$ in red, $TM8_{BetP}$ and $TM6_{BGT1}$ in blue, $TM5_{BetP}$ and $TM3_{BGT1}$ in orange and $TM10_{BetP}$ and $TM8_{BGT1}$ in yellow. (Inset) Coordination of betaine in BetP by several tryprophans from TM4 (W189, W194) and TM8 (W374, W377). Corresponding residues are found in TM2 and TM6 of BGT1.

Already an exchange of one tryptophan residue resulted in a significant lower K_M-value for transport, which was in a similar range of that detected for BGT1 (K_M = 146 µM) confirming that coordination of betaine by phenylalanines in a transporter decreases transport affinity (Figure 49). A substitution of functional important phenylalanines by tryptophanes in BGT1

might similarly result in an appreciably increase in affinity. This effect will be exploited to identify which phenylalanines in TM2 and TM6 of BGT1 are involved in betaine coordination.

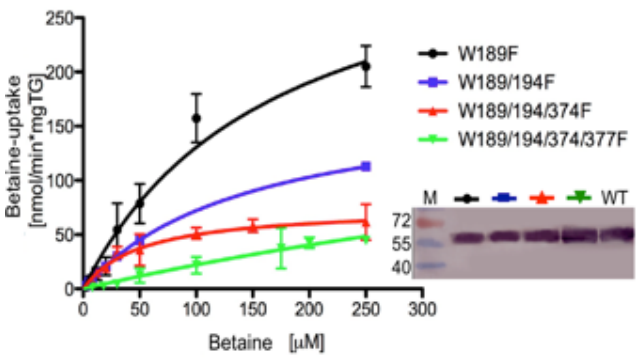

	K_m [µM]	V_{max} [nmol/min*mgTG]
W189F	169.1 ± 38.83	351.3 ± 41.94
W189/194F	149.5 ± 6.87	180.0 ± 4.93
W189/194/374/377F	577.0 ± 210.2	152.9 ± 36.51
WT	13.7 ± 6.01	166.5 ± 27.36

Figure 49: Betaine uptake rates in nmol per min and mg cell dry weight were measured dependent on the external betaine concentration in *E. coli* MKH13 cells expressing BetP mutants with phenylalanine substitutions. Mutations in the tryptophan box of BetP to phenylalanine resulted in a reduced affinity for the substrate in comparison to the wildtype (WT) of BetP as detected by uptake of 14[C]betaine in E.coli MKH13 cells. Western blot analysis demonstrates that all mutants are expressed to similar amounts.

3.3.2 GABA coordination in BetP

GABA coordination in BGT1 was investigated by a similar strategy. BGT1 comprises a glutamate residue in the unfold stretch of TM1 whereas the high affinity GABA transporter GAT1 habors a tyrosine residue at this position (Figure 50).

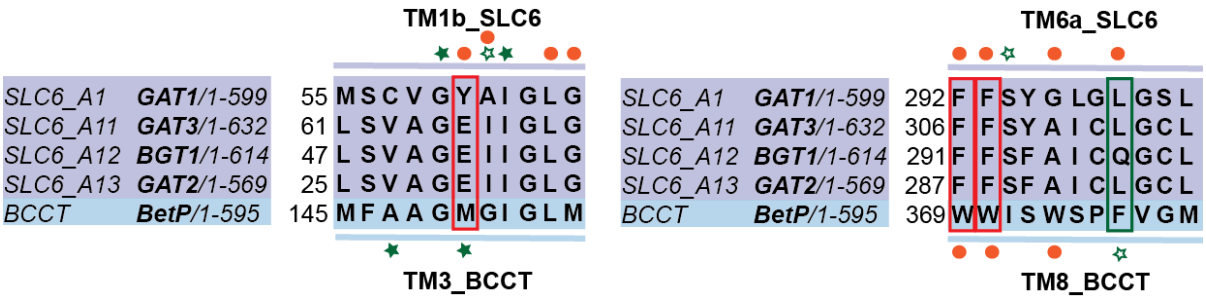

Figure 50: Sequence alignment of the amino acid sequences of TM domains 1b and 6a from the SLC6 transporters GAT1, GAT3, BGT1 and GAT2 and TM domains 3 and 8 of the BCCT family member BetP. Part of the TM domains 1b and 6a of human GAT1 (SLC6A1), human GAT3 (SLC6A11), dog BGT1 (SLC6A12) and human GAT2 (SLC6A13) were aligned with a part of the corresponding TM domains 3 and 8 of BetP. The red boxes highlight the position of the amino acid interacting with the substrate and which were mutated in BetP. The green box highlights the third position in TM3/TM8, which still needs to be investigated. The filled orange circles indicate the resdiues involved in substrate binding. The open and filled green stars show residues involved in coordinating sodium ions Na1 and Na2, respectively.

Interestingly, a substitution to glutamate in GAT1 abolished GABA uptake (Kanner, 2003) pointing towards a unique coordination of either GABA or sodium by this glutamate residue in BGT1 and the other two lower affinity GABA transporters GAT2 and GAT3. Whether this is a direct consequence of their second osmotically active substrates betaine, taurine and β-alanine for BGT1, GAT2 and GAT3, respectively, is unknown. One point mutation (M150E) was introduced in BetP and thereby transformed BetP into a GABA/betaine transporter with a K_M value of 334.5 ± 99.57 for GABA and 189 ± 37.5 for betaine (Figure 51, red and blue line, table). Additional substitution of a tryptophan to a phenylalanine at position 373 (M150E/W373F) in TM8 of BetP resulted in a GABA transport as well, however with a minor decrease in affinity for the substrate (Figure 51, brown line, table). An alternative

substitution of Trp374 to alanine (M150E/W374A) caused an increase in GABA affinity to 200.3 ± 10.93 (Figure 51, green line, Table aside).

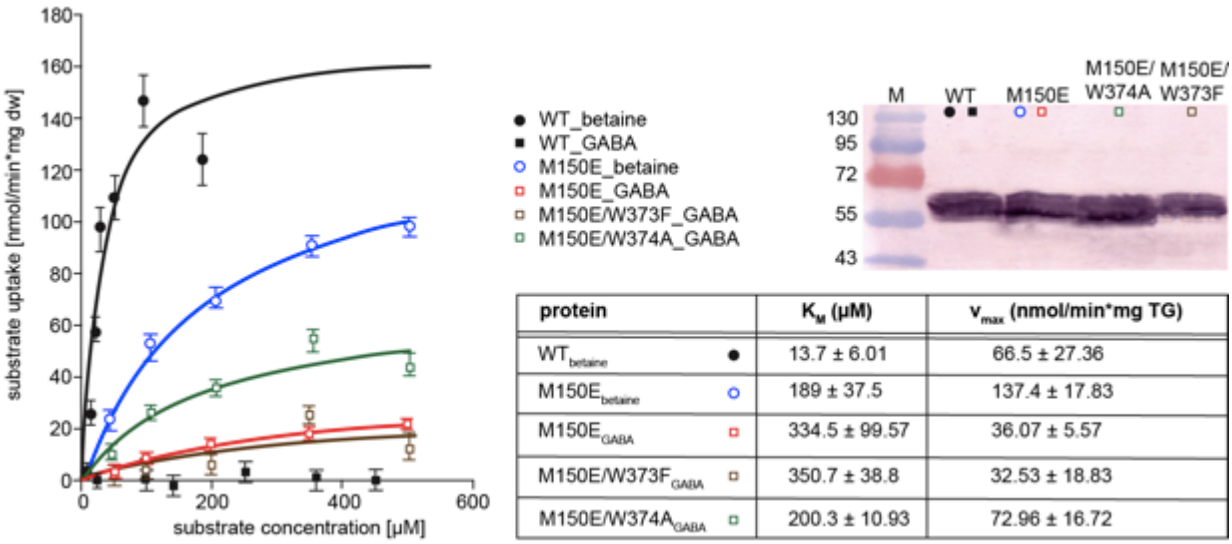

protein	K_M (µM)	v_{max} (nmol/min*mg TG)
$WT_{betaine}$ ●	13.7 ± 6.01	66.5 ± 27.36
$M150E_{betaine}$ ○	189 ± 37.5	137.4 ± 17.83
$M150E_{GABA}$ □	334.5 ± 99.57	36.07 ± 5.57
$M150E/W373F_{GABA}$ □	350.7 ± 38.8	32.53 ± 18.83
$M150E/W374A_{GABA}$ □	200.3 ± 10.93	72.96 ± 16.72

Figure 51: Point mutations of residues in TM3 and TM8 resulted in Na^+-coupled GABA transport in BetP. Substrate uptake rates in nmol per min and mg cell dry weight (dw) were measured dependent on the external betaine or GABA concentration in *E. coli* MKH13 cells expressing BetP M150E, M150E/W373F or M150E/W374A. Each point shows the average of three independent measurements. BetP WT (WT) was kindly provided by Camilo Perez. The error bars represent a mean ± SD. K_M and v_{max} values for betaine and GABA of M150E, M150E/W373F and M150E/W374A are listed in the table. Western blot analysis represents that all mutants are expressed to similar extend.

For crystallization trials the solubilisate of BetPΔN29EEE44/45/46AAA_M150E (BetA_M150E) was loaded onto a StrepTactin®-affinity chromatography column. The usual amount of protein loaded onto the SDS-PAGE gel was 10 µg. Most of the impurities were in the flow-through (FTO) fractions (Figure 52 A, FTO). After washing steps (Figure 52 A, W) with a detergent exchange from 0.01 % β-DDM to 0.6 – 1.2 % Cymal-5, the sample was eluted from the affinity column (Figure 52, E_Str) and was basically free of impurities, as judged by the Coomassie SDS-PAGE gel. The elution fraction (E_Str) shows a single band at 40 kDa with an additional band at ~ 95 kDa, the position of a possible BetA trimer. As membrane proteins are frequently observed to run at slightly lower apparent molecular mass in the SDS-PAGE gel than predicted, the bands in the gel most likely represent the monomeric form at 34-40 kDa and the trimeric form at ~ 100-120 kDa. The elution sample

from the affinity column was concentrated to ~ 5 mg/ml and loaded onto a size exclusion chromatography (SEC) Superose 6 10/300 column (Figure 52 A). An additional SEC purification step was necessary to obtain good quality 3D crystals.

BetA_M150E was co-crystallized in the presence of 5 mM GABA in 100 mM Hepes pH 7, 320 mM NaCl and 20 % (v/v) PEG 550 MME. A complete dataset of one crystal (Figure 52 B) was collected at the ESRF-ID29 beamline (Table 11). Data were collected in several data sub-sets by translation along one crystal axis to reduce the effects of radiation damage. All data sub-sets were processed and combined using the XDS package (Kabsch, 1993). Indexing revealed an orthorhombic crystal lattice with space-group $P2_12_12_1$, the same spacegroup as previously observed crystallized BetP mutants. A directional dependence of the diffraction pattern was observed (Figure 52 B) in which the resolution in the best direction was ~ 3.2 Å while in the worst was ~3.8 Å. Anisotropy correction (Strong et al., 2006) was applied and improved the statistics for the collected dataset. The crystal structure was determined by molecular replacement with BetA (pdb code: 4c7r) using the Phaser program (McCoy et al., 2007). The structure was refined using the Phenix refinement program without imposition of a three-fold non-crystallographic symmetry to account for the conformational asymmetry of individual protomers within the trimer (Adams et al., 2010). Model building was done manual with the COOT program (Emsley and Cowtan, 2004).

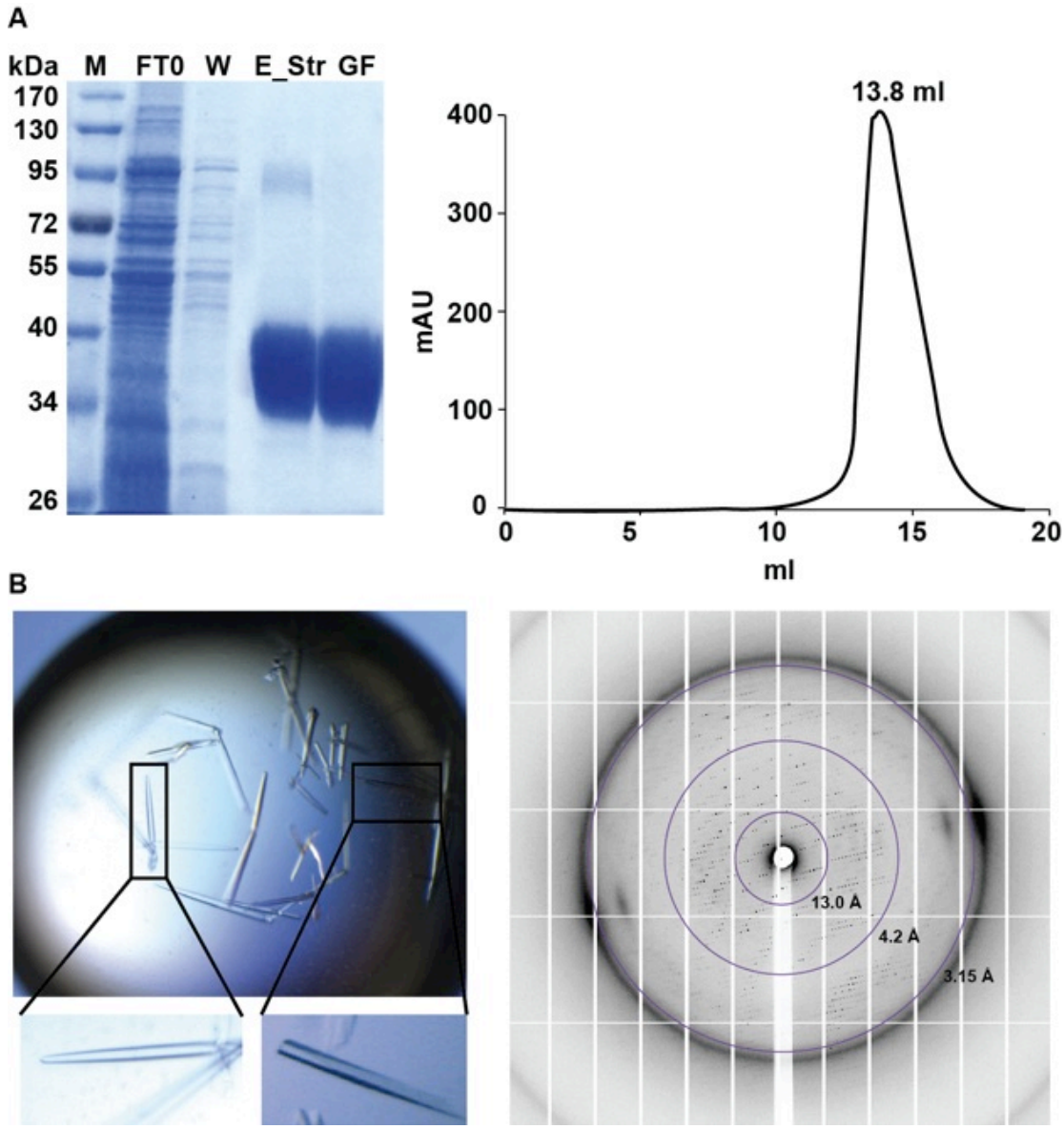

Figure 52: Purification, 3D Crystallization and Diffraction pattern of BetA_M150E. (**A**) SDS-gel of a BetA_M150E purification with StrepTactin®-affinity chromatography. The BetA_M150E solubilisate was loaded onto a column (FTO) and treated with 3 washing steps (W) before eluting the protein with desthiobiotin (E_Str). Size-exclusion chromatography of BetA_M150E was performed using a Superose 6 10/300 column. Purified protein samples were pooled and loaded onto the pre-equilibrated column. Separation was performed using a constant flow rate of 0.3 ml/min. The protein usually eluted in a single peak and an elution volume of 13.0 ml-15.0 ml. (**B**) Crystal needles of BetA_M150E were grown in 100 mM Hepes pH 7, 320 mM NaCl and 20 % (v/v) PEG 550 MME at 18 °C. Crystals diffracted to a resolution of ~ 3.2 Å in the best direction. Diffraction pattern image of the data set collected on the beamline ID29 at the ESRF (Granoble, France) from the BetA_M150E crystal.

The structure of BetA_M150E was solved with good statistical values (Table 11) to 3.2 Å resolution with the help of Caroline Koshy and Belinda Faust.

Table 11: Data collection and refinement statistics of BetA_M150E

Data collection	
Space group	$P2_1P2_1P2_1$
Cell dimensions	
a, b, c (Å)	120.26 129.78 186.89
α, β, γ (°)	90, 90, 90
Resolution (Å)*	48.73 - 3.2
R_{merge}[a]	0.144 (2.671)
$I/\sigma I$[a]	9.82 (0.79)
Completeness (%)*	81.5 (4.9)
Refinement	
Resolution (Å)	48.73 - 3.21
No. reflections	39696
R_{work}/R_{free} (%)	27.45/33.19
R.m.s.d.[b] bonds (Å)	0.003
R.m.s.d.[b] angles (°)	0.832

[a]Values in parentheses refer to data in the highest resolution shell.

[b]R.m.s.d., root mean square deviation

A GABA molecule was observed in two of the three protomers within the trimer (Figure 53) located close to the central binding site of the inward open facing state. GABA binds to BetA_M150E by forming a hydrogen bond between its carboxyl group and the carbonyl group of Glu150 as well as with its amino group and the indole ring of Trp377. Hereby the amino group of GABA is coordinated by Van der Waals interactions with Trp377 (Figure 53).

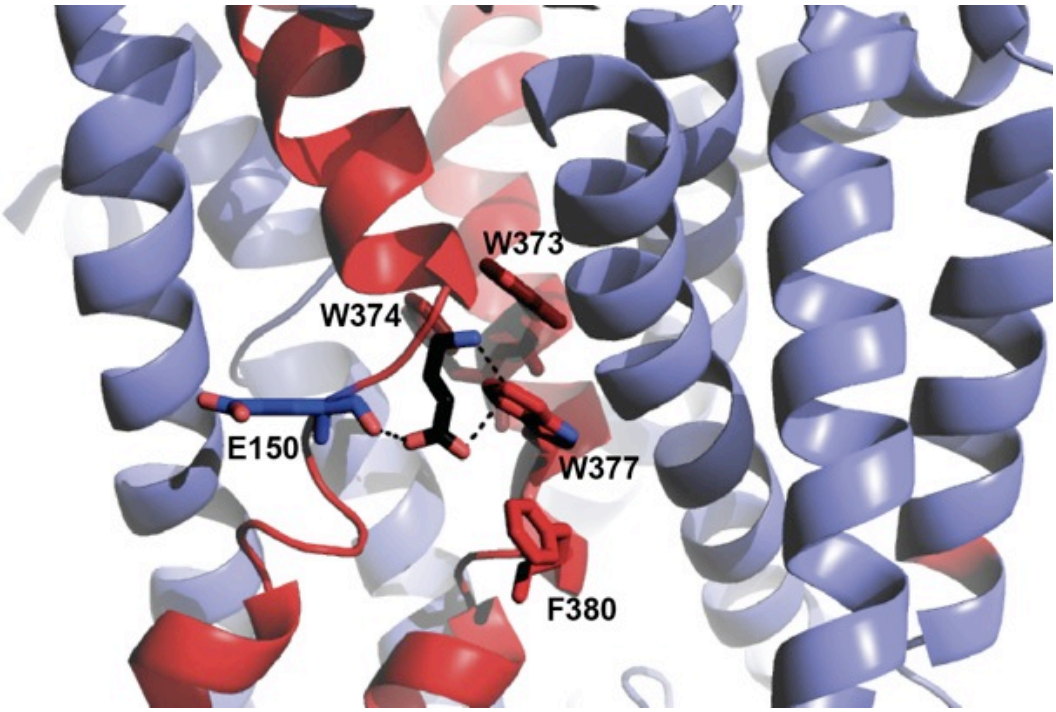

Figure 53: The X-ray structure of BetA_M150E in complex with GABA. View onto the GABA binding site in the BetA_M150E GABA mutant. The GABA molecule is shown in black. E150 and W377 coordinate the GABA molecule. Hydrogen bonds and Van der Waals interactions are depicted as dashed lines.

4 Discussion

4.1 Posttranslational modifications of BGT1

4.1.1 PKC dependent BGT1 downregulation *via* N-terminal regulatory components

The combination of electrophysiological studies in oocytes with radiotracer uptakes and localization of expressed proteins in cultured kidney cells provided complemantary information. The functional characteristics and kinetics of WT-BGT1 expressed in frog oocytes, including the preference for GABA over betaine (Figure 11), are in general agreement with a previous report (Matskevitch et al., 1999). Further, the inhibitory action of DOG on GABA dependent currents of WT-BGT1 in oocytes (Figure 14) confirms our previous report of DOG inhibition of endogenous BGT1 in MDCK cells (Kempson et al., 2006) and suggests that the response to DOG is not unique for MDCK cells but is an intrinsic property of BGT1. A previous study also showed that the endogenous system A transporter for amino acids was not sensitive to DOG, indicating a degree of specificity in the response (Kempson et al., 2006).

Three of the BGT1 mutants (T235A, S418A and S564A) displayed regular GABA dependent currents in oocytes (Figure 15), and GABA uptakes by the corresponding EGFP-BGT1 mutants were similar to native EGFP-BGT1 (Figure 18 A). Studies on localization of the EGFP-BGT1 mutants in MDCK cells revealed a primary integration into the plasma membrane during hypertonic stress, and cell internalization in response to PMA (Figure 17), likely by endocytosis. The inhibition of transport activity by PMA in HEK cells (Figure 18 B) was consistent with internalization, since cell uptake is determined in part by the surface abundance of the transport protein. Taken together, these observations suggest strongly that the mutations did not change the intrinsic transport activity of both WT-BGT1 and EGFP-BGT1, and show that the residues T235, S418 and S564 are not involved in the response to PKC activators.

The fourth mutant T40A showed an unexpected behavior. In oocytes it generated only a small GABA-dependent current that did not significantly respond to PMA, which stands in contrast to the observations with WT-BGT1 (Figure 15). In MDCK cells adapted to hypertonic stress the EGFP-tagged BGT1_T40A mutant was located in an intracellular compartment (Figure 16, Figure 17). This explains the low transport activity detected in HEK cells and the lack of measurable response to hypertonicity or PMA (Figure 18). The reasons why this mutant is trapped in intracellular compartments are not clear but some possibilities can be considered. One possible explanation is that T40A may have trafficked normally to the plasma membrane during hypertonic stress but was not retained there, similar to what was previously described for a truncated BGT1 mutant lacking the C-terminus (Massari et al., 2005). This mutant was recovered in a recycling compartment of MDCK cells (Massari et al., 2005), however, the intracellular location of T40A has to be determined. The mutant does not appear to be truncated because Western blots revealed a size similar to native EGFP-BGT1 and the other mutants that showed no effect (Figure 16). An alternative possibility is that T40A may remain intracellular due to a trafficking defect or improper folding. The former may be unlikely because it was previously established that signaling signals for exit from the endoplasmic reticulum and sorting to the basolateral plasma membrane of MDCK cells are contained within the cytoplasmic C-terminus of several proteins, including BGT1 (Matter et al., 1994; Muth et al., 1998). In BGT1 this signaling information lies within a short segment of amino acids (565-572), which is rich in basic residues (Perego et al., 1997). Attachment of a c-Myc tag (10 amino acids) or EGFP (238 amino acids) to the C-terminus did not affect basolateral targeting of BGT1 in MDCK cells (Ahn et al., 1996; Kempson et al., 2003). The remarkable effect of an alanine substitution at T40 in the cytoplasmic N-terminus might occur if the T40A mutant folds improperly at the N-terminus. This would likely result in retention of the T40A protein in the ER for degradation. However, attachment of EGFP to the N-terminus does not change plasma membrane trafficking compared to WT-BGT1, see (Kempson et al., 2003) and (Figure 17 B). Additional mutations and detailed co-localization studies with known markers for intracellular compartments will be needed to resolve some of these issues. Finally, it should be considered that PKC-dependent phosphorylation of T40 may be required

for normal trafficking and/or insertion of BGT1 into the basolateral plasma membrane of MDCK cells. This would explain the mis-localization of the T40A mutant. Related to this mechanism various reports show that hypertonicity can activate PKC isoforms in hepatocytes (Bierhals et al., 2007) and 3T3 cells (Zhuang et al., 2000), and that PKC may mediate hypertonic activation of cation channels in hepatocytes (Heinzinger et al., 2001) and the hypertonic induction of heat shock protein 70 in 3T3 cells (Lim et al., 2008).

In summary, the control of BGT1 transport activity likely occurs at several cellular levels, beginning at the regulation of gene expression by the TonEBP transcription factor in response to hypertonicity (Burg and Ferraris, 2008; Kwon et al., 2009), to the more rapid post-translational regulation of plasma membrane abundance *via* vesicular insertion (Kempson et al., 2003) and retrieval (Kempson et al., 2006; Kempson et al., 2008). Apart from T612 (Massari et al., 2005), the role of specific residues within BGT1 in transport regulation is not known. The Na^+- dependent betaine transporter in *Corynebacterium glutamicum*, BetP, provides a prime example of transport regulation upon hyperosmotic shock. In addition to its transport function, it is capable of both osmosensing and osmoregulation (Ott et al., 2008).

In BetP, both terminal domains are crucial for regulation of the trimeric transporter by interacting *via* salt bridges (Figure 54) with fold specific structural elements ($TM3_{BetP}$ and $TM8_{BetP}$).

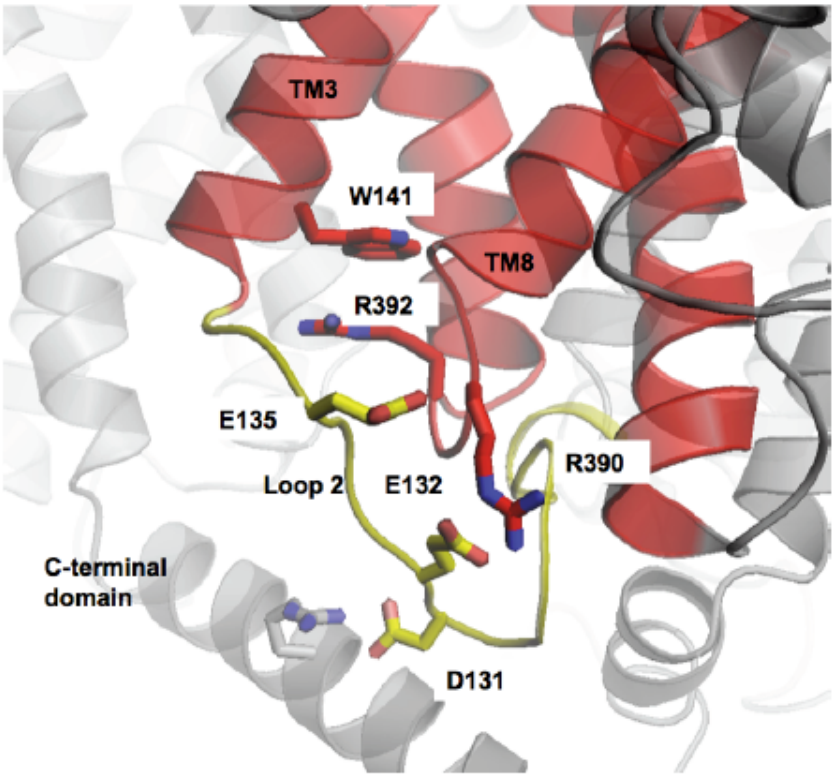

Figure 54: Cytoplasmic ionic interaction network of BetP. Due the mutual interaction of the C-terminal domains within the trimer, BetP can take advantage from the cytoplasmic ionic interaction network. Interactions comprise residues in Loop 2 (D131, E132) and TM3 (W141) with the C-terminal domain (R558) and Loop 8 (R390, R392).

A similar cytoplasmic salt bridge network was also observed in the NSS dopamine transporter DAT, formed by charged residues in the N-terminal domain close to the cytoplasmic tip of TM1, TM8 and TM6 and was suggested to modulate the transition of the transporter between the outward- and inward-facing conformations (Kniazeff et al., 2008). These residues are conserved in BGT1. Therefore, the BetP activation mechanism might be conserved also in eukaryotic NSS transporters. However, there is no indication for BGT1 being a homo-trimer (Figure 42) and the N- and C-terminal domains of BGT1 are shifted to different locations with respect to those in BetP. Interestingly, the topology shift places charged residues in both domains of BGT1 to positions that are crucial for the ionic interaction network in BetP (Figure 55).

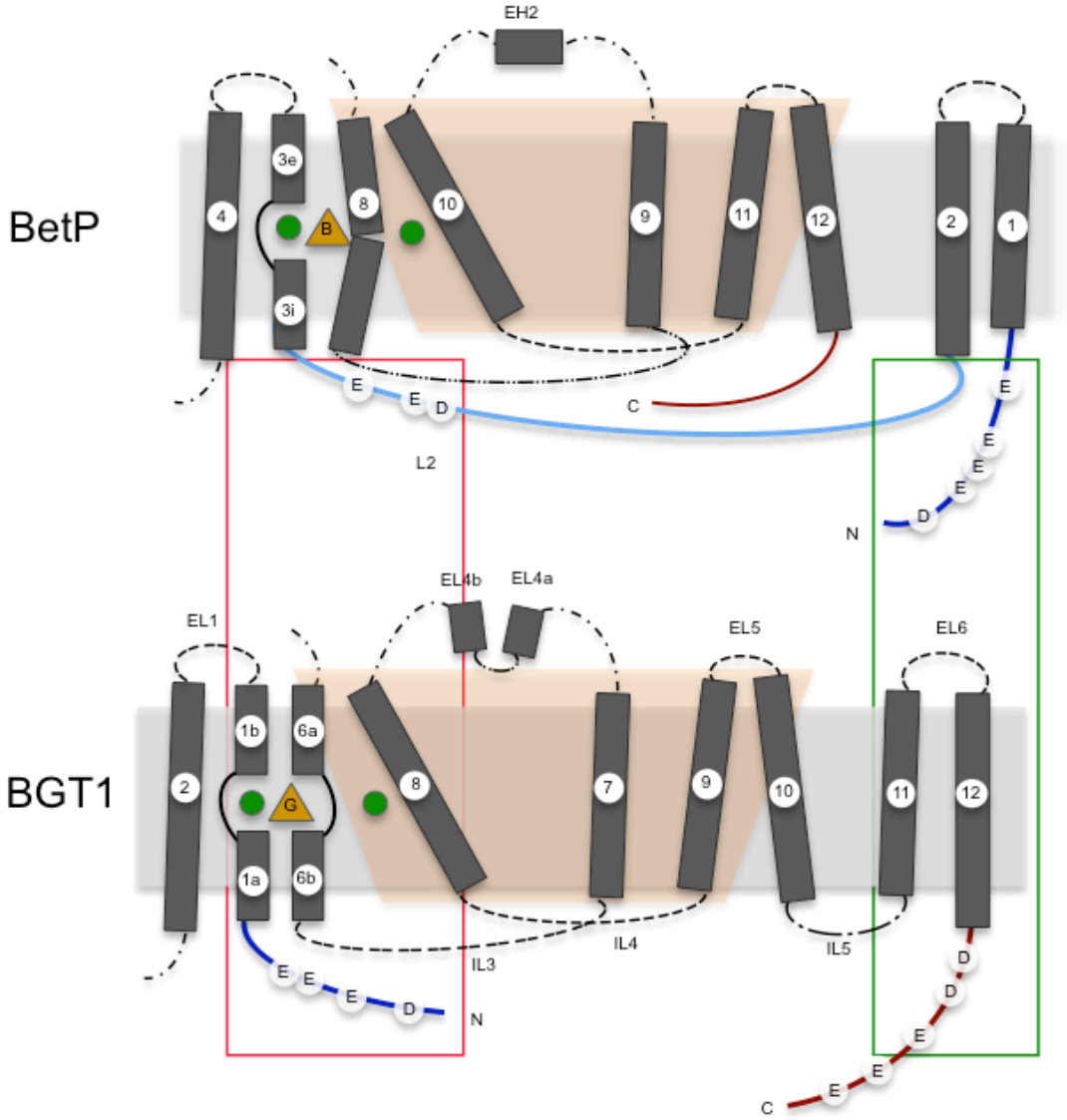

Figure 55: Topology shifts between BetP (TM2-TM12, missing TM5, 6 and h7) and BGT1 (TM1-12, missing TM3, 4 and 5). The positions of GABA and betaine are shown as yellow triangles labeled with 'B' for betaine and 'G' for GABA. The two sodium ions are shown as green circles. Due to a shift in topology by 2 TM helices, loop2 (L2) in BetP corresponds to the N-terminal domain of BGT1 (red rectangle) and the N-terminal domain of BetP corresponds to C-terminal domain of BGT1 (green rectangle). Charged clusters of glutamic acid (E) and aspartic acid (D) are found in BetP and BGT1 in the corresponding structural segments. L2 (D-E-X-X-E), N-terminal domain of BetP (D-X-E-E-E-X-X-X-E), N-terminal domain of BGT1 (E-E-X-E-X-X-D) and the C-terminal domain of BGT1 (E-X-E-5X-E-7X-D-5X-D).

Loop2 in BetP, which is involved in the regulatory interaction with the C-terminal domain, corresponds to the N-terminal domain of BGT1 (Figure 55, red rectangle). The N-terminal domain of BetP, which captures the C-terminal domain in specific stages of the regulatory cycle, corresponds to the C-terminal domain of BGT1 (Figure 55, green rectangle). Charged clusters of glutamic and aspartic acid are found in both BetP and BGT1 in corresponding structural segments. The osmo-sensing and osmoregulatory C-terminal domain of BetP lacks its counterpart in BGT1; however there is to date no indication that BGT1 is regulated on the activity level in the same way. Therefore, there is no need for BGT1 to form homo-oligomers in order to facilitate a similar activation mechanism involving its N- and C-terminal domains.
There is circumstantial evidence to suggest that the conformation of the N-terminus affects the transport cycle itself and particularly the translocation of substrate through the hydrophobic protein core as was shown for GAT1 (Deken et al., 2000).
N- and C-termini are in close vicinity and thus it is likely that there is also a cross-communication between the C-terminus and the hydrophobic core of the transporter.

4.1.2 *N*-glycosylation as a regulatory component in EL2

One of the most important and critical post-translational modifications of eukaryotic proteins is *N*-glycosylation (Stanley et al., 2009). This modification might be essential for correct folding, functionality and plasma membrane insertion of secreted proteins and offers greater proteomic diversity than other post-translational modifications (Stanley et al., 2009).
Deficiency in *N*-glycan association to the conserved site 3 was reported to reduce uptake rates in the NSS transporters GAT1 (Cai et al., 2005), CRT (Straumann et al., 2006), NET (Nguyen and Amara, 1996) and SERT (Tate and Blakely, 1994), which was mainly attributed to a reduced amount of protein inserted into the membrane. Lack of *N*-glycans at site 5 instead affected protein stability in DAT and GAT1 (Li et al., 2004; Cai et al., 2005). Aside from the obvious differences in the length of EL2, which might require a different quantity of *N*-glycosylation sites, the appearance of charged clusters flanking the sites also seems to affect the functional roles of *N*-glycosylation. Specifically, CRT, whose function is only slightly affected by *N*-glycosylation (Straumann et al., 2006), contains a charged cluster (Asp-Arg-

Arg) at *N*-glycosylation site 5 instead (Figure 20 A). By contrast, DAT and GAT1 lack this cluster at the same site and rely strongly on *N*-glycosylation for function (Li et al., 2004; Cai et al., 2005; Hu et al., 2011).

In order to obtain a first indication of the functional role of *N*-glycosylation in EL2 a homology model of BGT1 was constructed (Figure 20 B) based on a structure of the bacterial homologue $LeuT_{Aa}$ (Yamashita et al., 2005). EL2 in LeuT is not resolved completely; moreover, the sequence in this region is shorter than in the corresponding eukaryotic transporters (Figure 20 A). An additional chloride ion stabilizes the fold of EL2 by establishing crystal contacts (Yamashita et al., 2005). Moreover, simulations on the LeuT structure suggested EL2 to be flexible (Forrest and Rudnick, 2009). In the eukaryotic NSS transporter DAT, EL2 harbours residues to coordinate a zinc ion (Loland et al., 2003), while in others, e.g., in SERT disulphide bond formation is crucial to obtain a functional conformation of EL2 (Chen et al., 1997). In the same context, association with *N*-glycans seems to provide additional stabilizing interactions with most likely consequences for folding, trafficking and transport.

A functional role of *N*-glycans sems to be only associated with *N*-glycosylation site 5, N183 (Figure 20 A), while the putative, highly conserved *N*-glycosylation site 3, N171 (Figure 20 A), which is insensitive towards de-glycosylation with tunicamycin, is considered as silent *N*-glycosylation site in BGT1. Although *N*-glycan association is not essential on the BGT1 expression level, the conformation of EL2 might be crucially altered by the introduced mutations. Expression of BGT1 in oocytes could depend on a distinct conformation of EL2, which is compromised by the insertion of two negative charges in EL2. There are multiple factors specifically controlling functionally important conformations of EL2 in BGT1. Among those are the amount, kind and complexity of *N*-glycans that are required for plasma membrane insertion according to the tonicity of the membrane. In oocytes, BGT1 insertion is not regulated under hyperosmotic conditions (Figure 21 B) and shows only a comparatively simple form of *N*-glycans (Figure 21 D, Figure 22 A, judged from the small electrophoretic shift of ~ 10 kDa detected in Western blots) whereas it is *vice versa* in MDCK cells in which plasma membrane insertion of BGT1 is enhanced by hypertonicity (Figure 23 C, D; Hyp) and

associated *N*-glycans are more complex (Figure 23 A, judged from the band shift of ~ 35 kDa).

The overall effect of *N*-glycosylation on trafficking and transport is comparable to other NSS transporters including compromised trafficking and membrane insertion and a decrease in substrate affinity due to a lack of *N*-glycosylation (Tate and Blakely, 1994; Nguyen and Amara, 1996; Li et al., 2004; Cai et al., 2005; Straumann et al., 2006). Interestingly, a substitution of asparagine to aspartate for both *N*-glycosylation sites individually affected only trafficking (Figure 22 C), but not transport properties of BGT1 (Table 6). Taken all results into account the following interpretations can be drawn. They all point towards a distinct functional role of the extracellular loop 2 (EL2) within the NSS family, which was discussed already for other NSS transporters in previous studies (Tate and Blakely, 1994; Nguyen and Amara, 1996; Li et al., 2004; Cai et al., 2005; Straumann et al., 2006). Apparently, the structure of this loop in the absence of *N*-glycans is quite flexible and association with variable amounts of *N*-glycans modifies its plasticity towards a more stable conformation. It appears that the dynamic modification by *N*-glycans is important for expression (Figure 22 A) and trafficking (Figure 22 C), while a permanent putative stabilization by, e.g., mutagenesis decreases the amount of functional protein located in the plasma membrane (Figure 22 C). During transport, a more stable conformation of EL2 seems to be beneficial with respect to substrate affinity and can be mimicked by the introduction of a charged residue either at position 171 or 183 (Table 6, N183D, N171D). Introducing an aspartate at the conserved position 171 yielded a mutant with five times higher substrate affinity (Table 6, N171D) and hence might contribute to a more stable conformation of EL2, which could be additionally stabilized by salt bridges with neighbouring charged residues (Figure 20 C). This surprising finding points towards an altered architecture or conformation of EL2 by mutagenesis or association with *N*-glycans compared to the conformation adopted by the non-glycosylated BGT1-WT protein. Replacement of asparagine to aspartate at position 183 might even mimic the association with *N*-glycans yielding the nearly identical affinities of WT and N183D mutant (Table 6). Modifications of EL2 by either post-translational associated *N*-glycans or introduction of aspartic residue at position 183 (N183D)

could result in a stabilization of the flexible EL2. Considering that other GABA transporters like GAT1 comprise a functional *N*-glycosylation site at this position and at the same time show higher substrate affinity compared to BGT1, it can be assumed that in BGT1 the non-glycosylated N171 site contributes to its lower GABA affinity compared to GAT1 (Borden et al., 1992). This inactivation of the conserved N171 might be the result of specific interactions of non-conserved residues within EL2 of BGT1, which could render N171 inaccessible to *N*-glycans.

The data indicate that the dynamic association and putative stabilization of N183 by *N*-glycans is crucial for regulated membrane insertion (Figure 25). When N183 is genetically substituted by aspartate in EGFP-tagged BGT1, the protein loses its capability to counteract osmotic stress due to a reduced plasma membrane insertion (Figure 25 A, B; Hyp) compared to BGT1-WT during hypertonic stress (Figure 23 C, D; Hyp). Moreover, when *N*-glycans are enzymatically removed from EGFP-tagged BGT1_N183, its regulation is significantly impaired and the protein remains in the membrane even under isotonic conditions, which in the case of the glycosylated BGT1-WT protein would lead to depletion from the membrane to tune down transport (Figure 23 E).

In conclusion, three important processes in BGT1 can be proposed, which require *N*-glycosylation: firstly, translational regulation upon osmotic upshift; secondly, plasma membrane insertion and depletion and thirdly, substrate binding. To some point the data suggest a role of *N*-glycosylation for osmotic stress sensing of BGT1, which might rely on the sensory capability of N183-bound *N*-glycans in EL2. However, to resolve the exact *N*-glycan-mediated regulatory mechanism of BGT1 under osmotic stress conditions further detailed features have to be validated by additional experiments. It is an interesting fact that within the NSS family only the betaine transporting, osmotic stress regulated BGT1 has evolved an EL2 sequence quite distinct from other family members (Figure 20 A). The very distinctive role of *N*-glycosylation in BGT1 might draw attention to the non-conserved regions in EL2 of the other NSS transporters initiating more detailed investigations into this direction of these medical important transporters in future.

4.2 Heterologous expression of BGT1

High amounts of pure membrane proteins are needed for 3D crystallization to study their structure and function. From its natural source (MDCK cells) the expression level of BGT1 is not sufficiently high enough for extraction and purification. The best heterologous expression for a particular membrane protein results in high levels of functional protein production, a good cell surface distribution and the presence of functional, correctly folded protein. Therefore, the choice of a suitable heterologous protein expression system is a challenge, despite extensive experience from a wide variety of expression systems and expressed proteins (Grisshammer and Tate, 1995).

Overexpression of *bgt1* can be improved by manipulations such as gene optimization for expression in the desired organism with further optimization of expression in each host organism and to include affinity tags to facilitate protein purification to finally obtain milligram amounts of highly pure protein.

Expression studies were carried out in four different expression systems with analysis by different criteria depending on the amount of expressed protein and when possible on purified protein. Firstly, protein expression was analysed in membranes by Western blot analysis. Secondly, the BGT1 location within the cell was determined by immunogold labeling. Thirdly, the *N*-glycosylation status of natively expressed BGT1 was determined by Western blotting, and fourthly, the expression of functionally active BGT1 was measured by the uptake of radioactive-labeled substrate and specific inhibition in cells and proteoliposomes.

Indeed *E. coli*, *Sf9* cells and *P. pastoris* have successfully been used as expression systems in a wide variety of transporters, receptors and channels (Grisshammer and Tate, 1995; Reilander and Weiss, 1998). Nevertheless, if posttranslational modifications are required for the correct folding of a membrane protein and in order to obtain its fully functional state, all these expression systems have their limitations for the correct expression of mammalian membrane proteins.

Heterologous expression of proteins in *E. coli* and yeast has several advantages over the mammalian expression systems, which are the speed of producing overexpressing strains and the availablility of numerous expression vectors, the easy handeling and the low costs of

large-scale production. Expression of BGT1 in *E. coli* L-CF mode was a great chance because it could be shown that unglycosylated BGT1 was incorporated (Figure 28) and functionally active for [^{3}H]GABA uptake (Figure 29). Unfortunately, protein expression levels were too low and could not be increased. Furthermore, the protein can only be partially purified *via* the N-terminal His_6-tag (Figure 27). Explanations for the low expression yield might be, that the *E. coli* extract lacks the machinery for posttranslational modification of eukaryotic proteins and therefore a proper folding of the protein was not ensured and/or that the N-terminal His_6-tag might have a negative influence on the folding itself. Remarkably, it was not possible to express BGT1 in *E. coli in vivo*, though varying parameters like expression strains, growth media, temperatures and induction time. This could be due to the toxicity of the protein for *E. coli* leading to cell death and protein degradation.

Advantages of the *P. pastoris* expression system are the possibility of culturing *P. pastoris* in both shaking flasks and fermenter. Both are relatively easy to set-up and to maintain the growth culture. Nevertheless, these apparent advantages have many disadvantages. Most importantly for shaking flasks, which require five days for expression and the yield of cells per liter of culture is low. Besides this, during cell growth there is a lack to control the pH and oxygen levels. Nutrient levels and the temperature might fluctuate as well. On the other hand, a *P. pastoris* fermentation is also a laborintensive task, from setting-up the fermenter to harvesting of cells requires as well five days of work, but the advantage of fermentation is, that cells are supplemented with pure oxygen not just by increasing agitation but also by increasing air flow, which guaranties a constant sufficient oxygen level. Nutrients, like glycerol can be pumped into the vessel to replenish nutrients that are depleted, and the addition of methanol can be adjusted to prevent toxicity. Both systems were tested but unfortunately, during *P. pastoris* fermentation BGT1 protein production resulted in inhomogenous protein fractions in contrast to shaking flasks. Even though from a 5 l fermentation roughly one kilogram of cells could routinely be achieved whereas only about 10-15 g of cells were obtained per liter of media from shaking flasks, the production of homogenous protein predominated the decision to express BGT1 in shaking flasks, although with the resulting cell yield protein purification and further analysis were limited.

It might be that when the proper conditions of growth can be defined for BGT1 during *P. pastoris* fermentation, protein production might be improved and scaled-up in the near future. However, expression of eukaryotic membrane proteins in *P. pastoris* was reported to be difficult due to mannose hyper-glycosylation (Bretthauer, 2003). Severe folding problems were observed, e.g., for the NSS family member SERT, which showed high expression, but only small amounts of the expressed protein was functional active (Tate et al., 2003), most probably due to its dependency on cholesterol (Scanlon et al., 2001), which can not be mimicked by any other sterols, like ergosterol, which is found in yeast. Similarly, the codon-optimzed synthetic gene of *bgt1-wt* (WTsyn_Pp) was not stable after *P. pastoris* expression suffering plain degradation (Figure 56, WTsyn_Pp). In contrast, the codon-optimized synthetic gene with both *N*-glycosylation sites substituted to Asp, resulted in a stable protein expression (BGT1syn_PP) (Figure 39 and Figure 56, BGT1syn_Pp) and localisation in the ER and plasma membrane after expression as shown by immunogold-labelling with the FLAG-tag specific antibody (Figure 39 A).

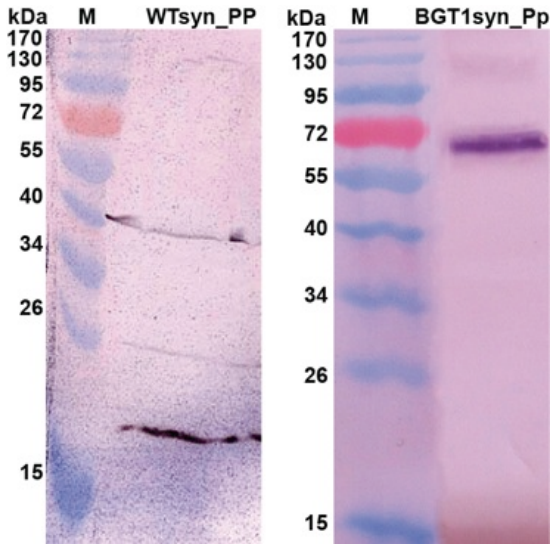

Figure 56: Improvement of expression for WTsyn_Pp and BGT1syn_Pp. The Western blot shows *P. pastoris* membranes containing overexpressed WTsyn_Pp (left) and BGT1syn_Pp. WT and BGT1 are coding for the same optimized gene but for BGT1syn both *N*-glycosylation sites were substituted to Aspartates. A major improvement in expression was obtained when using the optimized and deglycosylated gene for overexpression (BGT1syn_Pp, right), whereas the WT shows plain degradation (WTsyn_Pp_left).

Without modifying the amino acid sequence replacing rare codons with others that more closely reflect the host system's codon bias can dramatically increase the levels of functional protein expression. For optimization of the codon usage of BGT1 for heterologous expression in *P. pastoris* the codon table of the alcohol oxidase-gene AOX1 was used, which is the highest produced protein in *P. pastoris* when cells are grown in methanol media; AOX1 can make up as much as 30 % of the total cellular protein in the cell (Cregg, Madden et al. 1989; Daly and Hearn 2005). Therefore, it was considered that the choice of the codon table of a highly produced protein such as AOX1 might be advantageous over the more general *P. pastoris* codon bias. Notably, for a stable *bgt1* expression the codon-optimization was not sufficient, moreover a deglycosylated-optimized gene was essential.

Expression of *bgt1* in *Sf9* cells and in *Drosophila melanogaster* eyes resulted in sufficient amounts of protein for purification (Figure 31, Figure 35) and even for reconstitution of the *D. melanogaster* expressed *bgt1* (Figure 32). Both heterologous expression systems appear very encouraging and will be continued in large scale for further analysis and a fuller understanding of how *bgt1* expression is affected by cell type and the use of different expression systems with regard to subsequent purification and uptake measurements.

4.2.1 Solubilization and purification of BGT1 expressed from the codon-optimized gene (BGT1syn_Pp)

Detergents for solubilization of BGT1syn_Pp were screened as a first purification step. The goal was to find a certain detergent that solubilized as much BGT1syn_Pp as possible, while solubilizing the minimum of other membrane proteins. All tested detergents fulfilled these requirements (Figure 40). However, the milder maltoside detergents such as DM and DDM worked best, whereas the zwitterionic, harsher detergents like Fos-cholines and Zwittergent 3-12 as well as the anionic detergent Laurorylsarcosine were less effective (Figure 40), as they can disrupt internal protein interactions, which can lead to protein unfolding.

In the BGT1syn_Pp construct of the optimized gene a His_{10}-tag was fused to the protein's C-terminus for the first purification step and a FLAG-tag to the N-terminus for a second purification step. Both purification steps were necessary to obtain pure and homogenous

protein (Figure 41). 10 % glycerol in all purification buffers helped to improve monodispersity. Intriguingly, the choice of detergent during purification of BGT1syn_Pp influenced to some extent the running behavior of the protein during size exclusion chromatography. DM in all purification buffers resulted in one single monodisperse peak (Figure 41 A), DDM and Cymal-5 led to two peaks (Figure 41 B, C).

For membrane protein purification and crystallization the sugar-based, non-ionic detergents such as maltosides are often used. Most BGT1syn_Pp purifications were performed using these kinds of detergents. The Cymal-detergents have a cyclohexyl tail with which more hydrophobicity is packed into a shorter chain length compared to the maltoside-detergents. This could therefore be adavantageous for 3 D crystallization but so far it could not be robustly investigated due to limitations in protein amounts.

4.2.2 Monodispersity and oligomeric state of BGT1syn_PP

Blue native gradient gels and analytical size exclusion chromatography were used to determine the oligomeric state of BGT1. Size exclusion chromatography of BGT1 purified in DM gave a single peak, revealing a single monomeric state of the protein in this detergent (Figure 41 A) whereas BGT1 purified in Cymal-5 or DDM resulted in two peaks, revealing possibly two oligomeric states, a more prominent monomeric and a minor dimeric state (Figure 41 B, C). On the other hand, from BN gradient gel electrophoresis it can be assumed that the oligomeric state of BGT1 is monomeric, dimeric and even tetrameric independent of the detergent (Figure 42). Since the size exclustion chromotography profile of BGT1syn_Pp revealed a monomeric and to a lesser extent a dimeric oligomeric state, it could be that the presence of coomassie blue during BN gel electrophoresis increases electrostatic interactions between the protein molecules that might lead to the association of multiple monomeric proteins yielding in higher oligomeric states.

Interestingly, it was shown that neurotransmitter transporters form oligomers in the membrane (Schmid et al., 2001; Sorkina et al., 2003). The dopamine transporter, DAT and the glycine transporters, GlyT1 and GlyT2 form dimers at the cell surface (Hastrup et al., 2001; Sorkina et al., 2003; Torres et al., 2003; Bartholomaus et al., 2008). GAT1 (Schmid et al., 2001) and

SERT (Kilic and Rudnick, 2000; Schmid et al., 2001; Just et al., 2004; Sato et al., 2004) also form homo-oligomers in the membrane of living cells. Furthermore, it was suggested that oligomerization is thought to be a prerequisite for trafficking of transporters from the ER to the cell surface as mutations, which disrupt oligomer formation in GAT1 and DAT resulted in ER retention (Scholze et al., 2002; Torres et al., 2003). Even the bacterial member LeuT was crystallized as a dimer with TM11 and TM12 forming a dimerization interface (Yamashita et al., 2005). Although there is so far no functional reason to suggest homo-oligomer formation, it cannot be excluded that BGT1 might form dimers also under natural circumstances, especially considering the high tendency of other SLC6 family members to form homo-oligomers.

4.2.3 Lipid analysis of BGT1syn_Pp

Certain phospholipids are essential for the activity of several membrane proteins (Dowhan, 1997). Specific protein-lipid interactions might be important for correct folding of a membrane protein and membrane insertion (Dowhan and Bogdanov, 2012). For heterologous expression the specific phospholipid requirements of a membrane protein should be considered (Opekarova and Tanner, 2003) as the content and especially the complexity of phospholipid in different cell compartments vary greatly among organisms and even within mammalian cells (Fagone and Jackowski, 2009).

In general the zwitterionic phospholipids phosphatidylcholine (PC) and phosphatidylethanolamine (PE) are the most abundant phospholipids in eukaryotic cells, comprising 25 and 50 % of total cell phospholipid mass, respectively (Henneberry et al., 2001; van Meer et al., 2008; Fagone and Jackowski, 2009). PC forms bilayers in form of vesicles and other defined structures in solution (Dowhan, 1997). Moreover, PC and PE can be oriented by the electrical potential in the membrane and both, together with non-neutral lipids, have been suggested to be important to fulfill the “positive-inside-rule” for membrane insertion of membrane proteins (van Klompenburg et al., 1997).

PC usually adopts a cylindrical shape that spontaneously organizes itself into bilayers (Cullis and de Kruijff, 1979). With this feature, PC is ideally suited to serve as the bulk structural

element of biological membranes (de Kroon, 2007) and it makes up a high proportion of the lipids in the outer leaflet of the plasma membrane. The fluidity on the membrane is conferred through the kinked unsaturated acyl chains, acting as a balance to these lipids that do not form bilayers or that form specific micro-domains (rafts) (Petreus and Petreus, 2011). Curvature of membranes, which is required for membrane transport and fusion processes can be induced by metabolizing PC to e.g. lyso-phosphatidylcholine (lysoPC) or phospatidic acid (PA) (Petreus and Petreus, 2011).

A bound lipid after protein purification implies a high affinity of the lipid to the protein (McAuley et al., 1999). BGT1syn_Pp heterologously expressed in *P. pastoris* was purified and analysed by TLC (Figure 44). The lipid composition of the plasma membrane of yeast comprises mainly PC and PE with minor proportions of phosphatidylinositol (PI), phosphatidylserine (PS) or phosphatidyl-glycerol, as well as sterols, mainly ergosterol and zymosterol but no cholesterol (Ziółkowska et al., 2012).

TLC lipid analysis identified PC as being the major lipid bound to BGT1syn_Pp after purification (Figure 44), indicating a strong lipid-protein interactions through either the lipid head group or its unsaturated alcylchain or both, which most likely stabilize the protein.

4.2.4 Reconstitution of BGT1syn_Pp

Membrane proteins can be reconstituted into liposomes for either activity assays or 2D crystallization. For a successful reconstitution, detailed experimental investigation of the reconstitution parameters is needed (Racker, 1979). Positive reconstitution depends on correct liposome formation, suitable ionic conditions, the right temperature, stable lipids and protein and the right detergent used for reconstitution (Eytan, 1982; Rigaud and Levy, 2003). It is crucial that the protein maintains its full activity during the entire reconstitution procedure. At first, BGT1syn_Pp reconstitution was tested by gel chromatography as described for the GABA transporter 1, GAT1 (Shouffani and Kanner, 1990). Shouffani et al. controlled protein incorporation by measuring [^{3}H]GABA uptake into proteoliposomes. In this work, BGT1syn_Pp incorporation was first investigated by freeze-fracture imaging. Unfortunately, although gel chromatography is a fast method and only small amounts of protein are needed,

it can lead to inhomogenous and incomplete protein incorporation and heterogenous proteoliposome size (Rigaud and Levy, 2003). Removal of detergent (Na-cholate) resulted in the formation of heterogenous proteoliposomes with BGT1syn_Pp either not being incorporated at all or when incorporation was achieved the protein concentration was very low as seen in freeze-fracture images. Unfortunately, residual detergent was still present in the samples. Alternatively, Biobeads were used for detergent removal (Rigaud and Levy, 2003). The advantage of this method is that detergent removal can more precicely be controlled and even low cmc detergents can be removed completely. The detergent adsorption on the beads surface depends on several parameters, such as the initial detergent concentration in the sample, detergent properties, temperature and presence of phospholipids (Rigaud and Levy, 2003). Extrusion was tested for preformation of liposomes in combination with Triton X-100 titration for destabilizing the liposomes. Triton X-100 induced destabilisation of the preformed liposomes turned out to be a critical and important step for BGT1syn_Pp insertion. Due to the low protein yield liver polar lipids (LPL) were used for reconstitution as BGT1 naturally occurs mainly in kidneys and liver (chapter 1.5.1). LPL liposomes could not be destabilized easily but needed exact and continuous pipetting and mixing during Triton X-100 addition, which is most probably due to the cholesterol content in this lipid mixture. In the end, BGT1syn_Pp was evenly distributed in LPL liposomes as demonstrated by freeze fracture imaging (Figure 46). [^{3}H]GABA uptake into BGT1syn_Pp proteoliposomes was investigated and resulted in activity up to 800 nmol [^{3}H]GABA/mg protein. BGT1syn_Pp was fully inhibited by the specific BGT1 inhibitor NNC-05-2090 (Figure 47).

4.2.5 Crystallization of BGT1syn_Pp

4.2.5.1 2D crystallization of BGT1syn_Pp

2D crystallization of BGT1 or any other related eukaryotic transporter from the SLC6 family has not been reported elsewhere before this study.

Unfortunately, many factors hindered the crystallization of BGT1syn_Pp, mainly the low protein yield, although the purity of BGT1syn_Pp could be consistently reproduced

independent on individual expressions. But the protein usually had to be concentrated, ideally without any protein loss, to at least 1 mg/ml for 2D crystallization set-ups.

At low LPR (~ 0.5) only small lipid-protein patches formed, whereas at higher LPR (> 1) larger lipid-protein patches and sheets could be obtained (Figure 45). Even though PC stayed tightly bound to the protein during purification, which could be demonstrated by TLC (Figure 44), the use of DMPC, DOPC or POPC alone in 2D crystallization set-ups led to aggregation of the protein (Table 10), indicating that additionally to PC other lipid components like cholesterol are important to successfully crystallize the protein in the two dimensional lipid bilayer. Due to the low protein yield each crystallization set-up was done with a new batch of protein. This led to inconsistent results in 2D crystallization set-ups and beside occasional protein-lipid patch formation often resulting in protein aggregation, which could also be due to differences during protein expression. Nevertheless, protein-lipid patches and sheets only formed when liver polar lipid mixtures were used.

As dialysis temperature influences lipid fluidity, dialysis rate, protein stability and the cmc of the detergent used, dialysis temperatures at 27 °C and 37 °C could be tested in this work. No obvious dependency on temperature could be obtained but other temperatures like 20 °C or 4 °C should be tested in the near future. Nevertheless, initial protein-lipid patches could be obtained, which is a significant step forward for further 2D crystallization. These first lipid-protein sheets indicate that the protein has achieved already a kind of ordered packing.

4.2.5.2 3D crystallization of BGT1syn_Pp

Among other requirements for 3D protein crystallization a pure and monodisperse protein sample in sufficient amounts is needed. Protein stability is a prerequisite for protein crystallization since an unstable protein tends to either aggregate or degrade. Despite the low protein yield, initial 3D crystals of BGT1syn_Pp were carried out (Figure 43).

Notably, this is the first time that initial protein crystals of a higher eukaryotic SLC6 family member could be obtained. These first crystals are a significant progress for further 3D crystallization.

4.3 BGT1 and BetP: Common principles

BGT1 comprises several phenylalanines (Figure 57) in similar locations to aromatic residues in its structural homologue BetP, which suggests a different location and coordination for the substrate compared to GAT1 (Skovstrup et al., 2010) and TauT (Tomi et al., 2008). In fact phenylalanines could coordinate betaine, however, with a much lower affinity as observed in mutagenesis studies of betaine binding proteins (Schiefner et al., 2004).

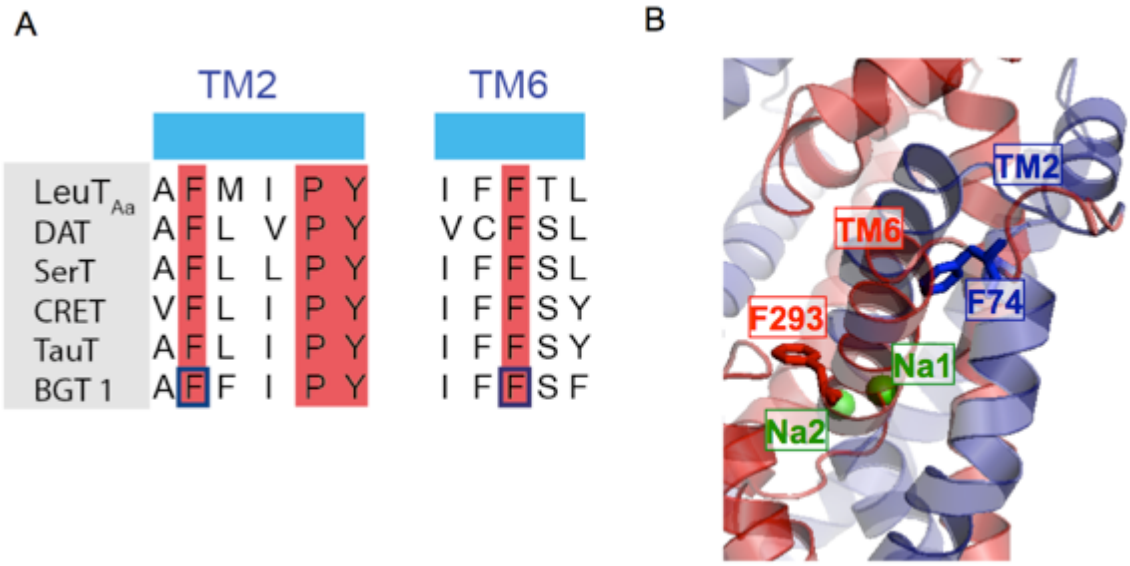

Figure 57: Amino acid sequence alignment of members of the SLC6 family and a corresponding homology model of BGT1. (**A**) Amino acid sequence alignment of conserved motifs in TM2 and TM6 of LeuT, DAT, SERT, CRET, TauT and BGT1 with strictly conserved residues highlighted in red. Conserved phenylalanines among all members are framed in blue in the BGT1 sequence. (**B**) The homology model of BGT1 shows TM2 (blue) and TM6 (red) with the two phenylalanines that are framed in BGT1 in the sequence alignment (A). Both sodium ions, Na1 and Na2 are labeled in green.

Indeed, BGT1 shows a significantly lower affinity for betaine ($K_{M\ (betaine)}$ = 200 - 400 µM) (Chen et al., 2004) compared to BetP ($K_{M\ (betaine)}$= 10 µM) (Farwick et al., 1995). It is not known if these phenylalanines form an aromatic box as they do in BetP, but with respect to the numerous Phe-residues halfway across TM2 and TM6 in BGT1 (Figure 57) it might be at least a possibility. Definitely, substitutions of tryptophanes to phenylalanines of the highly conserved aromatic box in BetP dramatically decreased the affinity for betaine (Figure 49)

indicating that the phenylalanines in BGT1 might contribute to some extent to betaine binding and coordination.

Although most of the residues coordinating the substrate are highly conserved in the osmolyte SLC6 subfamily, some residues identified in TM1 differ for GAT1, GAT2, GAT3 and BGT1, CRET and TauT (Figure 50). Substitution of residues in GAT1 by corresponding residues in TauT increased taurine uptake in GAT1 (Skovstrup et al., 2010). Amino acid substitutions at four positions (F60Y/C136L/A297G; GAT1 numbering) in CRET resulted in GABA-transport and in loss of creatine transport activity (Dodd and Christie, 2007). Remarkably, a substitution of residues in GAT1 by corresponding residues in BGT1 abolished GABA uptake pointing towards significant differences in GABA coordination in BGT1 compared to GAT1 (Skovstrup et al., 2010) and CRET, where single or multiple point mutations successfully altered substrate affinity (Dodd and Christie, 2007). However, without structural information of BGT1 it remains unknown if this is a direct consequence of its second osmotically active substrate betaine. It is assumed that the osmoregulatory role of BGT1 exceeds its role as a neurotransmitter transporter (Gadea and Lopez-Colome, 2001). Interestingly, the uptake data of BGT1's structural homolog BetP strongly support that Na^+-coordination in BetP is altered by the mutation M150E in the corresponding TM3, at the Na2 site (Figure 50). Surprisingly, this mutation also enabled (weak) GABA transport in BetP (Figure 51, M150E), which however is in good agreement with recent data that substrate specificity is linked to the coupling ion (Perez et al., 2011), assuming that the corresponding residue Glu51 is involved in Na^+- coordination in BGT1, too. Further modifications by an additional substitution of the Trp-box of BetP in TM8 to alanine (M150E/W374A) slightly increased the affinity for GABA in BetP (Figure 51) whereas the substitution to phenylalanine (M150E/W373F) showed similar GABA affinity as the single mutant, M150E (Figure 51).

In fact, the homology model of BGT1 points more towards a structural conservation of the BetP sodium-binding sites than to the sodium-binding sites found in $LeuT_{Aa}$ indicating that betaine (and perhaps GABA) transport in BGT1 might be facilitated by a mechanism more similar to that observed for BetP. However, it remains an intriguing question if the

mechanism of sodium-substrate coupling differs between the two substrates GABA and betaine in BGT1.

A crystal structure of the BetA_M150E mutant in complex with GABA could be obtained (Figure 53). GABA coordination was not yet shown in any transporter structure. The obtained X-ray data of the BetA_M150E-GABA complex enables to fit a reliable GABA molecule and its likely coordination in the already existing BGT1 homology model.

5 Summary

The betaine/GABA transporter BGT1 is one of the most important osmolyte transporters in the kidney. BGT1, which is a member of the neurotransmitter sodium symporter (NSS) family, facilitates Na^+/Cl^--coupled betaine uptake to cope with hyperosmotic stress as well as to counteract the deleterious effect of urea that is accumulated to high amounts during the urinary concentration cycle. Betaine transport in kidney cells is up-regulated under hypertonic conditions by a yet unknown mechanism when increasing amounts of intracellular BGT1 are inserted into the plasma membrane. Re-establishing isotonicity results in ensuing depletion of BGT1 from the membrane.

BGT1 phosphorylation on serines and threonines might be a regulation mechanism. In the present study, four potential PKC phosphorylation sites in BGT1 were mutated to alanines (T40A, T235A, S428A, S564A) and the responses to PKC activators, namely phorbol 12-myristate acetate (PMA) and a diacylglycerol analog (dioctanoyl-*sn*-glycerol, DOG) were determined. The sites chosen are highly conserved across species and are located at sites likely exposed to the cytoplasm. Since transport by BGT1 is electrogenic the intrinsic transport activity were monitored in frog oocytes expressing *bgt1*. The wild type and mutants were also expressed in cultured kidney cell lines to monitor intracellular distribution and for transport studies using radioactive-labelled substrate.

Superfusion of oocytes expressing WT-BGT1 with 1 mM GABA or betaine generates an inward current under voltage-clamp conditions. At -60 mV the K_M for GABA was 0.02 mM and for betaine 0.18 mM. GABA-sensitive currents were diminished after 30 min preincubation with the PKC activators PMA or DOG. Staurosporine blocked the response to DOG. Three mutants (T235A, S428A, S564A) evoked normal GABA-sensitive currents but currents in oocytes expressing the BGT1 mutant T40A were greatly diminished. [^{3}H]GABA uptake was also determined in HEK-293 cells expressing EGFP-tagged BGT1 with the same mutations. T235A, S428A and S564A showed normal upregulation of GABA uptake after hypertonic stress overnight, and downregulation by PMA was normal compared to EGFP-BGT1. In contrast, GABA uptake by the T40A mutant showed no response to hypertonicity

or PMA. Confocal microscopy of the EGFP-BGT1 mutants expressed in MDCK cells, grown on glass or filters, revealed that the T40A mutant was present in the cytoplasm after 24 h hypertonic stress while the other mutants and EGFP-BGT1 were predominantely present in the plasma membrane. All four mutants co-migrated with EGFP-BGT1 on Western blots suggesting they are full-length proteins. In conclusion, T235, S428, and S564 are not involved in downregulation of BGT1 due to phosphorylation by PKC. However, T40 near the N-terminus may be part of a hot spot important for normal trafficking or insertion of BGT1 into the plasma membrane.

Additionaly, a link between substrate transport regulation by BGT1, insertion of BGT1 into the plasma membrane and *N*-glycosylation in the extracellular loop 2 (EL2) of BGT1 could be revealed. The functional importance of two predicted *N*-glycosylation sites (N171 and N183), which are conserved in EL2 within the NSS family were investigated for trafficking, transport and regulated plasma membrane insertion by immunogold-labelling, electron microscopy, mutagenesis, two-electrode voltage clamp measurements in *Xenopus laevis* oocytes and uptake of radioactive-labelled substrate into MDCK cells. Trafficking and plasma membrane insertion of BGT1 was clearly promoted by proper *N*-glycosylation in both, oocytes and MDCK cells. De-glycosylation with PNGase F or tunicamycin led to a decrease in substrate affinity and transport rate. Mutagenesis studies revealed that in BGT1 N183 is the major *N*-glycosylation site responsible for full protein activity. Replacement of N183 with aspartate resulted in a mutant, which was not able to bind *N*-glycans suggesting that N171 is a non-glycosylated site in BGT1. N183D exhibited close to WT transport properties in oocytes. Surprisingly, in MDCK cells plasma membrane insertion of the N183D mutant was no longer regulated by osmotic stress indicating unambiguously that association with *N*-glycans at this position is linked to osmotic stress-induced transport regulation in BGT1.

The molecular transport mechanism of BGT1 remains largely unknown in the absence of a crystal structure. Therefore investigating the structure-function relationship of BGT1 by a combination of structural biology (2D and 3D crystallization) and membrane protein biochemistry (cell culture, substrate transport by radioactive labeled GABA uptake into cells

and proteoliposomes) was the aim of this work. While the functional assays are well established, structure determination of eukaryotic membrane transporters is still a challenge. Therefore, a suitable heterologous expression system could be defined, starting with cloning and overexpression of an optimized gene. The achieved expression levels in *P. pastoris* were high enough to proceed with isolation of BGT1. Furthermore, purification protocols could be established and resulted in pure protein, which could even be reconstituted in an active form. The quality and homogeneity of the protein allowed already 2D and 3D crystallization, in which initial crystals could be obtained.

Interestingly, the striking structural similarity of BGT1 to the bacterial betaine transporter BetP, which became a paradigm for osmoregulated betaine transport, provided infomation on substrate coordination in BGT1. The structure of a BetP mutant that showed activity for GABA was solved to 3.2 Å in complex with GABA in an inward facing open state. This structure shed som light into the molecular transport mechanisms in BGT1 and might help in future to design conformationally locked BGT1 to enforce the on-going structure determination.

6 Zusammenfassung

Nierenzellen sind extremen hyperosmotischen Bedingungen ausgesetzt, da bei der Bildung des konzentrierten Urins die interstitiellen NaCl- und Harnstoffkonzentrationen stark ansteigen. Zur Osmoadaptation akkumulieren Nierenzellen Osmolyte wie Betain, welches zudem die strukturelle Integrität von intrazellulären Proteinen vor zu hohen Harnstoffkonzentrationen schützt. Betain wird mittels des Na^+- gekoppelten und Cl^--abhängigen Co-Transporters BGT1 über die basolaterale Membran des Tubulusepithels transportiert. BGT1 ist über Transkription und Membraneinbau indirekt in die Osmoregulation der Niere involviert. Es stellt sich nun die Frage, ob der Transporter direkt auf Aktivitätsebene reguliert ist. Als Mitglied der Neurotransmitter-Sodium-Symporter (NSS)-Familie akzeptiert BGT1 auch GABA als Substrat, einen inhibitorischen Neurotransmitter, der u.a. im zentralen Nervensystem von großer Bedeutung ist.

Ein wichtiger Regulierungsmechanismus konnte über die Phosphorylierung mittels Protein Kinase C (PKC) an einem bestimmten Threonin-Rest (T40) im N-terminus von BGT1 gezeigt werden. Hierzu, wurden vier potentielle PKC Phosphorylierungsstellen gegen Alanine ausgetauscht und die Resonanz auf die PKC Aktivatoren, PMA und DOG, ermittelt. Die Transportaktivitäten wurden sowohl in Oozyten als auch in Zellkultur überprüft, letzteres wurde ebenfalls auch zur zellulären Lokalisierung des WT-BGT1 und der Mutanten genutzt. Drei der Mutanten wiesen ähnliche Transporteigenschaften, gleiche Herunterregulierung durch PMA bzw. DOG und eine gleiche zelluläre Verteilung unter hypertonischen Bedingungen auf, wie der Wildtyp (WT). Wohingegen kein Transport, weder nach hypertonischem Schock noch auf den PKC Aktivator bei der T40A Mutante zu detektieren war. Die zelluläre Verteilung dieser Mutante wies auf, dass diese nach 24h hypertonischem Stress im Cytoplasma verweilte, im Gegensatz zum WT und den anderen drei Mutanten, welche unter diesen Bedingungen primär in der Plasmamembran eingebaut waren. Dadurch lässt sich festhalten, dass T40 im N-Terminus von BGT1 eine wichtige Funktion in der Lokalisierung und Verankerung von BGT1 zur und in die Plasmamembran erfüllt.

Des Weiteren wurde die funktionelle Bedeutung zweier vorhergesagten *N*-Glykosylierungsstellen (N171, N183) in Bezug auf die zelluläre Verteilung, den Transport und den regulierten Einbau von BGT1 in die Plasmamembran untersucht. Hierbei konnte gezeigt werden, dass, sowohl in Oozyten als auch in Zellkultur, die Lokalisierung und der Plasmamembraneinbau von BGT1 durch die *N*-Glykosylierung eindeutig begünstigt wurde.
Eine Deglykosylierung mit PNGase F oder Tunicamycin führte zu einer Abnahme sowohl in der Substrataffinität als auch bei der Transportrate. Mittels Mutagenesestudien konnte aufgezeigt werden, dass N183 die Haupt-*N*-Glykosylierungsstelle und diese auch für die vollständige Proteinaktivität verantwortlich ist. Weiterhin konnte gezeigt werden, dass Zuckerreste an N183 unabdingbar für den osmoregulierten Regulationsmechanismus von BGT1 sind.

Der molekulare Mechanismus des GABA- und Betain-Transports in BGT1 ist in Ermangelung einer Struktur und dem Fehlen von *in vitro* Transportuntersuchungen weitgehend unbekannt. Deswegen wurde eine Kombination aus strukturbiologischen (2D und 3D Kristallisation) und biochemischen/biophysikalischen Methoden (Substrattransport mit radioaktiv-markiertem GABA in Zellen und Proteoliposomen) zur Struktur- und Funktionsuntersuchung dieses biologisch und medizinisch hoch relevanten eukaryotischen Sekundärtransporters angewendet.
Hierfür wurde BGT1 zunächst als Volllängenprotein heterolog in vier verschiedenen Expressionssystemen hergestellt. Anschließend erfolgte die Etablierung eines Reinigungsprotokolls, welches u.a. im Fall der Expression in *P. pastoris* zu reinem und stabilem Protein führte. Trotz der geringeren Ausbeute an gereinigtem Protein war es möglich Aktivitätsmessungen in Proteoliposomen, sowie 2D und gar 3D Kristallisation durchzuführen, welche sogar zu ersten Proteinkristallen führte.

In enger Anknüpfung an frühere Studien des bakteriellen, osmoregulierten Betain-Transporters BetP, welches als Modellsystem für osmoregulierten Sekundärtransport etabliert werden konnte, war es möglich eine Mutante herzustellen, welche nicht nur GABA

transportieren, sondern auch in Komplex mit GABA kristallisiert und strukturell untersucht werden konnte. Diese Erkenntnis ermöglicht nun eine weitere Etablierung des molekularen Transportmechanismus von BGT1 und könnte ferner dazu beitragen, BGT1 in einer bestimmten Konformation zu fixieren, um die Strukturaufklärung dieses Transporters voranzubringen.

7 Outlook

Role of the terminal domains in BGT1 activation

No structural information on the BGT1 N- and C-terminal domains is available to date. Based on *ab initio* structure determination of the N- and C-terminal domains of BGT1 provided by Dr. Cristina Fenollar-Ferrer (Computational Structural Biology Group, MPI of Biophysics) (Figure 12) several regulatory interaction sites were identified. As the N-terminal interaction with PKC could be inverstigated in this work, further attention can be focused on the following regulatory parameters:

(1) Interaction of Syntaxin 1A with the N-terminal residues E20, E21, E23, D26;

(2) Binding of Sec24D to the C-terminal residues R568 and L569;

(3) C-terminal PDZ binding at L605, I606 and V607.

In general, Syntaxin 1A, a major component of the exocytotic SNARE complex, acts as a down-regulator and modulates the transporter activity by affecting directly intrinsic transport properties. Indeed, the homology model proposes an ionic interaction network of the N-terminal domain (D26, E30 and W39) with either Loop6 (K310) or the C-terminal domain (R568), which would be very similar to the interaction network that inactivates betaine transport in BetP. These interactions might also be influenced by the phosphorylation of T40 through PKC leading to activation of endocytosis, and consequently result in a decreased number of transporters in the plasma membrane (shown in this work).

In the same context, binding of Sec24D to the C-terminal domain might be responsible of transporting the protein from the ER to the cell-surface.

Furthermore, the residues identified, which might be responsible for the interaction of BGT1 and the PDZ binding protein mLIN7 at the cell surface by preventing its internalization.

Hence, the above listed interaction sites can be investigated by mutagenesis studies and with further functional characterization of the mutants by [^{14}C]betaine and [^{3}H]GABA transport in Xenopus oocytes, MDCK cells and BGT1 proteoliposomes.

Thus, the *ab initio* model of the terminal domains can be validated and further information of BGT1 regulation can be revealed. With pull-down and co-immunoprecipitation assays the interaction partners can be identified and the predicted coordination sites can be confirmed by

mutagenesis. These investigations can be directly carried out in MDCK cells or in Xenopus oocytes.

In addition, introducing cysteines for cross-linking studies most likely will affect active coordination sites resulting in altered transport and trafficking.

Initial studies can be conducted in *Xenopus oocytes* and/or MDCK cells. The interaction of Syntaxin 1A with the N-terminal domain and binding of Sec24D to the C-terminal domain can be analyzed in MDCK cells by confocal microscopy to understand how trafficking of BGT1 is affected. Moreover, in an in vitro system the different interactions can be individually analysed.

Therefore, after a confirmation of the predicted interaction sites a heterologeous expression system, like *P. pastoris* could be used with a subsequent purification and reconstitution of individual mutants. As reconstitution experiments have already been shown to work successfully, [^{3}H]GABA uptake into proteoliposomes can be measured in the presence of activating partners and can eventually be optimized together with further lipid analysis and 2D crystallization. Freeze fracture can be used as a method to visualize the incorporation of the protein into liposomes.

Besides important functional characterization of the regulatory mechanism in BGT1 the results could provide valuable information to stabilize BGT1 when expressed heterologeously to improve the already existent 3D crystals. Not only should it be possible to lock the transporter in a distinct conformation, conformational stability might also be increased by promoting activating/inactivating interactions with soluble partner proteins.

Two-dimensional crystallization of BGT1

Two-dimensional crystallization of full-length BGT1 can further be improved to determine a 3D cryo-electron microscopy (EM) map to investigate BGT1 activation in the membrane in response to lipid composition, and internal ionic strength.

Heterologous expression and accompanied purification and reconstitution of BGT1 should be optimized in order to obtain higher amounts of purified protein to get tightly packed 2D crystals. Purified BGT1 can be analyzed regarding the content of associated lipids in addition

to the standard characterization techniques. As shown, BGT1 shows full activity in cholesterol-containing membranes, which indicates that membrane insertion might be dependent on the presence of lipid rafts. Lipid-rafts can be isolated by density gradient ultracentrifugation and immuno-affinity precipitation. Accordingly, reconstitution of BGT1 into different raft types can be investigated. Lipid analysis can be performed by MALDI-TOF, multiple precursor-ion MS and as already performed by thin-layer chromatography. In any case, as demonstrated in this work, the choice of lipids is the essential input parameter in 2D crystallization of BGT1. Natural lipids from MDCK cells might be advantageous. Lipids from MDCK cell membranes can be prepared by chloroform-methanol extraction. In addition, when using pure synthetic lipids, cholesterol could be used additionally, to better mimic the native MDCK membrane. Assuming an interaction between BGT1 and lipids, the crystallization conditions should be settled down for a defined protein-lipid mixture. To remove excess of detergent different dialysis set-ups (tubing, buttons or dialysis cassettes) can be tested as well as temperature ramping and sequential dialysis.

Cell-free expression of BGT1 could be continued in L-CF mode, and the cell-free produced protein can be further characterized and may be even crystallized.

Reconstituted protein and potential two-dimensional crystals should be examined first by freeze fracture and electron microscopy of negatively stained samples. In the case of well-diffracting crystals, high-resolution electron micrographs can be collected. Micrographs could then be digitized and analyzed with MRC and CCP4 programs to calculate a three-dimensional map of BGT1. To identify the N- and C-terminal domains in the resulting 3D EM map of the full-length protein it might be more effective to co-crystallize in the presence of Sec24D and different truncation mutants of the soluble part of Syntaxin 1A. The structures of both proteins were solved (pdb codes: 3EFO and 3C98), which would allow fitting them into the EM density of the complex.

Three-dimensional crystallization of BGT1

Expression and purification as well as three-dimensional crystallization of BGT1 can be continued and optimized to improve the size and quality of the existing crystals. Promising

3D crystals could be used for data collection. Alternatively, 3D crystallization in lipid cubic phase could be used, too.

The construction, characterization and crystallization of surface engineered mutants of BGT1 for 3D crystallization could be performed based on the existing homology model and the extended experience on

BetP. Understanding of betaine, GABA and sodium binding will be implemented in 3D crystallization to eventually lock BGT1 in a substrate-bound conformation. As described in the previous two sections the regulatory interaction with Syntaxin 1A and Sec24D might be helpful for 3D crystallization, too. However, the N- and C-terminal domains of BGT1 could also be expressed separately in E. coli by using the Maltose binding protein as a folding stabilizer to perform 3D crystallization together with the interaction partners Syntaxin 1A and Sec24D, respectively.

Very often mutations alter the expression behaviour of the protein. As a consequence, the expression of BGT1 mutants will probably require some efforts in testing of growth conditions for optimization.

Purification might be fine-tuned by careful screening of new detergents and additional purification steps

(size exclusion chromatography and/or ion exchanger) including removal of the affinity tag.

Crystallization studies should always be preceded by a careful analysis of the protein purity and stability by CD spectroscopy, native gel electrophoresis and dynamic light scattering. The functionality of each BGT1 construct should be tested by transport measurements before crystallization. Therefore, transport studies with [^{14}C]betaine and [^{3}H]GABA in cells and proteoliposomes could be performed. Most of the individual issues in 2D and 3D crystallization depend on each other; therefore a strict chronological separation is not possible. For instance, if point mutations will help to improve the structure determination due to a more rigid molecule, additional sites for mutation can be identified leading to a new round of cycling through mutation, optimization of expression, purification, crystallization and structure determination.

Coordination of betaine, GABA, sodium and chloride in BGT1

In BetP, the sodium sites are found at symmetric locations in the inverted repeats topology. These locations are slightly different to those identified in LeuT that serves as bacterial model for the neurostransmitter transporters, but not the osmolyte branch in the NSS-family. In analogy to the experiments in this study (GABA-specificity in BetP due to a single point mutation in TM3 -M150E - at the Na_2 site, and substitution of the Trp-box in TM4 and TM8 to alanine and phenylalanine, respectively) both sodium-binding sites can be further modified in BetP to reduce betaine affinity and to increase GABA affinity. Transport in WT BetP is not chloride dependent, however, chloride dependence of transport can be introduced by point mutations close to the Na1-site in analogy to the NSS-transporters SERT and GAT1. The effect of chloride on the transport of both substrates can be studied by measuring K_D-values for both substrates and co-substrate by Tryptophan-Fluorescence and K_M-values by [^{3}H]GABA transport in E. coli cells and proteoliposomes.

With a high-affinity GABA-BetP mutant in hand 3D crystallization could be continued to obtain a well diffracting crystal structure of BetP in complex with GABA to further enable a reliable GABA coordination in the already existing structure and homology model.

Later on, BetP can be exploited in a very similar way also for other osmolyte transporters of the SLC6 family as e.g. the creatine transporter (CRET) and the taurine transporter (TauT) to strengthen the hypothesis that osmolyte transport occurs by a different coupling mechanism than neurotransmitter transport.

In parallel substrate specificity and affinity in BGT1 can be examined directly. Therefore, crucial residues involved in betaine coordination should be identified by an increase in affinity by determining K_M-values in Xenopus oocytes when systematically conserved phenylalanine residues in TM2 and TM6 are substituted to tryptophan residues. Identification of betaine coordinating residues would serve further to dock betaine into the homology model of BGT1. In return, the homology model in complex with betaine could be a valuable tool to subsequently investigate sodium binding sites in BGT1 by mutagenesis, ITC, [^{14}C]betaine and [^{3}H]GABA transport in Xenopus oocytes.

Based on the reconstitution results for the heterologeously expressed BGT1 into proteoliposomes allowing now to investigate the order of sodium binding during substrate transport by using Tryptophan-Fluorescence and solid-supported membrane-based electrophysiology with improved time resolution.

In a next step, sodium binding and coupling in heterologeously expressed TauT and CRET could be investigated in a similar way, too.

The more general goal could be to establish BetP as a structural and functional model system to investigate the osmolyte branch of SLC6 transporter.

Literature

Abramson, J., and E.M. Wright. 2009. Structure and function of Na(+)-symporters with inverted repeats. *Curr Opin Struct Biol*. 19:425-432.

Adams, P.D., P.V. Afonine, G. Bunkoczi, V.B. Chen, I.W. Davis, N. Echols, J.J. Headd, L.W. Hung, G.J. Kapral, R.W. Grosse-Kunstleve, A.J. McCoy, N.W. Moriarty, R. Oeffner, R.J. Read, D.C. Richardson, J.S. Richardson, T.C. Terwilliger, and P.H. Zwart. 2010. PHENIX: a comprehensive Python-based system for macromolecular structure solution. *Acta crystallographica. Section D, Biological crystallography*. 66:213-221.

Ahn, J., O. Mundigl, T.R. Muth, G. Rudnick, and M.J. Caplan. 1996. Polarized expression of GABA transporters in Madin-Darby canine kidney cells and cultured hippocampal neurons. *J Biol Chem*. 271:6917-6924.

Almilaji, A., C. Munoz, Z. Hosseinzadeh, and F. Lang. 2013. Upregulation of Na,Cl-Coupled Betaine/ gamma-Amino-Butyric Acid Transporter BGT1 by Tau Tubulin Kinase 2. *Cell Physiol Biochem*. 32:334-343.

Andre, N., N. Cherouati, C. Prual, T. Steffan, G. Zeder-Lutz, T. Magnin, F. Pattus, H. Michel, R. Wagner, and C. Reinhart. 2006. Enhancing functional production of G protein-coupled receptors in Pichia pastoris to levels required for structural studies via a single expression screen. *Protein Sci*. 15:1115-1126.

Armsen, W., B. Himmel, H. Betz, and V. Eulenburg. 2007. The C-terminal PDZ-ligand motif of the neuronal glycine transporter GlyT2 is required for efficient synaptic localization. *Mol Cell Neurosci*. 36:369-380.

Barnard, T.J., J.L. Wally, and S.K. Buchanan. 2007. Crystallization of integral membrane proteins. *Current protocols in protein science / editorial board, John E. Coligan ... [et al.]*. Chapter 17:Unit 17 19.

Bartholomaus, I., L. Milan-Lobo, A. Nicke, S. Dutertre, H. Hastrup, A. Jha, U. Gether, H.H. Sitte, H. Betz, and V. Eulenburg. 2008. Glycine transporter dimers: evidence for occurrence in the plasma membrane. *J Biol Chem*. 283:10978-10991.

Bauernschmitt, H.G., and R.K. Kinne. 1993. Metabolism of the 'organic osmolyte' glycerophosphorylcholine in isolated rat inner medullary collecting duct cells. II. Regulation by extracellular osmolality. *Biochim Biophys Acta*. 1150:25-34.

Beck, F.X., A. Burger-Kentischer, and E. Muller. 1998. Cellular response to osmotic stress in the renal medulla. *Pflügers Arch*. 436:814-827.

Beck, F.X., M. Schmolke, W.G. Guder, A. Dorge, and K. Thurau. 1992a. Osmolytes in renal medulla during rapid changes in papillary tonicity. *Am J Physiol*. 262:F849-856.

Beck, F.X., M. Sone, A. Dorge, and K. Thurau. 1992b. Effect of loop diuretics on organic osmolytes and cell electrolytes in the renal outer medulla. *Kidney Int*. 42:843-850.

Becker, D.M., and L. Guarente. 1991. High-efficiency transformation of yeast by electroporation. *Methods Enzymol*. 194:182-187.

Beckman, M.L., E.M. Bernstein, and M.W. Quick. 1998. Protein kinase C regulates the interaction between a GABA transporter and syntaxin 1A. *J Neurosci*. 18:6103-6112.

Bennion, B.J., and V. Daggett. 2003. The molecular basis for the chemical denaturation of proteins by urea. *Proceedings of the National Academy of Sciences of the United States of America*. 100:5142-5147.

Berntsson, R.P., S.H. Smits, L. Schmitt, D.J. Slotboom, and B. Poolman. 2010. A structural classification of substrate-binding proteins. *FEBS Lett*. 584:2606-2617.

Beuming, T., J. Kniazeff, M.L. Bergmann, L. Shi, L. Gracia, K. Raniszewska, A.H. Newman, J.A. Javitch, H. Weinstein, U. Gether, and C.J. Loland. 2008. The binding sites for cocaine and dopamine in the dopamine transporter overlap. *Nat Neurosci*. 11:780-789.

Bierhals, K., A.C. Sondersorg, C.T. Lin, C. Rosenbaum, H. Waldmann, and F. Wehner. 2007. The epsilon-isoform of PKC mediates the hypertonic activation of cation channels in confluent monolayers of rat hepatocytes. *Cell Physiol Biochem*. 20:397-404.

Borden, L.A. 1996. GABA transporter heterogeneity: pharmacology and cellular localization. *Neurochem Int*. 29:335-356.

Borden, L.A., K.E. Smith, P.R. Hartig, T.A. Branchek, and R.L. Weinshank. 1992. Molecular heterogeneity of the gamma-aminobutyric acid (GABA) transport system. Cloning of

two novel high affinity GABA transporters from rat brain. *J Biol Chem*. 267:21098-21104.

Borowitzka, L.J., and A.D. Brown. 1974. The salt relations of marine and halophilic species of the unicellular green alga, Dunaliella. The role of glycerol as a compatible solute. *Arch Mikrobiol*. 96:37-52.

Bourque, C.W. 2008. Central mechanisms of osmosensation and systemic osmoregulation. *Nat Rev Neurosci*. 9:519-531.

Bowlus, R.D., and G.N. Somero. 1979. Solute compatibility with enzyme function and structure: rationales for the selection of osmotic agents and end-products of anaerobic metabolism in marine invertebrates. *J Exp Zool*. 208:137-151.

Bradford, M.M. 1976. A rapid and sensitive method for the quantitation of microgram quantities of protein utilizing the principle of protein-dye binding. *Analytical biochemistry*. 72:248-254.

Braun, E.J. 1985. Comparative aspects of the urinary concentrating process. *Ren Physiol*. 8:249-260.

Brett, C.L., M. Donowitz, and R. Rao. 2005. Evolutionary origins of eukaryotic sodium/proton exchangers. *Am J Physiol Cell Physiol*. 288:C223-239.

Bretthauer, R.K. 2003. Genetic engineering of Pichia pastoris to humanize N-glycosylation of proteins. *Trends in Biotechnology*. 21:459-462.

Brocker, C., N. Lassen, T. Estey, A. Pappa, M. Cantore, V.V. Orlova, T. Chavakis, K.L. Kavanagh, U. Oppermann, and V. Vasiliou. 2010. Aldehyde dehydrogenase 7A1 (ALDH7A1) is a novel enzyme involved in cellular defense against hyperosmotic stress. *J Biol Chem*. 285:18452-18463.

Broer, S. 2006. The SLC6 orphans are forming a family of amino acid transporters. *Neurochem Int*. 48:559-567.

Broer, S. 2010. Xenopus laevis Oocytes. *Methods Mol Biol*. 637:295-310.

Broer, S., and U. Gether. 2012. The Solute Carrier Family 6. *Br J Pharmacol*. 167:256-278.

Burg, M.B., and J.D. Ferraris. 2008. Intracellular organic osmolytes: function and regulation. *J Biol Chem*. 283:7309-7313.

Burg, M.B., E.D. Kwon, and E.M. Peters. 1996. Glycerophosphocholine and betaine counteract the effect of urea on pyruvate kinase. *Kidney International*. 50:S100-S104.

Burg, M.B., and E.M. Peters. 1998. Effects of glycine betaine and glycerophosphocholine on thermal stability of ribonuclease. *American Journal of Physiology-Renal Physiology*. 274:F762-F765.

Caffrey, M. 2003. Membrane protein crystallization. *Journal of structural biology*. 142:108-132.

Cai, G., P.S. Salonikidis, J. Fei, W. Schwarz, R. Schulein, W. Reutter, and H. Fan. 2005. The role of N-glycosylation in the stability, trafficking and GABA-uptake of GABA-transporter 1. Terminal N-glycans facilitate efficient GABA-uptake activity of the GABA transporter. *FEBS J*. 272:1625-1638.

Caldas, T., N. Demont-Caulet, A. Ghazi, and G. Richarme. 1999. Thermoprotection by glycine betaine and choline. *Microbiology-Uk*. 145:2543-2548.

Cannon, J.G., C.F. Anderson, and M.T. Record. 2007. Urea−Amide Preferential Interactions in Water: Quantitative Comparison of Model Compound Data with Biopolymer Results Using Water Accessible Surface Areas. *The Journal of Physical Chemistry B*. 111:9675-9685.

Chen, J.G., S. Liu-Chen, and G. Rudnick. 1997. External cysteine residues in the serotonin transporter. *Biochemistry*. 36:1479-1486.

Chen, N.H., M.E. Reith, and M.W. Quick. 2004. Synaptic uptake and beyond: the sodium- and chloride-dependent neurotransmitter transporter family SLC6. *Pflügers Arch*. 447:519-531.

Chen, V.B., W.B. Arendall, 3rd, J.J. Headd, D.A. Keedy, R.M. Immormino, G.J. Kapral, L.W. Murray, J.S. Richardson, and D.C. Richardson. 2010. MolProbity: all-atom structure validation for macromolecular crystallography. *Acta crystallographica. Section D, Biological crystallography*. 66:12-21.

Chern, M.K., and R. Pietruszko. 1999. Evidence for mitochondrial localization of betaine aldehyde dehydrogenase in rat liver: purification, characterization, and comparison

with human cytoplasmic E3 isozyme. *Biochemistry and Cell Biology-Biochimie Et Biologie Cellulaire*. 77:179-187.

Christie, D.L. 2007. Functional insights into the creatine transporter. *Subcell Biochem*. 46:99-118.

Chung, C.T., S.L. Niemela, and R.H. Miller. 1989. One-step preparation of competent Escherichia coli: transformation and storage of bacterial cells in the same solution. *Proc Natl Acad Sci U S A*. 86:2172-2175.

Cowley, B.D., Jr., J.D. Ferraris, D. Carper, and M.B. Burg. 1990. In vivo osmoregulation of aldose reductase mRNA, protein, and sorbitol in renal medulla. *Am J Physiol*. 258:F154-161.

Creighton, T.E. 1991. Stability of folded conformations : Current opinion in structural biology 1991, 1: 5-16. *Current Opinion in Structural Biology*. 1:5-16.

Crowther, R.A. 1972. The Molecular Replacement Method. *Gordon and Breach, New York*.

Cullis, P.R., and B. de Kruijff. 1979. Lipid polymorphism and the functional roles of lipids in biological membranes. *Biochim Biophys Acta*. 559:399-420.

Curless, C., J. Baclaski, and R. Sachdev. 1996. Phosphate glass as a phosphate source in high cell density Escherichia coli fermentations. *Biotechnology progress*. 12:22-25.

de Kroon, A.I. 2007. Metabolism of phosphatidylcholine and its implications for lipid acyl chain composition in Saccharomyces cerevisiae. *Biochim Biophys Acta*. 1771:343-352.

Deken, S.L., M.L. Beckman, L. Boos, and M.W. Quick. 2000. Transport rates of GABA transporters: regulation by the N-terminal domain and syntaxin 1A. *Nat Neurosci*. 3:998-1003.

DeLano, W. 2002. The PyMOL Molecular Graphics System. . *In* DeLano Scientific LLC, San Carlos, CA; USA.

Dmitrieva, N.I., and M.B. Burg. 2005. Hypertonic stress response. *Mutat Res-Fund Mol M*. 569:65-74.

Dodd, J.R., and D.L. Christie. 2007. Selective amino acid substitutions convert the creatine transporter to a gamma-aminobutyric acid transporter. *J Biol Chem*. 282:15528-15533.

Doring, F., T. Michel, A. Rosel, M. Nickolaus, and H. Daniel. 1998. Expression of the mammalian renal peptide transporter PEPT2 in the yeast Pichia pastoris and applications of the yeast system for functional analysis. *Mol Membr Biol*. 15:79-88.

Dowhan, W. 1997. Molecular basis for membrane phospholipid diversity: why are there so many lipids? *Annual review of biochemistry*. 66:199-232.

Dowhan, W., and M. Bogdanov. 2012. Molecular genetic and biochemical approaches for defining lipid-dependent membrane protein folding. *Biochim Biophys Acta*. 1818:1097-1107.

Drenth, J. 2007. Principles of Protein X-Ray Crystallography. *Third edn.: Springer Science + Business Media LLC*.

Emsley, P., and K. Cowtan. 2004. Coot: model-building tools for molecular graphics. *Acta Crystallographica Section D*. 60:2126-2132.

Eytan, G.D. 1982. Use of liposomes for reconstitution of biological functions. *Biochim Biophys Acta*. 694:185-202.

Fagone, P., and S. Jackowski. 2009. Membrane phospholipid synthesis and endoplasmic reticulum function. *Journal of lipid research*. 50 Suppl:S311-316.

Farhan, H., V. Reiterer, V.M. Korkhov, J.A. Schmid, M. Freissmuth, and H.H. Sitte. 2007. Concentrative export from the endoplasmic reticulum of the gamma-aminobutyric acid transporter 1 requires binding to SEC24D. *J Biol Chem*. 282:7679-7689.

Farhan, H., V. Reiterer, A. Kriz, H.P. Hauri, M. Pavelka, H.H. Sitte, and M. Freissmuth. 2008. Signal-dependent export of GABA transporter 1 from the ER-Golgi intermediate compartment is specified by a C-terminal motif. *J Cell Sci*. 121:753-761.

Farwick, M., R.M. Siewe, and R. Kramer. 1995. Glycine betaine uptake after hyperosmotic shift in Corynebacterium glutamicum. *J Bacteriol*. 177:4690-4695.

Fedan, J.S., L.X. Yuan, V.C. Chang, J.O. Viola, D. Cutler, and L.L. Pettit. 1999. Osmotic regulation of airway reactivity by epithelium. *J Pharmacol Exp Ther*. 289:901-910.

Feng, Y.X., V. Muller, B. Friedrich, T. Risler, and F. Lang. 2001. Clinical significance of cell volume regulation. *Wiener Klinische Wochenschrift*. 113:477-484.

Forrest, L.R., R. Kramer, and C. Ziegler. 2011. The structural basis of secondary active transport mechanisms. *Biochim Biophys Acta*. 1807:167-188.

Forrest, L.R., and G. Rudnick. 2009. The rocking bundle: a mechanism for ion-coupled solute flux by symmetrical transporters. *Physiology (Bethesda, Md.)*. 24:377-386.

Forrest, L.R., Y.W. Zhang, M.T. Jacobs, J. Gesmonde, L. Xie, B.H. Honig, and G. Rudnick. 2008. Mechanism for alternating access in neurotransmitter transporters. *Proc Natl Acad Sci U S A*. 105:10338-10343.

Gadea, A., and A.M. Lopez-Colome. 2001. Glial transporters for glutamate, glycine, and GABA: II. GABA transporters. *J Neurosci Res*. 63:461-468.

Galinski, E.A., and H.G. Trüper. 1994. Microbial behaviour in salt-stressed ecosystems. *FEMS Microbiology Reviews*. 15:95-108.

Gallazzini, M., J.D. Ferraris, M. Kunin, R.G. Morris, and M.B. Burg. 2006. Neuropathy target esterase catalyzes osmoprotective renal synthesis of glycerophosphocholine in response to high NaCl. *Proceedings of the National Academy of Sciences of the United States of America*. 103:15260-15265.

Garcia-Perez, A., and M.B. Burg. 1991. Renal medullary organic osmolytes. *Physiological Reviews*. 71:1081-1115.

Garman, E.F., and S. Doublie. 2003. Cryocooling of macromolecular crystals: optimization methods. *Methods Enzymol*. 368:188-216.

Garman, E.F., and T.R. Schneider. 1997. Macromolecular Cryocrystallography. *Journal of Applied Crystallography*. 30:211-237.

Gedeon, P.C., M. Indarte, C.K. Surratt, and J.D. Madura. 2010. Molecular dynamics of leucine and dopamine transporter proteins in a model cell membrane lipid bilayer. *Proteins*. 78:797-811.

Glasel, J.A. 1995. Validity of nucleic acid purities monitored by 260nm/280nm absorbance ratios. *BioTechniques*. 18:62-63.

Gouaux, E. 2009. Review. The molecular logic of sodium-coupled neurotransmitter transporters. *Philos Trans R Soc Lond B Biol Sci*. 364:149-154.

Grisshammer, R., and C.G. Tate. 1995. Overexpression of integral membrane proteins for structural studies. *Quarterly reviews of biophysics*. 28:315-422.

Guastella, J., N. Nelson, H. Nelson, L. Czyzyk, S. Keynan, M.C. Miedel, N. Davidson, H.A. Lester, and B.I. Kanner. 1990. Cloning and expression of a rat brain GABA transporter. *Science*. 249:1303-1306.

Hastrup, H., A. Karlin, and J.A. Javitch. 2001. Symmetrical dimer of the human dopamine transporter revealed by cross-linking Cys-306 at the extracellular end of the sixth transmembrane segment. *Proc Natl Acad Sci U S A*. 98:10055-10060.

Haussinger, D. 1996. The role of cellular hydration in the regulation of cell function. *Biochemical Journal*. 313:697-710.

Heinzinger, H., F. van den Boom, H. Tinel, and F. Wehner. 2001. In rat hepatocytes, the hypertonic activation of Na(+) conductance and Na(+)-K(+)-2Cl(-) symport--but not Na(+)-H(+) antiport--is mediated by protein kinase C. *The Journal of physiology*. 536:703-715.

Henneberry, A.L., T.A. Lagace, N.D. Ridgway, and C.R. McMaster. 2001. Phosphatidylcholine synthesis influences the diacylglycerol homeostasis required for SEC14p-dependent Golgi function and cell growth. *Molecular biology of the cell*. 12:511-520.

Hosseinzadeh, Z., M. Shojaiefard, S.K. Bhavsar, and F. Lang. 2012. Up-regulation of the betaine/GABA transporter BGT1 by JAK2. *Biochem Biophys Res Commun*. 420:172-177.

Hu, J., J. Fei, W. Reutter, and H. Fan. 2011. Involvement of sialic acid in the regulation of gamma--aminobutyric acid uptake activity of gamma-aminobutyric acid transporter 1. *Glycobiology*. 21:329-339.

Indarte, M., J.D. Madura, and C.K. Surratt. 2008. Dopamine transporter comparative molecular modeling and binding site prediction using the LeuT(Aa) leucine transporter as a template. *Proteins*. 70:1033-1046.

Ishmukhametov, R.R., M.A. Galkin, and S.B. Vik. 2005. Ultrafast purification and reconstitution of His-tagged cysteine-less Escherichia coli F1Fo ATP synthase. *Biochim Biophys Acta*. 1706:110-116.

Ito, T., Y. Fujio, M. Hirata, T. Takatani, T. Matsuda, S. Muraoka, K. Takahashi, and J. Azuma. 2004. Expression of taurine transporter is regulated through the TonE (tonicity-responsive element)/TonEBP (TonE-binding protein) pathway and contributes to cytoprotection in HepG2 cells. *Biochemical Journal*. 382:177-182.

Just, H., H.H. Sitte, J.A. Schmid, M. Freissmuth, and O. Kudlacek. 2004. Identification of an additional interaction domain in transmembrane domains 11 and 12 that supports oligomer formation in the human serotonin transporter. *J Biol Chem*. 279:6650-6657.

Kabsch, W. 1993. Automatic processing of rotation diffraction data from crystals of initially unknown symmetry and cell constants. *Journal of Applied Crystallography*. 26:795-800.

Kanner, B.I. 2003. Transmembrane domain I of the gamma-aminobutyric acid transporter GAT-1 plays a crucial role in the transition between cation leak and transport modes. *J Biol Chem*. 278:3705-3712.

Kaufmann, K.W., G.H. Lemmon, S.L. Deluca, J.H. Sheehan, and J. Meiler. 2010. Practically useful: what the Rosetta protein modeling suite can do for you. *Biochemistry*. 49:2987-2998.

Kempf, B., and E. Bremer. 1998. Uptake and synthesis of compatible solutes as microbial stress responses to high-osmolality environments. *Arch Microbiol*. 170:319-330.

Kempson, S.A., J.A. Beck, P.E. Lammers, J.S. Gens, and M.H. Montrose. 2005. Membrane insertion of betaine/GABA transporter during hypertonic stress correlates with nuclear accumulation of TonEBP. *Biochim Biophys Acta*. 1712:71-80.

Kempson, S.A., J.M. Edwards, A. Osborn, and M. Sturek. 2008. Acute inhibition of the betaine transporter by ATP and adenosine in renal MDCK cells. *Am J Physiol Renal Physiol*. 295:F108-117.

Kempson, S.A., J.M. Edwards, and M. Sturek. 2006. Inhibition of the renal betaine transporter by calcium ions. *Am J Physiol Renal Physiol*. 291:F305-313.

Kempson, S.A., and M.H. Montrose. 2004. Osmotic regulation of renal betaine transport: transcription and beyond. *Pflügers Arch-Eur J Physiol*. 449:227-234.

Kempson, S.A., V. Parikh, L. Xi, S. Chu, and M.H. Montrose. 2003. Subcellular redistribution of the renal betaine transporter during hypertonic stress. *Am J Physiol Cell Physiol*. 285:C1091-1100.

Kilic, F., and G. Rudnick. 2000. Oligomerization of serotonin transporter and its functional consequences. *Proc Natl Acad Sci U S A*. 97:3106-3111.

Klammt, C., D. Schwarz, K. Fendler, W. Haase, V. Dotsch, and F. Bernhard. 2005. Evaluation of detergents for the soluble expression of alpha-helical and beta-barrel-type integral membrane proteins by a preparative scale individual cell-free expression system. *FEBS J*. 272:6024-6038.

Kniazeff, J., L. Shi, C.J. Loland, J.A. Javitch, H. Weinstein, and U. Gether. 2008. An intracellular interaction network regulates conformational transitions in the dopamine transporter. *J Biol Chem*. 283:17691-17701.

Kramer, R. 2009. Osmosensing and osmosignaling in Corynebacterium glutamicum. *Amino Acids*. 37:487-497.

Kramer, R., and C. Ziegler. 2009. Regulative interactions of the osmosensing C-terminal domain in the trimeric glycine betaine transporter BetP from Corynebacterium glutamicum. *Biol Chem*. 390:685-691.

Kraus, L.M., and A.P. Kraus. 2001. Carbamoylation of amino acids and proteins in uremia. *Kidney International*. 59:S102-S107.

Krishnamurthy, H., C.L. Piscitelli, and E. Gouaux. 2009. Unlocking the molecular secrets of sodium-coupled transporters. *Nature*. 459:347-355.

Krissinel, E., and K. Henrick. 2004. Secondary-structure matching (SSM), a new tool for fast protein structure alignment in three dimensions. *Acta Crystallographica Section D*. 60:2256-2268.

Kuhlbrandt, W. 1992. Two-dimensional crystallization of membrane proteins. *Quarterly reviews of biophysics*. 25:1-49.

Kukuruzinska, M.A., and K. Lennon. 1998. Protein N-glycosylation: molecular genetics and functional significance. *Crit Rev Oral Biol Med*. 9:415-448.

Kwon, M.S., S.W. Lim, and H.M. Kwon. 2009. Hypertonic Stress in the Kidney: A Necessary Evil. *Physiology*. 24:186-191.

Laemmli, U.K. 1970. Cleavage of structural proteins during the assembly of the head of bacteriophage T4. *Nature*. 227:680-685.

Lamark, T., I. Kaasen, M.W. Eshoo, P. Falkenberg, J. McDougall, and A.R. Strom. 1991. DNA sequence and analysis of the bet genes encoding the osmoregulatory choline-glycine betaine pathway of Escherichia coli. *Mol Microbiol*. 5:1049-1064.

Lang, F. 2007. Mechanisms and significance of cell volume regulation. *Journal of the American College of Nutrition*. 26:613S-623S.

Laryea, M.D., F. Steinhagen, S. Pawliczek, and U. Wendel. 1998. Simple method for the routine determination of betaine and N,N-dimethylglycine in blood and urine. *Clin Chem*. 44:1937-1941.

Leslie, A.G.W. 1992. Recent changes to the MOSFLM package for processing film and image plate data. *Joint CCP4 + ESF-EAMCB Newsletter on Protein Crystallography*. 26.

Lever, M., P.C. Sizeland, C.M. Frampton, and S.T. Chambers. 2004. Short and long-term variation of plasma glycine betaine concentrations in humans. *Clin Biochem*. 37:184-190.

Lever, M., and S. Slow. 2010. The clinical significance of betaine, an osmolyte with a key role in methyl group metabolism. *Clinical Biochemistry*. 43:732-744.

Li, L.B., N. Chen, S. Ramamoorthy, L. Chi, X.N. Cui, L.C. Wang, and M.E. Reith. 2004. The role of N-glycosylation in function and surface trafficking of the human dopamine transporter. *J Biol Chem*. 279:21012-21020.

Lim, Y.S., J.S. Lee, T.Q. Huang, and J.S. Seo. 2008. Protein kinase Cmu plays an essential role in hypertonicity-induced heat shock protein 70 expression. *Experimental & molecular medicine*. 40:596-606.

Lis, H., and N. Sharon. 1993. Protein glycosylation. Structural and functional aspects. *Eur J Biochem*. 218:1-27.

Liu, Q.R., B. Lopez-Corcuera, S. Mandiyan, H. Nelson, and N. Nelson. 1993. Molecular characterization of four pharmacologically distinct gamma-aminobutyric acid transporters in mouse brain [corrected]. *J Biol Chem*. 268:2106-2112.

Liu, Q.R., B. Lopez-Corcuera, H. Nelson, S. Mandiyan, and N. Nelson. 1992. Cloning and expression of a cDNA encoding the transporter of taurine and beta-alanine in mouse brain. *Proc Natl Acad Sci U S A*. 89:12145-12149.

Livesay, D.R., P.D. Kidd, S. Eskandari, and U. Roshan. 2007. Assessing the ability of sequence-based methods to provide functional insight within membrane integral proteins: a case study analyzing the neurotransmitter/Na+ symporter family. *Bmc Bioinformatics*. 8.

Loland, C.J., K. Norgaard-Nielsen, and U. Gether. 2003. Probing dopamine transporter structure and function by Zn2+-site engineering. *Eur J Pharmacol*. 479:187-197.

Lolkema, J.S., and D.J. Slotboom. 2003. Classification of 29 families of secondary transport proteins into a single structural class using hydropathy profile analysis. *J Mol Biol*. 327:901-909.

Lolkema, J.S., and D.J. Slotboom. 2008. The major amino acid transporter superfamily has a similar core structure as Na+-galactose and Na+-leucine transporters. *Mol Membr Biol*. 25:567-570.

Lopez-Corcuera, B., Q.R. Liu, S. Mandiyan, H. Nelson, and N. Nelson. 1992. Expression of a mouse brain cDNA encoding novel gamma-aminobutyric acid transporter. *J Biol Chem*. 267:17491-17493.

Massari, S., C. Vanoni, R. Longhi, P. Rosa, and G. Pietrini. 2005. Protein kinase C-mediated phosphorylation of the BGT1 epithelial gamma-aminobutyric acid transporter regulates its association with LIN7 PDZ proteins: a post-translational mechanism regulating transporter surface density. *J Biol Chem*. 280:7388-7397.

Matskevitch, I., C.A. Wagner, C. Stegen, S. Broer, B. Noll, T. Risler, H.M. Kwon, J.S. Handler, S. Waldegger, A.E. Busch, and F. Lang. 1999. Functional characterization of

the Betaine/gamma-aminobutyric acid transporter BGT-1 expressed in Xenopus oocytes. *J Biol Chem*. 274:16709-16716.

Matter, K., E.M. Yamamoto, and I. Mellman. 1994. Structural requirements and sequence motifs for polarized sorting and endocytosis of LDL and Fc receptors in MDCK cells. *The Journal of cell biology*. 126:991-1004.

McAuley, K.E., P.K. Fyfe, J.P. Ridge, N.W. Isaacs, R.J. Cogdell, and M.R. Jones. 1999. Structural details of an interaction between cardiolipin and an integral membrane protein. *Proc Natl Acad Sci U S A*. 96:14706-14711.

McCoy, A.J., R.W. Grosse-Kunstleve, P.D. Adams, M.D. Winn, L.C. Storoni, and R.J. Read. 2007. Phaser crystallographic software. *Journal of Applied Crystallography*. 40:658-674.

McPherson, A. 1999. Crystallization of biological macromolecules. i-ix, 1-586 pp.

Melikian, H.E., S. Ramamoorthy, C.G. Tate, and R.D. Blakely. 1996. Inability to N-glycosylate the human norepinephrine transporter reduces protein stability, surface trafficking, and transport activity but not ligand recognition. *Mol Pharmacol*. 50:266-276.

Messerschmidt, A. 2007. Front Matter. *In* X-Ray Crystallography of Biomacromolecules. Wiley-VCH Verlag GmbH & Co. KGaA. I-XIII.

Michea, L., D.R. Ferguson, E.M. Peters, P.M. Andrews, M.R. Kirby, and M.B. Burg. 2000. Cell cycle delay and apoptosis are induced by high salt and urea in renal medullary cells. *American Journal of Physiology-Renal Physiology*. 278:F209-F218.

Miyakawa, H., S.K. Woo, C.P. Chen, S.C. Dahl, J.S. Handler, and H.M. Kwon. 1998. Cis- and trans-acting factors regulating transcription of the BGT1 gene in response to hypertonicity. *American Journal of Physiology-Renal Physiology*. 274:F753-F761.

Motulsky, H. 1999. Analyzing Data with GraphPad Prism. GraphPad Software Inc., San Diego, CA, USA.

Muller, H.K., O. Wiborg, and J. Haase. 2006. Subcellular redistribution of the serotonin transporter by secretory carrier membrane protein 2. *J Biol Chem*. 281:28901-28909.

Munoz, C., M. Sopjani, M. Dermaku-Sopjani, A. Almilaji, M. Foller, and F. Lang. 2012. Downregulation of the osmolyte transporters SMIT and BGT1 by AMP-activated protein kinase. *Biochem Biophys Res Commun*. 422:358-362.

Muñoz-Clares, R.A., Á.G. Díaz-Sánchez, L. González-Segura, and C. Montiel. 2010. Kinetic and structural features of betaine aldehyde dehydrogenases: Mechanistic and regulatory implications. *Archives of Biochemistry and Biophysics*. 493:71-81.

Muth, T.R., J. Ahn, and M.J. Caplan. 1998. Identification of sorting determinants in the C-terminal cytoplasmic tails of the gamma-aminobutyric acid transporters GAT-2 and GAT-3. *J Biol Chem*. 273:25616-25627.

Na, K.Y., S.K. Woo, S.D. Lee, and H.M. Kwon. 2003. Silencing of TonEBP/NFAT5 transcriptional activator by RNA interference. *Journal of the American Society of Nephrology*. 14:283-288.

Nakanishi, T., F. Nishihara, A. Yamauchi, S. Yamamoto, M. Sugita, and Y. Takamitsu. 1996. NaCl and/or urea infusion fails to increase renal inner medullary myo-inositol in protein-deprived rats. *Am J Physiol*. 271:F1255-1263.

Nakanishi, T., Y. Takamitsu, H. Nakahama, and M. Sugita. 1994. Impairment of renal medullary osmolyte accumulation in potassium-depleted rats. *Am J Physiol*. 267:F139-145.

Nakanishi, T., O. Uyama, H. Nakahama, Y. Takamitsu, and M. Sugita. 1993. Determinants of relative amounts of medullary organic osmolytes: effects of NaCl and urea differ. *Am J Physiol*. 264:F472-479.

Nelson, N. 1998. The family of Na+/Cl- neurotransmitter transporters. *J Neurochem*. 71:1785-1803.

Nesterenko, M.V., M. Tilley, and S.J. Upton. 1994. A simple modification of Blum's silver stain method allows for 30 minute detection of proteins in polyacrylamide gels. *Journal of biochemical and biophysical methods*. 28:239-242.

Nguyen, T.T., and S.G. Amara. 1996. N-linked oligosaccharides are required for cell surface expression of the norepinephrine transporter but do not influence substrate or inhibitor recognition. *J Neurochem*. 67:645-655.

Nozaki, Y., and C. Tanford. 1963. Solubility of amino acids and related compounds in aqueous urea solutions. *Journal of Biological Chemistry*. 238:4074-&.

Nystrom, T. 2005. Role of oxidative carbonylation in protein quality control and senescence. *EMBO J*. 24:1311-1317.

Opekarova, M., and W. Tanner. 2003. Specific lipid requirements of membrane proteins--a putative bottleneck in heterologous expression. *Biochim Biophys Acta*. 1610:11-22.

Ott, V., J. Koch, K. Spate, S. Morbach, and R. Kramer. 2008. Regulatory properties and interaction of the C- and N-terminal domains of BetP, an osmoregulated betaine transporter from Corynebacterium glutamicum. *Biochemistry*. 47:12208-12218.

Pallo, A., A. Bencsura, L. Heja, T. Beke, A. Perczel, J. Kardos, and A. Simon. 2007. Major human gamma-aminobutyrate transporter: in silico prediction of substrate efficacy. *Biochem Biophys Res Commun*. 364:952-958.

Parcej, D.N., and L. Eckhardt-Strelau. 2003. Structural characterisation of neuronal voltage-sensitive K+ channels heterologously expressed in Pichia pastoris. *J Mol Biol*. 333:103-116.

Penmatsa, A., K.H. Wang, and E. Gouaux. 2013. X-ray structure of dopamine transporter elucidates antidepressant mechanism. *Nature*.

Perego, C., A. Bulbarelli, R. Longhi, M. Caimi, A. Villa, M.J. Caplan, and G. Pietrini. 1997. Sorting of two polytopic proteins, the gamma-aminobutyric acid and betaine transporters, in polarized epithelial cells. *J Biol Chem*. 272:6584-6592.

Perez, C., C. Koshy, S. Ressl, S. Nicklisch, R. Kramer, and C. Ziegler. 2011. Substrate specificity and ion coupling in the Na+/betaine symporter BetP. *EMBO J*. 30:1221-1229.

Perez, C., C. Koshy, Ö. Yildiz, and C. Ziegler. 2012. Alternating-access mechanism in conformationally asymmetric trimers of the betaine transporter BetP. *Nature Letter*.

Peter, H., A. Burkovski, and R. Kramer. 1998. Osmo-sensing by N- and C-terminal extensions of the glycine betaine uptake system BetP of Corynebacterium glutamicum. *J Biol Chem*. 273:2567-2574.

Peterson, D.P., K.M. Murphy, R. Ursino, K. Streeter, and P.H. Yancey. 1992. Effects of dietary protein and salt on rat renal osmolytes: covariation in urea and GPC contents. *Am J Physiol*. 263:F594-600.

Petreus, O., and T. Petreus. 2011. Phosphorus-Containing Polysulfones. *In* High Performance Polymers and Engineering Plastics. V. Mittal, editor. John Wiley & Sons, Salem, Massachusetts. 167-205.

Poolman, B., P. Blount, J.H. Folgering, R.H. Friesen, P.C. Moe, and T. van der Heide. 2002. How do membrane proteins sense water stress? *Mol Microbiol*. 44:889-902.

Preston, A.S., A. Yamauchi, H.M. Kwon, and J.S. Handler. 1995. Activators of protein kinase A and of protein kinase C inhibit MDCK cell myo-inositol and betaine uptake. *Journal of the American Society of Nephrology : JASN*. 6:1559-1564.

Racker, E. 1979. Reconstitution of membrane processes. *Methods Enzymol*. 55:699-711.

Radian, R., and B.I. Kanner. 1985. Reconstitution and purification of the sodium- and chloride-coupled gamma-aminobutyric acid transporter from rat brain. *J Biol Chem*. 260:11859-11865.

Ramachandran, G.N., C. Ramakrishnan, and V. Sasisekharan. 1963. Stereochemistry of polypeptide chain configurations. *J Mol Biol*. 7:95-99.

Rasola, A., L.J. Galietta, V. Barone, G. Romeo, and S. Bagnasco. 1995. Molecular cloning and functional characterization of a GABA/betaine transporter from human kidney. *FEBS Lett*. 373:229-233.

Ravna, A.W., M. Jaronczyk, and I. Sylte. 2006. A homology model of SERT based on the LeuT(Aa) template. *Bioorg Med Chem Lett*. 16:5594-5597.

Ravna, A.W., I. Sylte, and S.G. Dahl. 2003. Molecular model of the neural dopamine transporter. *J Comput Aided Mol Des*. 17:367-382.

Reilander, H., and H.M. Weiss. 1998. Production of G-protein-coupled receptors in yeast. *Curr Opin Biotechnol*. 9:510-517.

Reinehr, R., and D. Haussinger. 2006. Hyperosmotic activation of the CD95 death receptor system. *Acta Physiol*. 187:199-203.

Reizer, J., A. Reizer, and M.H. Saier, Jr. 1994. A functional superfamily of sodium/solute symporters. *Biochim Biophys Acta*. 1197:133-166.

Ressl, S., A.C. Terwisscha van Scheltinga, C. Vonrhein, V. Ott, and C. Ziegler. 2009a. Molecular basis of transport and regulation in the Na(+)/betaine symporter BetP. *Nature*. 458:47-52.

Ressl, S., A.C.T. van Scheltinga, C. Vonrhein, V. Ott, and C. Ziegler. 2009b. Molecular basis of transport and regulation in the Na+/betaine symporter BetP. *Nature*. 458:47-U41.

Rhodes, D., and A.D. Hanson. 1993. Quaternary Ammonium and Tertiary Sulfonium Compounds in Higher Plants. *Annual Review of Plant Physiology and Plant Molecular Biology*. 44:357-384.

Rigaud, J.L., and D. Levy. 2003. Reconstitution of membrane proteins into liposomes. *Methods Enzymol*. 372:65-86.

Rubenhagen, R., H. Ronsch, H. Jung, R. Kramer, and S. Morbach. 2000. Osmosensor and osmoregulator properties of the betaine carrier BetP from Corynebacterium glutamicum in proteoliposomes. *J Biol Chem*. 275:735-741.

Sato, Y., Y.W. Zhang, A. Androutsellis-Theotokis, and G. Rudnick. 2004. Analysis of transmembrane domain 2 of rat serotonin transporter by cysteine scanning mutagenesis. *J Biol Chem*. 279:22926-22933.

Scanlon, S.M., D.C. Williams, and P. Schloss. 2001. Membrane cholesterol modulates serotonin transporter activity. *Biochemistry*. 40:10507-10513.

Schaffner, W., and C. Weissmann. 1973. A rapid, sensitive, and specific method for the determination of protein in dilute solution. *Analytical biochemistry*. 56:502-514.

Schagger, H., and G. von Jagow. 1991. Blue native electrophoresis for isolation of membrane protein complexes in enzymatically active form. *Analytical biochemistry*. 199:223-231.

Schiefner, A., J. Breed, L. Bosser, S. Kneip, J. Gade, G. Holtmann, K. Diederichs, W. Welte, and E. Bremer. 2004. Cation-pi interactions as determinants for binding of the compatible solutes glycine betaine and proline betaine by the periplasmic ligand-binding protein ProX from Escherichia coli. *J Biol Chem*. 279:5588-5596.

Schiller, D., R. Rubenhagen, R. Kramer, and S. Morbach. 2004. The C-terminal domain of the betaine carrier BetP of Corynebacterium glutamicum is directly involved in sensing K+ as an osmotic stimulus. *Biochemistry*. 43:5583-5591.

Schliess, F., and D. Haussinger. 2002. The cellular hydration state: A critical determinant for cell death and survival. *Biological Chemistry*. 383:577-583.

Schmid, J.A., P. Scholze, O. Kudlacek, M. Freissmuth, E.A. Singer, and H.H. Sitte. 2001. Oligomerization of the human serotonin transporter and of the rat GABA transporter 1 visualized by fluorescence resonance energy transfer microscopy in living cells. *J Biol Chem*. 276:3805-3810.

Scholze, P., M. Freissmuth, and H.H. Sitte. 2002. Mutations within an intramembrane leucine heptad repeat disrupt oligomer formation of the rat GABA transporter 1. *J Biol Chem*. 277:43682-43690.

Schulze, S., S. Koster, U. Geldmacher, A.C. Terwisscha van Scheltinga, and W. Kuhlbrandt. 2010. Structural basis of Na(+)-independent and cooperative substrate/product antiport in CaiT. *Nature*. 467:233-236.

Shouffani, A., and B.I. Kanner. 1990. Cholesterol is required for the reconstruction of the sodium- and chloride-coupled, gamma-aminobutyric acid transporter from rat brain. *J Biol Chem*. 265:6002-6008.

Singh, L.R., T.A. Dar, and F. Ahmad. 2009a. Living with urea stress. *Journal of Biosciences*. 34:321-331.

Singh, L.R., T.A. Dar, S. Rahman, S. Jamal, and F. Ahmad. 2009b. Glycine betaine may have opposite effects on protein stability at high and low pH values. *Biochimica et Biophysica Acta (BBA) - Proteins & Proteomics*. 1794:929-935.

Skovstrup, S., O. Taboureau, H. Brauner-Osborne, and F.S. Jorgensen. 2010. Homology modelling of the GABA transporter and analysis of tiagabine binding. *ChemMedChem*. 5:986-1000.

Smith, P.E. 2004. Cosolvent interactions with biomolecules: Relating computer simulation data to experimental thermodynamic data. *Journal of Physical Chemistry B*. 108:18716-18724.

Smyth, M.S., and J.H. Martin. 2000. x ray crystallography. *Molecular pathology : MP*. 53:8-14.

Sone, M., G.J. Albrecht, A. Dorge, K. Thurau, and F.X. Beck. 1993. Osmotic adaptation of renal medullary cells during transition from chronic diuresis to antidiuresis. *Am J Physiol*. 264:F722-729.

Sone, M., A. Ohno, G.J. Albrecht, K. Thurau, and F.X. Beck. 1995. Restoration of urine concentrating ability and accumulation of medullary osmolytes after chronic diuresis. *Am J Physiol*. 269:F480-490.

Sorkina, T., S. Doolen, E. Galperin, N.R. Zahniser, and A. Sorkin. 2003. Oligomerization of dopamine transporters visualized in living cells by fluorescence resonance energy transfer microscopy. *J Biol Chem*. 278:28274-28283.

Stanley, P., H. Schachter, and N. Taniguchi. 2009. N-Glycans. *In* Essentials of Glycobiology. 2nd edition. A. Varki, R. Cummings, J. Esko, H. Freeze, P. Stanley, C. Bertozzi, G. Hart, and M. Etzler, editors. Cold Spring Harbor Laboratory Press, NY.

Stratton, J., V. Chiruvolu, and M. Meagher. 1998. High cell-density fermentation. *Methods Mol Biol*. 103:107-120.

Straumann, N., A. Wind, T. Leuenberger, and T. Wallimann. 2006. Effects of N-linked glycosylation on the creatine transporter. *Biochem J*. 393:459-469.

Strong, M., M.R. Sawaya, S. Wang, M. Phillips, D. Cascio, and D. Eisenberg. 2006. Toward the structural genomics of complexes: crystal structure of a PE/PPE protein complex from Mycobacterium tuberculosis. *Proc Natl Acad Sci U S A*. 103:8060-8065.

Strutz-Seebohm, N., M. Shojaiefard, D. Christie, J. Tavare, G. Seebohm, and F. Lang. 2007. PIKfyve in the SGK1 mediated regulation of the creatine transporter SLC6A8. *Cell Physiol Biochem*. 20:729-734.

Studier, F.W. 2005. Protein production by auto-induction in high density shaking cultures. *Protein expression and purification*. 41:207-234.

Sucic, S., S. Dallinger, B. Zdrazil, R. Weissensteiner, T.N. Jorgensen, M. Holy, O. Kudlacek, S. Seidel, J.H. Cha, U. Gether, A.H. Newman, G.F. Ecker, M. Freissmuth, and H.H.

Sitte. 2010. The N terminus of monoamine transporters is a lever required for the action of amphetamines. *J Biol Chem*. 285:10924-10938.

Tate, C.G., and R.D. Blakely. 1994. The effect of N-linked glycosylation on activity of the Na(+)- and Cl(-)-dependent serotonin transporter expressed using recombinant baculovirus in insect cells. *J Biol Chem*. 269:26303-26310.

Tate, C.G., J. Haase, C. Baker, M. Boorsma, F. Magnani, Y. Vallis, and D.C. Williams. 2003. Comparison of seven different heterologous protein expression systems for the production of the serotonin transporter. *Biochim Biophys Acta*. 1610:141-153.

Terwilliger, T.C., R.W. Grosse-Kunstleve, P.V. Afonine, N.W. Moriarty, P.H. Zwart, L.W. Hung, R.J. Read, and P.D. Adams. 2008. Iterative model building, structure refinement and density modification with the PHENIX AutoBuild wizard. *Acta crystallographica. Section D, Biological crystallography*. 64:61-69.

Thomsen, C., P.O. Sorensen, and J. Egebjerg. 1997. 1-(3-(9H-carbazol-9-yl)-1-propyl)-4-(2-methoxyphenyl)-4-piperidinol, a novel subtype selective inhibitor of the mouse type II GABA-transporter. *Br J Pharmacol*. 120:983-985.

Tomi, M., A. Tajima, M. Tachikawa, and K. Hosoya. 2008. Function of taurine transporter (Slc6a6/TauT) as a GABA transporting protein and its relevance to GABA transport in rat retinal capillary endothelial cells. *Biochim Biophys Acta*. 1778:2138-2142.

Torres, G.E., A. Carneiro, K. Seamans, C. Fiorentini, A. Sweeney, W.D. Yao, and M.G. Caron. 2003. Oligomerization and trafficking of the human dopamine transporter. Mutational analysis identifies critical domains important for the functional expression of the transporter. *J Biol Chem*. 278:2731-2739.

Trama, J., W.Y. Go, and S.N. Ho. 2002. The osmoprotective function of the NFAT5 transcription factor in T cell development and activation. *Journal of Immunology*. 169:5477-5488.

Uchida, S., H.M. Kwon, A. Yamauchi, A.S. Preston, F. Marumo, and J.S. Handler. 1993a. Molecular cloning of the cDNA for an MDCK cell Na(+)- and Cl(-)-dependent taurine transporter that is regulated by hypertonicity. *Proc Natl Acad Sci U S A*. 90:7424.

Uchida, S., T. Nakanishi, H.M. Kwon, A.S. Preston, and J.S. Handler. 1991. Taurine behaves as an osmolyte in Madin-Darby canine kidney cells. Protection by polarized, regulated transport of taurine. *J Clin Invest*. 88:656-662.

Uchida, S., A. Yamauchi, A.S. Preston, H.M. Kwon, and J.S. Handler. 1993b. Medium tonicity regulates expression of the Na(+)- and Cl(-)-dependent betaine transporter in Madin-Darby canine kidney cells by increasing transcription of the transporter gene. *J Clin Invest*. 91:1604-1607.

Urban, J.P., A.C. Hall, and K.A. Gehl. 1993. Regulation of matrix synthesis rates by the ionic and osmotic environment of articular chondrocytes. *J Cell Physiol*. 154:262-270.

van Klompenburg, W., I. Nilsson, G. von Heijne, and B. de Kruijff. 1997. Anionic phospholipids are determinants of membrane protein topology. *EMBO J*. 16:4261-4266.

van Meer, G., D.R. Voelker, and G.W. Feigenson. 2008. Membrane lipids: where they are and how they behave. *Nat Rev Mol Cell Biol*. 9:112-124.

Venkatesu, P., M.J. Lee, and H.M. Lin. 2007. Thermodynamic characterization of the osmolyte effect on protein stability and the effect of GdnHCl on the protein denatured state. *Journal of Physical Chemistry B*. 111:9045-9056.

Venkatesu, P., M.J. Lee, and H.M. Lin. 2009. Osmolyte Counteracts Urea-Induced Denaturation of alpha-Chymotrypsin. *Journal of Physical Chemistry B*. 113:5327-5338.

Wang, A., and D.W. Bolen. 1996. Effect of proline on lactate dehydrogenase activity: testing the generality and scope of the compatibility paradigm. *Biophys J*. 71:2117-2122.

Wang, D., S.L. Deken, T.L. Whitworth, and M.W. Quick. 2003. Syntaxin 1A inhibits GABA flux, efflux, and exchange mediated by the rat brain GABA transporter GAT1. *Mol Pharmacol*. 64:905-913.

Watson, D., R.D. Sleator, P.G. Casey, C. Hill, and C.G. Gahan. 2009. Specific osmolyte transporters mediate bile tolerance in Listeria monocytogenes. *Infect Immun*. 77:4895-4904.

Wirthensohn, G., S. Lefrank, M. Schmolke, and W.G. Guder. 1989. Regulation of organic osmolyte concentrations in tubules from rat renal inner medulla. *Am J Physiol*. 256:F128-135.

Woo, S.K., S.C. Dahl, H. Miyakawa, J.S. Handler, and H.M. Kwon. 1999. Tonicity-responsive enhancer binding protein (TonEBP): A transcription factor regulating cellular accumulation of compatible osmolytes(CO). *Faseb Journal*. 13:A710-A710.

Wood, J.M. 2007. Bacterial osmosensing transporters. *Methods Enzymol*. 428:77-107.

Wu, J.W., and Z.X. Wang. 1999. New evidence for the denaturant binding model. *Prot Sci*. 8:2090-2097.

Yamashita, A., S.K. Singh, T. Kawate, Y. Jin, and E. Gouaux. 2005. Crystal structure of a bacterial homologue of Na+/Cl--dependent neurotransmitter transporters. *Nature*. 437:215-223.

Yamauchi, A., S. Uchida, H.M. Kwon, A.S. Preston, R.B. Robey, A. Garciaperez, M.B. Burg, and J.S. Handler. 1992. Cloning of a Na^+-dependent and Cl^--dependent betaine transporter that is regulated by hypertonicity. *Journal of Biological Chemistry*. 267:649-652.

Yancey, P.H. 2005. Organic osmolytes as compatible, metabolic and counteracting cytoprotectants in high osmolarity and other stresses. *Journal of Experimental Biology*. 208:2819-2830.

Yancey, P.H., and M.B. Burg. 1990. Counteracting effects of urea and betaine in mammalian-cells in culture *American Journal of Physiology*. 258:R198-R204.

Yancey, P.H., M.E. Clark, S.C. Hand, R.D. Bowlus, and G.N. Somero. 1982. Living with Water Stress: Evolution of Osmolyte Systems. *Science*. 217:1214-1222.

Yancey, P.H., and G.N. Somero. 1979. Counteraction of urea destabilization of protein-structure by methylamine osmoregulatory compounds of elasmobranch fishes *Biochemical Journal*. 183:317-323.

Zhou, Y., S. Holmseth, R. Hua, A.C. Lehre, A.M. Olofsson, I. Poblete-Naredo, S.A. Kempson, and N.C. Danbolt. 2012. The betaine-GABA transporter (BGT1, slc6a12) is

predominantly expressed in the liver and at lower levels in the kidneys and at the brain surface. *Am J Physiol Renal Physiol*. 302:F316-328.

Zhou, Y.Y., J.A. Yao, and G.N. Tseng. 1997. Role of tyrosine kinase activity in cardiac slow delayed rectifier channel modulation by cell swelling. *Pflügers Arch*. 433:750-757.

Zhuang, S., S.I. Hirai, and S. Ohno. 2000. Hyperosmolality induces activation of cPKC and nPKC, a requirement for ERK1/2 activation in NIH/3T3 cells. *Am J Physiol Cell Physiol*. 278:C102-109.

Ziegler, C., E. Bremer, and R. Krämer. 2010. The BCCT-family of carriers: from physiology to crystal structure. *Molecular Microbiology*:no-no.

Ziółkowska, N.E., R. Christiano, and T.C. Walther. 2012. Organized living: formation mechanisms and functions of plasma membrane domains in yeast. *Trends in Cell Biology*. 22:151-158.

Zomot, E., A. Bendahan, M. Quick, Y. Zhao, J.A. Javitch, and B.I. Kanner. 2007. Mechanism of chloride interaction with neurotransmitter:sodium symporters. *Nature*. 449:726-730.

Zou, Q., S.M. Habermann-Rottinghaus, and K.P. Murphy. 1998. Urea effects on protein stability: Hydrogen bonding and the hydrophobic effect. *Proteins-Structure Function and Genetics*. 31:107-115.

List of Figures

List of Figures

List of Tables

Appendix

Gene sequences

1) wt-bgt1

atggacagaaaagtggcagtccccgaggacgggcctcccgttgtctcctggctccctgaggagggagagaagttggaccaggaagggga
ggaccaggtgaaggatcggggccaatggaccaacaagatggagtttgtgctgtcagtggccggggagatcattgggctgggcaatgtctg
gaggtttccctatctctgctacaaaaatggaggtggggccttcttcatcccctacttcatcttcttcttcacctgcggcatcccggtgttcttcctgg
aggtggcgttgggccagtacaccagccagggcagcgtgacagcctggaggaagatctgccccccttcttcagggcatcggtctggcgtctgt
ggtcattgagtcctatctgaacatctactacatcatcatcctcgcctgggctctcttctacctgttcagctcctttacctctgagctgccctggacga
cctgtaccaacacctggaacacagagcattgcatggactttcttaaccactcgggagcccgcacagcgacctcctctgagaacttcacctcac
ctgtcatggaattctgggagagacgtgttttgggcatcacctcaggcatccatgatttgggggctctgcgctgggagctagctctgtgccttctg
ctggcctggcttatctgctacttctgcatctggaagggagtcaagaccacaggcaaggtggtgtatttcacagccacgtttccctacctgatgct
ggtcatcctgctgatccgaggcatcacccttcccggagcctaccagggtgtcatctattacctgaagcctgatttgcttcgcctcaaggacccc
caagtatggatggacgcgggcacccagatcttcttctccttcgccatctgccaggggtgcctgactgccctgggcagctacaacaagtatcac
aacaactgctacagggacagcatcgccctctgcttcctgaacagtgccaccagcttcgcggctggcttcgtggtcttctccatcctgggcttcat
ggcccaagagcaggggctgcccatctctgaggtggccgagtccggtcctggtctagccttcatcgcgttccccaaggctgtgacaatgatgc
ccttatctcagctgtggtcctgccttttcttcatcatgctcatcttccttgggctggacagccagtttgtctgtgtggagtgcctggtgacagcctcc
atggacatgttccccagtcagctccggaagagtgggcggcgggagctcctcatccttgccattgctgtcttctgctacctggcggggctttttct
ggtcacggagggcgggatgtatatcttccagctgtttgattattatgcctccagtggcatatgcctgctcttcctggcgatgttcgaagtgatctg
catcagctgggtgtacggggctgatcgtttctatgacaacattgaagacatgattggctaccggccatggcccttggtgaagatttcctggctct
ttctgacccctggactctgcctggccaccttcctcttctccttgagccagtacacacctctcaaatacaacaacatctacgtgtaccctccctggg
gctactccatcggctggttcttggctctctcctccatgatctgcgtcccactctttgtcatcatcactcttctgaagacccggggttccttcaagaag
cgcctacgacagcttaccacccctgaccccagcctgccacagcccaagcaacacctgtatctggatggtggtaccagccaggactgcggg
ccttccccaacaaaggagggactaatagttggggagaaggagacccacttgtag

2) codon-optimized BGT1syn_Pp

atggactacaaggacgatgacgataaggatggcggactggaagttcttttccagggaccaatggacagaaaggtcgctgtcccagaagacg
gtccaccagttgtttcttggttgccagaagaaggtgaaaagttggaccaagagggtgaggaccaagttaaggacagaggtcaatggactaac
aagatggagttcgttttgtccgtcgctggtgagatcattggtttgggtaacgtctggagattcccatacttgtgttacaagaacggtggtggtgctt
tcttcatcccatacttcatcttcttcttcacttgtggtatccctgtcttcttcttggaggttgctttgggtcaatacacctctcaaggttccgttaccgctt

ggagaaagatttgtccattgttgcaaggtattggtttggcttctgttgtcatcgaatcttacttgaacatctactacattatcatcttggcctgggcctt
gttctacttgttctcttccttcacttctgagttgccatggactacttgcaccaacacttggaacaccgaacactgtatggacttcttggaccactctg
gtgctagaactgctacctcctctgaagacttcacctccccagtcatggagttctgggaaagaagagttttgggtattacctccggtatccacgac
ttgggtgctttgagatgggagttggctttgtgtttgttgttggcttggttgatttgttacttctgtatctggaagggtgttaagaccaccggtaaggtc
gtttacttcaccgctaccttcccatacttgatgttggttatcttgttgatcagaggtattaccttgcctggtgcttaccaaggtgttatttactacttgaa
gccagacttgttgagattgaaggacccacaagtttggatggacgctggtactcaaatcttcttctccttcgctatctgtcaaggttgtttgactgctt
tgggttcctacaacaagtaccacaacaactgctacagagactccatcgccttgtgtttcttgaactccgctacttccttcgctgctggtttcgttgtt
ttctccatcttgggtttcatggctcaagaacagggtttgccaatttctgaggttgccgaatccggtccaggtttggctttcatcgctttcccaaagg
ccgttactatgatgccattgtcccagttgtggtcctgtttgttcttcattatgttgatcttcttgggtttggactcccaattcgtttgtgtcgaatgtttggt
taccgcttccatggacatgttcccatcccaattgagaaagtctggtagaagagagttgttgattttggctattgctgtcttctgttacttggctggttt
gttcttggtcactgaaggtggtatgtacatcttccaattgttcgactactacgcctcctctggtatctgcttgttgttcttggctatgttcgaggttattt
gtatctcttgggtttacggtgctgacagattctacgacaacattgaggacatgatcggttacagaccatggcctttggttaagatttcctggttgttc
ttgactccaggtttgtgtttggccaccttcttgttctctttgtctcaatacaccccattgaagtacaacaacatttacgtttacccaccatggggttact
ccattggttggttcttggctttgtcttctatgatctgtgttccattgttcgttatcatcaccttgttgaagaccagaggttctttcaagaagagattgag
acagttgactactcctgacccttctttgcctcaaccaaagcagcacttgtacttggacggtggtacctcccaggactgcggtccttccccaacca
aggagggtttgatcgtcggtgaaaaggagactcacttgggcggacatcatcatcatcatcatcatcatcattgataggcggccgc

Protein constructs

1) WT-BGT1

UniProtKB entry name: S6A12_CANFA UniProtKB accession no.: P27799

>sp|P27799|S6A12_CANFA Sodium- and chloride-dependent betaine transporter OS=Canis familiaris GN=SLC6A12 PE=1 SV=2

MDRKVAVPEDGPPVVSWLPEEGEKLDQEGEDQVKDRGQWTNKMEFVLSVAGEIIGLGN
VWRFPYLCYKNGGGAFFIPYFIFFFTCGIPVFFLEVALGQYTSQGSVTAWRKICPLLQGIGL
ASVVIESYLNIYYIIILAWALFYLFSSFTSELPWTTCTNTWNTEHCMDFLNHSGARTATSSE
NFTSPVMEFWERRVLGITSGIHDLGALRWELALCLLLAWLICYFCIWKGVKTTGKVVYF
TATFPYLMLVILLIRGITLPGAYQGVIYYLKPDLLRLKDPQVWMDAGTQIFFSFAICQGCL
TALGSYNKYHNNCYRDSIALCFLNSATSFAAGFVVFSILGFMAQEQGLPISEVAESGPGLA
FIAFPKAVTMMPLSQLWSCLFFIMLIFLGLDSQFVCVECLVTASMDMFPSQLRKSGRRELL
ILAIAVFCYLAGLFLVTEGGMYIFQLFDYYASSGICLLFLAMFEVICISWVYGADRFYDNIE

DMIGYRPWPLVKISWLFLTPGLCLATFLFSLSQYTPLKYNNIYVYPPWGYSIGWFLALSS
MICVPLFVIITLLKTRGSFKKRLRQLTTPDPSLPQPKQHLYLDGGTSQDCGPSPTKEGLIVG
EKETHL

2) BetP

UniProtKB entry name: BETP_CORGL UniProtKB accession no.: P54582

>sp|P54582|BETP_CORGL Glycine betaine transporter BetP OS=Corynebacterium glutamicum (strain ATCC 13032 / DSM 20300 / JCM 1318 / LMG 3730 / NCIMB 10025) GN=betP PE=1 SV=1

MTTSDPNPKPIVEDAQPEQITATEELAGLLENPTNLEGKLADAEEEIILEGEDTQASLNWS
VIVPALVIVLATVVWGIGFKDSFTNFASSALSAVVDNLGWAFILFGTVFVFFIVVIAASKF
GTIRLGRIDEAPEFRTVSWISMMFAAGMGIGLMFYGTTEPLTFYRNGVPGHDEHNVGVA
MSTTMFHWTLHPWAIYAIVGLAIAYSTFRVGRKQLLSSAFVPLIGEKGAEGWLGKLIDIL
AIIATVFGTACSLGLGALQIGAGLSAANIIEDPSDWTIVGIVSVLTLAFIFSAISGVGKGIQY
LSNANMVLAALLAIFVFVVGPTVSILNLLPGSIGNYLSNFFQMAGRTAMSADGTAGEWL
GSWTIFYWAWWISWSPFVGMFLARISRGRSIREFILGVLLVPAGVSTVWFSIFGGTAIVFE
QNGESIWGDGAAEEQLFGLLHALPGGQIMGIIAMILLGTFFITSADSASTVMGTMSQHGQ
LEANKWVTAAWGVATAAIGLTLLLSGGDNALSNLQNVTIVAATPFLFVVIGLMFALVKD
LSNDVIYLEYREQQRFNARLARERRVHNEHRKRELAAKRRRERKASGAGKRR

PKC specific antibody design

Antigen design:

MDRKVAVPEDGPPVVSWLPEEGEKLDQEGEDQVKDRGQWTNKMEFVLSVAGEI

for immunization:

CQVKDRGQW(pThr)NKMEF